Bridging Scales: Flood Projection and Attribution at 150-m Resolution across Japan under Climate Change

CHEN JIACHAO

2025

Bridging Scales: Flood Projection and Attribution at 150-m Resolution across Japan under Climate Change

（スケールの架橋：気候変動下における日本全域 150 m 解像度洪水予測と要因寄与解析）

by

CHEN JIACHAO

A dissertation submitted in partial fulfillment of the requirement for the degree of Doctor of Philosophy

Department of Civil and Earth Resources Engineering

Kyoto University, Japan

2025

Declaration of Authorship

I affirm that, this dissertation, entitled “Bridging Scales: Flood Projection and Attribution at 150-m Resolution across Japan under Climate Change” and the content presented in it is my investigation, with any external contributions explicitly acknowledged within the text. I also confirm that I have not previously submitted this work for any academic degree or qualification at Kyoto University for other educational institution.

CHEN JIACHAO

Acknowledgement

Many years later as he faced the flowers and applause, Dr. Jiachao Chen was to remember that distant afternoon when Professor **Takahiro Sayama** discussed his research progress with him. Throughout the three-year doctoral journey, Professor Sayama offered professional guidance and rigorous training with unwavering responsibility, holding nearly fifty one-on-one seminars—each lasting more than two hours. Beyond academic mentorship, his diligence and his philosophy of encouraging independent thinking and expression deeply moved me. These admirable qualities continue to inspire me even after graduation, as enduring ideals I strive to emulate.

I have always believed that meeting a good supervisor is an extraordinary stroke of luck ($\frac{1}{n}$). Even rarer and more precious is the good fortune of joining a team where every member is both accomplished and generously supportive ($\frac{1}{n^x}$). I was honored to be part of such a team. Associate Professor **Tomohiro Tanaka** and Assistant Professor **Masafumi Yamada** are scholars I hold in the highest regard. I was often impressed by the agility of their thinking and their incisive grasp of key issues. Their insightful feedback and suggestions greatly enriched this research. I am also deeply grateful to our assistant professors—Dr. **Eva Yamamoto**, Dr. **Kodai Yamamoto**, and Dr. **Yoshito Sugawara**—for their constant willingness to answer my questions and offer practical advice and encouragement. Each gesture may have seemed small, but together they formed the fabric of my doctoral life. I also extend my heartfelt thanks to our laboratory secretary, Ms. **Sono Inoue**, whose dedication created an environment where every researcher could focus entirely on academic pursuits, free from administrative burdens.

Pursuing a Ph.D. alone in a foreign country is an immense challenge—both physically and mentally. I will always remember Dr. **Shuangtao Wang**, who came to meet me on my disoriented first day in Kyoto; Dr. **Ting Yan**, who visited and took me to the hospital when I suffered acute gastroenteritis; Dr. **Jiaqi Peng**, who accompanied me through winters and summers in an otherwise empty lab; and Dr. **Shi Feng**, who helped me communicate with a doctor when I had a fractured foot. These are but a few moments among countless days of mutual support. Knowing they were waiting

in the lab gave me reason to look forward to each day, and it was their trust and encouragement that helped me persist through self-doubt when facing research challenges.

I also owe a profound debt of gratitude to my mother, Ms. **Xiaoyan Xu**, whose nurturing and support were essential to the completion of my doctoral studies. A great, open-minded, and hardworking woman, she raised me alone and stood by me all the way to my Ph.D. Although she never received higher education and faced many obstacles, she believed more than anyone in the transformative power of education. No words can capture the sacrifices she made, nor the depth of my gratitude.

The Ph.D. journey was not only a process of constructing academic foundations but also of cultivating a philosophical worldview. Philosophy was refined and tested through practice, and in turn guided that practice—helping me resolve research challenges. I wish here to acknowledge someone long gone: **Zedong Mao**. His biography deeply influenced me, motivating me to overcome adversity and introducing me to philosophical inquiry. His writings *On Contradiction* and *On Practice* were particularly enlightening, shaping my understanding of how to approach research.

Lastly, I express sincere appreciation to the Ministry of Education, Culture, Sports, Science and Technology (MEXT) for the scholarship that supported me—not only financially, but also through the immersive language environment that enabled me to spend an unforgettable year at Northeast Normal University. There, I met lifelong friends who supported and encouraged me throughout my doctoral studies. I am especially grateful to Ms. **Guiping Liu**, Ms. **Li Zhang**, Ms. **Muyun Liu**, Ms. **Jun Li**, and other faculty and staff of the MEXT preparatory program, who offered invaluable help during my Japanese studies. Their dedication during the difficult era of the COVID-19 pandemic remains especially heartfelt and inspiring.

This acknowledgment is a tribute to the cherished years of my doctoral journey (2022.10–2025.09), and to all those who helped me along the way—I offer my deepest respect and heartfelt gratitude.

CHEN JIACHAO

July, 2025

Abstract

Climate change is expected to intensify the global hydrological cycle by increasing atmospheric moisture capacity, thereby amplifying the frequency and severity of extreme weather events. Coupled with complex environmental and anthropogenic factors, this results in more devastating flood disasters, leading to heightened casualties, economic losses, and constraints on sustainable development. As scientific understanding is undergoing a critical transition from global to regional and local scales—where the actual impacts of disasters unfold— a range of detailed, interdisciplinary studies are being conducted to provide insights and data support for reliable and actionable location-specific disaster risk reduction strategies.

However, current local-scale insights often remain fragmented, derived from disparate datasets, modeling approaches, and spatial scales. This inconsistency limits cross-scale integration and hampers comprehensive assessments of climate change impacts. Effective flood-related decision-making across national, regional, and community levels demands a unified and consistent insights and data foundation.

Focusing on Japan, this study aims to conduct nationwide, high-resolution (150 m, hourly) flood simulations for events exceeding a 10-year return period under historical and future climate stages (+2 ˚C and +4 ˚C warming) and analyze the future flood change patterns and the transformation of meteorological drivers. A core challenge lies in achieving computational feasibility for nationwide hydrodynamic modeling across multiple scales and climate stages while ensuring analytical accuracy and robustness.

To address this, the study innovatively developed the Aggregating Grid Event (AGE) method extracting precipitation events from large climate ensembles, which trigger floods exceeding a specified return period (10 years in this study) at least at one river cross-section within a given region. The AGE method incorporates river concentration time into the calculation of precipitation contributions to flood peaks and retrieves events across multiple scales and locations to ensure comprehensive capture of impactful events. By simulating only the most critical events, AGE dramatically reduces computational demands and supports parallel processing strategies.

Validation on Shikoku Island shows that 2,966 events extracted by the AGE method can yield comparable discharge quantile estimations to those based on all 25,700 valid events from the same climate ensemble. The relative bias in estimated 100-year flood remained within ±5% across the region, without introducing additional uncertainty. The AGE method outperforms alternative methods by selecting events accounting for spatiotemporal precipitation variability and preserving the complete hydrological process.

Building upon the antecedent investigation, the study constructs a three-step simulation–estimation framework: (1) identification of regional extreme precipitation events from a climate ensemble using the AGE method, (2) obtaining flood responses at each river cross-section using an efficient distributed hydrodynamic model, and (3) estimating flood frequency curve for each river cross-section using the top 72 discharge peaks and the Peaks-Over-Threshold (POT) method. The 5-km dynamically downscaled climate projection ensemble, derived from the database for Policy Decision-making for Future climate change (d4PDF) project, was employed to provide hourly precipitation data under historical, +2°C, and +4°C warming stages, while avoiding issues of non-stationarity. The Rainfall–Runoff–Inundation (RRI) model, which integrates local river cross-section data and reservoir operation, was used for high-resolution flood simulation.

Applying the simulation–estimation framework to Japan, this study estimated the 100-year flood peak for every river cross-section with a resolution of 150 m, and analyzed their changes pattern at future climate stages. Nationwide results show that 100-year flood peaks are projected to increase by factors of 1.16 and 1.37 under +2 °C and +4 °C warming stages, respectively. Northern regions, including Tohoku and Hokkaido, exhibit the greatest increases and climate sensitivity. Within-region variability is also substantial, with small basins and mountain–plain transition zones facing disproportionately larger increases. Flood hydrographs are projected to become steeper, with 10%–20% faster rising limbs, signaling heightened flash flood risks. Statistically significant increases in flashiness in northern Japan highlight the need to integrate emerging risks into future flood management plans.

To elucidate the meteorological drivers behind these flood projections, each flood event is attributed to one of three dominant weather systems using a d4PDF-based tropical cyclone (TC) track dataset: TC-induced, non-TC events in June–July (NT67, associated with Meiyu–Baiu fronts), and non-TC events in August–September (NT89,

linked to autumnal fronts). These three systems account for over 90% of historical floods, with TCs being the predominant driver (>50%). While the frequency of TC-driven floods is projected to decline—particularly in northern Japan—due to a reduction in TC number, shifts in TC tracks and intensification cause a ~20% increase in TC-driven flood events in the Chugoku region under +2 ˚C warming stage. Both TC and non-TC floods show increasing peak discharge and flashiness, with the contributions of NT67 and NT89 projected to rise by 20%–30%, exhibiting strong regional characteristics. The increasing complexity and intra-basin heterogeneity in flood causation challenge traditional flood management practices. Notably, attribution varies even within individual basins, and climate change is expected to significantly reorder the dominant drivers of extreme floods (e.g., top 10 events), underscoring the need for basin-specific, climate-informed flood attribution analysis and developing countermeasures for different weather-induced floods.

In summary, this study bridges the gap between global flood research and local-scale flood risk assessments. It establishes a detailed and computationally feasible framework for mesoscale flood analysis and delivers high-resolution nationwide projections. The findings reveal emerging high-risk regions and critical shifts in flood-generating mechanisms, providing essential insights for enhancing adaptive flood management strategies and strengthening Japan's resilience to future floods. Additionally, the generated future flood database offers a valuable resource for further research on localized flood hazards and their cascading societal impacts.

Abbreviations

1D: one-dimensional
2D: two-dimensional
48h-AMS: 48 h Annual Maximum precipitation Series
+2°C: The future climate stage that the global mean temperature is 2°C higher than preindustrial level
+4°C: The future climate stage that the global mean temperature is 4°C higher than preindustrial level
AEP: Annual Exceedance Probability
AGE: Aggregating Grid Event
AM48: Annual Maximum 48 h rainfall events
AMFS: Annual Maximum Flood Series
AOGCM: Atmosphere–Ocean General Circulation Model
BIAS: relative bias
BM: Block Maxima
CaMa-Flood: CAtchment-based MAcro-scale FLOODplain model
CC: Correlation Coefficient
CI: Confidence Interval
CAs: upstream Contribution Areas
CMIP6: Coupled Model Intercomparison Project sixth phase
CORDEX: COordinated Regional climate Downscaling EXperiment
d4PDF: Database for Policy Decision-making for Future climate change
d4PDF DDSJP: 5-km dynamically downscaled d4PDF over Japan
DEM: Digital Elevation Model
ECMWF: European Centre for Medium-Range Weather Forecasts
ENSO: El Niño–Southern Oscillation
FFA: Flood Frequency Analysis
FFC: flood frequency curve
GCM: Global Climate Model
GAN: Generative Adversarial Network
GEV: Generalized Extreme Value distriution

GLO: Generalized Logistic distribution

GloFAS: Global Flood Awareness System

GLOFRIS: GLObal Flood RISk

GNO: Generalized Normal distribution

GPD: Generalized Pareto Distribution

IBTrACS: International Best Track Archive for Climate Stewardship

IDF: Intensity-Duration-Frequency

IPO: Interdecadal Pacific Oscillation

J-FlwDir: Japan Flow Direction map

JRRI: localized Japan RRI

KGE: Kling-Gupta Efficiency

KS: Kolmogorov–Smirnov test

MAPE: Mean Absolute Percentage Error

M-CV: Modified Coefficient of Variation

MLIT: Ministry of Land, Infrastructure, Transport and tourism, Japan

MRI-AGCM 3.2: Meteorological Research Institute Atmospheric General Circulation Model 3.2

M-K: Mann-Kendall test

NEX-GDDP: NASA Earth Exchange Global Daily Downscaled Projections

NHRCM: Non-Hydrostatic Regional Climate Model

NSE: Nash-Sutcliffe Efficiency

NT67: Non-TC events in June–July

NT89: Non-TC events in August–September

PE3: Pearson Type III distribution

PGW: Pseudo Global Warming

POT: Peaks–Over–Threshold

PrecStre: Precipitation Stretching method

PrecStre-I: Estimates precipitation frequency using all ensemble members

PrecStre-S: Obtains precipitation quantiles from the ensemble mean

Q50: Discharge at 50-year return period

Q100: Discharge at 100-year return period

R: correlation coefficient

RBA: Relative Basin Area

RCP: Representative Concentration Pathway

RCID: Relative Confidence Interval Difference

RCM: Regional Climate Model
RDCT: Rainfall During the Concentration Time
REC: Regional Envelope Curve
RMSE: Root Mean Square Error
RPD: Relative Peak Difference
RRI: Rainfall-Runoff-Inundation model
RRAR: Radar Rain gauge Analyzed Rainfall
RRMSE: Relative Root Mean Square Error
SI-CAT DDS5TK: Dynamical DownScaling data for near future atmospheric projection (from Tohoku to Kyushu) by the Social Implementation program on Climate change Adaptation Technology
SST: Sea Surface Temperature
SSP: Shared Socioeconomic Pathway
TAD: Total Absolute Displacement
TC: Tropical Cyclone
TR: Total Rainfall
WAK: Wakeby (a five-parameter distribution)
WEB-RRI: Water and Energy Budget-based RRI

Table of contents

Declaration of Authorship I
Acknowledgement III
Abstract V
Abbreviations VIII
Table of contents i
List of figures v
List of tables xi
1. Introduction 1
1.1 Background 1
1.1.1 Floods and climate change 1
1.1.2 Floods in Japan 2
1.1.3 Climate projection ensemble 3
1.1.4 Flood projections under climate change 5
1.2 Research objectives 6
1.3 Outlines 6
2. Evaluation of Regional event-based frequency analysis methods 9
Abstract 9
2.1 Introduction 10
2.2. Methods 12
2.2.1 Regional approach 12
2.2.2 Rainfall-Runoff-Inundation model 14
2.2.3 Frequency analysis method 15
2.3 Study Area and Data 17
2.3.1 Study area 17
2.3.2 Data 18
2.4 Results 20
2.4.1 Evaluation of the current scenario 20
2.4.2 Evaluation on future scenarios 23
2.5 Discussion 26
2.6 Conclusions 29

3. Development of the Aggregating Grid Event method 30
Abstract 30
3.1 Introduction 31
3.2 Methodology 34
3.2.1 Aggregating grid event (AGE) method 34
3.2.3 Rainfall-runoff-inundation (RRI) model 38
3.2.4 Peak-over-threshold (POT) 39
3.2.5 Evaluation indicators 40
3.3 Study Area and Data 40
3.3.1 Shikoku Island 40
3.3.2 5-km d4PDF dataset 41
3.4 Results 42
3.4.1 Discharge peaks 42
3.4.2 Discharge quantiles 44
3.5 Discussion 49
3.6 Conclusions 52
4. Evaluation on process-based flood quantile estimation methods 54
Abstract 54
4.1 Introduction 55
4.2 Study area & data 57
4.2.1 Shikoku Island 57
4.2.2 Data 58
4.3 Methodology 58
4.3.1 Aggregating Grid Event Method 60
4.3.2 Precipitation Stretching Method 62
4.3.3 Rainfall-Runoff-Inundation Model 64
4.3.4 Evaluation Indicators 66
4.4 Results 67
4.1 Evaluation on the AGE method 67
4.4.2 Evaluation on the precipitation stretching method 68
4.4.3 Error and uncertainty pattern 71
4.5 Discussion 74
4.6 Conclusions 76
5. Projecting future floods at multiscale rivers over Japan 78
Abstract 78

5.1 Introduction 79
5.2 Study area and data description 81
5.2.1 Study area 81
5.2.2 Ensemble climate projection dataset 82
5.3 Methodology 83
5.3.1 Event extraction method 83
5.3.2 Rainfall-Runoff-Inundation (RRI) model 84
5.3.3 Flood frequency analysis 85
5.3.4 Evaluation method 85
5.4 Results 87
5.4.1 National trend 87
5.4.2 Regional trends 90
5.4.3 Flood process changes 95
5.5 Discussion 97
5.5.1 Increase ratio and flashiness at major basin outlets 97
5.5.2 Extreme precipitation pattern changes 99
5.5.3 Comparison of flood projection studies 100
5.5.4 “by All” Policy 101
5.5.5 Limitations 101
5.6 Conclusions 102
6. Meteorological driver transitions of projected floods 104
Abstract 104
6.1 Introduction 105
6.2 Results 108
6.2.1 Changes in flood contributions 108
6.2.2 Basin scale effect changes 111
6.2.4 Changes in flood responses 113
6.3 Discussion 118
6.4 Conclusions 122
6.5 Methods 123
6.5.1 Data sources 123
6.5.2 Hydrodynamic model 124
6.5.3 Extreme precipitation event extraction method 124
6.5.4 Flood attribution method 125
6.5.5 Index and Statistical Testing 125

7. Concluding remarks 127
Supporting information 131
Supplemental figures 131
Supplemental tables 149
References 155

List of figures

Figure 1-1 Outline of this dissertation 7

Figure 2-1 Flow chart of the basin and regional approaches for this chapter 13

Figure 2-2 Overview of Shikoku Island 18

Figure 2-3 Accuracy comparison of applying the POT and BM methods using different parameters for Watari basin. 20

Figure 2-4 RRMSEs of the eight basins using different methods and parameters under the current scenario. The grey dash line represents the RRMSE between the predictions of the basin approach and the basin AMFS 21

Figure 2-5 Estimation results of discharge quantiles for different basins using the POT methods with the top 10% AMFS. The meaning of elements in the figure can refer to Figure 2-3 23

Figure 2-6 Estimation results of discharge quantiles for different basins using the POT methods with the top 10% AMFS for the 2 K warming scenario 24

Figure 2-7 Estimation results of discharge quantiles for different basins using the POT methods with the top 10% AMFS for the 4 K warming scenario 25

Figure 2-8 Distribution of processed (POT and BM) and original regional AMFS with optimal selection parameters in the current scenario 28

Figure 3-1 Flowchart portraying the study methodology used in this study. Abbreviations: rainfall-runoff-inundation (RRI), aggregating grid event (AGE). 34

Figure 3-2 Process schematic of aggregating grid events (AGE) method used in this study. Abbreviations: resolution (res.). 37

Figure 3-3 Map of Shikoku Island, Japan. Abbreviations: digital elevation model (DEM). 41

Figure 3-4 Relative bias (BIAS) of river grids. Comparison of the highest 72 discharges between aggregating grid event (AGE) method and all valid precipitation events. 43

Figure 3-5 Evaluation of the 72 highest discharges of all river grids, based on the events extracted by the aggregating grid event (AGE) method. 44

Figure 3-6 Flood quantile maps for the return periods of (a) 10, (b) 50, (c) 100, and (d) 1000 years.....45

Figure 3-7 Spatial distribution of discharge-quantile relative bias (BIAS) values for return periods of (a) 10, (b) 50, (c) 100, and (d) 1000 years.....46

Figure 3-8 Changes in the relative bias (BIAS) values of discharge quantiles with basin area, for return periods of 10 (RP10), 50 (RP50), 100 (RP100), 1000 (RP1000) years.47

Figure 3-9 Comparison of the discharge quantiles for all river sections on the Shikoku Island for different return periods. Abbreviations: correlation coefficient (R), relative bias (BIAS), root mean square error (RMSE). 47

Figure 3-10 Results of confidence interval (CI) ratios for all river grids within Shikoku Island at different return periods. Abbreviations: aggregating grid event (AGE) model and reference (Ref) values.....48

Figure 4-1 Overview of the Shikoku Island 57

Figure 4-2 Flows of obtaining quantile maps for evaluation 59

Figure 4-3 Conceptual illustration of the Aggregating Grid Event method (derived from Chapter 3).....61

Figure 4-4 Conceptual illustration of precipitation stretching method.....62

Figure 4-5 Locations of gauge and validation results of the JRRI model in the study area.....66

Figure 4-6 BIAS of discharge at 100-year return period (AGE method V.S. all valid events).....67

Figure 4-7 BIAS of discharge at 100-year return period (PrecStre-I method V.S. all valid

events).....69

Figure 4-8 BIAS of discharge at 100-year return period (PrecStre-S method V.S. all valid events).....70

Figure 4-9 Evaluation results of discharge quantiles at 100-year return period (a) across Shikoku Island, and (b) at the basin outlets.....71

Figure 4-10 Distributions of BIAS of discharge quantiles obtained from the AGE, PrecStre-I, and PrecStre-S methods vary with relative basin area.....73

Figure 4-11 Distributions of relative confidence interval differences (RCID) values in different relative basin area (RBA) ranges.....74

Figure 5-1 Topography of Japan and the locations of 14 regions, adjusted from official administrative divisions based on basin boundaries 82

Figure 5-2 Spatial distribution of Q100 increase ratios at +2˚C (a) and +4˚C (b) stages. Osaka bay (red rectangle) is enlarged as an example to show tributary details in this study. Abbreviation: 100-year return period discharge (Q100).....88

Figure 5-3 Distributions of increase ratios (a) and equivalent return period of historical Q100 (b) on the national level and 14 regions. Abbreviation: 100-year return period discharge (Q100) 89

Figure 5-4 Q100 increase ratios of each region vary with contribution areas at the +2˚C stage. 91

Figure 5-5 Q100 increase ratios of each region vary with contribution areas at the +4˚C stage. 92

Figure 5-6 Q100 increase ratios of each region vary with elevation at the +2˚C stage. Abbreviation: modified coefficient of variation (*M-CV*) 93

Figure 5-7 Q100 increase ratios of each region vary with elevation at the +4˚C stage. Abbreviation: modified coefficient of variation (*M-CV*) 94

Figure 5-8 Spatial distribution of flashiness medians and their relative changes at the +2˚C and +4˚C stages. 96

Figure 5-9 Spatial distribution of increase ratios for outlets of 109 national basins at the +2˚C (a) and +4˚C (b) stages.....98

Figure 6-1 Overview of the four major islands in Japan..... 107

Figure 6-2 Proportion of TC-, NT67-, NT89-induced floods at the past climate stage and projected changes at the +2˚C and +4˚C stages. 109

Figure 6-3 REC slope of TC-, NT67-, NT89-induced floods at the past climate stage, and their changes at the +2˚C, and +4˚C stages, with TC-induced floods in Watari River Basin as an example. 112

Figure 6-4 Discharge peak median of categorized floods at 109 national basin outlets under the past climate stage and the projected changes. 114

Figure 6-5 Effective duration median of categorized floods at 109 national basin outlets under the past climate stage and the projected changes. 116

Figure 6-6 Flashiness of categorized floods at 109 national basin outlets under the past climate stage and the projected changes. 117

Figure 6-7 Representative precipitation processes of the largest flood event in Ishikari basin from the past climate ensemble. 119

Figure S1 Comparison of fitting methods for basin annual maximum series..... 131

Figure S2 Evaluation of the peak discharges of all river grids, based on the events extracted by the aggregating grid event (AGE) method using the total rainfall (TR) indicator. 132

Figure S3 Evaluation of the peak discharges of all river grids, based on the events extracted by the aggregating grid event (AGE) method using the rainfall during concentration time (RDCT) indicator..... 134

Figure S4 Spatial distribution of the relative bias (BIAS) values in the peak discharges, based on the aggregating grid event (AGE method) using the (a) total rainfall (TR) and (b) rainfall during concentration time (RDCT) indicators..... 135

Figure S5 Box plots of the evaluation indices, including NSE, RPD, CC, and KGE at 711

national stations (2,723 events in total). 136

Figure S0-6 Spatial distribution of average NSE values at 711 national stations. Abbreviations: Nash–Sutcliffe Efficiency (NSE). 137

Figure S7 Comparisons of observed events against discharge simulated with and without initial conditions at the major basins of the study area. 137

Figure S8 Locations of the discharge gauges (a) and comparisons between observation-based frequency curve and simulated extremes (b~d). 138

Figure S9 Spatial distribution of 121 national dams in the RRI model. Abbreviations: Rainfall-Runoff-Inundation (RRI) 139

Figure S10 Comparison of 10-year discharge for each river grid across 14 regions of Japan. 140

Figure S11 Spatial distribution of Q50 increase ratios at +2˚C (a) and +4˚C (b) stages. Osaka bay (red rectangle) is enlarged as an example to show tributary details in this study. Abbreviation: 50-year return period discharge (Q50). 141

Figure S12 Spatial distribution of contours for increase ratio median peak in Figure 5-7. The attached table provides the contour values for the corresponding region.142

Figure S13 Increase ratio trend of TC-induced max discharge along basin area at the +2℃ stage..... 143

Figure S14 Increase ratio trend of TC-induced max discharge along basin area at the +4℃ stage..... 144

Figure S15 Increase ratio trend of NT67-induced max discharge along basin area at the +2℃ stage..... 145

Figure S16 Increase ratio trend of NT67-induced max discharge along basin area at the +4℃ stage..... 146

Figure S17 Increase ratio trend of NT89-induced max discharge along basin area at the +2℃ stage..... 147

Figure S18 Increase ratio trend of NT89-induced max discharge along basin area at the +4℃ stage. 148

List of tables

Table 2-1 Parameters of the POT and BM data selection methods.....16

Table 2-2 Morphological parameters of the eight major river basins of Shikoku Island 17

Table 2-3 Performance of regional results in different scenarios 24

Table 4-1 Topographic parameters of the eight major basins in Shikoku Island...58

Table 4-2 Relationship between pixel area and approximate river concentration time 62

Table 4-3 Target rainfall amount of each basin and their 95% upper and lower limits from the PrecStre-I method.....63

Table 4-4 Representative member, target rainfall amount of each basin and their 95% upper and lower limits from the PrecStre-S method 64

Table 4-5 Statistical evaluation results of the PrecStre-S, PreStre-I, and AGE methods at different scales.....72

Table S1 Goodness-of-fit Z of the eight basins under current scenario..... 149

Table S2 Goodness-of-fit Z of the eight basins under 2k scenario..... 149

Table S3 Goodness-of-fit Z of the eight basins under 4k scenario..... 149

Table S4 Relationship between pixel area and approximate basin concentration time. 150

Table S5 Parameter sets of the Rainfall-Runoff-Inundation model for each soil type. 150

Table S6 Estimated scaling ratios and corresponding upper and lower 95% limits for candidate events using in PrecStre-I. 151

Table S7 Estimated scaling ratios and corresponding upper and lower 95% limits for candidate events using in PrecStre-S. 152

1. Introduction

1.1 Background

1.1.1 Floods and climate change

Throughout the long arc of human history, the struggle against flooding has remained a persistent challenge intertwined with societal advancement. This struggle has seen a profound shift—from passive endurance to active defense. Yet, victory remains elusive, as climate change propels flood risks into unprecedented and uncertain territory.

Climate change entails long-term alterations in temperature and climate patterns across atmospheric, oceanic, and terrestrial systems, predominantly driven by anthropogenic greenhouse gas emissions. Its most prominent effects include global warming and the increasing frequency of extreme weather events (IPCC, 2021). By enhancing atmospheric water capacity at approximately 6.5% per degree Celsius (Allen and Ingram, 2002), climate change accelerates the hydrological cycle, thereby increasing the frequency and severity of extreme precipitation and amplifying flood hazards (Donat et al., 2016; Dong et al., 2020; Fowler et al., 2021; Prein et al., 2017; Westra et al., 2014). Beyond atmospheric moisture, climate change exacerbates flood risks through multiple pathways. Warmer oceans fuel more destructive tropical cyclones by providing more latent heat energy (Emanuel, 2005; Li et al., 2017; Tu et al., 2018). Storm surges during landfall—especially when coinciding with sea-level rise and astronomical high tides—can trigger compound flooding, intensifying risks in coastal areas (Bates et al., 2021; Maymandi et al., 2022; Mitu et al., 2023; Wang et al., 2024; Ward et al., 2018). In some regions, accelerated glacial melt may raise flood peaks and cause glacial lake outburst floods (Ikeda et al., 2016; Shugar et al., 2020). Additionally, emerging environmental features associated with human development—such as urbanization that reduces infiltration through surface hardening, and increased aerosol concentrations that intensify extreme precipitation risks—further expose human society to unprecedented flood hazards (Miller et al., 2014; Rosenfeld et al., 2014; Tang et al., 2024; Zhang et al., 2018; Zhao et al., 2024)

As one of the deadliest natural hazards, floods impact society across numerous dimensions, including loss of life, destruction of infrastructure and property, and

disruption of agriculture (Koks et al., 2019; Sun et al., 2019a; Verschuur et al., 2024). These direct impacts often cascade into secondary crises in public health, food and energy security, and ecosystem stability (Ivers and Ryan, 2006; Liu et al., 2019; Vestby et al., 2024; Ye et al., 2024). Between 1998 and 2017, floods accounted for 43.4% of all global disasters, affecting two billion people, causing over 142,000 deaths, and incurring USD 656 billion in economic losses (Wallemacq et al., 2018).

To curb global warming and mitigate disaster-related losses, the international community has reached a series of agreements, including the Kyoto Protocol, the Paris Agreement, and the Sendai Framework for Disaster Risk Reduction. The Paris Agreement aims to limit global warming to well below 2 ˚C above pre-industrial levels, with efforts constrain it to 1.5 ˚C. Notably, as the responses of human and ecological systems to climate change are non-linear, the 1.5 ˚C target is regarded as a critical threshold triggering irreversible tipping points (Hoegh-Guldberg et al., 2019). Unfortunately, 2024 marked the first year in which the global mean temperature surpassed 1.5 ˚C above pre-industrial levels, suggesting the Paris target may be exceeded within the next two decades (Bevacqua et al., 2025). This milestone **underscores the urgent necessity of addressing flood risks under more severe climate scenarios** through proactive adaptation, disaster risk reduction, emergency preparedness, and resilience-building initiatives.

1.1.2 Floods in Japan

Floods in Japan is primarily driven by intense precipitation associated with tropical cyclones, frontal systems, and mesoscale convective systems. Owing to Japan's mountainous terrain and small river basins, **flash flood is a common flood type**, which is characterized by rapid flow velocities and short durations, typically reaching peak discharge within 12–24 hours of rainfall onset (Collier, 2007; Georgakakos, 1986; Marchi et al., 2010; Raynaud et al., 2015), and are often accompanied by landslides and debris flows (Mori and Ono, 2019; Yokoya et al., 2022).

Several recent events underscore the diversity and destructive of Japan's floods. In October 2019, Typhoon Hagibis struck eastern Japan, damaging 325 rivers, breaching 142 levees, and resulting in 114 fatalities or missing persons (Cabinet Office, 2020; MLIT, 2020). In July 2018, heavy rainfall associated with the Baiu front—a quasi-stationary frontal system—damaged 315 rivers and breached 37 levees, causing 245 deaths or missing persons in western Japan (Cabinet Office, 2019; MLIT, 2019). Most

recently, in September 2024, record-breaking rainfall from a line-shaped rainband—a mesoscale convective system—caused 63 casualties and displaced 244 people on a Ishikawa prefecture (Cabinet Office, 2024).

The simulation and forecasting of flash floods—especially in ungauged basins—remain challenging due to the complex hydrological responses in mountainous terrain and the rapid concentration of runoff (Ciervo et al., 2015; Wang et al., 2023; Zhai et al., 2021). **Hydrodynamic models**, which capture the physical processes of flood generation and propagation, **offer a robust approach for simulating flash floods in ungauged regions** (Ciervo et al., 2015; Liu et al., 2025). Accordingly, flood studies in Japan typically rely on hydrodynamic modeling, with a strong emphasis on high spatial and temporal resolution (Huang et al., 2023; Tanaka et al., 2020; Taniguchi et al., 2022; Tezuka et al., 2014). However, **hydrodynamic models require much more computational resources than statistical or hydrological methods, which hinder their application on large domains**.

Japan's flood risk management has evolved through several paradigm shifts. The first era (1910–1935) marked the initial development of modern flood control plans during Japan's transition to a modern state. The second era (1935–1970) responded to major flood disasters by revising flood control strategies and introducing techniques such as frequency analysis. The third era (1970–2010) focused on addressing urban flooding and environmental concerns amid rapid urbanization and economic growth (Nakamura and Oki, 2018).

Currently, **Japan is entering a new phase of flood risk governance shaped by climate change and growing emphasis on public awareness and engagement**. The government's recent policy initiative, "River Basin Disaster Resilience and Sustainability by All," advocates for comprehensive stakeholder involvement, spanning both public and private sectors (MLIT, 2024a). **High-resolution flood projections that incorporate climate change** are becoming increasingly critical for informing the public and facilitating effective policy implementation.

1.1.3 Climate projection ensemble

Scientists have developed a series of Global Climate Models (GCMs) to project future climate under various greenhouse gas emission and socioeconomic development scenarios. However, due to the climate system's high sensitivity to initial conditions,

substantial uncertainties remain in future projections (Deser et al., 2012, 2014; Lorenz, 1963; Palmer, 1999; Shepherd, 2014). To quantify and mitigate these uncertainties—stemming from models, parameters, inputs, and scenarios—the Coupled Model Intercomparison Project (CMIP) was established to support standardized simulations and enhance the robustness of climate impact assessments (Eyring et al., 2016). CMIP is currently in its sixth phase (CMIP6), utilizing Representative Concentration Pathways (RCPs) and Shared Socioeconomic Pathways (SSPs) to characterize emission trajectories and socioeconomic futures (Riahi et al., 2017; van Vuuren et al., 2011).

However, GCMs typically operate at coarse spatial resolutions (~100–200 km), limiting their ability to capture the structure details of mesoscale weather systems, and their complex interactions with topography, thereby constraining regional-scale impact assessments (Chen et al., 2021a; Kitoh et al., 2016a; Pontoppidan et al., 2017; Prein et al., 2015, 2017; Rasmussen et al., 2014). To overcome this, Regional Climate Models (RCMs) have been developed to dynamically downscale GCM outputs using physically based processes tailored to specific regions, yielding more reliable regional projections (Sasaki et al., 2011).

The above climate projection schemes are inherently evolutionary, meaning the climate state continuously changes throughout the simulation period. This introduces non-stationarity into Flood Frequency Analysis (FFA), as changing climate conditions undermine the assumption of stationary statistics (Milly et al., 2008). The Pseudo Global Warming (PGW) technique provides a viable solution by coupling reanalysis data with detrended future climate signals for targeted future periods (Taniguchi et al., 2022). This method is commonly applied to assess future changes in specific events, such as tropical cyclones, known as storyline analysis (Shepherd et al., 2018; Takemi, 2019; Tanaka et al., 2023).

Recently, the PGW approach has been extended to longer-term projections, leading to the development of the database for Policy Decision making for Future climate change (**d4PDF**), a high-resolution large ensemble global climate dataset (Fujita et al., 2019; Mizuta et al., 2017). Regions surrounding Japan have been further **downscaled to fine spatial (5 km) and temporal (hourly) resolutions** (Kawase et al., 2023), **enabling robust assessments of future frequencies of extreme events**, including heavy rainfall, snowfall, floods, and droughts (Hatsuzuka et al., 2020; Kawase et al., 2020; Miyasaka et al., 2020; Ohba et al., 2022; Tanaka et al., 2018; Zhao et al., 2023).

1.1.4 Flood projections under climate change

Current research on future flood projections can be broadly divided into two spatial scales: macroscale and microscale. Macroscale studies address global or continental extents, aiming to identify long-term trends and broad spatial patterns (Alfieri et al., 2015b; Hirabayashi et al., 2013; Pappenberger et al., 2012). These studies typically employ cascade modeling frameworks that couple land surface or large-scale hydrological models with computationally efficient global flood models (Hoch and Trigg, 2019). In contrast, microscale studies target individual river basins, tributaries, or specific flood events, focusing on detailed transformations in flood mechanisms under future climate conditions. These studies often utilize high-resolution hydrological and hydrodynamic models to capture localized processes (Shi and Shiraiwa, 2023; Yamamoto et al., 2021; Yu et al., 2019; Zhao et al., 2016).

However, a mesoscale framework is needed to bridge the gap between macroscale projections and microscale process understanding. Mesoscale modeling refers to simulations encompassing **large domains**—such as entire countries or major transboundary river basins—while maintaining sufficiently **high spatiotemporal resolution** to resolve local hydrological dynamics. At this scale, local features such as reservoirs, levees, river cross-section geometries, and tributary divergences critically influence flood behavior and should be explicitly represented.

Achieving consistency and complementarity between macro- and micro-scale projections is essential for national flood risk management and regional disaster analysis, but presents significant technical challenges. The incorporation of physical processes in hydrodynamic models is indispensable for reliable outcomes, especially in ungauged basins or when representing flash flood dynamics. **High-resolution, large-domain hydrodynamic simulations inherently demand considerable computational resources. Utilizing climate projection ensembles will further exacerbate the number of required simulations.** The computational feasibility should be guaranteed, while avoiding excessive simplification that compromises accuracy.

Therefore, **the core challenge of this dissertation** lies in developing methods to balance accuracy and computational feasibility, serving for projecting future flood frequencies across all river sections in Japan using an ultra-high spatiotemporal resolution hydrodynamic model.

1.2 Research objectives

The overarching goal of this study is to investigate changes in flood patterns across Japan—encompassing national and regional trends, flash flood risks, and meteorological driver transitions—under climate change from a hyper-resolution perspective. To achieve this, the study incorporates methodology development, flood projections, and pattern change analysis. The specific objectives are as follows:

1. **To evaluate the impact of precipitation variability on different FFA methods**, thereby identifying the most suitable approach for a regional event-based flood quantile estimation framework.

2. **To develop a method for detecting regional extreme precipitation events** that preserve the spatiotemporal coherence of rainfall across multiple locations and scales, enabling robust estimation of flood frequency curves at all river grid cells within the study domain.

3. **To assess the performance of the proposed methodology** in processing climate ensemble datasets, with a focus on estimating flood quantiles (e.g., 100-year flood), and to compare results with those derived from conventional flood design approaches.

4. **To analyze projected changes in flood patterns over Japan** by applying the developed methodology to a large climate ensemble dataset and simulating floods at 2˚C and 4˚C warmer climate stages using a nation-wide hydrodynamic model.

5. **To characterize the transitions in weather system** associated with projected extreme floods, providing actionable insights for local flood prevention and adaptation strategies.

The successful completion of these objectives will establish a novel methodological framework for future flood risk assessment, enhance scientific and public understanding of climate-induced flood hazards in Japan, support the implementation of participatory flood risk management policies, and inform critical decision-making at the national and regional levels.

1.3 Outlines

The structure of this dissertation is outlined in Figure 1-1. To enable hyper-resolution

flood simulations across Japan—at 150 m spatial and 1-hour temporal resolution—and to project changes in flood regimes at all river cross-sections using a large dynamically downscaled climate ensemble (totaling 2,160 simulation years), a novel methodology is required to balance accuracy and computational feasibility. This challenge propels the research presented in Chapters 2 and 3.

Chapter 2 attempts to reduce computational demand associate with FFA by constructing a regional extreme precipitation event set, and subsequently evaluates the applicability of two mainstream FFA methods—Block Maxima and Peaks-Over-Threshold.

Chapter 3 is motivated by the limitations of conventional event selection methods, such as the basin-averaged annual maximum approach, which fails to capture the spatiotemporal variability of precipitation, resulting in inaccurate FFA in tributaries. To address this, the chapter developed the Aggregating Grid Event (AGE) method, which extracts precipitation extremes across multiple locations and scales, and aggregates them into a coherent regional event set.

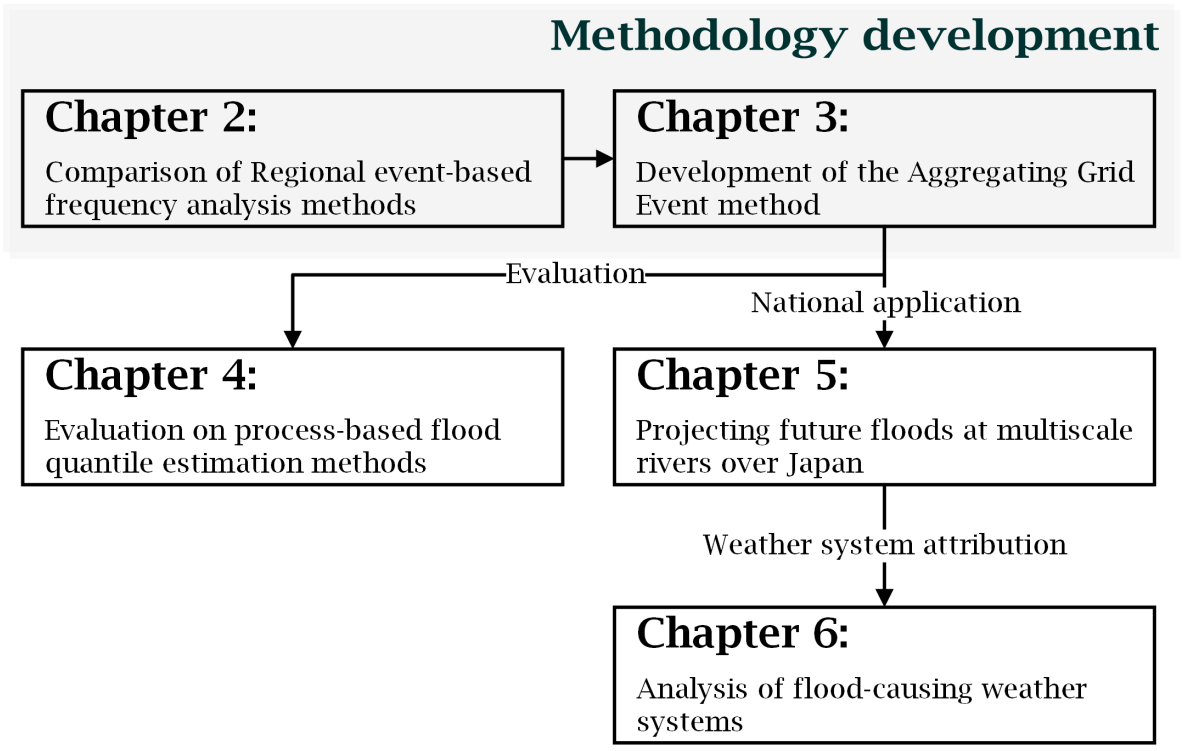


Figure 1-1 Outline of this dissertation

Chapter 4 validates the AGE method by comparing its performance against the flood quantile estimation results from a full event set and a conventional flood design

approach, demonstrating its reliability and methodological advantages.

Chapter 5 applies the AGE method at the national scale to process the large climate ensemble and perform comprehensive flood simulations and pattern analyses.

Chapter 6 integrates a global tropical cyclone track dataset to identify the dominant meteorological systems responsible for projected extreme floods and assesses how shifts in these systems influence future flood characteristics in Japan.

Together, these chapters offer novel insights into projected flood regime changes and their meteorological drivers under varying climate warming stages. The findings contribute to advancing climate change impact assessment, informing disaster risk reduction, and supporting adaptive flood management strategies in Japan.

2. Evaluation of Regional event-based frequency analysis methods[1]

Abstract

High-resolution nationwide hydrodynamic simulations across climate stages requires a brand-new framework to reduce computational cost. This chapter proposes an event-based regional approach to estimate discharge quantiles at all river sections of a given region (i.e., Shikoku Island in this chapter). The distributed rainfall-runoff-Inundation (RRI) model and a large climate projection ensemble are used for flood simulations. Peak discharges based on regional annual maximum 48 h rainfall events (AM48) are obtained for Flood Frequency Analysis (FFA). Meanwhile, the peak discharges based on basin AM48 are prepared for obtaining reference results. The Peak-Over-Threshold (POT) and Block Maxima (BM) methods are used as alternative FFA approaches, which can exclude abnormal high-frequency discharges by elevating thresholds. The POT-based FFA showed good and stable accuracy when using peak discharges in the range of the top 10% to 50%. The BM method, employing block sizes of 2 to 5 years, can generate relatively accurate frequency curves, but the choice of block size introduces significant variations in results among certain basins. Generally, the accuracy of results based on the POT method surpasses that of the BM method. Considering the accuracy, computational cost, and result stability, the POT method is preferred. The error introduced by the regional approach was acceptable with more than half of the relative root mean square errors remaining within 10% and basically all of the results are within 20%. The results of the regional approach exhibited good accuracy across climate stages and provided consistent information regarding future flood quantiles. This study serves as the foundation for high-resolution future flood risk assessment.

[1] This chapter is based on the publication:

Chen, J., Sayama, T., Yamada, M., & Sugawara, Y. (2024). Regional event-based flood quantile estimation method for large climate projection ensembles. ***Progress in Earth and Planetary Science***, 11(1), 16

2.1 Introduction

Floods, whose risk are influenced by climate change have substantial economic and social ramifications (Hirabayashi et al. 2013; Winsemius et al. 2018; Tellman et al. 2021). Flood intensity and frequency have been reported to increase due to climate change (IPCC, 2021). These changes necessitate proactive risk-management strategies for human settlements, urban planning, and socioeconomic development.

Typical flood hazard assessments rely on extensive data collection, detailed hydraulic engineering surveys, and hydrological and hydrodynamic modeling (Martínez et al., 2018; Zeng et al., 2022). Such approaches (e.g. Institute of Hydrology, 1999) often adopt statistical methods, such as intensity-duration-frequency or depth–area–duration methods, to design rainfall intensity for a specified return period (Gellens, 2002; Sun et al., 2019b) and rainfall pattern (Yan et al., 2020). However, because of the variability in precipitation, the impact to different river sections of an event is different. While statistical method selecting events by specifying an outlet first, which means the simulation result cannot be used for investigating other river sections in the same basin (e.g., precipitation events that cause a 100-year flood in a particular basin may not necessarily result in floods with the same return period in its sub-basins). Moreover, preparing designed rainfall and conducting hydrologic simulations for all river sections, including sub-basins, over a large region is impractical (Packman and Kidd, 1980; Watt and Marsalek, 2013). Another issue is that the return period of rainfall and floods have no unified correspondence; thus, results obtained from the design storm may not represent the actual river flood intensities for the return periods (Breinl et al., 2021).

To achieve reliable national- or global-scale flood risk assessment, several approaches have been proposed, including analysis-based and cascade modeling approaches (Dottori et al., 2016; Hoch and Trigg, 2019). The analysis-based modeling approach utilizes regional Flood Frequency Analysis (FFA) with observed discharge datasets to estimate peak discharge and employs cluster algorithms to extend the results to ungauged basins based on catchment descriptors (Sampson et al. 2015; Smith et al. 2015; Wing et al. 2017, 2020). The cascade modeling approach, exemplified by the utilizations of GloFAS (Dottori et al., 2016), GLOFRIS (Winsemius et al., 2013), and ECMWF (Pappenberger et al., 2012) typically employ a land surface model with a river routing model such as CaMa-Flood (Yamazaki et al., 2013) or LISFLOOD (Bates et al.,

2010) to compute flood peaks over large domains based on long-term simulations. The simulated flood peak discharges at each river section can then be statistically analyzed to compute those with certain frequencies. The estimated discharges are used as inputs to high-resolution hydrodynamic models. For example, Alfieri et al. (2014) employed LISFLOOD to generate a continuous 21-year daily discharge sequence for the pan-European region at a resolution of 5 km, and mapped flood hazards at a resolution of 100 m. However, these approaches have difficulties in handling large climate projection ensembles. The analysis-based modeling approach relies on an observed discharge dataset, which is unavailable for future scenarios. Thus, the cascade modeling approach is more applicable for climate change impact assessment. Nevertheless, even with low-resolution cascade simulations, the computational requirements are significant because of the numerous climate projection ensembles spanning several decades. Moreover, errors and uncertainties are associated with discharge results from simulations at low resolutions (Meade et al. 1991; Alfieri et al. 2014; Zhao et al. 2017). Sampson et al. (2015) suggested that its applicability in regions with low-quality topographic data is yet to be demonstrated and quantified. Therefore, considering new approaches for large-scale flood simulations under climate change and obtaining accurate peak discharges at specific return periods for local flood hazard mapping is necessary.

In this study, we propose an event-based approach to obtain the peak discharge in all river sections. To distinguish this approach from the conventional event-based approach (called the basin approach in this study), which focuses only on a single-basin outlet, the new approach is hereafter referred to as the regional approach. The regional approach aims to reduce the computational burden with relatively low errors for large climate projection ensembles.

Event-based simulations, including the regional approach, confront the challenge of precipitation variability. Some events lead to high discharge in specific river sections and low discharge in others. These cases ultimately result in severe errors in the FFA. To reduce these impacts and obtain accurate peak discharges for each river section at specific return periods, we further exam screening methods using Block Maxima (BM) and Peak Over Threshold (POT). The problems addressed in this study are as follows:

1. Which method–BM or POT–is more suitable for frequency analysis based on the result using regional approach? How should its corresponding parameters be

selected?

2. How much error will be introduced by the regional approach?

3. Will the approach be valid under future climate conditions?

Based on the challenges faced when studying floods under climate change, this study provides a novel approach for large-scale and high-resolution flood simulations. Additionally, the cases selected in this study shed light on the potential magnitude of errors and uncertainties introduced by the regional approach, which can inform efforts for further improvement.

2.2. Methods

2.2.1 Regional approach

Figure 2-1 compares the key steps of the conventional basin approach and the proposed regional approach. Both approaches extract extreme rainfall events. While the basin approach extracts events based on basin average precipitation, the regional approach extracts them based on an entire region, in this case Shikoku Island, which contains multiple river basins. The former approach has been adopted in Japan for estimating annual maximum peak discharges corresponding to different return periods (i.e., flood quantiles) by simulating flood discharges with a rainfall-runoff model. In case we use a distributed rainfall-runoff model, we can simulate discharges even at tributaries within the basin. However, the estimated discharges do not necessary represent the quantiles at each river section, except for the outlet of the basin, because of the spatial variability of precipitation of the extracted events. In order to obtain a flood quantile map, which is our objective here, we have to apply the basin approach for each river sections even within a river basin. Obviously, that requires enormous computation, which is not practically possible. As an alternative approach, we introduce the regional approach. The method extracts large number of rainfall events from a climate projection ensemble based on the amount of rainfall over a region. Then we estimate flood peak discharges using a distributed rainfall-runoff model. Here we hypothesize that discharges with longer return periods at different river sections have high probability to be affected by a series of extreme precipitation events. That means if we extract sufficient number of events and adequately screen the peak discharge data based on POT or BM, we can estimate the flood quantiles at all river sections. To evaluate the accuracy, we can compare the one

estimated by the basin approach (at the outlet) and the regional approach. Given the ample data provided by climate projection ensembles spanning centuries, the criterion for extreme events in this study was the annual maximum 48 h precipitation (48h-AMS). Subsequently, a distributed high-resolution hydrologic model, the Rainfall-Runoff-Inundation (RRI) model, was employed to simulate the discharges for each river section. Because of the variability in precipitation, event-based simulation results may contain low discharges, which necessitate the adoption of the POT and BM methods as potential solutions for estimating the frequency curves. The flood quantiles were obtained by further screening the discharge and conducting FFA.

In this study, discharges from the basin outlets derived via the basin approach were considered as references. The criterion for extreme events in the basin approach remains the 48h-AMS, and computed for each basin within the study area. A comparison was made between the results obtained from the basin and regional approaches.

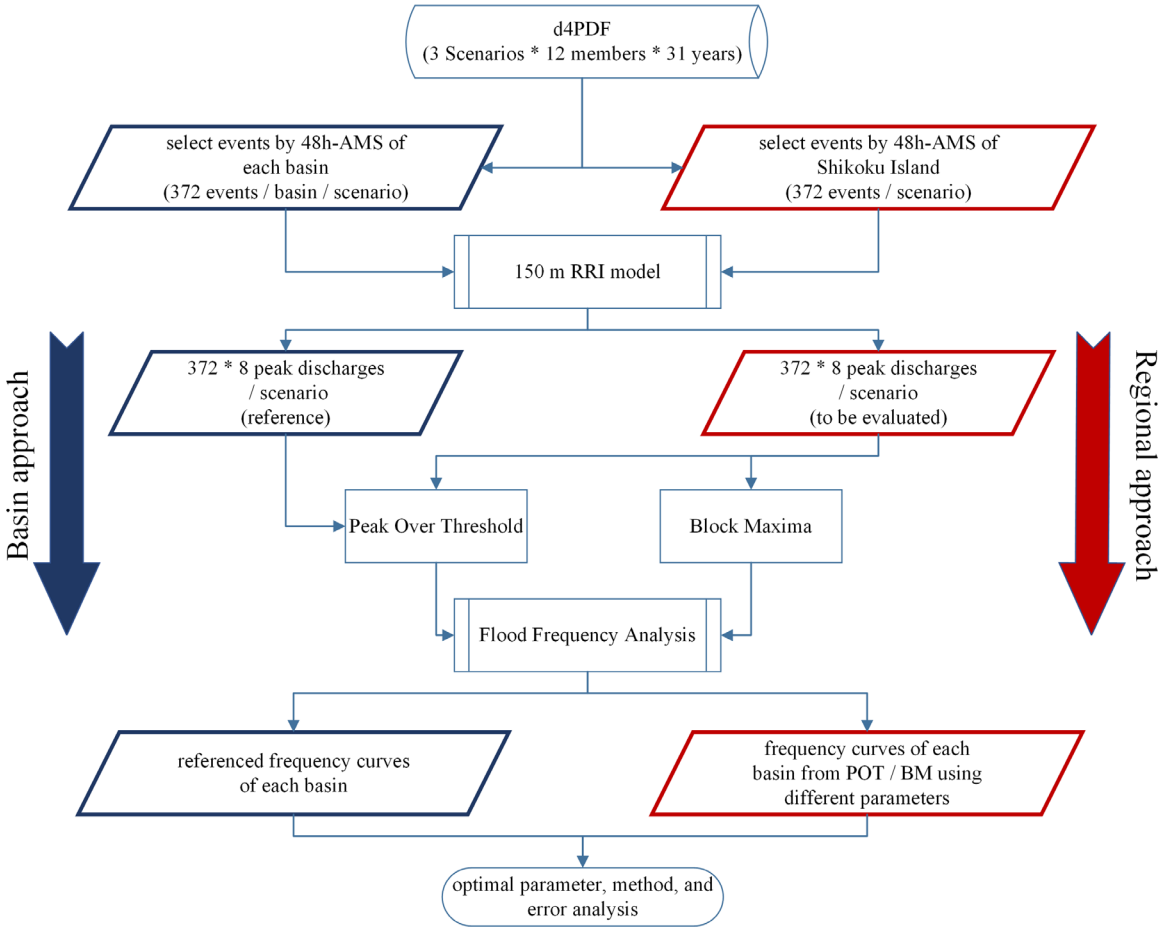


Figure 2-1 Flow chart of the basin and regional approaches for this chapter

A numerical experiment was conducted on Shikoku Island (applying the regional

approach) and its eight major river basins (applying the basin approach as a reference). In particular, we evaluated the performance of the regional approach with different screening parameters. For the POT method, the screening parameter is a threshold above which they will be included in the frequency analysis. For the BM method, the screening parameter is an interval at which the maximum value is determined, referred to as block size (Zou et al., 2021). In addition, we verified the performance of the regional approach in the 2 K and 4 K scenarios (the Sea Surface Temperature (SST) rises 2 K and 4 K, respectively) by comparing the flood quantiles with those from the basin approach. The effects of the frequency analysis method and sources of error are discussed later in this paper.

2.2.2 Rainfall-Runoff-Inundation model

This study used the RRI model, a two-dimensional distributed hydrodynamic model, to simulate the physical processes involved in the transition from precipitation to runoff (Sayama et al. 2012). It discretizes the study area and divides it into land and river channel grids using two-dimensional and one-dimensional diffusion wave equations to describe water movement, respectively. River channel grids contain information of levees, allowing the RRI model to simulate runoff overflows and returns in the river grids. In terms of runoff components, the RRI model considers surface and lateral subsurface flows, which are important in mountainous areas (Sayama and McDonnell 2009). The Green-Ampt model (Green and Ampt, 1911) was used to model infiltration. The fifth-order Runge-Kutta formula (Cash and Karp, 1990) was used as the numerical scheme to ensure efficiency and accuracy. The RRI model performs well in Japan and Southeast Asian countries (Sayama et al. 2015, 2017, 2020; Bhagabati and Kawasaki 2017; Yamamoto et.al 2021; Try et al. 2022). Due to the good performance, Rasmy et al. (2019) further developed a Water and Energy Budget-based RRI (WEB-RRI) model in Sri Lanka for local water resources and disaster management under a changing climate. Even though the WEB-RRI model is advantageous in terms of estimating long-term water and energy budget, which is essential for the applications of the model to water resources management, the original RRI model is thought to be suitable for the present study because of the physically sound and simple representations of the subsurface and surface runoff processes, essential for event-based storm runoff predictions even in ungauged basins. In a previous study, the RRI model had been well calibrated across Japan, and these model parameters were followed in this study (Yamada et al., 2022; Yamakita, 2023).

The peaks of the RRI model results based on the 48h-AMS extracted for each basin are called the basin Annual Maximum Flood Series (AMFS), which was used as the reference for this study and has a total of 372 (discharge peaks) × 8 (basins) × 3 (scenarios) values. The simulation results using 48h-AMS which were extracted for Shikoku Island and then extracted at the outlet of each basin, are called the regional AMFS, which also has 372 × 8 × 3 values.

2.2.3 Frequency analysis method

Depending on the sample selection method, frequency analysis can be classified into the BM and POT methods (Mostofi Zadeh et al., 2019). The BM method divides a time series into equal-sized blocks and extracts the maximum value for each block. The most typical application of the BM method in hydrology is the annual maximum method. The L-moment method is used to estimate parameters of each distribution (Hosking and Wallis, 1993). For the BM method, the optimal distribution is ultimately determined to be the Pearson Type III (PE3), as given by Eq. 2-1, among those tested distributions including Generalized Logistic (GLO), Generalized Extreme Value (GEV), Generalized Normal (GNO), Generalized Pareto Distribution (GPD) and PE3. The results of the goodness-of-fit statistic Z, used for selecting the optimal distribution, are detailed in Tables S1 to S3. However, according to the definition of block maxima, only one value can be selected within a block. That means, in years with abundant precipitation, multiple flood events may occur, but the second-largest discharge cannot be chosen as an “extreme value”, even if it surpasses the maximum in a drought year. While in a drought year, no matter how low the discharge was, it will be selected as an “extreme value”. Due to the abovementioned limitation, the BM method is possible to miss high values and select low values, causing inaccurate frequency analysis results (Ferreira and de Haan, 2015). The POT method selects all data above a certain threshold. The newly created sequence theoretically follows the GPD (Eq. 2-2) (Lang et al., 1999).

$$\boldsymbol{PE3}(\boldsymbol{x}) = \frac{\sigma^{\xi}}{\Gamma(\xi)}(x-\mu)^{\xi-1} exp\,(-\sigma(x-\mu)) \tag{2-1}$$

$$\boldsymbol{GPD}(\boldsymbol{x}) = \begin{cases} 1-(1+\xi\left(\frac{x-\mu}{\sigma}\right))^{-1/\xi} & for\ \xi \neq 0 \\ 1-exp\left(-\frac{x-\mu}{\sigma}\right) & for\ \xi = 0 \end{cases} \tag{2-2}$$

where ξ, μ, and σ are the shape, location, and scale parameter, respectively.

The distribution for reference results refers to Figure S1. All three parameters are estimated by L-moment method. The block size and threshold are the key parameters that must be artificially determined for the BM and POT, respectively. Although many studies have been conducted on the choice of a reasonable threshold for a POT, the aim is to find a low threshold for using as much data as possible (Langousis et al., 2016; Mostofi Zadeh et al., 2019; Swetapadma and Ojha, 2021). In this study, because of the numerous climate projection ensembles, we attempted to use high thresholds to balance efficiency and accuracy. Due to the spatial variability of precipitation, some of the regional 48h-AMS may result in low discharges in specific sub-basins. Therefore, using a high threshold is advantageous for filtering low discharges. Furthermore, because the POT method allows for more precise threshold control, it was chosen as the frequency analysis method for the basin AMFS. As the design floods of most infrastructures focus on a return period longer than 10 years, the maximum threshold for the POT was set to the top 10% of the AMFS in descending order. Correspondingly, the maximum block size of the BM was set to 10 years. A series of possible parameters, categorized as Model 1 to 6, are listed in Table 2-1. The extracted AMFS were nonstandard annual series, the probability P corresponding to the standard return period T must be calculated using Eq. 2-3, where the *npy* refers to the number of discharge peaks per year.

Table 2-1 Parameters of the POT and BM data selection methods

Models	1	2	3	4	5	6
POT (threshold)	10%	20%	30%	40%	50%	100%
BM (block size)	10 Years	5 Years	4 Years	3 Years	2 Years	1 Years

$$P = 1 - \frac{1}{T \times npy} \tag{3}$$

The FFA results were evaluated using the relative bias (BIAS; Eq. 2-4) and Relative Root Mean Square Error (RRMSE; Eq. 2-5).

$$BIAS = \frac{y_e - y_r}{y_r} \times 100\% \tag{4}$$

$$RRMSE = \frac{\sqrt{\frac{1}{n}\sum(y_{e*} - y_{r*})^2}}{\frac{1}{n}\sum y_{r*}} \tag{5}$$

where y_e and y_r are the quantiles corresponding to different return periods between 10 to 1000 years every one-year. They are estimated based on the fitted curves to the simulated peak discharges by the regional and the basin approaches, respectively. The *BIAS* indicates how the regional approach is biased compared to the basin one. On the other hand, *RRMSE* compares the simulated peak discharges by the basin approach (y_{r*}) and the fitted curve by the regional approach denoted as y_{e*}, which are corresponding to discrete return periods. Hence unlike the *BIAS* index, the *RRMSE* indicates the degree of errors more directly by the regional approach compared to the reference one without uncertainty associated to the curve fitting to the y_{r*}. The model results can be regarded as excellent if RRMSE ≤ 10%, good if 10% < RRMSE ≤ 20%, fair if 20% < RRMSE ≤ 30%, and poor if RRMSE > 30% (dos Santos et al., 2016).

2.3 Study Area and Data

2.3.1 Study area

The study area of Shikoku Island, Japan, is located between 132–135°E and 32.5–34.55°N (Figure 2-2). It is a relatively independent area separated from Honshu Island by the Seto Inland Sea to the north and surrounded by the Pacific Ocean on its three other sides. The area of Shikoku Island is 18,785 km^2, 70% of which is covered by forests. Similar to other regions of Japan, it is mountainous and steep, with the highest peak on the island (with a summit of 2,000 m) descending to sea level within 50 km.

Table 2-2 Morphological parameters of the eight major river basins of Shikoku Island

Basin	**Area (km^2)**	**Length (km)**	**Elevation of river source (m)**
Yoshino	3750	194	1897
Watari	2186	196	1336
Niyodo	1560	124	1982
Hiji	1210	103	460
Naka	874	125	1929
Monobe	508	71	1770
Shigenobu	445	36	1233
Doki	140	33	1059

Shikoku Island has an average annual temperature of nearly 14 °C, making it a major producer of early rice crops in Japan (Yoshida et al., 2012). The spatial distribution of

average annual precipitation varies considerably due to frontal storms and typhoons (Kamahori and Arakawa 2018; Tada et al. 2018; Otaki et al. 2022), from about 1,200 mm in the north to 2,500 mm in the south and 4,000 mm in the mountains (Yao and Creed, 2005)

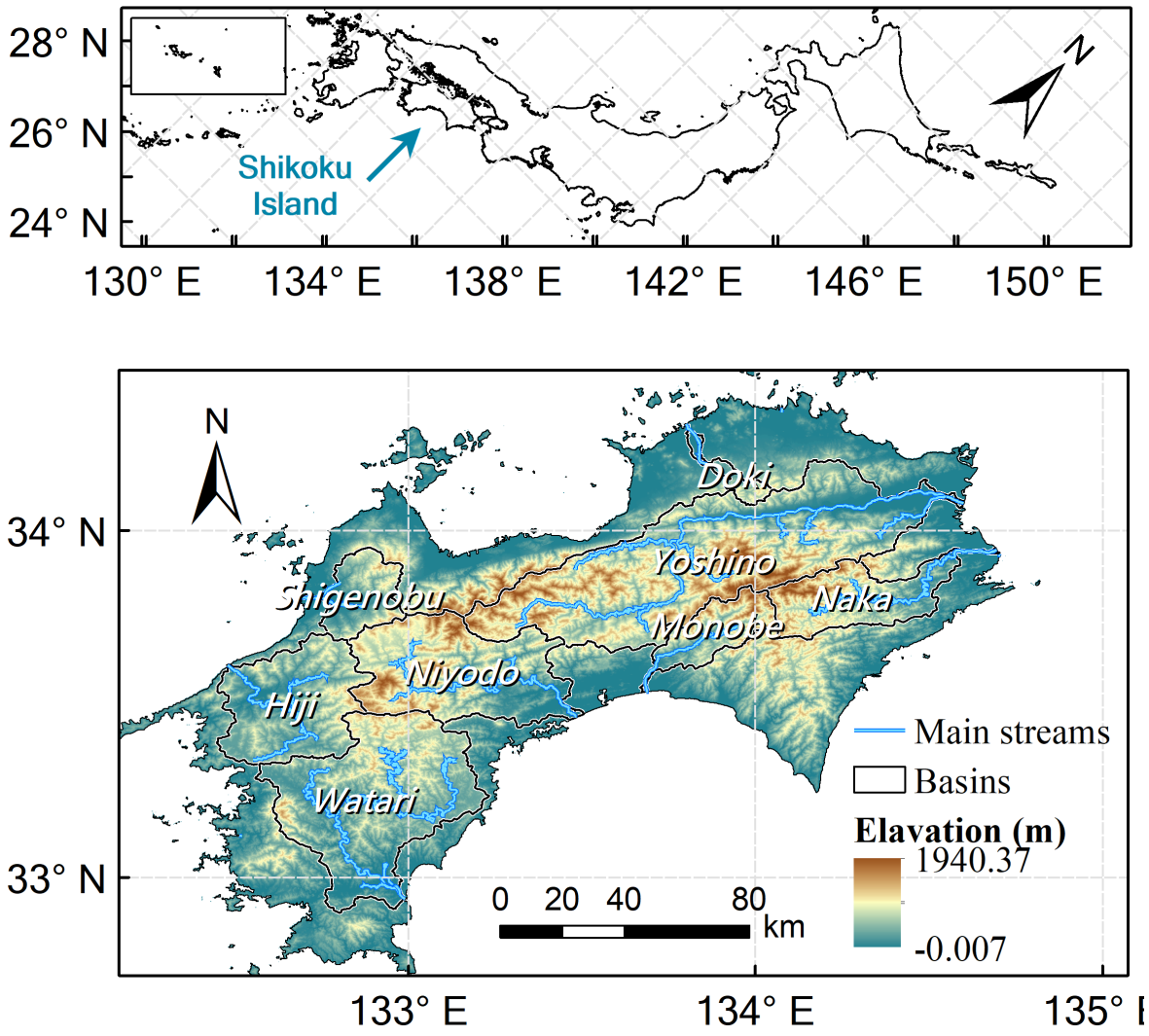


Figure 2-2 Overview of Shikoku Island

The main reasons for selecting Shikoku Island as the study area were its relatively independent geographical conditions, significant differences in precipitation, and flood-prone terrain. The morphological parameters of its eight major river basins are listed in Table 2-2.

2.3.2 Data

The database for Policy Decision-making for Future climate change (d4PDF) is an

open-access dataset used to study climate change impacts and plan adaptation (Mizuta et al., 2017). The dataset was dynamically downscaled from the 60 km Meteorological Research Institute Atmospheric General Circulation Model 3.2 (MRI-AGCM 3.2), using a 20 km Non-Hydrostatic Regional Climate Model (NHRCM) (Sasaki et al., 2011). External forcing was derived from MRI-AGCM 3.2 and the boundary conditions were derived from MRI-CM (Deushi and Shibata, 2011) and MRI-CGCM3 (Yukimoto et al., 2012). The differences between simulations in the same scenario were mainly caused by the difference in SST between current and future climate (ΔSST) and perturbations (δSST). The spatiotemporal distributions of ΔSST was provided by six CMIP5 (Coupled Model Intercomparison Project phase 5) models (Mizuta et al., 2017). Owing to the large number of ensembles that facilitate uncertainty reduction and good extreme event reproducibility (Tanaka et al. 2018; Ishii and Mori 2020), d4PDF has been widely used to study extreme precipitation, snowfall, drought, and water resource assessment (Kawase et al. 2016, 2020; Ohba and Sugimoto 2019; Hatsuzuka et al. 2020; Miyasaka et al. 2020; Ohba et al. 2022).

The data used in this study were further downscaled using the 5 km NHRCM. This dataset is called dynamical downscaling data for near-future atmospheric projection (from Tohoku to Kyushu) by the Social Implementation program on Climate change Adaptation Technology (SI-CAT DDS5TK), which is funded by the Ministry of Education, Culture, Sports, Science and Technology, and covers the Tohoku to Kyushu regions of Japan. This included three scenarios (current, 2 K ΔSST, and 4 K ΔSST) with 31 years × 12 members (2 × 6 SST patterns) (Mizuta et al. 2017; Fujita et al. 2019). More specific parameter settings can be found in Sasai et al. (2019). These 12 members were used as a complete dataset.

2.4 Results

2.4.1 Evaluation of the current scenario

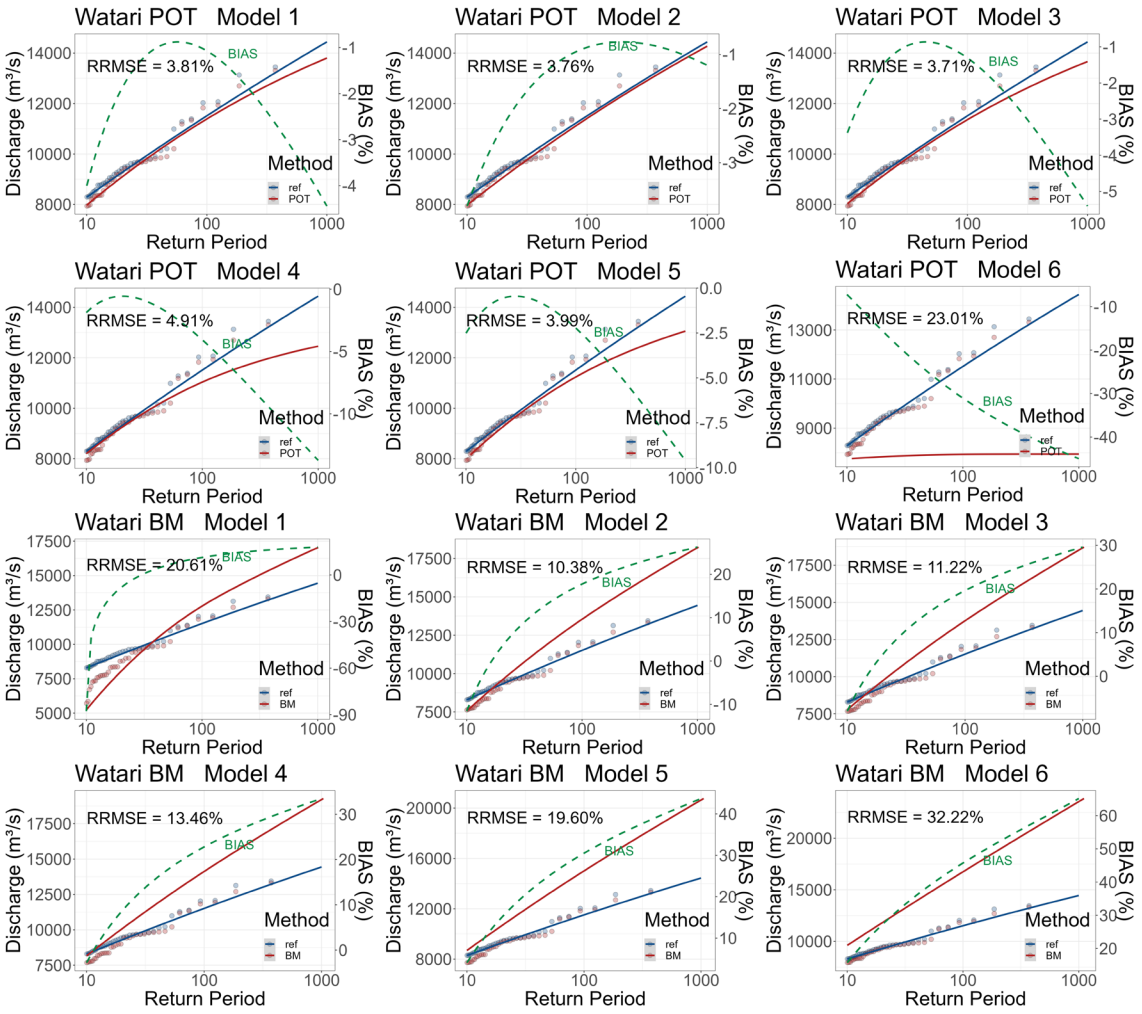


Figure 2-3 Accuracy comparison of applying the POT and BM methods using different parameters for Watari basin.

Model 1–6 indicate the precipitation data come from current scenario and the parameter corresponds to the value of Model 1–6 in Table 2-1. Blue points and lines represent the basin AMFS and frequency curve, respectively. Red points and lines indicate the regional AMFS and frequency curve, respectively. Green dashed lines show the BIAS between the basin and regional results

A primary objective of this study was to determine the optimal combination of frequency analysis methods for integration into the regional approach. Figure 2-3, using the Watari river basin as an example, illustrates the frequency curves fitted by the POT and BM methods using the six parameters from Table 2-1. It is crucial to note that different parameters can result in varying data samples, causing the x-axis's starting position to be less than 10 years. However, since this study primarily focuses

on fitting beyond a 10-year return period, the calculation of RRMSE and the display of fitting results only use results exceeding 10-year return period. The RRMSE in Figure 2-3 calculates the error between the predictions of the regional approach and the basin AMFS, and used for assessing the accuracy of the regional approach-based frequency curve. According to the RRMSE, models 1 to 5 using the POT method in the Watari Basin (i.e., employing the top 10% to 50% of basin AMFS as the threshold) yield stable and satisfactory results.

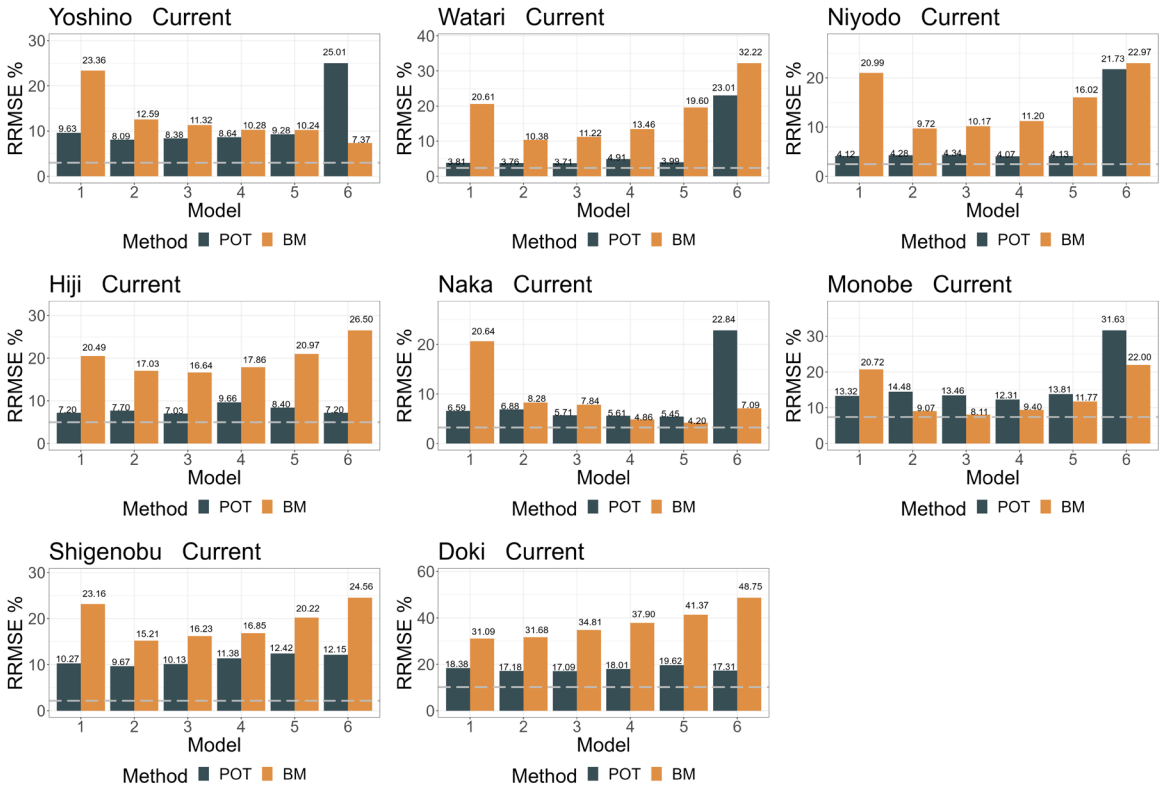


Figure 2-4 RRMSEs of the eight basins using different methods and parameters under the current scenario. The grey dash line represents the RRMSE between the predictions of the basin approach and the basin AMFS

To obtain robust conclusions, we examined the results for eight major basins across Shikoku Island, and their RRMSE are summarized in Figure 2-4. The blue histograms represent RRMSE based on the POT method, the orange histograms represent RRMSE based on the BM method, and the grey line reflects the error of the fitted curve under reference conditions (i.e., the RRMSE from basin approach). The reference RRMSEs demonstrate excellent goodness of fit of the basin approach, which indicates the capacity of being reference, with values consistently below 10%, meeting the criteria for excellence. Overall, the POT method appears to offer higher accuracy. Specifically, models 1 to 5, corresponding to the use of the top 10% to 50% of regional AMFS,

demonstrate high accuracy across basins. Their results show no significant difference in magnitude from the reference RRMSE (i.e., the grey line). Model 6, which utilizes 100% of the regional AMFS, tends to yield inferior results. As analyzed in the issue of the limitations of event-based simulations, the simulation results of event set in some river sections may include extremely low discharges, which is caused by precipitation variability, and thereby influence the fitting of the frequency curve. This further underscores the necessity of employing high thresholds to prevent these "non-extreme" data from frequency analysis.

For the BM method, models 1 and 6 (corresponding to block sizes of 10 years and 1 year, respectively) typically exhibit the poorest performance. The results of models 2 to 5 vary by basin, making it challenging to determine the optimal block size or provide a recommended range. This variability is attributed to the inability of the BM sampling method to effectively exclude "non-extreme" discharges. Additionally, the order of occurrence of peak discharges influences the sampling results, introducing considerable uncertainty. Therefore, considering the accuracy and the robust of threshold, the POT method is recommended.

Figure 2-5 shows the POT-based frequency curves for the current scenario with threshold of 10%. According to the RRMSE values, all the regional results have a good fit. The distribution of data points in Figure 2-5 shows that most of the regional AMFS and basin AMFS overlap or have small differences, especially for extreme discharges with long return periods, which confirms our hypothesis that most of the peak discharges in different river sections originate from different events, but ultimately from an extreme event group.

The Monobe River Basin presents a unique case, showing a poor overlap of discharge with long return periods and a large error in the maximum value. By manual checking, we found that the maximum values of the basin AMFS and regional AMFS originated from two different precipitation events. This suggests that the maximum value of the basin AMFS originated from a local extreme precipitation event. Due to the spatial variability of precipitation, it was missed in the search for extreme precipitation across the entire region. The maximum value of the regional AMFS corresponded to the second-largest value of the basin AMFS. Similar mismatches were observed in the subsequent AMFS in the Monobe River Basin. Theoretically, the longer the return period of discharges, the greater the FFA model error caused by the mismatch. This indicates that the regional approach can be further improved by determining new

extraction approaches that can identify these crucial local extreme precipitation events or alternative frequency analysis methods that can reduce the sensitivity to ranking.

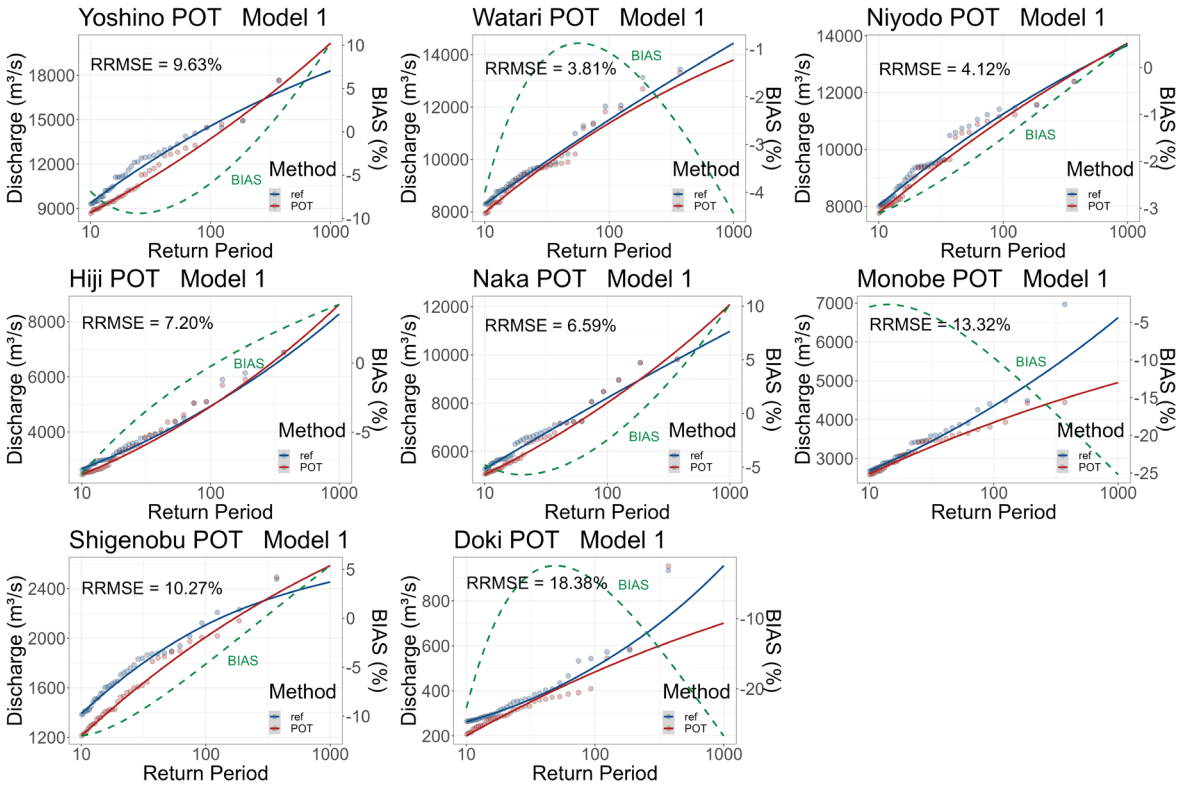


Figure 2-5 Estimation results of discharge quantiles for different basins using the POT methods with the top 10% AMFS. The meaning of elements in the figure can refer to Figure 2-3

A relatively high BIAS was observed in the Doki river basin, which has the smallest area among the eight basins, consequently having low discharge in most years. However, because of their topography and morphology, they are more sensitive to precipitation, which leads to an extremely high discharge from the largest precipitation event, and therefore, the frequency curve fails to fit discharge with return period longer than 100 years.

Overall, the BIAS varied between ±10% for different return periods and the interval of BIAS variation was limited to 0 to -5% in some basins. The regional approach mitigates but does not entirely eliminate the influence of precipitation variability.

2.4.2 Evaluation on future scenarios

In the 2 K and 4 K warming scenarios, the POT method with the top 10% AMFS yielded

good outcomes. The RRMSEs of each basin when employing the top 10% AMFS are summarized in Table 2-3. In the current scenario, five basins were rated as excellent, whereas three basins received good ratings, consistent with the results presented in Figure 2-5. In the 2 K warming scenario, four basins were rated excellent, two good, and two fair. In the 4 K warming scenario, five basins achieved excellent ratings, and three received good ratings. Notably, none of the basins were rated as poor in any of the three scenarios. Hence, we concluded that the constructed quantile estimation model performs well and is stable across the three scenarios.

Table 2-3 Performance of regional results in different scenarios

Scenarios	Excellent (RRMSE ≤ 10%)	Good (10< RRMSE ≤ 20%)	Fair (20% < RRMSE ≤30%)	Poor (RRMSE > 30%)
Current	5	3	0	0
2 K	4	2	2	0
4 K	5	3	0	0

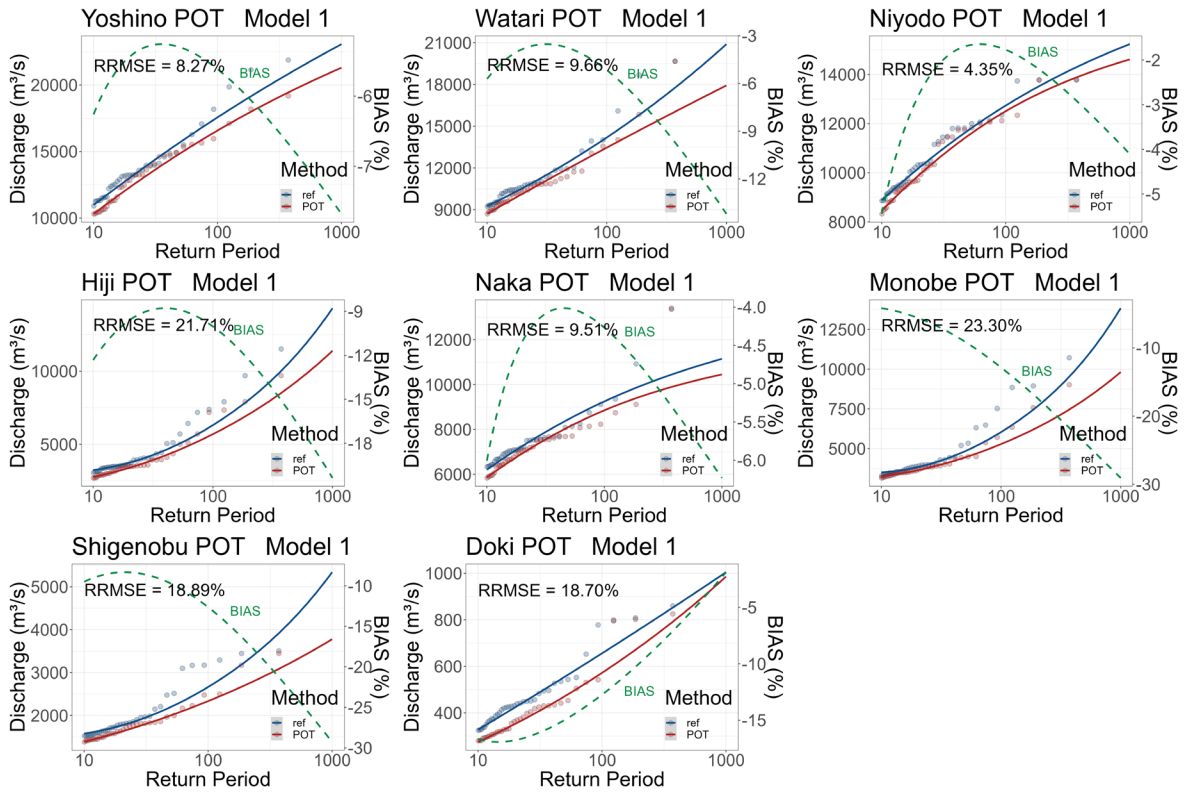


Figure 2-6 Estimation results of discharge quantiles for different basins using the POT methods with the top 10% AMFS for the 2 K warming scenario

Figure 2-6 shows the estimation results of the discharge quantiles for each basin with the POT method and 10% AMFS in the 2 K warming scenario. In this scenario, we

observed a general underestimation in discharges from regional approach. Manual checking revealed that these discharges originated from the same precipitation event, with peak times differing by several hours. This situation arose mainly because the precipitation only extracted for 48 h, whereas some extreme events lasted longer than 48 h and exhibited variations in peak times among the different basins. Consequently, in some basins, precipitation input ceased before the true peak was reached. Climate change affects the characteristics and durations of extreme precipitation events. Therefore, in the future, event extraction schemes that do not depend on fixed durations must be considered. Overall, BIAS varied between ±20% and within ±10% in some basins.

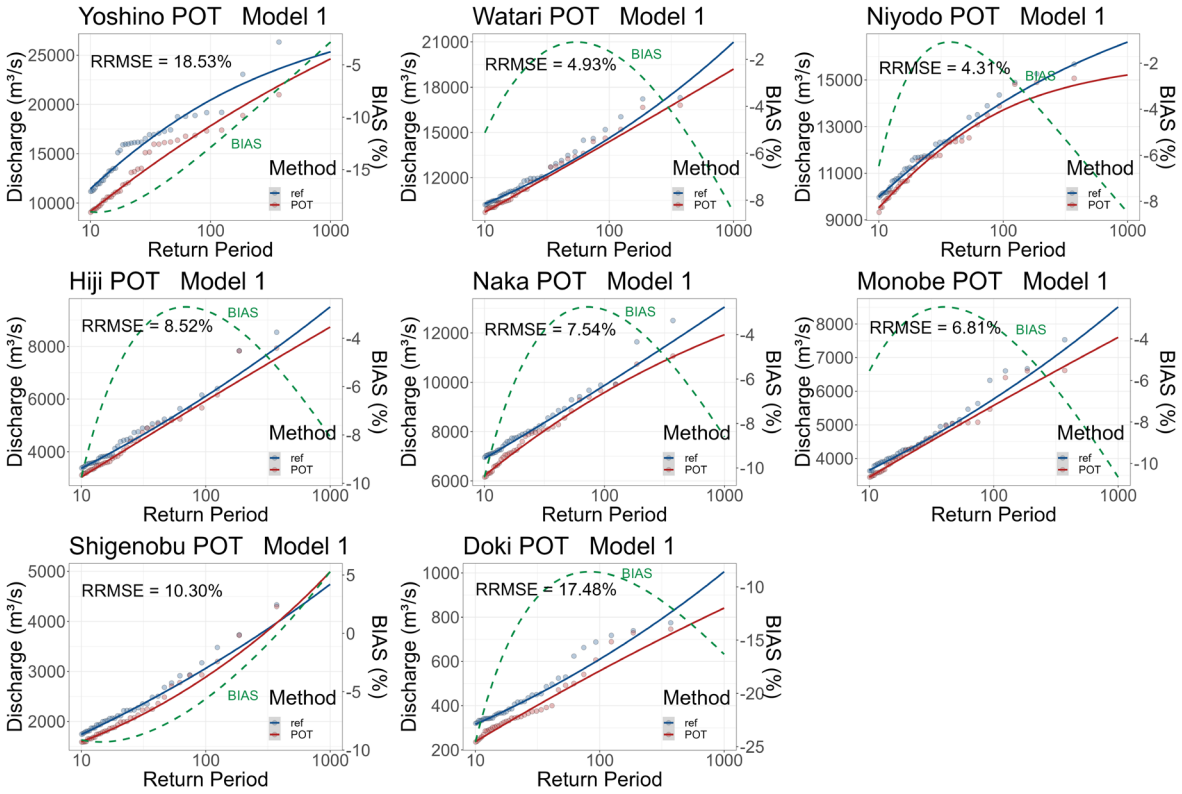


Figure 2-7 Estimation results of discharge quantiles for different basins using the POT methods with the top 10% AMFS for the 4 K warming scenario

Figure 2-7 shows the estimation results of the discharge quantiles for each basin using the POT method and 10% AMFS under the 4 K warming scenario. In this scenario, large RRMSE values were observed in the Yoshino and Doki basins. From the perspective of precipitation events, the maximum 48 h-AMS in the Yoshino basin, whether extracted by the basin approach or the regional approach, is associated with the same precipitation event. However, due to the actual precipitation process exceeding 48 h and the event selection method being set with a 48-hour time window, the start times

of the basin 48 h-AMS and the regional 48 h-AMS differ by 4 h. During this time, the precipitation center shifts from the Yoshino basin to another basin, resulting in a significant reduction in the discharge calculated by the regional method, ranking it 30th instead of the first. This further underscores the need to develop an event extraction method with non-fixed durations in future studies. In the Doki Basin, the frequency curves fit well with the corresponding points, indicating that the GPD distribution is capable to fit the extreme discharges. While due to the limitation on precipitation extraction method, there is a significant difference between the regional AMFS and basin AMFS, leading to large error.

Overall, increasing the threshold for the FFA can effectively improve the accuracy of the results by excluding low discharges. 10% to 50% of the AMFS were found to be reasonable threshold. Considering the accuracy and result stability, the POT method is the preferred frequency analysis method. The spatiotemporal variability of precipitation remains the primary source of error, and its impact may become more pronounced with climate change. However, this impact is expected to be mitigated in the future by improving precipitation event extraction methods. In summary, the regional approach yielded relatively accurate flood quantiles for each basin at a relatively low computational cost.

2.5 Discussion

This study proposes a regional approach to estimate the flood quantiles of all river sections from finite extreme precipitation events. This approach is expected to be valid under diverse climatic conditions. In the regional approach framework, a crucial step is aimed at further screening discharges, offering two alternatives: POT and BM. “Which option, accompanied by what parameters, proves optimal? What is the magnitude of the error and how does it perform in future scenarios?” These three fundamental questions have become the focal points of this study.

The initial purpose of the POT method was to avoid missing high discharges during rainy years, which likely occurs when employing the BM method. To perform a more reliable FFA, the POT method typically sets a relatively low threshold to maximize the data utilization. This study sets a high threshold mainly based on two considerations. Firstly, it aims to eliminate the influence of low values at short return periods, ensuring a robust fit for extreme values at long return periods. Secondly, the availability of multi-year data from climate ensembles, such as the 372 years of

precipitation data provided by SI-CAT DDS5TK in this study, allows for the construction of reliable FFA even when employing a higher threshold. Hence, a relatively high threshold value was established. Notably, the selection of the threshold constitutes a highly technical task within the POT method as it affects data independence, distribution assumptions, and sample size (Lang et al. 1999; Beguería 2005). Previous studies have predominantly focused on threshold selection (Langousis et al., 2016; Swetapadma and Ojha, 2021). Nevertheless, the demand arises from attempts to employ a low threshold instead of a high threshold. This is because the lower threshold limit (more than once per year) for satisfying the GPD is ambiguous, whereas it is tenable if the threshold is adequately high. Independence was guaranteed because the discharges were from different precipitation events, and a large ensemble ensured the data size.

The POT and BM methods have two primary distinctions: sampling technique and assumed distribution. The divergent outcomes of the sampling techniques are shown in Figure 2-8. After the screening process, the BM method still retained discharges close to zero in certain basins, such as Watari, Hiji, Shigenobu, and Doki. However, the POT method does not encounter this issue. Due to its inability to entirely eliminate periodic fluctuations that may exist in the data (e.g., missing several flood peaks in wet years and including low discharges in dry years as extremes), the BM method may not be suitable for filtering low discharges using the regional approach. This limitation introduces uncertainty into the results. Low discharges play a more significant role in estimating the distribution curve parameters because they constitute a substantial proportion of the extremes. Consequently, greater emphasis is placed on fitting short return periods, whereas the accuracy of long return period predictions, which hold greater importance for decision-makers, is disregarded. Theoretically, the GPD exhibits better adaptability to heavy-tailed distributions (Madsen et al., 1997). Cunnane (1973) demonstrated that POT performed better when the average annual occurrence was higher than 1.6, and a similar conclusion was derived in other studies (Madsen et al. 1997; Bezak et al. 2014). According to the results of this study, the POT method exhibits excellent robustness and accuracy, making it a superior choice for integration into the regional approach.

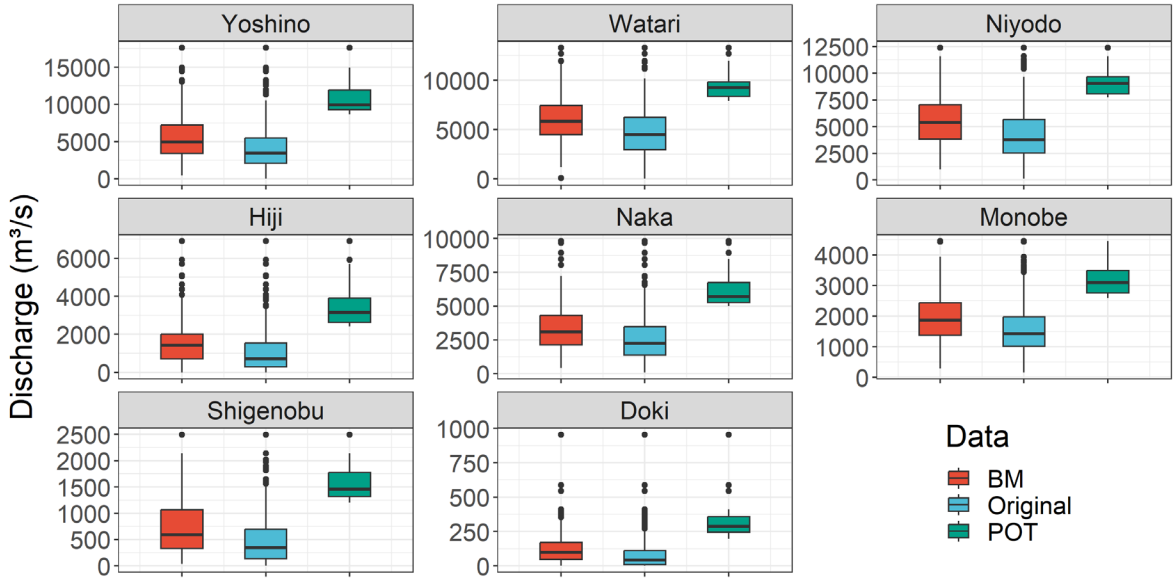


Figure 2-8 Distribution of processed (POT and BM) and original regional AMFS with optimal selection parameters in the current scenario

Errors in the quantile estimations can be classified into two types. The first type comes from the gap between the sample data and population distribution, which is unavoidable. This type of error can be considered as the goodness-of-fit of the results from the basin approach (Figure 2-3) when the basin approach is regarded as a reference. Generally, the first type of error accounted for over half of the total errors. The second type of error stems from the differences in discharge when employing a regional approach, which mainly caused by the precipitation variability.

The accuracy of the results provided two important insights. First, despite recent research indicating that storm temporal patterns under climate change will become more acute and have shorter durations (Wasko et al., 2021), the regional approach remains valid under future scenarios without a significant increase in error. This suggests that the regional approach is compatible with the potential changes in climatic conditions. Second, the error underscores the pivotal role of local extreme precipitation events in future flood risk assessments, emphasizing the importance of utilizing detailed climate projection ensembles. Recent studies on the dynamic downscaling of climate data have focused on convection-permitting models with higher resolution (Ishizaki, 2022) because convection is a potential mechanism of extreme precipitation that varies with climate warming (Pendergrass, 2020) and causes extremely severe precipitation (Qin et al., 2022).

To meet the emerging demand for handling high-resolution climate projection

ensembles in flood research, developing event-based regional approach is crucial. Future studies should prioritize the reduction of the second type of error. A potential direction could be developing event extraction methods that independent from statistical indicators, keeping natural evolution of precipitation and capturing local extreme precipitation.

2.6 Conclusions

To fully leverage large climate projection ensembles and provide discharges at specific return periods for large-scale flood hazard maps with limited computing resources, this study proposes an event-based high-resolution simulation and analysis scheme called the regional approach. Using Shikoku Island and its eight major basins as an example, the applicability of this approach was verified using a 150 m resolution RRI model, and the sources of error were analyzed. This study contributes to the development of big data processing techniques in hydrology. The conclusions are as follows:

(1) The top 10% to 50% of AMFS for the POT method are the reasonable combinations for the regional approach. The POT method is more recommended than BM method.
(2) Using the regional approach, the RRMSE of each basin was maintained within 20%. The main source of error was attributed to the fixed duration of 48 h being unable to fully cover the peak occurrence times of all basins. Moreover, using annual maximum 48 h rainfall as the extraction criterion may miss extreme precipitation events with short durations.
(3) The regional approach designed in this study showed good accuracy under current, 2 K warming, and 4 K warming scenarios and can provide future flood quantiles consistent with those obtained from the basin approach.

3. Development of the Aggregating Grid Event method[1]

Abstract

The generation of flood projection ensembles for large areas and at a high resolution has been a long-standing computational challenge. Previous studies focused on improving model efficiency and hardware acceleration. An intriguing question arises; is it possible to reduce the computational demand for obtaining specific flood characteristics (e.g., flood frequency curves, FFCs) through precipitation data preprocessing, while maintaining high accuracy? In this study, we developed an aggregating grid event (AGE) method based on hydrological concepts to extract essential precipitation events from large-ensemble climate-change dataset. A total of 2,966 events were extracted from dynamically downscaled 720-year precipitation data covering all over Japan with the 5-km spatial resolution. By inputting the precipitation data into the Rainfall–Runoff–Inundation model at a 150 m resolution, we computed hourly discharges across all river grids in the study area, Shikoku Island, Japan. Based on the simulated peak discharges, we computed FFCs for return periods exceeding 10 years at each river grid using the peak-over-threshold method. The results demonstrated the effectiveness of the AGE method, with a relative bias (BIAS) of -1.38% and a root mean square error (RMSE) of 36.45 m^3/s for flood peaks across locations. Furthermore, the BIAS of quantiles at 100-year return period was -1.04% compared to the references, which were estimated from all the valid 25,700 precipitation events. By using 2,966 events instead of 25,700 events, the AGE method significantly reduces the computational burden in estimating FFCs at all river grids while maintaining accuracy. This approach is applicable for any grid-based precipitation dataset, marking a crucial advancement in regional hyper-resolution flood studies based on climate projection ensembles.

---

[1] This chapter is based on the publication:

Chen, J., Sayama, T., Yamada, M., & Sugawara, Y. (2025) Reducing the computational cost of process-based flood frequency estimation by extracting precipitation events from a large-ensemble climate dataset ***Journal of Hydrology***. 655, 132946.

3.1 Introduction

Owing to climate change, rapid economic development, and population growth, global flood risk is increasing (Ceola et al., 2014; Liu et al., 2022; Winsemius et al., 2016). Comprehensive and detailed flood hazard maps that account for current and future climatic conditions are essential for effective flood prevention, emergency services, resilience enhancement, and informed intergovernmental cooperation and multinational investment. However, a significant gap exists between the demand for complex, large-scale, high-resolution modeling and the constraints of limited computational resources, emphasizing the growing need for innovative simulation approaches that balance accuracy and efficiency.

Previous efforts to develop global flood hazard maps were conducted within the context outlined above. Broadly, these approaches can be categorized into two primary types (Hoch and Trigg, 2019). The first type is the basin descriptor-based scheme which extracts relationships between basin descriptors and features of flood frequency curves (FFCs) derived from historical discharge data. These relationships are used to estimate flood peaks in ungauged basins, which are subsequently input into two-dimensional (2D) hydrodynamic models to create flood hazard maps. Smith et al. (2015) proposed a method based on hybrid clustering and a flood index to estimate the FFCs for major global basins. Building upon that work, Sampson et al. (2015) used intensity–duration–frequency curves to estimate the local extreme rainfall, improving FFC estimation for small basins, and generating flood hazard maps at a 90-m resolution for the region between 56° S and 60° N. According to Wing et al. (2017, 2020), that simulation approach can reach an average hit rate of 90 % on flood extent. The second type pertains to the cascade-modeling scheme, which begins by simulating discharge processes at a coarse resolution using macro-scale hydrological or land-surface models. FFCs for each river section are then derived from these simulations, with peak discharge values for specific return periods subsequently incorporated into high-resolution hydrodynamic models. The key to this scheme lies in efficient routing models, because even for low-resolution conditions, large-scale and long-duration simulations require significant computational resources. Previous studies utilizing cascade modeling to develop global flood warning systems, such as the global flood awareness system (GloFAS) (Dottori et al., 2016), GLObal Flood RISk (GLOFRIS) (Winsemius et al., 2013), and European Centre for Medium-Range Weather Forecasts (ECMWF) (Pappenberger et al., 2012), primarily employ CAtchment-based

MAcro-scale FLOODplain (CaMa-Flood) (Yamazaki et al., 2013) or LISFLOOD-FP (Bates et al., 2010) as their routing models. Hirabayashi et al. (2013) used CaMa-Flood to simulate and analyze global future flood risks at a spatial resolution of 15' (approximately 28 km). Similarly, Alfieri et al. (2014) utilized LISFLOOD-FP at a resolution of 5 km to simulate the daily river discharges for the pan-European region for 1990–2010, ultimately generating flood hazard maps at a resolution of 100 m. The development of global flood models has significantly broadened the scope of flood research, providing detailed flood hazard information at the continental and global scales.

Macro-scale schemes, however, are inadequate for national-scale simulations, which demand more detailed and precise results. Both basin descriptor-based and cascade-modeling schemes exhibit limitations when applied to the assessment of national flood risks. A notable commonality between these methods is that large-scale simulations often involve tradeoffs, sacrificing accuracy and introducing uncertainties to improve computational efficiency (Alfieri et al., 2014; Meade et al., 1991; Sampson et al., 2015; Zhao et al., 2017). The tradeoff between modeling efficiency and accuracy may be acceptable for studies relying on observed data, the substantial uncertainties inherent in climate models necessitate a more cautious approach to avoid compounding uncertainties (Vetter et al., 2017; Zelinka et al., 2017). The basin descriptor-based scheme relies on observed discharge data and the relationship between basin descriptors and IDF curves, both of which will change under future climatic conditions (Mirhosseini et al., 2013); therefore, this scheme is unsuitable to provide accurate simulations for future scenarios. The cascade-modeling scheme is comparatively more suitable for studying future flood changes; however, it struggles to manage the intensive computational demands required for such large-scale simulations.

Recent advancements in downscaling techniques have made it possible to provide high-resolution large-ensemble precipitation projections for certain regions (Ishizaki, 2022; Kawase et al., 2023; Kitoh et al., 2016). These data are promising for studying detailed subdaily-scale flood processes (Sunyer et al., 2017). To comprehensively utilize such a dataset, we need to explore new methods to improve simulation efficiency.

In the abovementioned schemes, a critical challenge for flood hazard mapping lies in ensuring necessary water level and discharge data for all river sections with minimal

computational effort. Specifically, obtaining discharge frequency curves for all river sections is essential. This raises a key question: can peak discharges (for estimating frequency curves) for all sections be directly derived from simulations driven by a limited set of precipitation events? Such an approach would offer an efficient and direct method to create high-resolution national flood hazard maps while avoiding the errors and uncertainties associated with resolution transformations.

However, precipitation variability and scaling challenges make it difficult to extract the required events solely based on rainfall-runoff relationships or other indicators prior to simulation (Liu et al., 2018). Note that different events with the same total precipitation is possible to result in different peak discharges in the same river section because of different spatiotemporal patterns of precipitation (Balbastre-Soldevila et al., 2019; Saharia et al., 2021). Furthermore, spatial variations in precipitation present additional complexities: a precipitation event that triggers a flood at an outlet with a specific return period might not necessarily result in high discharges at other river sections. Moreover, the difference in event scale may also present challenges. For example, extreme precipitation events with short durations occurring over a small area (localized extreme events) may lead to significant localized floods; however, these events may be easily overlooked when extracting events based on basin-averaged precipitation (Ohba and Sugimoto, 2019; Thomassen et al., 2021). In the future, these localized extreme events are expected to become more frequent and play a significant role in extreme floods (Li et al., 2019). To accurately estimate flood frequency curves for each river cross-section, it is imperative to account for both basin-scale and localized floods. However, due to the challenges discussed, no existing method can comprehensively extract flood-triggering precipitation events for process-based flood frequency estimations. This gap highlights the need for innovative approaches to address the inherent complexities of precipitation variability, scale, and spatiotemporal dynamics.

To address this issue, we propose an aggregating grid event (AGE) method for extracting precipitation events that led to extreme flooding from large-ensemble climate datasets. The extracted precipitation events were input into the rainfall-runoff-inundation (RRI) model, and the simulated discharges were used for estimating the corresponding FFC of particular river cross-section. In this study, we focus on evaluating the accuracy of peak discharges and discharge quantiles, along with analyzing the uncertainty associated with these quantiles.

3.2 Methodology

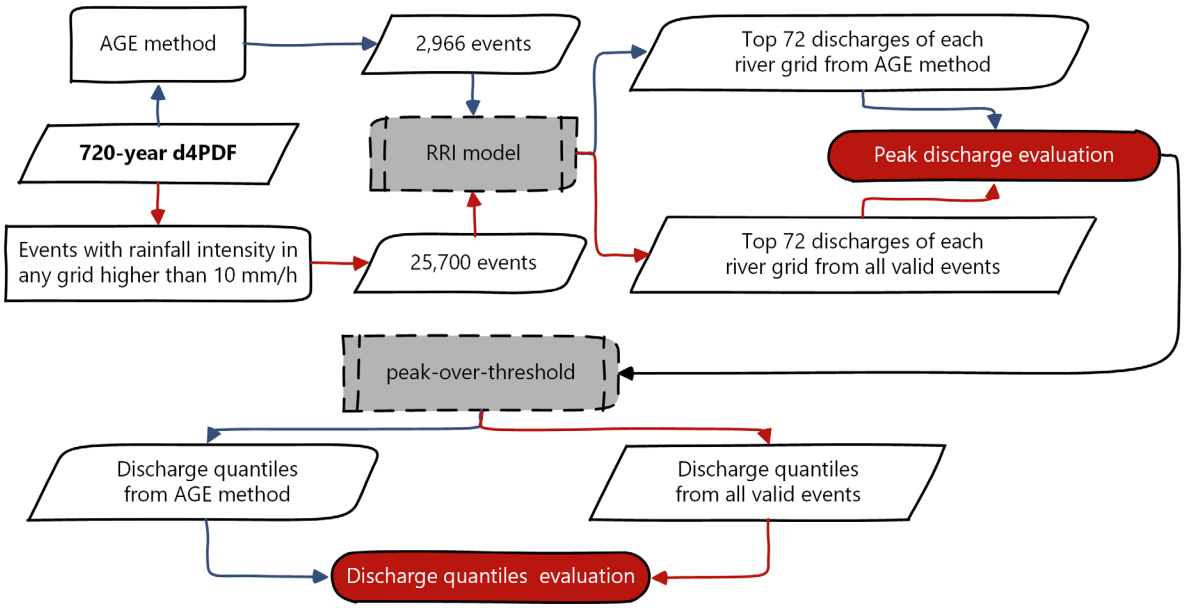


Figure 3-1 Flowchart portraying the study methodology used in this study. Abbreviations: rainfall-runoff-inundation (RRI), aggregating grid event (AGE).

The evaluation outline is shown in Figure 3-1. To create the reference discharges, 25,700 valid precipitation events were identified from a 720-year ensemble climate dataset within the study area. A valid event was defined as any event with rainfall intensity exceeding 10 mm/h in at least one grid. Concurrently, the AGE method was applied to the same dataset, extracting 2,966 precipitation events. The resulting discharges were simulated using the high-resolution RRI model, with a spatial resolution of 150 m and a temporal resolution of 1 hour. Discharges with an annual exceedance probability (AEP) lower than 0.1 (i.e., the largest 72 discharges over 720 years) were selected for evaluation and FFC estimation. By using the peak-over-threshold (POT) method, we estimated FFC for each river grid and conducted accuracy and uncertainty evaluation.

3.2.1 Aggregating grid event (AGE) method

A comprehensive consideration of precipitation heterogeneity and its interaction with basin characteristics is the key to reliable flood design (Wright et al., 2014). Conventional methods often rely on spatio-temporal averaged indicators, such as basin averaged 48-h precipitation, to rank and extract extreme events. However, those approaches introduce significant inaccuracies in flood simulations. Firstly, neglecting precipitation outside the fixed 48-hour window can bias flood simulation results.

Secondly, spatial averaging overlooks localized extreme events that may cause severe localized flooding (Chen et al., 2024). Therefore, the first two challenges in developing a new method are preserving the natural spatio-temporal variability of precipitation and accounting for extreme events at different scales. After successfully separating precipitation events, a third challenge arises: identifying the events that lead to higher discharges. In this study, we considered both the total rainfall and the rainfall intensity to rank the events.

Figure 3-2 illustrates the AGE method used in this study, which begins by analyzing the whole precipitation time series for each grid cell in the climate dataset. This approach enables the detection of the most localized floods driven by extreme precipitation events occurring within individual grid cells. Step 1 in Figure 3-2 applies a threshold and interval to differentiate events. The threshold, determined based on the local precipitation regime, must strike a balance: excessively high thresholds risk omitting significant events, while overly low thresholds increase computational demands. To construct FFCs for flood events exceeding a 10-year return period, the threshold was set at 10 mm/h—well below the flood-triggering intensity for the study area. The interval duration was approximated based on the time of concentration, which varies with spatial scale as detailed in Table S4. An independent precipitation event was separated when the intensity remained below the threshold for more than one interval.

To rank the events, a flood-peak-correlated indicator was selected, accounting for regional variations in climatic and geographical factors. This study compared total rainfall and rainfall during the concentration time (RDCT), finding RDCT to be more effective, as shown in Figures S2–S4. Highlighted in step 2 of Figure 3-2, RDCT focuses on precipitation intensity over a critical period, outperforming total rainfall by excluding long-duration, low-intensity precipitation events.

As shown in Figure 3-2, step 3, all grid events were ranked by the indicator (RDCT in this study), and those surpassing a frequency threshold were selected. To construct FFCs for return periods over 10 years, the top 72 events from a 720-year climate ensemble were chosen. Steps 1 through 3 were iteratively applied to each grid cell.

Subsequently, the precipitation data were then upscaled to various resolutions until a single grid cell encompassed the entire basin, employing mean pooling—a technique from deep learning used to modify data resolution while preserving features (Babenko

and Lempitsky, 2015). Typically, mean pooling averages four adjacent grids. The aforementioned procedures were applied across resolutions to identify extreme events at different spatial scales. At the resolution where one grid covers the entire basin, results align with those from basin-averaged indicators. Notably, the time of concentration for step 1 and RDCT in step 3 adjusts as per Table S4 with spatial resolution changes.

Selected events across all grids and resolutions were placed on a timeline (step 4, Figure 3-2). Two distinct relationship types were identified: overlap and isolation. Overlap represents a large-scale event impact massive grids at varying timings and durations as it develops spatiotemporally. Conversely, isolation refers to localized extreme events occurring within a single grid at a specific resolution. By merging overlapping events and retaining isolated ones, extreme events across scales were aggregated with reduced complexity while maintaining event integrity.

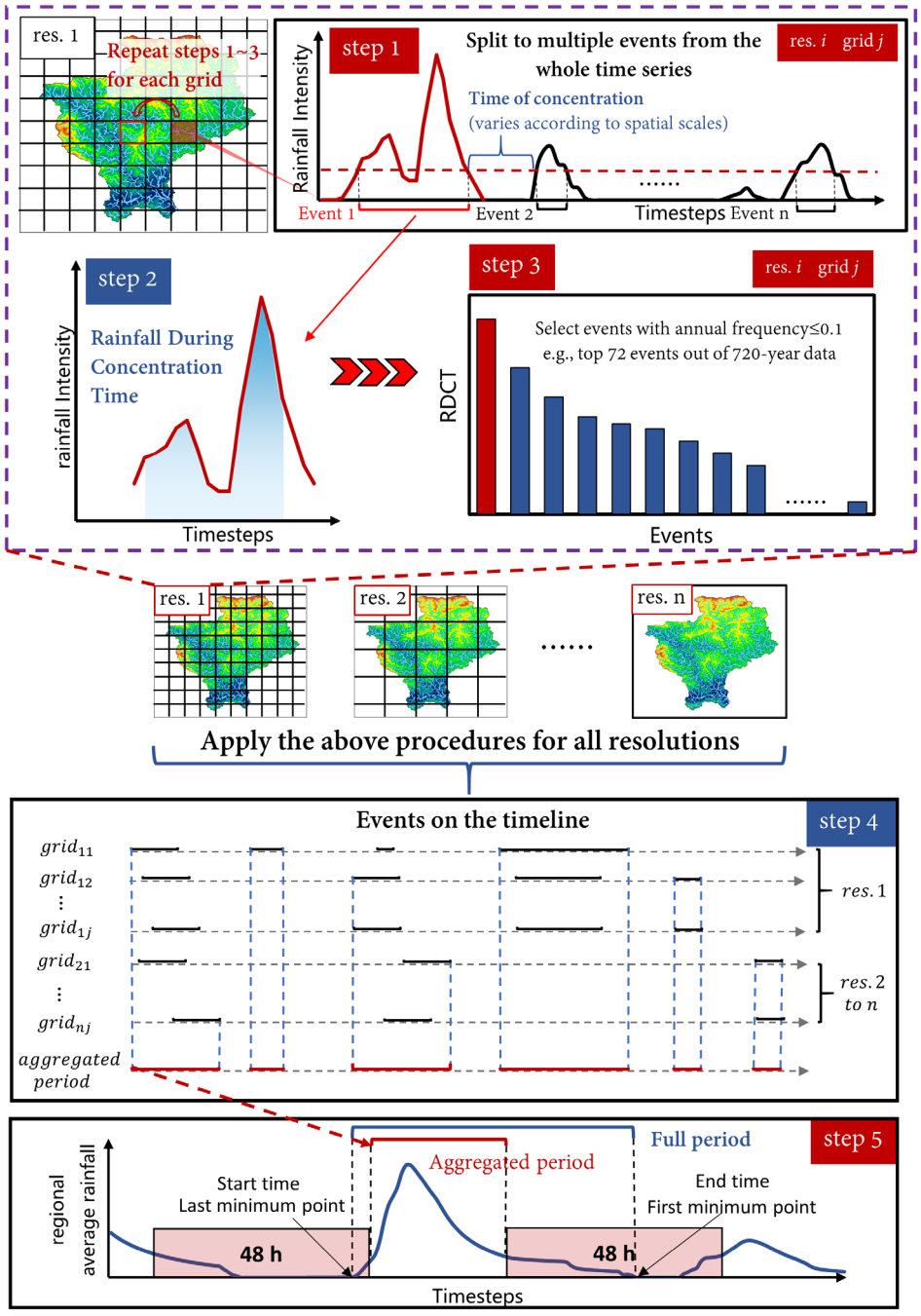


Figure 3-2 Process schematic of aggregating grid events (AGE) method used in this study. Abbreviations: resolution (res.).

Since events were initially separated by a threshold in step 1, aggregated events might be incomplete. To capture the actual event duration, as shown in step 5 (Figure 3-2), a 48-hour extension was applied to both start and end timesteps. The earliest and latest timesteps with minimal basin-averaged precipitation within the extensions are marked as the actual event boundaries. Precipitation data were then extracted for the entire period. The extension length is region-specific, relating to the precipitation

pattern, though a larger value is preferred.

In summary, the AGE method was developed while considering the above challenges associated with identifying precipitation events that lead to extreme floods. First, by summarizing the precipitation time series across all grids, the method maintained the natural temporal changes in precipitation. Furthermore, extracting the data based on aggregated periods preserved the natural spatial structure of the precipitation. Second, by traversing all grids at various resolutions, we effectively avoided ignoring the extreme localized events at different scales. Finally, the RDCT enabled the AGE method to theoretically identify the precipitation events that resulted in high discharges.

3.2.3 Rainfall-runoff-inundation (RRI) model

The rainfall-runoff-inundation (RRI) model is a distributed hydrologic model developed by Sayama et al. (2012); the model considers the coupling of one-dimensional (1D) and 2D processes, allowing for the simultaneous simulation of runoff and inundation. In land grids, the RRI model represents water movement, using a 2D diffusion wave equation, while a 1D diffusion wave equation is used for river grids. The Green-Ampt model (Green and Ampt, 1911) was employed for estimating the infiltration in flat areas, and an integrated subsurface and surface model (Sayama & McDonnell, 2009; Tachikawa et al., 2004) was employed for mountainous areas. The model does not prepare schemes for computing evapotranspiration, but allows users to provide evapotranspiration data if available. As this study focuses on extreme flood events, we did not consider the evapotranspiration process. The numerical scheme of the model was optimized using the fifth-order Runge-Kutta formula (Cash and Karp, 1990), to ensure both accuracy and efficiency. In river grids, the model can simulate reservoir operations, as well as the reciprocating interactions of water with levees. In this study, we applied simple operational rules based on the local reservoir operation data. Notably, the RRI has been widely applied in Southeast Asia and Japan (Rasmy et al., 2019; Sayama et al., 2017; Try et al., 2022; Yamamoto et al., 2021). Sayama et al. (2020) developed a nationwide real-time flood forecasting system for Japan, based on the RRI model.

The resolution of the RRI model used in this study was set to 150 m. The required elevation and flow direction data were obtained from the Japan flow direction map (J-FlwDir) developed by Yamazaki et al. (2020). The original dataset, with a resolution of

30 m, was upscaled to a resolution of 150 m using an upscaling algorithm developed by Masutani et al. (2006), while preserving the location of the main streams. The model parameters were derived from a calibrated national RRI model (see Table S5) (Sayama et al., 2024). Figures S5 to S6 show the performance of the RRI model applied to the entire Japan evaluated by a total of 2,723 events at 711 gauging stations. Because of the extensive computational requirements, the RRI model in this study was deployed on the fourth-generation Earth Simulator, a vector engine-based supercomputer (Habata et al., 2003, 2004).

3.2.4 Peak-over-threshold (POT)

In general, frequency analysis methods can be classified into two categories, based on their approaches to extreme value selection: the block maxima and POT methods (Mostofi Zadeh et al., 2019). The annual maxima method, a common block maxima application, sets the block size to 1 year and selects the largest flood event within each year for the frequency analysis. A limitation of this method is its susceptibility to interannual variability, where the highest value is always included regardless of how low the discharges are in dry years, while the second highest discharge is consistently excluded irrespective of how high the discharges are in rainy years. (Ferreira and de Haan, 2015). As we used a precipitation dataset that spanned 720 years, the limitations of the block maxima method could be exacerbated. In general, the POT method encompasses all the discharges above a defined threshold in the analysis and employs a generalized Pareto distribution (GPD) to describe the distribution of extreme values (Lang et al., 1999), thereby avoiding the shortcomings of the block maxima method. Another advantage of the POT method, especially when dealing with long-duration data, as in the case of large climate projection ensembles, is its ability to analyze the data based on higher thresholds (resulting in fewer discharge data points), thus, significantly reducing the hydrologic simulations. Consequently, in this study, the POT method was used to predict the frequency curves for each river cross-section.

The high thresholds were set to select the largest 72 discharges (i.e., AEP $\leq$0.1) for each river section. The GPD was determined using Eq. (3-1), as follows:

$$\boldsymbol{GPD}(\boldsymbol{x}) = \begin{cases} 1 - (1 + \xi\left(\frac{x-\mu}{\sigma}\right))^{-1/\xi} & for\ \xi \neq 0 \\ 1 - \exp\left(-\frac{x-\mu}{\sigma}\right) & for\ \xi = 0 \end{cases} \quad (3\text{-}1)$$

where, ξ, μ, and σ represent the shape, location, and scale parameters.

3.2.5 Evaluation indicators

In this study, the accuracy of the discharge peaks was assessed using the correlation coefficient (R), relative bias (BIAS), and root mean square error (RMSE), using Eqs. (3-2), (3-3), and (3-4), respectively. To depict the width of the 95% confidence interval (CI) and ensure that it is comparable across different river grids, a CI ratio was used Eq. (3-5).

$$\mathrm{R} = \frac{\sum(y_e - \overline{y_e})(y_r - \overline{y_r})}{\sqrt{\sum(y_e - \overline{y_e})^2 \sum(y_r - \overline{y_r})^2}} \quad (3\text{-}2)$$

$$\mathrm{BIAS} = \frac{\sum y_e - \sum y_r}{\sum y_r} \times 100\% \quad (3\text{-}3)$$

$$\mathrm{RMSE} = \sqrt{\frac{1}{n}\sum(y_e - y_r)^2} \quad (3\text{-}4)$$

$$\mathrm{CI\ ratio} = \frac{y_{97.5\%} - y_{2.5\%}}{y_e} \times 100\% \quad (3\text{-}5)$$

where y_e and y_r denote the estimated and reference series, respectively; $y_{97.5\%}$ is the 97.5th percentile of the estimated value y_e, and $y_{2.5\%}$ is the 2.5th percentile.

3.3 Study Area and Data

3.3.1 Shikoku Island

As shown in Figure 3-3, Shikoku Island (Japan) is located between 132°–135° E and 32.5°–34.6° N, covering a total area of approximately 21,000 km^2. The island includes eight major river basins (listed in descending order of area, as follows): the Yoshino, Watari, Niyodo, Hiji, Naka, Monobe, Shigenobu, and Doki river basins. In addition, numerous small rivers exist along the coast. The island is surrounded by the Seto Inland Sea and the Pacific Ocean and is frequently affected by quasi-stationary band-shaped precipitation and typhoons (Kamahori and Arakawa, 2018; Kato, 2020; Otaki et al., 2022; Tada et al., 2018). The spatial distribution in the annual rainfall in the region exhibits significant variations, portraying higher values in the central region

(~4000 mm) and lower values in the northern (~1200 mm) and southern (~2500 mm) regions (Yao and Creed, 2005). This disparity is primarily due to the northward progression of warm and moist air masses and typhoons that encounter the mountainous terrain in the central region, leading to concentrated rainfall. Moreover, the island is predominantly mountainous; the minimum distance from the coast (sea level) to the region with an elevation of ~2000 m above sea level is only 50 km. The rivers on the island exhibit steep slopes and high flow velocities, rendering them susceptible to flooding.

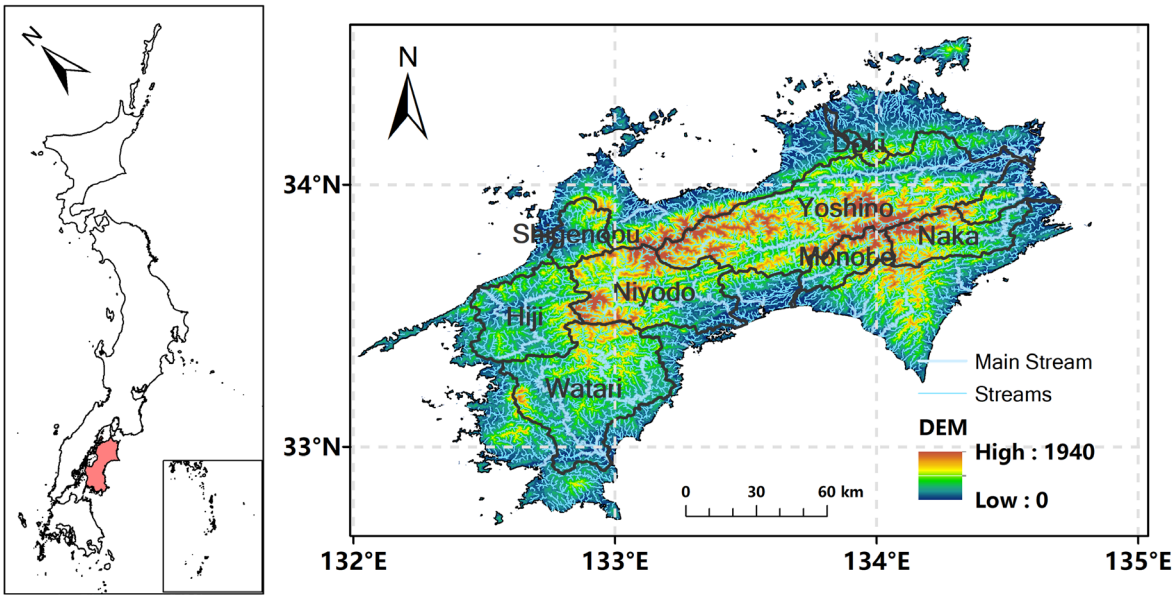


Figure 3-3 Map of Shikoku Island, Japan. Abbreviations: digital elevation model (DEM).

In this study, at a resolution of 150 m, the entire study area was divided into 948,162 grids. Among these, the grids with an upstream contribution area greater than 1.125 km^2 (i.e., 50 grids) were identified as river grids (a total of 95,021 grids).

3.3.2 5-km d4PDF dataset

The full name of d4PDF is database for Policy Decision-making for Future climate change. The basic idea of d4PDF is to provide extensive climate projection data at specific stages of global warming (e.g., the global-mean surface air temperature is 2K, 4K warmer than the preindustrial era) through repeated simulation, so as to robustly assess the climate-change impact on extreme events. To account for the uncertainty of most general circulation models (GCMs), the original experiment of d4PDF used the sea surface temperature (SST) results of different GCMs as the initial and boundary

conditions, together with perturbations (Mizuta et al., 2017). Each member of the d4PDF stands for the climatic system (at specific initial conditions and perturbations) runs for 60 years without a warming trend. The experiment employed the Meteorological Research Institute atmospheric general circulation model 3.2 (MRI-AGCM 3.2) (Kusunoki and Mizuta, 2013) and performed global simulations at 60 km resolution. To conduct detailed studies in specific regions, the d4PDF was partially dynamically downscaled by 20 km and 5 km (Mizuta et al., 2017, Kawase et al., 2023). The detailed data facilitated numerous investigations on hydroclimatic extremes (e.g., extreme precipitation, snowfall, and drought) and water resource assessment (Hatsuzuka et al., 2020; Kawase et al., 2020; Miyasaka et al., 2020; Ohba et al., 2022; Tanaka et al., 2018; Zhao et al., 2023). In studies on precipitation frequency and floods, data from different members is treated as independent and identically distributed series for robustly estimating the quantiles (Cheng et al., 2021; Tanaka et al., 2020; Try et al., 2020).

In this study, we employed the latest dynamically downscaled d4PDF, which covers Japan, referred to as d4PDF DDS JP (Kawase et al., 2023). The data was downscaled by a 5-km non-hydrostatic regional climate model (NHRCM) (Sasaki et al., 2011). The d4PDF DDS JP encompasses three scenarios: historical, 2K warming, and 4K warming, each containing 12 members (6 SSTs ×2 perturbations). Each member has 60-year hourly data. Compared with previous downscaled outcomes, the d4PDF DDS JP can fully cover Japan, while enhancing the accuracy of the estimations of precipitation, sea ice, and radiations (Sasai et al., 2019). Because this study focuses on evaluating the AGE method, instead of evaluating the climate change impact, we only use the data at historical stage (i.e., 60 years ×12 members =720 years).

3.4 Results

3.4.1 Discharge peaks

We employed the AGE method to process the full d4PDF DDS JP, extracting 2,966 precipitation events from the 720-year historical stage. In comparison, 25,700 valid precipitation events were identified to generate reference discharges. Both sets of the precipitation events were simulated using the RRI model, and the highest 72 discharges (corresponding to AEP ≤ 0.1) for each river grid were extracted from the results. This comparison allows us to evaluate whether the AGE method successfully identifies the key precipitation events necessary for obtaining the highest 72 peak

discharges across different river sections.

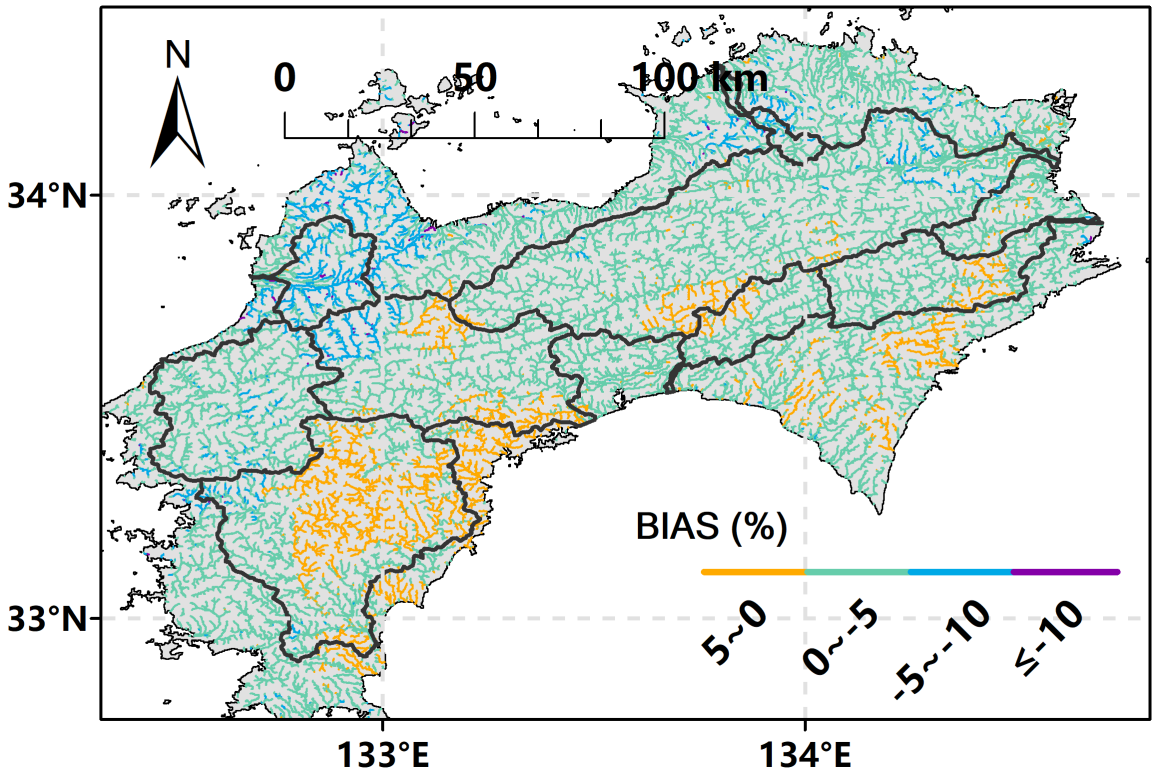


Figure 3-4 Relative bias (BIAS) of river grids. Comparison of the highest 72 discharges between aggregating grid event (AGE) method and all valid precipitation events.

As shown in Figure 3-4, we assessed the highest 72 discharges of each river grid by calculating the BIAS values. The results indicate that the BIAS of most river grids falls within the range of 0 to -5%. A smaller fraction of river grids exhibits BIAS values ranging from 5% to 0. Only a limited number of river grids show BIAS values between -5% and -10%. Overall, the results demonstrate high accuracy.

Figure 3-5 portrays a comprehensive evaluation for eight major river basins (a~h) and the overall Shikoku Island (i). This figure provides further insights into the characteristics of discharge peaks. The R values exceed 0.999 for all basins, indicating a strong linear relationship between the peak discharges obtained through the AGE method and the reference discharges. The RMSE values are significantly smaller than discharge peaks, indicating acceptable error levels. BIAS, being dimensionless, serves as an additional indicator for cross-basin comparisons. In Figure 3-5 (i), a BIAS of -1.38% and an RMSE of 36.45 m^3/s support the conclusion that peak discharges derived from the AGE method exhibit high accuracy.

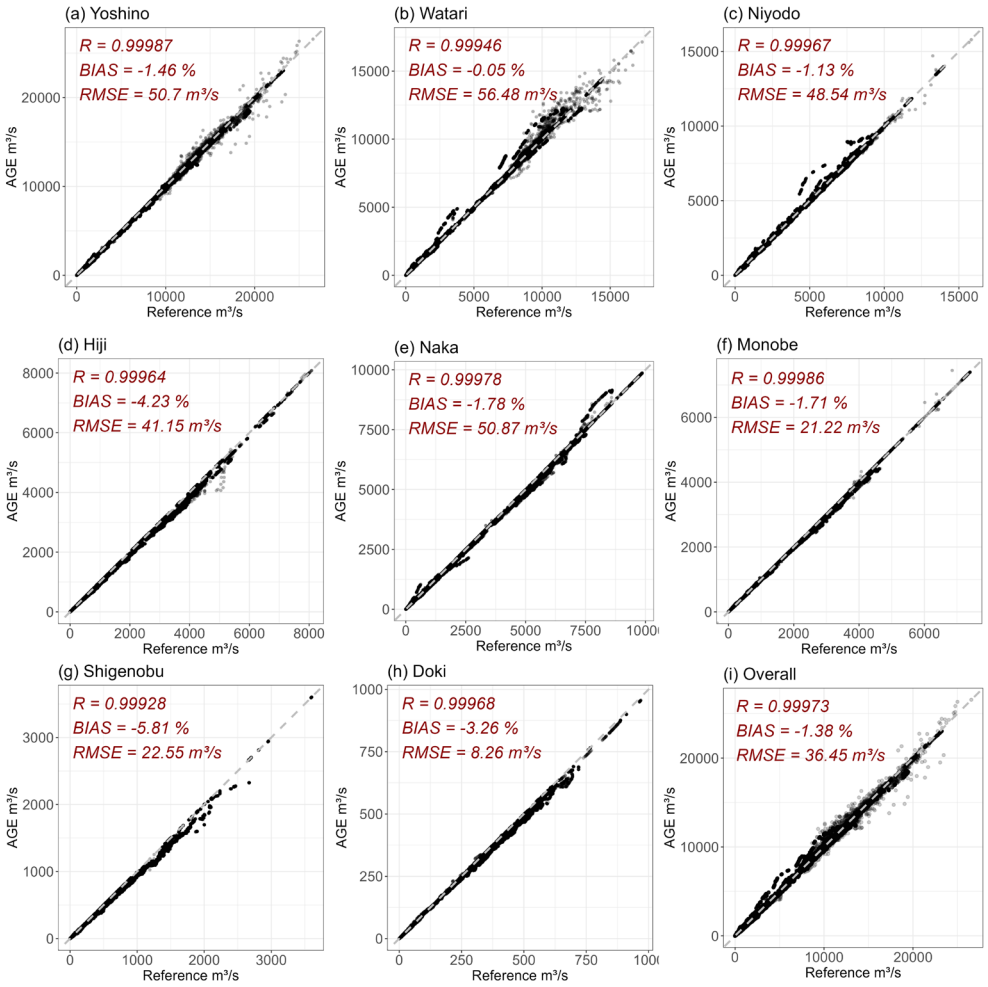


Figure 3-5 Evaluation of the 72 highest discharges of all river grids, based on the events extracted by the aggregating grid event (AGE) method.

(a)~(h) portray the results for the eight basins considered in this study; (i) portrays the overall results for Shikoku Island. Abbreviations: correlation coefficient (R), relative bias (BIAS), root mean square error (RMSE).

Overall, the AGE method substantially reduces the required number of events for peak discharge estimation from 25,700 to 2,966, while maintaining high accuracy. Therefore, estimating FFCs based on these peak discharges is reasonable.

3.4.2 Discharge quantiles

The highest 72 discharges correspond to AEP ≤0.1 (i.e., return period ≥ 10 years). We selected these highest 72 discharges for each river grid and then, estimated the FFCs using the POT method. The discharge quantiles were obtained from the corresponding FFCs. Figure 3-6 portrays the flood quantile maps based on the AGE method for 10-, 50-, 100-, and 1000-year return periods. To create the reference quantiles, we repeated the abovementioned procedures, replacing the AGE-based

discharge with the reference discharge. Note that discharge quantiles are important variables for hydrology research and infrastructure design projects.

Figure 3-7 portrays the BIAS values of discharge quantiles for 10-, 50-, 100-, and 1000-year return periods. Each BIAS represents the error of a specific river grid. The bar charts in the bottom right corner of each map display the statistical distribution of the BIAS values across Shikoku Island. The majority of BIAS values fall within the range of 0 to -10 %. The BIAS of most river grids concentrates on the range between 0 and –5 %. These BIAS values were dominated by underestimations. However, some discharge quantiles for the 1000-year return period depict overestimation, likely due to the higher uncertainty associated with longer return periods.

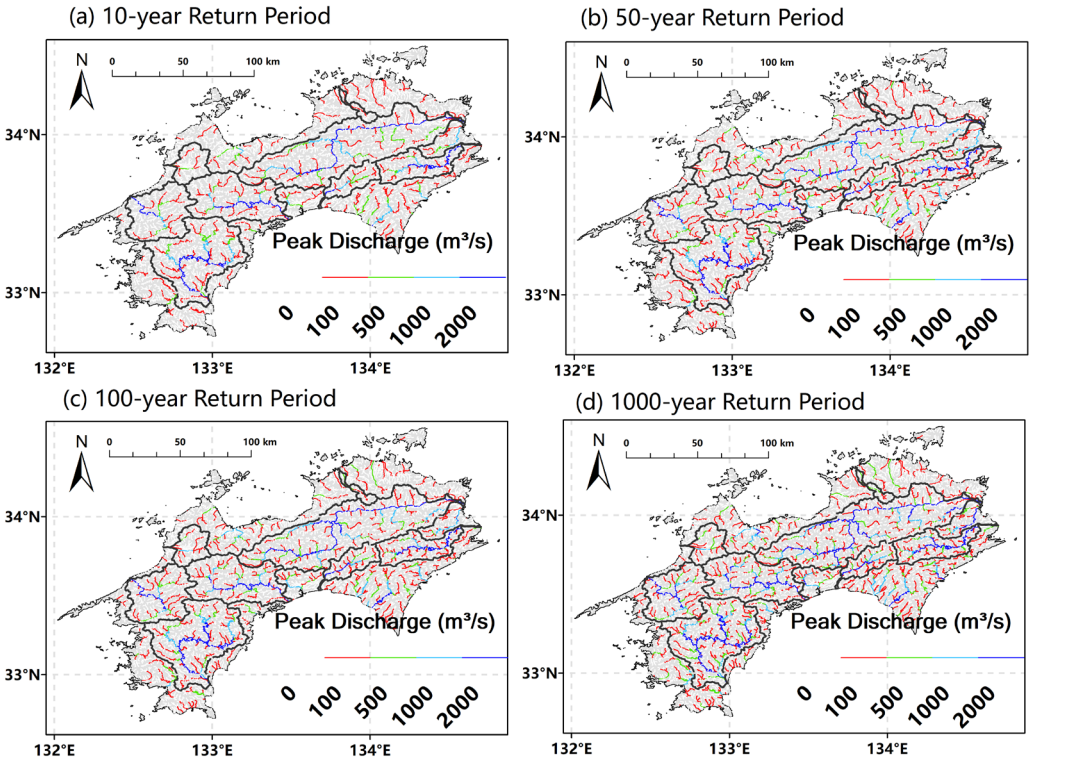


Figure 3-6 Flood quantile maps for the return periods of (a) 10, (b) 50, (c) 100, and (d) 1000 years.

To understand how the BIAS values vary with basin areas, we categorized the data based on upstream contribution area and depicted the results in Figure 3-8. The results indicated that, except for the 1000-year return period, all the outliers were exclusively identified in river grids with basin areas smaller than 25 km², which typically represent the source of the river network. Owing to their limited basin areas, these river sections exhibited relatively low discharges. Consequently, even a minor difference in the discharge can result in substantial BIAS. For river sections with basin

areas greater than 25 km², the BIAS values typically varied from 0 to –10 %. When the basin area exceeded 500 km², the BIAS values varied from 0 to –5 % (portraying a reduction in the range). Despite the relatively larger uncertainties in results for the 1000-year return period, leading to a scattered BIAS distribution, it was still evident that the majority of the BIAS values for each river cross-section were within the range of ±10 %. In river grids with basin areas larger than 500 km², the BIAS values were maintained within the range of ±5 %. In summary, the error decreases as the basin area increases, with larger basin areas having the potential to experience higher discharges, which typically garner greater attention.

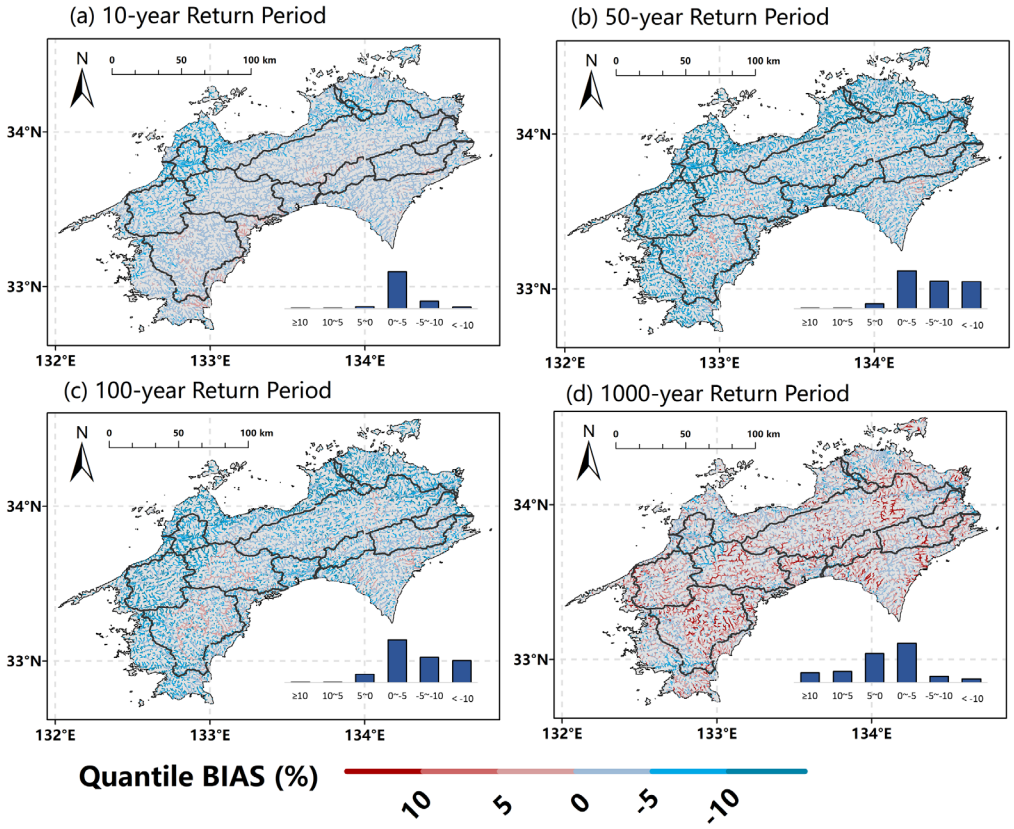


Figure 3-7 Spatial distribution of discharge-quantile relative bias (BIAS) values for return periods of (a) 10, (b) 50, (c) 100, and (d) 1000 years.

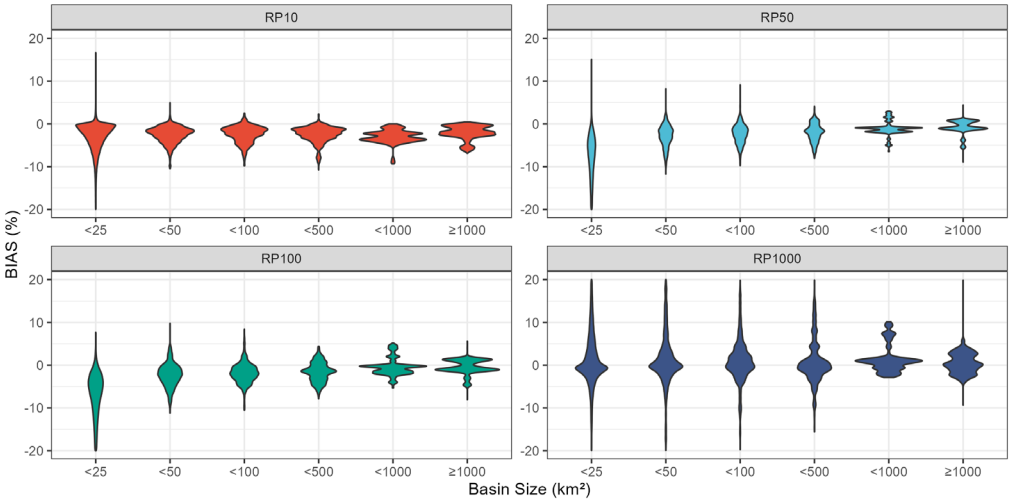


Figure 3-8 Changes in the relative bias (BIAS) values of discharge quantiles with basin area, for return periods of 10 (RP10), 50 (RP50), 100 (RP100), 1000 (RP1000) years.

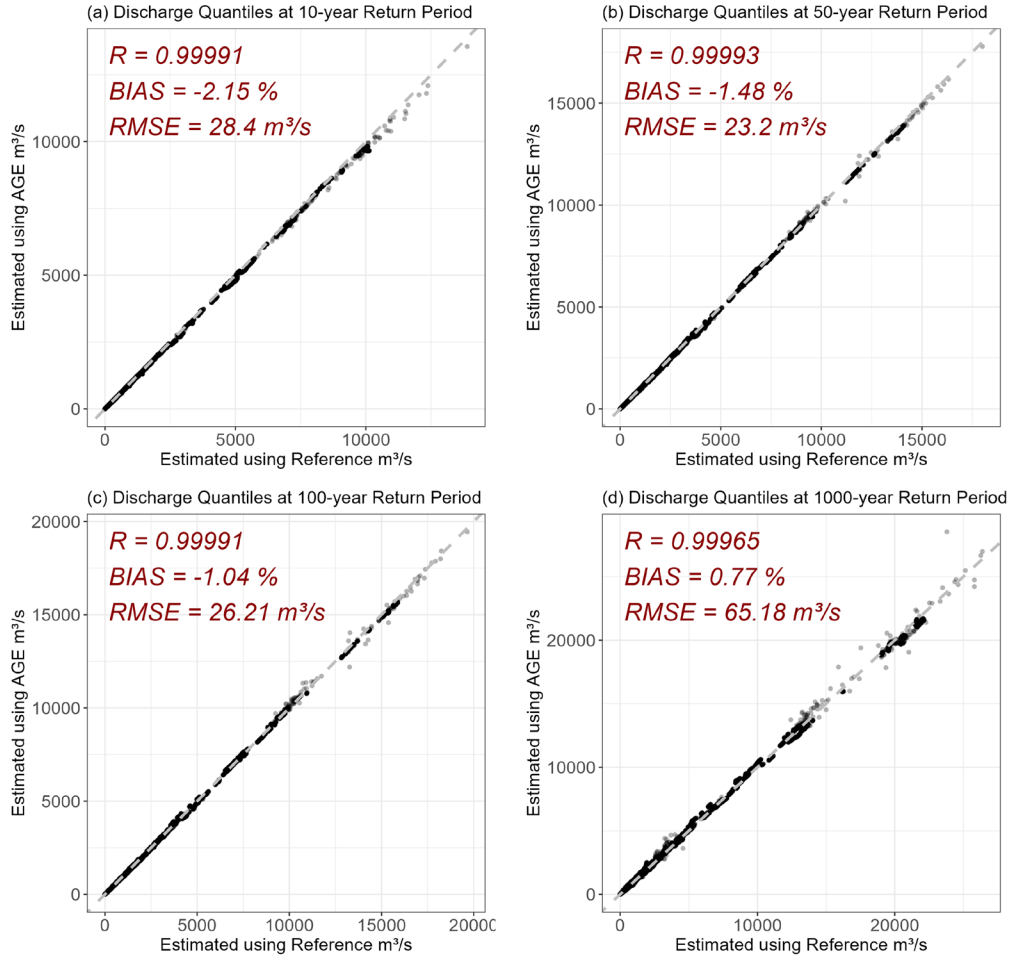


Figure 3-9 Comparison of the discharge quantiles for all river sections on the Shikoku Island for different return periods. Abbreviations: correlation coefficient (R), relative bias (BIAS), root mean square error (RMSE).

Figure 3-9 illustrates the overall accuracy of the AGE-based discharge quantiles across

Shikoku Island. Accurate estimates of peak discharges facilitate accurate quantile estimation. The BIAS values are -2.15%, -1.48%, -1.04%, and -0.77% for return periods of 10, 50, 100, and 1000 years. Regarding the RMSE, its values remain below 30 m^3/s for the return period up to 100 years, increasing to 65.18 m^3/s for the 1000-year return period. In summary, highly accurate estimates of discharge quantiles can be obtained by using the AGE method for extracting extreme precipitation events.

Figure 3-10 compares the uncertainties of the AGE-based quantiles with those of reference quantiles for different return periods. The CI ratio was employed to access the relative width of the 95% confidence interval. Each boxplot summarizes the CI ratios of river grids across Shikoku Island for the respective return period. As expected, uncertainties increase with the rise in the return period. Note that outliers are not shown in the figure. Compared with the reference results, the CI ratios of AGE-based results exhibit slightly higher values at the return period of 1000 years but remain nearly the same at the return periods of 10, 50, and 100 years. The CI ratios at the 10-year return period were generally close to zero, and median CI ratios at the 50-, 100-, and 1000-year return periods were 14, 17, and 43 %, respectively. Overall, the uncertainty of discharge quantiles obtained through the AGE method is comparable to the reference results.

In summary, employing the AGE method to develop flood quantile maps allowed for accurate and reliable discharge estimates.

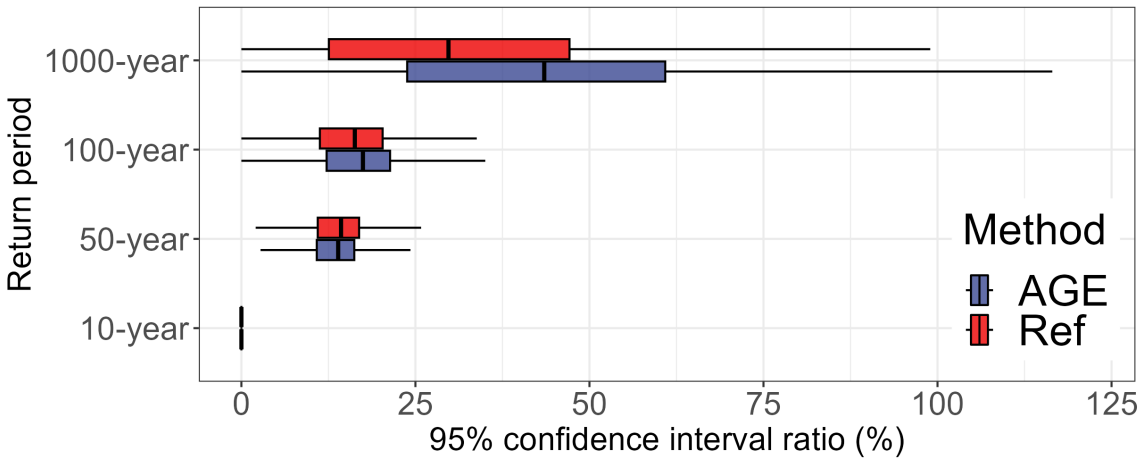


Figure 3-10 Results of confidence interval (CI) ratios for all river grids within Shikoku Island at different return periods. Abbreviations: aggregating grid event (AGE) model and reference (Ref) values.

3.5 Discussion

This study proposes an AGE method as an innovative approach to reduce the computational cost of process-based flood frequency estimation by extracting the precipitation events that lead to extreme discharges from large climate ensembles. Based on the extracted events, the AGE method enables high-resolution flood simulations through the RRI model. Flood quantiles of each river grid were estimated based on filtered peak discharges and the POT method. The high accuracy demonstrated by the AGE method suggests its significant potential for facilitating extensive and high-resolution flood simulations. A typical application scenario could involve detailed assessment of climate change impacts on regional-scale floods.

In recent years, concerted efforts by governmental organizations and scientists have proposed a series of downscaled climate ensembles —such as ENSEMBLE (van der Linden and Mitchell, 2009), coordinated regional climate downscaling experiment (CORDEX) (Gutowski Jr. et al., 2016; Jacob et al., 2020), NASA Earth Exchange Global Daily Downscaled Projections (NEX-GDDP) (Bao and Wen, 2017), ClimEx (Leduc et al., 2019), and d4PDF (Ishii & Mori, 2020; Kawase et al., 2023) database—to enhance regional climate change impact studies. These datasets, with resolutions ranging from 5 km to 25 km, facilitate research on heatwaves, droughts, floods, and extreme precipitation (Ali et al., 2018; Di Sante et al., 2021; Huang et al., 2015; Smith et al., 2014; Xu et al., 2021). Flood research predominantly employs distributed hydrological models aligned with precipitation data resolutions or semi-distributed models (Alfieri et al., 2015; Di Sante et al., 2021; Huang et al., 2015; Köplin et al., 2014). However, due to the considerable computational burden, the studies that employ distributed hydrologic models at resolutions significantly higher than the precipitation input (i.e., hyper-resolution simulations), generating ensemble results, are currently scarce.

For regional- or national-scale studies, hyper-resolution simulations are imperative for supporting local government decision-making and providing detailed risk information to residents. Current studies mainly focus on the outlets of large basins, where dense populations reside (Arnell and Gosling, 2016; Tanaka et al., 2021). However, small- to medium-sized basins, which are intricately tied to local livelihoods, are often neglected or parameterized in coarse-resolution models. For instance, grids spanning several kilometers may contain multiple river channels but fail to accurately represent critical parameters such as flow direction, river slope, and roughness. Flash floods, prevalent in smaller basins, are particularly challenging to simulate with daily

temporal resolutions, as daily averaging can underestimate their intensity (Shehata and Mizunaga, 2018). Additionally, artificial flood control measures, such as reservoirs, levees, and water gates, significantly affect discharge patterns and must be explicitly accounted for (Boulange et al., 2021; Hanazaki et al., 2022; Zhou, 2020). Therefore, hyper-resolution simulations are imperative for evaluating flood dynamics at regional scales in the context of global warming.

Event-based simulation is a crucial method in flood research and is commonly employed in flood design and performing hyper-resolution simulations (Huang et al., 2018; Mei et al., 2020; Zeng et al., 2022). Nevertheless, performing hyper-resolution simulations at a national scale for all events remains a significant challenge, necessitating innovative approaches to optimize efficiency.

The AGE method, which avoids reliance on specific hydrologic models or model remodeling, e.g., the application of graphics processing unit acceleration (Vacondio et al., 2014; Yan et al., 2015), fundamentally involving the pre-processing of precipitation data based on the available hydrological knowledge. This approach offers considerable flexibility, essential for regional studies that necessitate incorporating extensive survey data. Additionally, local stakeholders often prefer proprietary or familiar models, underscoring the importance of adaptable methods for achieving accurate regional flood assessments.

Various methods are used for extracting extreme precipitation, including those based on spatial connectivity (Tan et al., 2021), extreme precipitation indicators (Sun et al., 2021), percentiles (Mahbod and Rafiee, 2021), and thresholds and intervals (Mascaro et al., 2013). These approaches stem from climatic or meteorological perspectives, consider physical or statistical features, and partial methods only focus on specific sites. In contrast, the AGE method is tailored to hydrological requirements, attributing hydrological significance to parameters such as approximate river concentration time while integrating both regional and localized events. Furthermore, the AGE method is versatile and can be applied to various gridded precipitation data.

Similar to the majority of hydrological methods, the AGE method provides approximations, rather than strict numerical results. The separation and arrangement of the precipitation events primarily refer to the unit hydrograph concept, employing an approximate value (e.g., 6 h or 12 h), instead of calculating the specific concentration times. In extreme cases, this approximation may miss certain events,

warranting further investigation. Nevertheless, our study indicates that the sensitivity of event selection and peak discharge to the approximation is minimal. Another potential concern is the lack of validation for such approximations for larger basins. The data and empirical formulae collected in this study mainly pertain to small–medium-sized basins, with the largest being the Tone River Basin (area of 16,840 km^2). Nevertheless, the AGE method is expected to remain effective at larger basin scales if the time of concentration is carefully determined from empirical formulae, or redesigning another ranking indicator to consider more complex factors (e.g., snowmelt, antecedent soil moisture). However, the benefits of the AGE method may diminish as simulation periods approach those of continuous simulations under extreme conditions. Essentially, the AGE method works by excluding isolated events that have minimal impact on major flood peaks across locations and resolutions. However, if all events are shown to significantly influence flood peaks somewhere within the basin, then all events must be simulated. Key factors influencing these benefits are basin scale and climate conditions. Larger basins generally have longer times of concentration, increasing the likelihood of overlap with events across grids and resolutions. Conversely, overlap probability decreases when local precipitation is more temporally and spatially concentrated.

Initial conditions, such as antecedent soil moisture, influence simulated flood peaks (Grimaldi et al., 2012; Yu et al., 2019), with varying importance across regions depending on factors like soil properties, land use, basin size, climate conditions, and model structure (Bhagabati and Kawasaki, 2017; Mitková et al., 2016; Schumann et al., 2016; Singh et al., 2022; Stephens et al., 2018). A pre-test in this study assessed the impact of initial conditions by simulating 10 storm events and using the final timestep's spatial distributions of soil moisture and water levels as wet initial conditions. Simulations with and without initial conditions were compared against observations (Figure S7). Results show that initial conditions slightly affect runoff at the onset but have minimal impact on flood peaks. Flood peaks were accurately reproduced without initial conditions, indicating that precipitation is the primary driver of flood peaks in the study area. Consequently, the RDCT was selected as the ranking indicator. For applications in other regions, pre-analysis of the influence of initial conditions is recommended. In case of more frequent storms, the AGE method should be applied with caution, as initial conditions and the spatio-temporal distribution of precipitation may exert a greater influence on flood wave timing. As understanding of initial conditions improves (Shokri et al., 2023; Yu et al., 2019), the

AGE method can be effective if the ranking indicator is redesigned while statistically considering other key factors.

As the AGE method is intended to support further studies, such as those assessing climate change impacts, the overall bias and uncertainty remain important concerns for future research. Process-based methods—comprising climate simulations, hydrologic simulations, and flood frequency analysis—introduce cumulative bias and uncertainty at each step (Clark et al., 2016), including the use of the AGE method to process climate data. Although results using the AGE method align well with those based on all valid events in this study, further validation against observed data is crucial to ensure reliability. A robust evaluation would require a careful methodological approach and sufficient observational data. Nevertheless, we gathered around 20-year annual maximum discharges from three gauges of Yoshino river basin to perform flood frequency analysis for comparison. As shown in Figure S8, the analysis revealed a 10% to 20% bias at the 20-year return period, with simulated results falling within the 95% confidence interval. Notably, this is not a rigorous evaluation due to the limited data length and its potential lack of representativeness.

The spatio-temporal resolution of the climate data is another concern when discussing the impact of climate change. Even though hyper-resolution simulations can better represent the geographical conditions and hydrodynamic changes, the reliability of results in extremely small basins is constrained by the resolution of climate data. Fine-scale convective processes can trigger severe floods in small basins, yet these processes are challenging to replicate in climate models with coarser resolutions (Archer et al., 2024; Chen et al., 2021; Thomassen et al., 2021). To address this, utilizing convection-permitting models with higher resolutions (e.g., 1 km, 15-minute intervals) can yield more robust and accurate results (Li et al., 2022; Prein et al., 2015; Yu et al., 2019).

3.6 Conclusions

This study proposes and validates a novel, simple, and efficient precipitation extraction method, the AGE method, for high-resolution national flood simulations, while using large-ensemble climate projection data. The AGE method separates and ranks precipitation events based on hydrological concepts and aggregates these events across multiple scales. It enables the identification of precipitation events that lead to flooding over a specific frequency.

The study focuses on Shikoku Island in Japan, where the AGE method extracted 2,966 events from a 720-year hourly ensemble climate dataset. For reference, 25,700 events were identified from the same dataset, and corresponding discharges were simulated using the 150-m resolution RRI model. Discharge quantiles for each river grid were estimated using the highest 72 discharges and the POT method. The evaluation assessed both peak discharges and discharge quantiles.

Results demonstrate that the AGE method reliably identifies precipitation events causing discharges with AEP $\leqslant 0.1$ for all river cross-sections. Combining the RDCT with the AGE method achieved high accuracy in peak discharge estimations, with a BIAS of −1.38% and an RMSE of 36.45 m^3/s. This accuracy translates into reliable discharge quantile estimations without significantly increasing uncertainty. Notably, BIAS values for river grids with basin areas exceeding 500 km^2 mostly fall within ±5%.

These findings underscore the capability and practicality of the AGE method in effectively managing extensive precipitation datasets for targeted hydrological applications.

4. Evaluation on process-based flood quantile estimation methods

Abstract

Utilizing ensemble data facilitates robust flood quantile estimation at arbitrary locations, enhancing regional flood risk management but posing significant computational challenges. This chapter assesses two event-based computational reduction methods: the aggregating grid event (AGE) method, which extracts critical events, and the precipitation stretching method, subdivided into PrecStre-I (full ensemble) and PrecStre-S (ensemble mean). Evaluations in eight basins on Shikoku Island, Japan, employed 25,700 precipitation events from a 720-year ensemble as a benchmark. High-resolution (hourly, 150 m) discharge simulations via the Rainfall-Runoff-Inundation model estimated 100-year peak discharges. The AGE method consistently achieved quantile relative biases within ±10% across river sections, whereas the precipitation stretching method exhibited greater variability, with biases up to ±40% due to precipitation uncertainties. Notably, downstream accuracy improved in basins with relative areas >90%, where outlets showed mean absolute percentage errors of 23% (PrecStre-S) and 16% (PrecStre-I), compared to basin-level errors of 38% and 34%, respectively. Using the full ensemble preserved original confidence intervals, while the ensemble mean inflated them by 25%–50%. Accordingly, the AGE method is preferable for process-based estimations, with PrecStre-I viable for downstream analyses, offering valuable insights for adaptive flood risk management under climate change.

4.1 Introduction

In recent years, the frequent occurrence of extreme weather events has resulted in significant loss in life and property (Tellman et al., 2021; Winsemius et al., 2018), prompting heightened societal awareness of climate change and the exploration of adaptive measures. In flood management, infrastructure construction and adaptive strategy formulation, the discharge quantile (e.g., discharge at 100-year return period) serves as a pivotal benchmark. In recent years, flood management has become increasingly sophisticated, with decision-makers obtaining discharge quantiles not only at basin and sub-basin outlets but also across various cross-sections within the basin.

Process-based approaches utilize distributed hydrological models to derive peak discharges, which are then incorporated into flood frequency analysis (FFA) for estimating discharge quantiles at any location (Chen et al., 2024; Dottori et al., 2016; Pappenberger et al., 2012; Yu et al., 2019). However, due to the limited availability of historical extreme event records, these methods often depend on stochastic weather generators or climate ensembles to expand sample sizes for reliable flood quantile estimation (Ishii and Mori, 2020; Tanaka et al., 2023; Wright et al., 2020). This reliance, however, presents scalability challenges for large-scale applications (Li et al., 2014; Peleg et al., 2017). Among these methods, climate ensemble approaches offer high physical reliability by simulating long-term meteorological variations. However, they also generate a substantial number of non-extreme events, leading to excessive computational demands for large-scale simulations, especially when accounting for inundation dynamics and backwater effects in the modeling process.

Event-based simulation is widely used in flood management, infrastructure design, and climate change impact analysis (Mei et al., 2020; Tamm et al., 2023). By focusing exclusively on extreme events, these approaches enhance the efficiency of climate ensemble utilization. Typically, event-based methods derive hydrological model inputs from intensity-duration-frequency (IDF) curves, which are constructed through frequency analysis of regional precipitation data (Hernes et al., 2020; Tamm et al., 2023).

However, conventional event-based simulations struggle to incorporate spatiotemporal precipitation variability and antecedent conditions, both of which significantly influence simulation accuracy. As a result, a 100-year precipitation event

does not necessarily correspond to a 100-year flood event (Kim et al., 2019; Najibi and Devineni, 2023; Zhou et al., 2021). Various studies have sought to integrate antecedent conditions into event-based simulations. Approaches include estimating lead time for antecedent rainfall (Cea and Fraga, 2018), incorporating antecedent moisture as a calibration parameter (Soriano et al., 2020), and stochastic matching of antecedent rainfall (Yu et al., 2019). Additionally, probabilistic methods have been explored, such as the Hybrid-CE approach, which combines continuous and event-based simulations to improve flood quantile estimation (Li et al., 2014), and the probabilistic spatial estimation of antecedent water conditions (Salgado-Cassiani et al., 2022).

To address spatiotemporal precipitation variability, weather generators are commonly used to create structured precipitation fields (Peleg et al., 2017; Peleg and Morin, 2014; Wright et al., 2017). Recent advancements include a generalized linear model-based weather generator that integrates multiple climate covariates (Verdin et al., 2018), a multipoint statistics-based precipitation generation method for projecting future precipitation types (Benoit et al., 2020), and a GAN-based (Generative Adversarial Network) stochastic weather generator enhancing spatial reliability (Ji et al., 2024). Additionally, stochastic storm transposition has been combined with high-resolution radar rainfall fields to generate extreme precipitation events for FFA (Wright et al., 2014). However, few event-based methods explicitly accounting for spatiotemporal variability are applicable to precipitation ensembles.

Among emerging techniques, the precipitation stretching method scales precipitation fields by estimating scaling factors based on the ratio between basin-averaged precipitation of multiple events and a target quantile (e.g., 100-year return period) (Saito et al., 2022). This method expands the sample size of precipitation distributions to reduce discrepancies between precipitation and discharge quantiles. Alternatively, the Aggregating Grid Event (AGE) method retrieves extreme precipitation events across multiple scales from ensembles while preserving spatiotemporal variability (Chen et al., 2025c). However, when applied to distributed hydrological models, precipitation variability affects flood quantile estimation not only at basin outlets but also at sub-basin locations. Research remains limited on the performance of event-based methods for precipitation ensembles in estimating flood quantiles across tributaries. Moreover, applying these methods to precipitation ensembles introduces new challenges related to implementation strategies and uncertainty propagation.

This study evaluates the performance of event-based simulation methods that incorporate improvements for addressing spatiotemporal precipitation variability, with a focus on the AGE method and the precipitation stretching method in ensemble-based flood quantile estimation. Key research questions include: (1) Can event-based methods accurately estimate flood quantiles for different tributaries within a basin? (2) Should event selection be based on the entire ensemble or the ensemble member average? (3) How does ensemble uncertainty propagate in different methods?

4.2 Study area & data

4.2.1 Shikoku Island

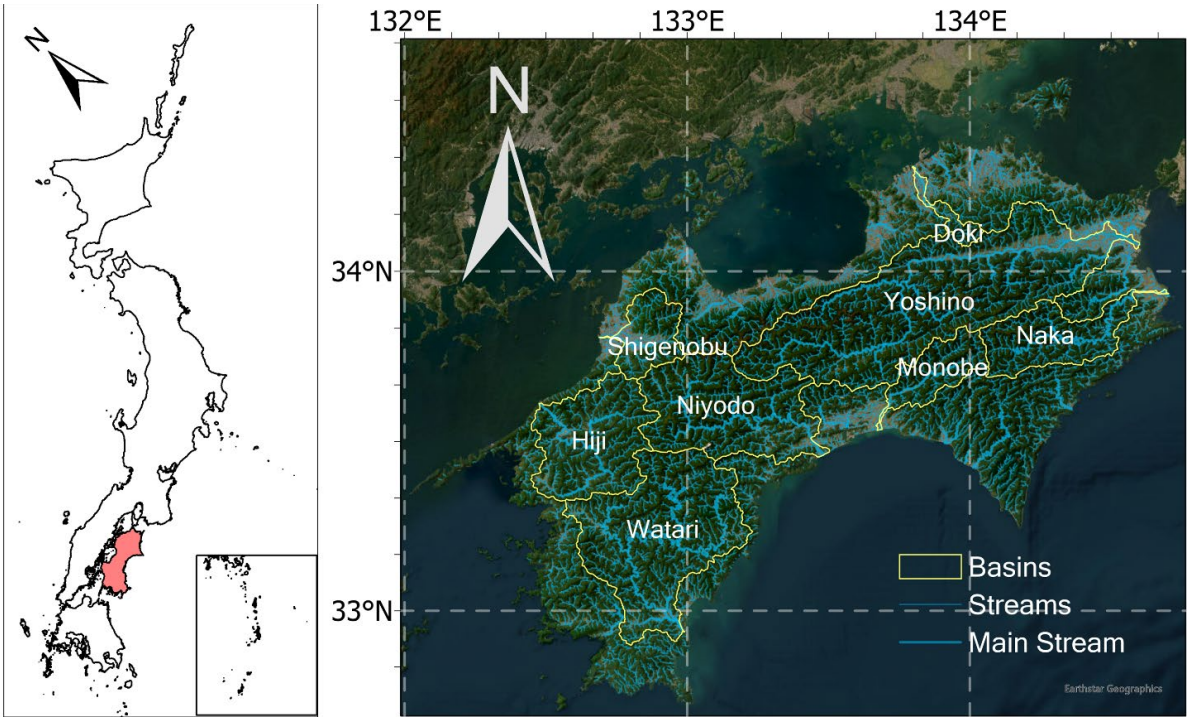


Figure 4-1 Overview of the Shikoku Island

As Figure 4-1 shows, this study focuses on Shikoku Island in Japan, encompassing eight major river basins and numerous coastal river channels, with a total area of 21,000 km². The eight major river basins' topographic characteristics are detailed in Table 4-1. Shikoku Island is frequently impacted by typhoons, leading to intense precipitation. The precipitation exhibits significant spatial variations influenced by the topography, with annual precipitation ranging from 1200 mm to 4000 mm. Simultaneously, owing to the mountainous terrain on the island, the river channels experience steep gradients, resulting in rapid streamflow. The combination of climatic

and topographic factors makes Shikoku Island prone to flooding disasters.

Table 4-1 Topographic parameters of the eight major basins in Shikoku Island

Basin	Area (km^2)	Length (km)	Elevation of river source (m)
Yoshino	3750	194	1897
Watari	2186	196	1336
Niyodo	1560	124	1982
Hiji	1210	103	460
Naka	874	125	1929
Monobe	508	71	1770
Shigenobu	445	36	1233
Doki	140	33	1059

4.2.2 Data

This study utilizes a nation-wide climate ensemble called d4PDF_5kmDDS_JP, which is dynamically downscaled from the 60-km d4PDF climate projection ensemble (Kawase et al., 2023). The ensemble provides climate variables at historical and future stages, featuring a spatial resolution of 5 km and a temporal resolution of 1 hour. Since this study does not focus on climate change impacts, only the historical ensemble data is adopted. To ensure a comprehensive representation of extreme events for robust frequency analysis, the historical d4PDF_5kmDDS_JP dataset includes 12 ensemble members, each covering the period 1951–2010 (60 years), generated with 12 initial perturbations. The detailed experimental design and downscaling procedures of d4PDF can be found in Mizuta et al. (2017) and Kawase et al. (2023). The 12 ensemble members (HPB_m001 to HPB_m012) are independent and identically distributed, allowing them to be treated as a single dataset (i.e., using 720-year data) for frequency analysis. Evaluation of this ensemble has demonstrated improved performance in simulating radiation, sea ice, and precipitation, aligning more closely with observational records (Kawase et al., 2023).

4.3 Methodology

Figure 4-2 shows the experiment framework of this study. An intensity threshold is required to extract precipitation event while exclude transient light precipitation. Given the hydroclimatic characteristics of the study area, precipitation bellow 10 mm/h is unlikely to generate annual flood peaks. Therefore, 10 mm/h is defined as a valid precipitation threshold. To capture all potentially influential events leading to

high discharges, all the timestep experienced valid precipitation is marked. A total of 25,700 precipitation events were extracted from the 720-year ensemble. The AGE method was applied to the same ensemble, extracting precipitation events for flood simulations. The precipitation stretching method is classified into two approaches: (1) integrated (PrecStre-I): estimates precipitation frequency using all ensemble members. (2) separated (PrecStre-S): obtains precipitation quantiles from the ensemble mean. The details of the methods are described in the next subsections.

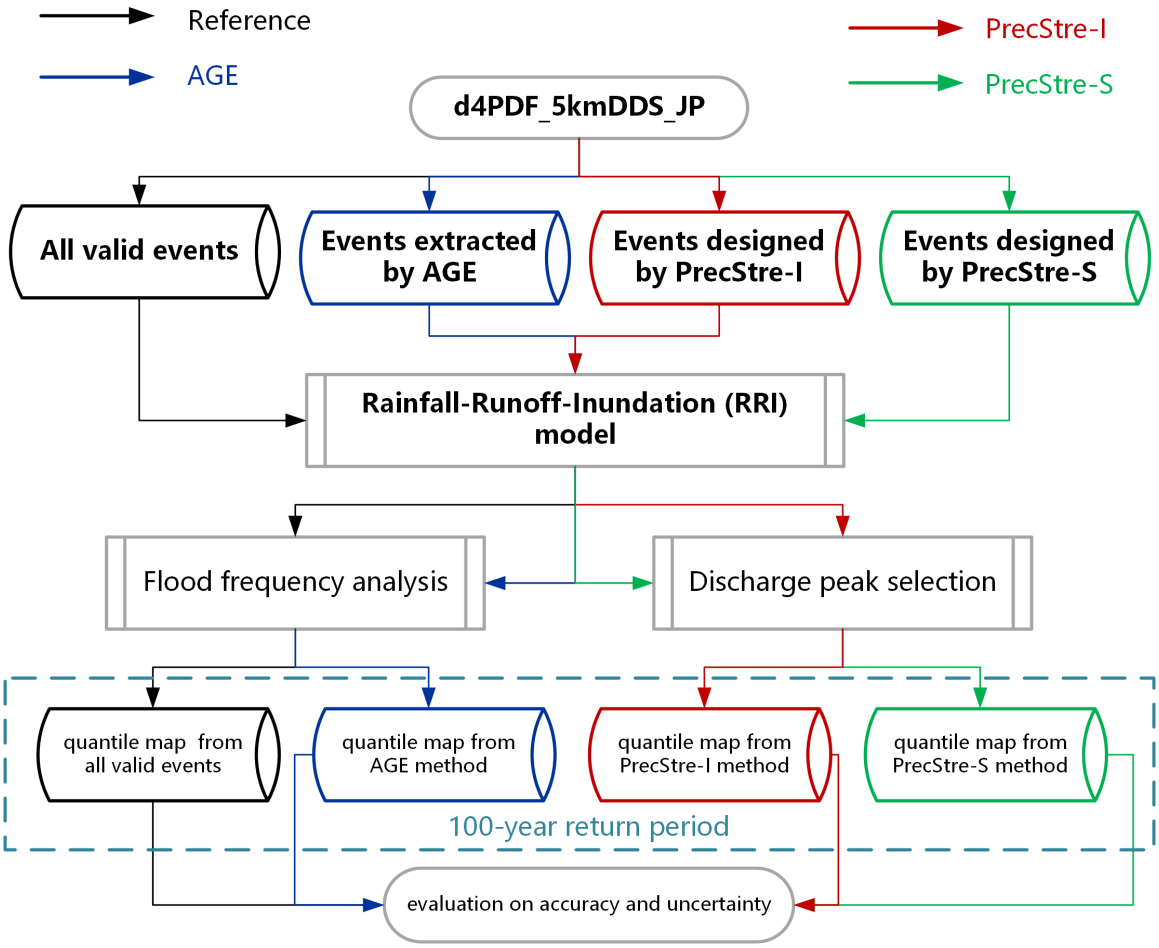


Figure 4-2 Flows of obtaining quantile maps for evaluation

The Rainfall-Runoff-Inundation (RRI) model is then used to obtain flood peaks from the extracted events. Based on the simulation results, the peak-over-threshold (POT) method is used to estimate the 100-year discharge and its 95% confidence interval for each river cross-section (Chen et al., 2024; Mostofi Zadeh et al., 2019). In this study, the POT threshold is set to a 10-year return period, corresponding to the top 72 events from the 720-year ensemble. The cumulative distribution function of the generalized pareto distribution (GPD) used in the POT method is given in Eq. 4-1. Wherein, ξ is the shape parameter, μ is the location parameter, and σ is the scale parameter. The

conversion equation of return period T and probability P is shown in Eq. 4-2, where *npy* means the number of peaks per year.

$$\boldsymbol{GPD}(\boldsymbol{x}) = \begin{cases} 1 - (1 + \xi\left(\frac{x-\mu}{\sigma}\right))^{-1/\xi} & for\ \xi \neq 0 \\ 1 - \exp\left(-\frac{x-\mu}{\sigma}\right) & for\ \xi = 0 \end{cases} \tag{4-1}$$

$$P = 1 - \frac{1}{T \times npy} \tag{4-2}$$

By comparing with reference discharge quantiles based on all valid events, the accuracy and uncertainty of these three methods are evaluated.

4.3.1 Aggregating Grid Event Method

The AGE method was developed to retrieve critical precipitation events for FFA at multiple locations within a region (Chen et al., 2025c). Its advantages include preserving the natural spatiotemporal distribution of precipitation and identifying extreme events across multiple scales. As shown in Figure 4-3, the core procedures of the AGE method comprise discretization, sorting, preliminary selection, upscaling, aggregation, and completion.

First, precipitation data for each grid is discretized using a 10 mm/h (valid precipitation threshold for the study area) threshold (Step 1). If the interval between two precipitation slices is shorter than a specified value, they are considered part of the same event. To ensure hydrological independence (i.e., subsequent precipitation does not influence the flood peak), this interval is set to the approximate time of concentration (Table 4-2). The values in Table 4-2 are estimated using an empirical formula (Kadoya and Fukushima, 1976) and summarized from the planned precipitation durations outlined in local flood prevention plans of 109 national river basins. Detailed guidelines can be found in MLIT (2024). The rainfall amount over approximate river concentration time is then calculated (step 2) and used for sorting. The top 72 events are preliminarily selected (step 3). Repeating Steps 1–3 across all grids yields an event set at the original spatial scale.

Subsequently, precipitation data is upscaled until a single pixel encompasses the target basin, with event sets derived at various scales through repeated application of the above steps. When events from different grids and scales are placed on a timeline (step 4), two patterns emerge: overlap and isolation, reflecting different impact scales

of extreme events. The final event set is obtained by aggregating overlapping events while preserving isolated ones.

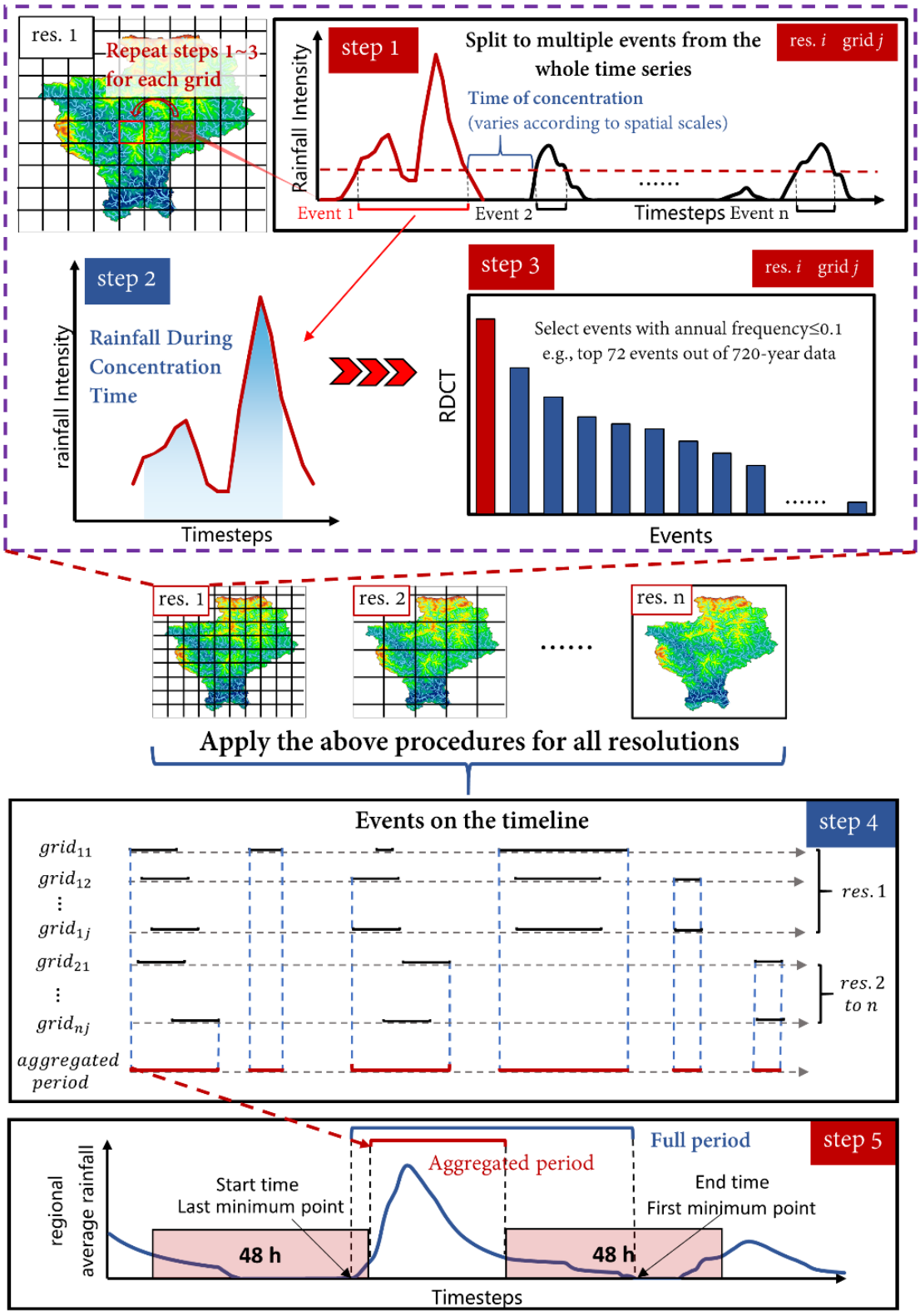


Figure 4-3 Conceptual illustration of the Aggregating Grid Event method (derived from Chapter 3)

Lastly, using regionally averaged rainfall, each event period is refined by identifying the first and last minimum points within an extended 48-hour time window (step 5). Based on the AGE method, this study identifies 2,966 events from the 720-year ensemble.

Table 4-2 Relationship between pixel area and approximate river concentration time

Area (km^2)	Time (h)
0~200	6
200~500	12
500~5000	24
≥ 5000	48

4.3.2 Precipitation Stretching Method

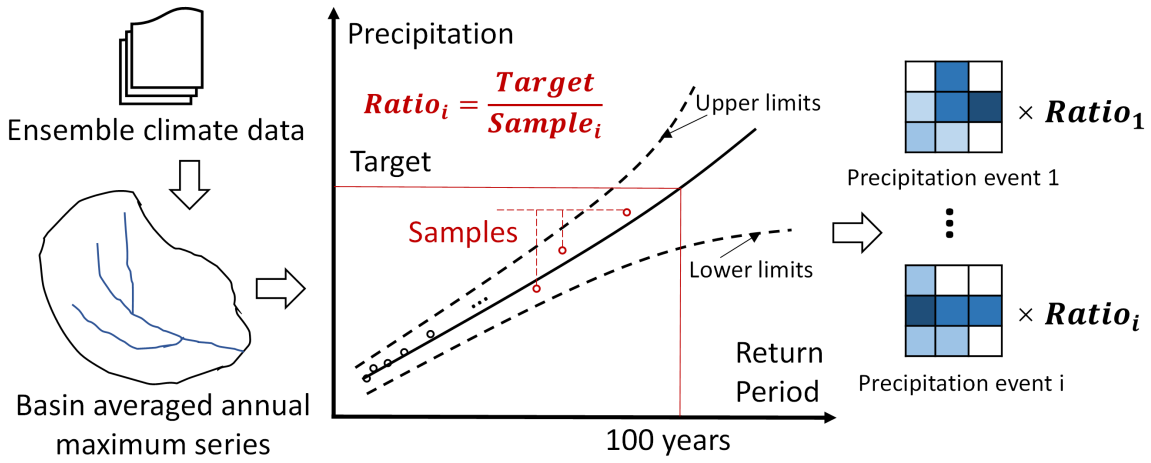


Figure 4-4 Conceptual illustration of precipitation stretching method

The concept of the precipitation stretching method is illustrated in Figure 4-4. For each target river basin, spatially averaged rainfall is computed to derive hourly time series from the ensemble climate data. Subsequently, the annual maximum 48-hour precipitation is extracted for frequency analysis. Given the small catchment areas and short concentration times of the study basins, a 48-hour duration is recommended for storm event design in the study area. The Generalized Extreme Value (GEV) distribution (Eq. 4-3) is used to fit the annual maximum sequence, with its parameter meaning consistent with those in Eq. 4-1. These parameters are estimated using the

L-moment method (Hosking and Wallis, 1993). Precipitation events with totals approximating the 100-year return level are selected, as their spatiotemporal structures are considered representative of potential 100-year events. The 100-year return period precipitation serves as the target value, and six 48-h precipitation events retaining their original spatiotemporal distributions are selected for stretching. By applying the scaling ratio to each grid and timestep of the corresponding event, precipitation is proportionally scaled with total rainfall equals to the target value (i.e., 100-year return level). The six stretched events are then used as input to the RRI model for discharge simulation. Finally, the maximum discharge at each river grid is extracted to represent the estimated discharge corresponding to the 100-year return period.

$$\boldsymbol{GEV}(\boldsymbol{x}) = \begin{cases} \exp\left(-\left(1+\xi\left(\frac{x-\mu}{\sigma}\right)\right)^{-1/\xi}\right) & for\ \xi \neq 0\ with\ 1+\xi\left(\frac{x-\mu}{\sigma}\right) > 0 \\ \exp\left(-\exp\left(-\frac{x-\mu}{\sigma}\right)\right) & for\ \xi = 0 \end{cases} \quad (4\text{-}3)$$

Based on ensemble treatment methods, the precipitation stretching approach is categorized into PrecStre-I and PrecStre-S. For estimating 100-year precipitation, PrecStre-I directly utilizes annual maximum precipitation from the 720-year ensemble, whereas PrecStre-S estimates quantiles for each ensemble member using 60-year data and subsequently averages the results. Since PrecStre-S treats each member as an independent dataset, candidate events are extracted from the same member. Thus, selecting a representative member is essential. The member yielding a 100-year precipitation estimate closest to the ensemble mean is designated as the representative member for the corresponding basin.

To quantify discharge uncertainty, the upper and lower limits of the 95% confidence interval for 100-year precipitation are recorded. In PrecStre-S, these limits are averaged across all members. Candidate events are then proportionally stretched to match the upper and lower limits, and the corresponding simulation results define the confidence interval for discharge estimates, allowing an assessment of uncertainty propagation. Information on 100-year precipitation for each basin is provided in Tables 4-3 and 4-4, while scaling ratios for candidate events are detailed in Tables S6 and S7.

Table 4-3 Target rainfall amount of each basin and their 95% upper and lower limits

from the PrecStre-I method

Basins	Target (mm)	Upper Limit (mm)	Lower Limit (mm)
Yoshino	480	521	442
Watari	545	585	509
Niyodo	567	603	531
Hiji	414	465	370
Naka	710	762	668
Monobe	686	733	640
Shigenobu	415	471	370
Doki	411	457	367

Table 4-4 Representative member, target rainfall amount of each basin and their 95% upper and lower limits from the PrecStre-S method

Basins	Representative member	Target (mm)	Upper Limit (mm)	Lower Limit (mm)
Yoshino	HPB_m006	485	654	364
Watari	HPB_m006	547	709	429
Niyodo	HPB_m004	573	724	456
Hiji	HPB_m002	410	611	288
Naka	HPB_m011	712	916	564
Monobe	HPB_m006	688	885	544
Shigenobu	HPB_m005	412	613	285
Doki	HPB_m010	414	623	282

4.3.3 Rainfall-Runoff-Inundation Model

The Rainfall-Runoff-Inundation (RRI) model employed in this study was initially developed by Sayama et al. (2012), and currently had been localized, including the incorporation of surveyed river cross-sections (Yamada et al., 2022), embedding a reservoir operation model (Ly et al., 2021), and nationwide calibration based on soil and geological attributes (Sayama et al., 2025) over Japan. At present, the localized Japan RRI (JRRI) with a 150m resolution has been developed into a real-time

forecasting system (Sayama et al., 2020). For floods with medium to long return periods (e.g., 100 years), cross-section shape of river channels and flood control structures have important effect to the simulation results (Boulange et al., 2021; Hanazaki et al., 2022; Zhou, 2020). Therefore, to accurately projecting future flood risk, this study conducted simulations based on the RRI model.

The RRI model is a naturally coupled one-dimensional and two-dimensional model capable of simultaneously calculating the evolution of streamflow and overflow to provide information on discharge and inundation depths. It divides the study area into river grids and land grids, applying one-dimensional diffusion wave equations to river grids and two-dimensional diffusion wave equations to land grids. The infiltration scheme employs the Green-Ampt model (Green and Ampt, 1911) in gentle topography, while an integrated stage-discharge relationship (Sayama and McDonnell, 2009; Tachikawa et al., 2004) taking unsaturated, saturated subsurface and surface flows is applied to mountainous regions. The numerical computations are conducted using the fifth-order Runge-Kutta formula (Cash and Karp, 1990). Due to its computational efficiency, accuracy, and open source, the RRI model has found extensive applications in Japan and Southeast Asia (Rasmy et al., 2019; Sayama et al., 2015; Try et al., 2020, 2022; Yamamoto et al., 2021).

Terrain data is a crucial input for the RRI model, and in this study, the 30m resolution J-FlwDir developed by Yamazaki et al. (2020) was utilized. The resolution was upscaled to 150m using an algorithm developed by (Masutani et al., 2006), while retaining the main stream locations.

The validation results of the JRRI model are shown in Figure 4-5, with a total of 519 flood processes evaluated across the study area. Model performance is assessed using the Correlation Coefficient (CC, Eq. 4-4), Nash-Sutcliffe Efficiency (NSE, Eq 4-5), and Relative Peak Difference (RPD, Eq. 4-6).

$$CC = \frac{\sum_{t=1}^{T}(Q_o^t - \overline{Q_o})(Q_s^t - \overline{Q_s})}{\sqrt{(\sum_{t=1}^{T}(Q_o^t - \overline{Q_o})^2)(\sum_{t=1}^{T}(Q_s^t - \overline{Q_s})^2)}} \tag{4-4}$$

$$NSE = 1 - \frac{\sum_{t=1}^{T}(Q_s^t - Q_o^t)^2}{\sum_{t=1}^{T}(Q_o^t - \overline{Q_o})^2} \tag{4-5}$$

$$RPD = \frac{Q_{p,s} - Q_{p,o}}{Q_{p,o}} \tag{4-6}$$

where Q_o^t and Q_s^t are the observed and simulated discharges at timestep t, $\overline{Q_o}$ and

$\overline{Q_s}$ are the temporal means, and $Q_{p,o}$ and $Q_{p,s}$ are the peak discharges of Q_o^t and Q_s^t.

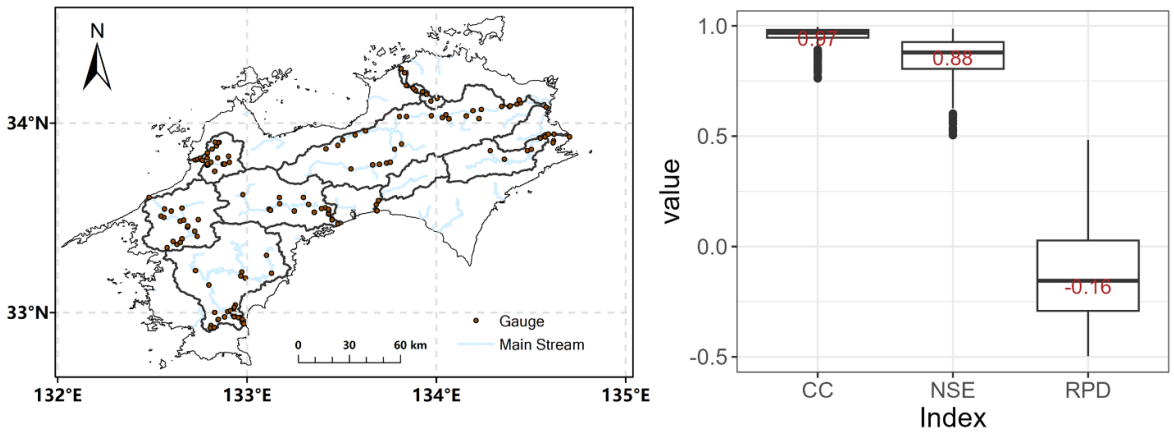


Figure 4-5 Locations of gauge and validation results of the JRRI model in the study area

The JRRI model demonstrates strong agreement, achieving median values of 0.97, 0.88, and -0.16 for CC, NSE, and RPD, respectively. Furthermore, as the reference discharge quantiles and those derived from the AGE, PrecStre-I, and PrecStre-S methods are based on the same model, any biases are considered systematic and do not impact subsequent analyses.

Given the substantial computational tasks involved in the validation work of this study, JRRI was developed as a vectorized version deployed on the fourth-generation Earth Simulator, a supercomputer based on vector engines (Habata et al., 2003). In this study, Shikoku Island is divided into 948,162 grids with a resolution of 150 m, and the simulation results are outputted with 1-hour temporal resolution. Among these, grids with more than 50 contributing grids from upstream are defined as river grids and serve as the objects for estimating the 100-year return period discharge in this study, totalling 95,021 grids.

4.3.4 Evaluation Indicators

In this study, we employed relative bias (BIAS), and mean absolute percentage error (MAPE), as defined by Eqs. 4-7 and 4-8, to comprehensively assess the error between the discharges obtained from the AGE or precipitation stretching methods and the benchmark at the 100-year return period. To evaluate the uncertainty changes for discharge quantiles from different river cross-sections, the relative confidence interval difference (RCID), as defined by Eq 4-9, was employed.

$$BIAS = \frac{\sum y_e - \sum y_r}{\sum y_r} 100\% \quad (4\text{-}7)$$

$$MAPE = \frac{1}{n}\sum\left(\frac{y_e - y_r}{y_r}\right) 100\% \quad (4\text{-}8)$$

$$RCID = \frac{(y_{e\_up} - y_{e\_low}) - (y_{r\_up} - y_{r\_low})}{y_{r\_pred}} \quad (4\text{-}9)$$

where, y_e is the estimated series, y_r is the reference series, y_{e_up} and y_{e_low} are the upper and lower limits of 95% confidence interval of the estimated discharge, y_{r_up} and y_{r_low} are the upper and lower limits of 95% confidence interval of the reference discharge y_{r_pred}.

4.4 Results

4.1 Evaluation on the AGE method

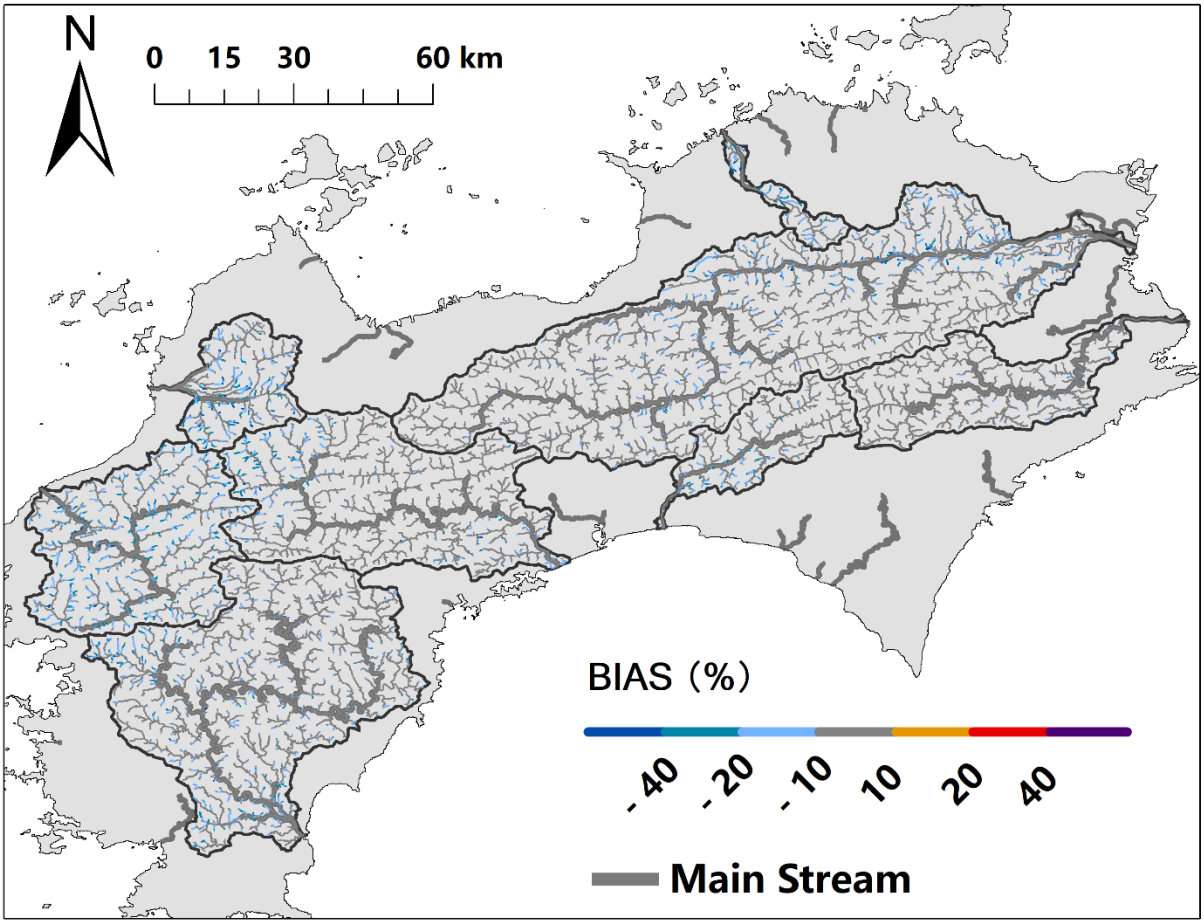


Figure 4-6 BIAS of discharge at 100-year return period (AGE method V.S. all valid events)

Based on the 2,966 events extracted by the AGE method, the 100-year discharge at each river grid is estimated. BIAS values, computed by comparing these estimates with those from all valid events, are mapped in Figure 4-6. The results show that BIAS generally falls within ±10%, with only a few upstream grids exhibiting errors between -20% and -10%. These larger upstream errors are attributed to the smaller catchment areas (0.1–0.2 km²) and low discharge quantiles (1–2 m³/s), making BIAS more sensitive to minor fluctuations. However, this error remains acceptable, as infrastructure design and adaptation planning primarily rely on discharge quantiles in middle and downstream reaches.

Overall, the AGE method demonstrates high accuracy in estimating discharge quantiles across multiple locations. Precipitation variability is expected to enhance event variability (i.e., FFA-relevant events in downstream areas differ from those upstream), yet the high accuracy across most river grids indicates that the 2,966 identified events effectively capture these differences. Furthermore, compared to simulating 720 years of hourly data, the AGE method significantly reduces computational demands. This efficiency is particularly valuable for regional applications, as small river basins, characterized by rapid hydrodynamic responses, require high-resolution yet computationally intensive simulations, such as hourly modeling (Shehata and Mizunaga, 2018). Both infrastructure design, which relies on historical ensembles, and climate change assessments using climate projection ensembles can benefit from the AGE method.

4.4.2 Evaluation on the precipitation stretching method

Figure 4-7 shows the BIAS between the 100-year return level discharge obtained using the PrecStre-I method and the benchmark. The results reveal significantly larger errors compared with those based on the AGE method, with no discernible spatial distribution characteristics or consistent error patterns along river channels. The results from the PrecStre-I method show both overestimation and underestimation. A typical example is the Monobe river basin, where the distribution of BIAS reveals overestimation ranging from 20% to 40% in the main stream, with some segments on tributaries exhibiting overestimation exceeding 40%, while others show underestimation exceeding -40%. Conversely, the Hiji river basin generally presents underestimated results, with BIAS mostly below -20%, and some segments even below -40%. These errors stem from the uncertainty in the spatial and temporal distribution of the six precipitation events, which were selected for stretching. Due to the

nonlinear effect of basins, precipitation events with different spatiotemporal distribution can lead to varying discharges, even if they share the same total precipitation. When the distribution patterns of the selected events are dominated by patterns that tend to cause low discharge, the estimated discharge quantiles will be underestimated even if using the largest value among the six events. The results suggest that designing precipitation events to estimate discharge quantiles at multiple locations within a basin, based on a limited number of precipitation patterns, poses significant risks, potentially leading to large errors and spatial uncertainty.

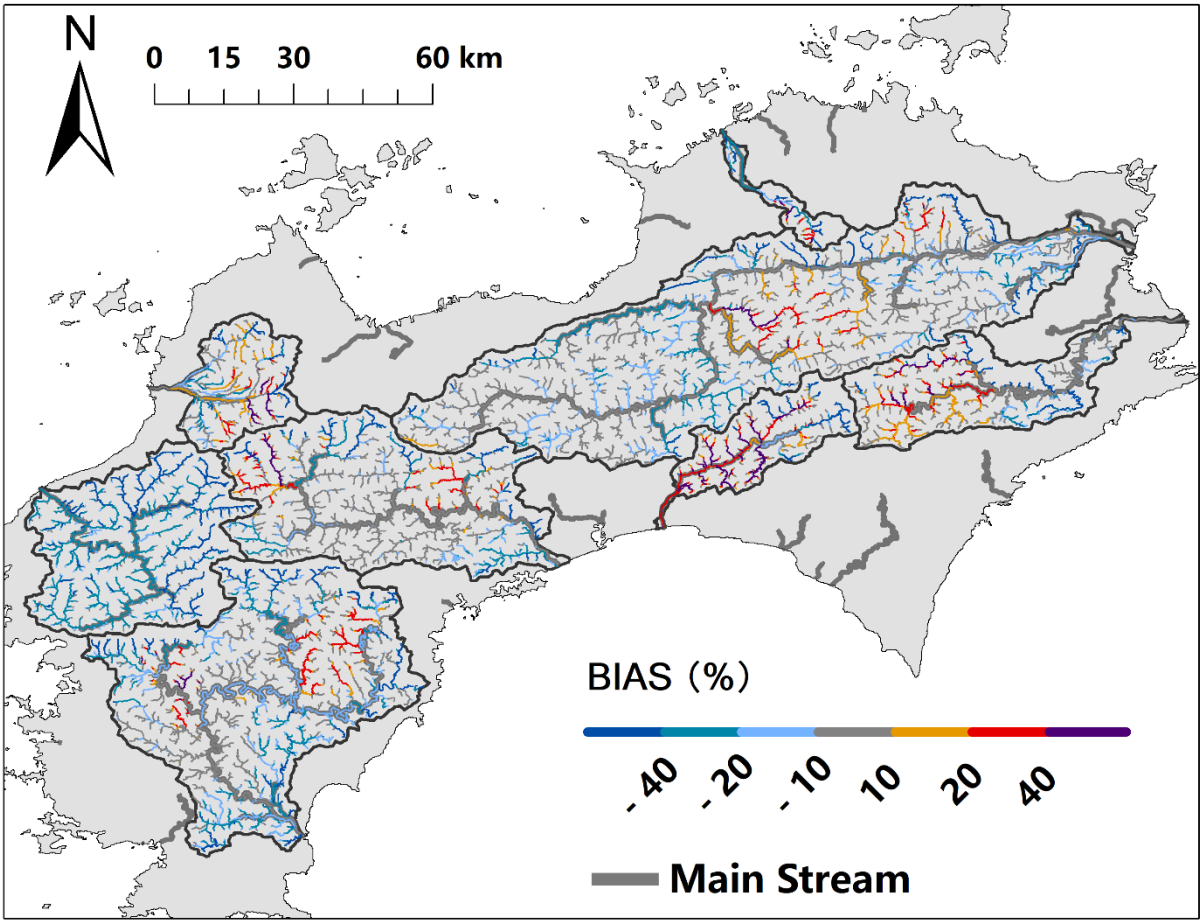


Figure 4-7 BIAS of discharge at 100-year return period (PrecStre-I method V.S. all valid events)

Figure 4-8 portrays the BIAS of discharge quantiles at 100-year return period, obtained through the PrecStre-S method. Similar to Figure 4-7, the results of the PrecStre-S method exhibit large errors and unpredictable error patterns. In Figure 4-7, both the Hiji and Watari river basins primarily show underestimations, whereas they exhibit significant overestimations in Figure 4-8. This discrepancy is related to the uncertainty in spatiotemporal distribution of the selected events. According to

Tables 4-3 and 4-4, the target rainfall amount derived from the PrecStre-I and PrecStre-S methods show no significant difference for the Watari river basin (545 mm and 547 mm) and the Hiji river basin (414 mm and 410 mm), respectively. Both event sets, i.e., the six events selected by PrecStre-I and PrecStre-S, respectively, were stretched to similar total precipitation. However, the selected events of PrecStre-S were dominated by patterns that tend to lead to severe floods, whereas the PrecStre-I exhibited the opposite, resulting in the opposing error patterns. This outcome highlights the sensitivity of discharge response to the spatiotemporal distribution of precipitation events. Underestimations can be mitigated by incorporating a larger number of precipitation events; however, this may also introduce extreme precipitation patterns, potentially exacerbating overestimations.

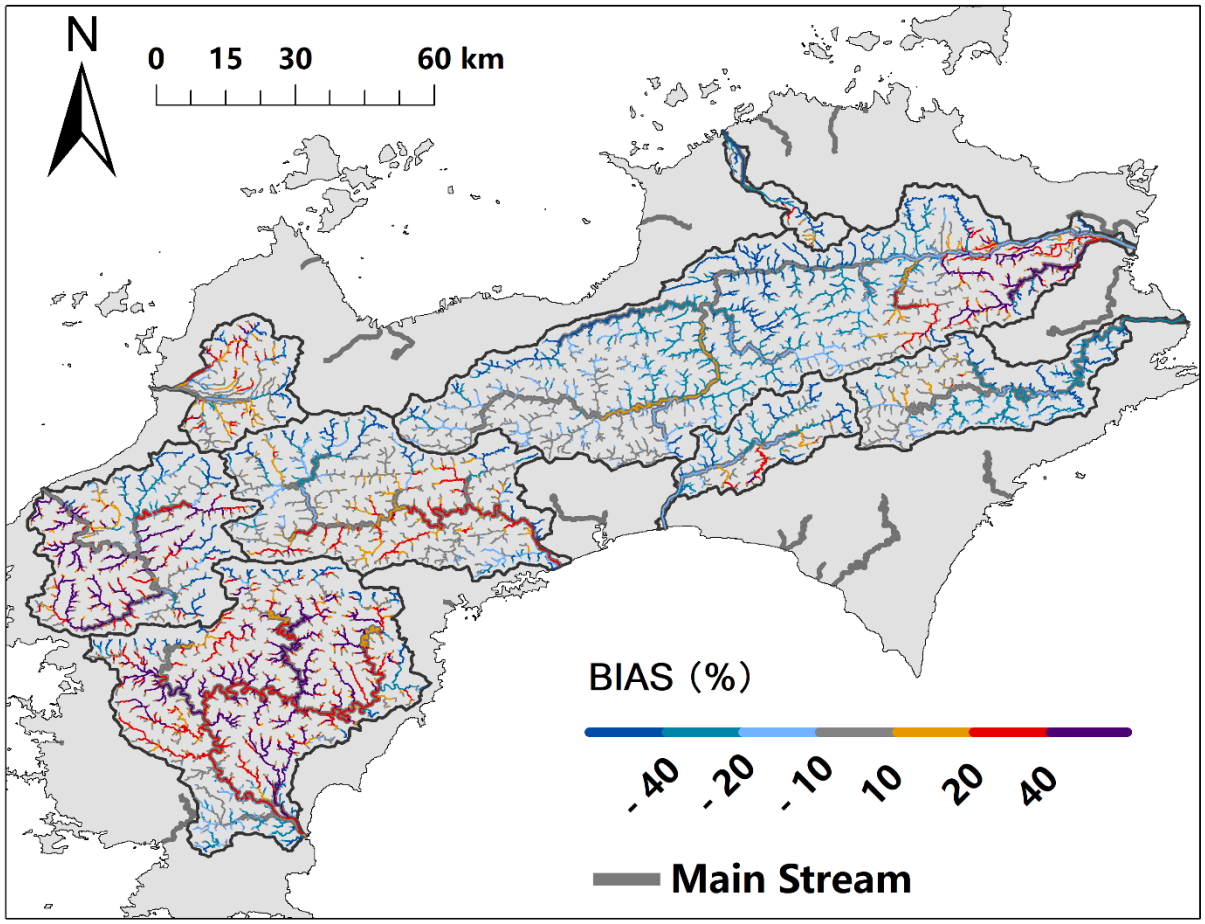


Figure 4-8 BIAS of discharge at 100-year return period (PrecStre-S method V.S. all valid events)

In summary, the precipitation stretching method, whether treating the ensemble data as an integrity in the PrecStre-I approach or as separate, independent members in the PrecStre-S approach, struggles to accurately estimate design discharges for multiple

river cross-sections within a basin. The variability of precipitation and the sensitivity of discharge response are the primary reasons for the errors and uncertainties. These results underscore the importance of considering the effect of precipitation variability and the advantages of the AGE method.

4.4.3 Error and uncertainty pattern

In this section, we further compared the performance of the three methods, focusing on the accuracy and uncertainty of discharge quantiles (at 100-year return period) in different relative locations of a basin. Firstly, we compared the accuracy of discharge quantiles across all river grids on Shikoku Island and the outlets of the eight main basins. Figure 4-9 shows the results, and Table 4-5 provides the statistical evaluation outcomes.

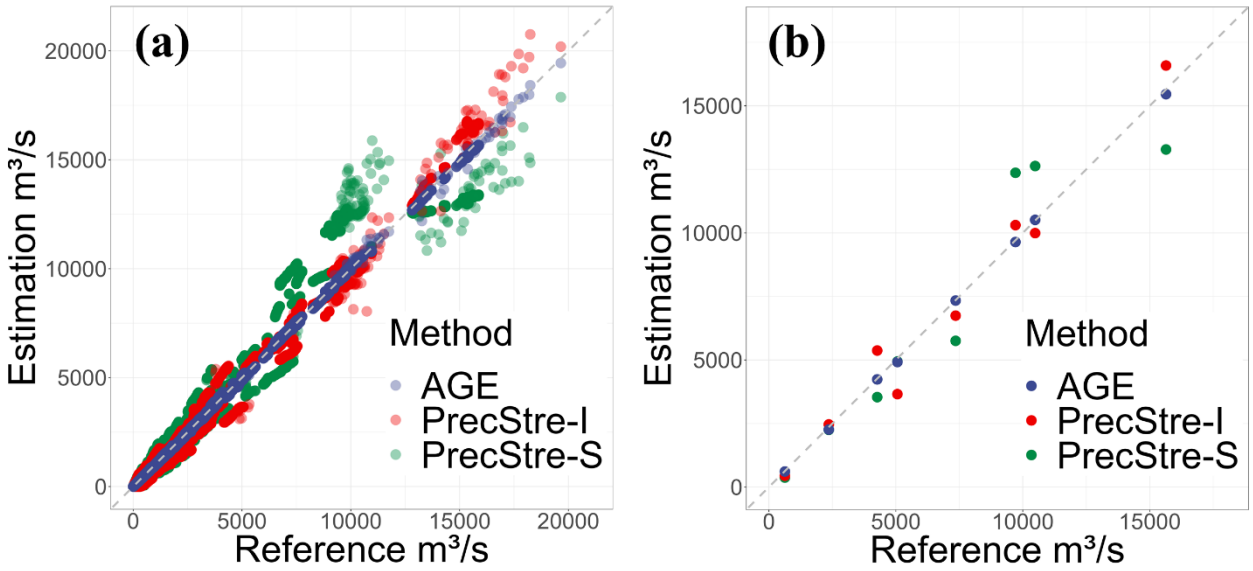


Figure 4-9 Evaluation results of discharge quantiles at 100-year return period (a) across Shikoku Island, and (b) at the basin outlets

The AGE method demonstrated consistent and high accuracy both across Shikoku Island and at the outlets, with BIAS values of 1%, as well as MAPE values of 6% and 2%, respectively. Both the PrecStre-I and PrecStre-S methods exhibited small BIAS values, indicating accurate estimation of total precipitation. However, the large MAPE values suggest inaccuracies in the estimations at individual river grids, which can be attributed to discrepancies in the spatiotemporal distribution of precipitation. In the outlets, the MAPE of the precipitation stretching method showed a significant improvement, decreasing from 38% to 23% (PrecStre-S) and 34% to 16%, indicating its potential as an alternative method for designing discharges in the downstream. Basin

outlets typically have high demands for flood control infrastructures due to concentrated populations and properties. Despite achieving higher accuracy, the AGE method requires relatively higher computational resources. The precipitation stretching method holds engineering value for designing discharges at basin outlets in scenarios with limited computational resources.

Table 4-5 Statistical evaluation results of the PrecStre-S, PreStre-I, and AGE methods at different scales

Scale	Method	BIAS (%)	MAPE (%)
Shikoku	PrecStre-S	-4	38
	PrecStre-I	4	34
	AGE	1	6
Outlets	PrecStre-S	1	23
	PrecStre-I	0	16
	AGE	1	2

Secondly, we calculated the ratio of the upstream contribution area to basin area for each river grid (i.e., relative basin area, RBA). Figure 4-10 portrays the categorized BIAS values of river grids based on their RBA. In the upstream areas of basins (RBA ≤ 20%), outliers appear more frequently as low discharges are more sensitive to the changes. Neglecting the outliers, the AGE method performs better than the precipitation stretching method with BIAS more concentrated and closer to 0. Moving to the middle parts of basins (20% < RBA ≤ 90%), the occurrence of exceptionally large BIAS values significantly reduces. BIAS values of the AGE method are concentrated around 0, whereas those of the precipitation stretching method distribute within a range of ±50%. The BIAS values of PrecStre-I are close to 0 in sections with 50% < RBA ≤70%, while PrecStre-S did not exhibit similar favorable results. This phenomenon does not imply that PrecStre-I outperforms PrecStre-S within this range. Rather, as the only difference lies in the spatial distribution of precipitation, the performance variation is primarily attributed to the uncertainty in precipitation variability. In the downstream areas (RBA > 90%), the AGE method continues to outperform the other methods. BIAS values of both PrecStre-I and PrecStre-S methods reduce to a range of ±25%. Discharges in the downstream are less susceptible by precipitation variability.

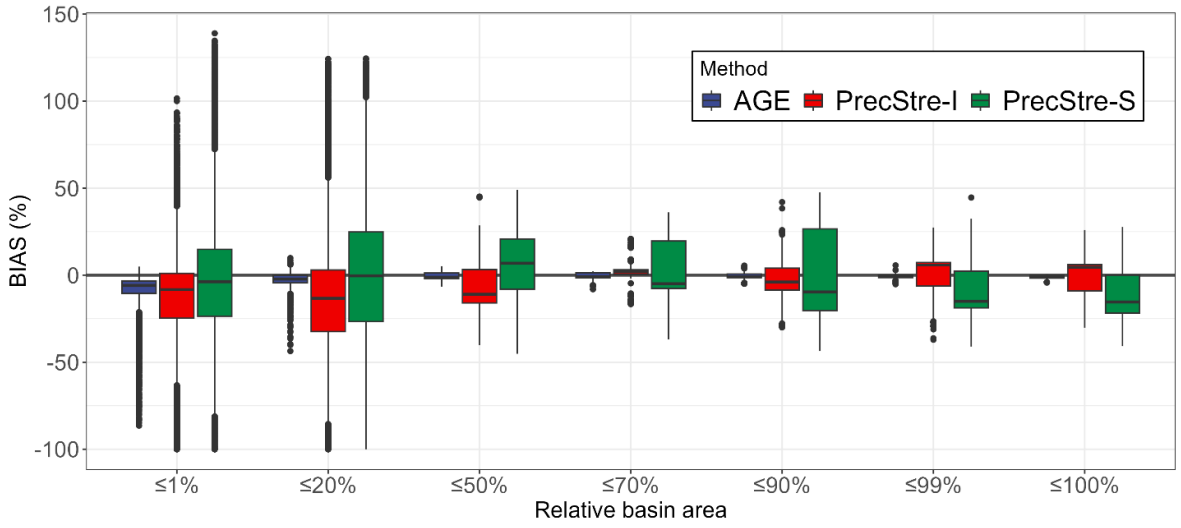


Figure 4-10 Distributions of BIAS of discharge quantiles obtained from the AGE, PrecStre-I, and PrecStre-S methods vary with relative basin area

The RCID was used to evaluate the relative changes in the 95% confidence interval associated with the estimation of discharge quantiles. Positive RCID values denote an increase in uncertainty compared to the reference, while negative values indicate a decrease. Notably, the uncertainty here pertains specifically to the uncertainty related to quantile estimation, rather than the accuracy uncertainty or inherent uncertainty of model outputs.

Figure 4-11 portrays the categorization of RCID values based on the RBA. RCID values derived from the AGE method are predominantly centered around zero, suggesting a consistent uncertainty level relative to the reference results. Similarly, RCID values from the PrecStre-I method demonstrate a comparable distribution to those from the AGE method. In contrast, the PrecStre-S method exhibits substantially increasing uncertainty levels at all RBA ranges, highlighting that data utilization plays a more critical role in uncertainty than the frequency analysis method or basin scale. Since PrecStre-S estimates 100-year precipitation using 60-year data, its confidence interval is wider than that derived from 720-year data, and hydrodynamic simulations are likely to sustain or even amplify this uncertainty. Therefore, for minimizing uncertainty in frequency analysis, it is recommended to treat ensemble data as a whole, rather than averaging individual members.

In summary, owing to the well design towards precipitation variability, the AGE method can obtain accurate and reliable discharge quantiles for all river cross-sections in a region. The precipitation stretching method offers simplicity, and can be used for providing discharge quantiles downstream, while to limit the uncertainty

of estimations, the PrecStre-I method is recommended for enhanced reliability.

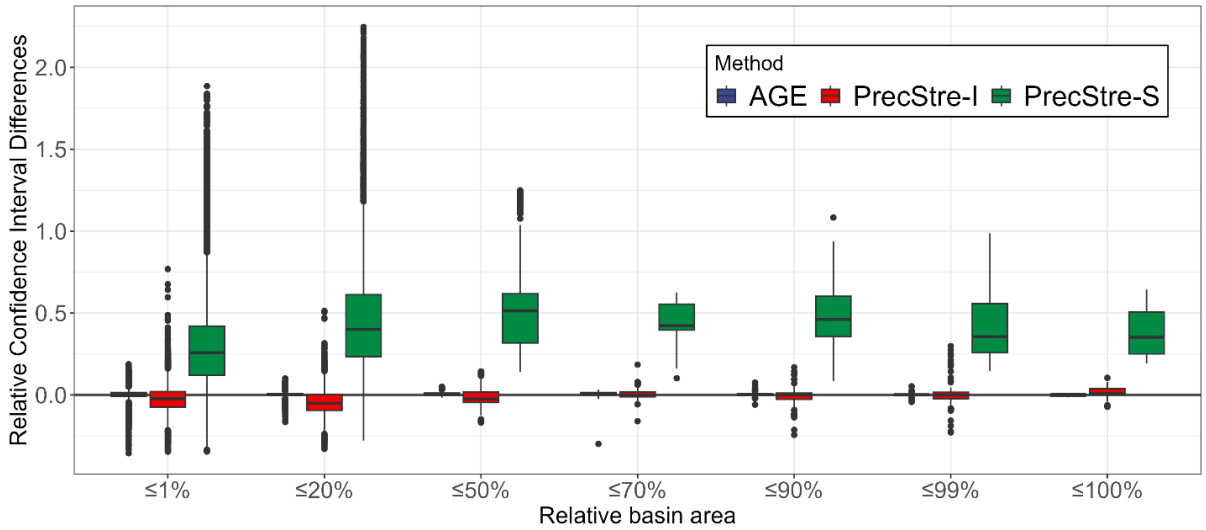


Figure 4-11 Distributions of relative confidence interval differences (RCID) values in different relative basin area (RBA) ranges

4.5 Discussion

The interaction between ensembles and flood modeling is a common focus in flood forecasting, primarily aimed at quantifying uncertainty and enhancing reliability (Caseri et al., 2016; Zsoter et al., 2020). Unlike short-term forecasting, advances in high-performance computing have enabled the generation of long-duration climate ensembles, facilitating robust flood frequency estimation under specific climate conditions (Kawase et al., 2023). For instance, historical ensemble outputs from d4PDF are being explored for infrastructure planning, while ensembles representing 2˚C and 4˚C warming above pre-industrial levels are widely used to assess climate change impacts and inform disaster prevention strategies (Budhathoki et al., 2022; Ishii and Mori, 2020; Sasai et al., 2019; Tanaka et al., 2021; Zhao et al., 2023c). Notably, unlike most scenario-based ensembles, d4PDF employs pseudo-global warming simulations (Tanaka et al., 2023; Zhao et al., 2023c), allowing for frequency analysis under specific climatic conditions while avoiding non-stationarity issues (Taniguchi et al., 2022), enhancing practicability. Climate ensembles are expected to play an increasingly critical role in flood risk management, and advancements in downscaling techniques will further enhance research on localized disaster events. To fully leverage high-resolution climate ensembles, the development of information distillation techniques—methods for extracting key information from large datasets—remains essential.

Spatiotemporal precipitation variability is a key factor influencing flood simulation outcomes and is expected to intensify under climate change (Wasko et al., 2021; Zhao et al., 2023c). This study evaluates methods that account for such variability when estimating flood quantiles across a basin. The results show that while the precipitation stretching method incorporates multiple possible precipitation distributions, it still introduces substantial errors, particularly in upstream areas where localized precipitation patterns are more pronounced than in downstream regions. This underscores the risks of designing precipitation scenarios based purely on statistical approaches, which may overlook critical physical variability. In contrast, the AGE method directly extracts precipitation events from the ensemble, preserving the physical consistency of spatiotemporal distributions. Additionally, its multi-location and multi-scale event identification strategy ensures robust performance across different basin regions. Thus, when computational resources allow, the AGE method serves as a superior alternative to precipitation stretching, as it more effectively accounts for precipitation variability.

A primary function of ensembles is to reduce uncertainty in projection results, which is particularly crucial for climate change studies where minimizing uncertainty is a key objective (Kita and Yamazaki, 2023; Satoh et al., 2018; Zelinka et al., 2017). This study highlights that different ensemble utilization strategies result in significant variations in uncertainty, which then propagate through the modeling chain. To mitigate uncertainty, it is recommended to maximize sample usage, such as treating the ensemble as an integrated dataset rather than relying on individual members. It is important to note that d4PDF members originate from the same model and can be considered independent identically distributed (Fujita et al., 2019; Kawase et al., 2023; Mizuta et al., 2017). In contrast, climate projection ensembles (e.g., ensembles from Coupled Model Intercomparison Project) are derived from different general circulation models, meaning their members should not be indiscriminately combined for analysis.

The duration used for frequency analysis and simulation in the precipitation stretching method is longer than the approximate river concentration times listed in Table 4-2, as it is intended to incorporate not only the peak flow processes but also the initial and post-event hydrological responses. More detailed stretching approaches could be considered—for example, calculating scaling factors based solely on precipitation within the concentration time and applying them to 48-hour events, or stretching only the precipitation within the concentration time while

preserving the original initial and post-event rainfall. However, these alternative schemes introduce additional uncertainties and lack validations. Therefore, this study adopts a consistent 48-hour duration throughout the process—from frequency analysis to event stretching. While incorporating concentration time could potentially lead to the selection of more concentrated precipitation segments and thus higher discharge peaks, Figure 4-9(c) shows no significant underestimation when compared with the reference results. This supports the validity of using the 48-hour duration in this study.

A limitation of this study is that we did not evaluate how the performance of the precipitation stretching method changes with variations in the number of selected events and more complex designing strategies, such as manually designing for multiple sub-basins. It is possible that their performance could be further improved through such adjustments. However, despite this limitation, we still recommend the AGE method due to its automation and universality, which make it a robust choice for a wide range of applications.

4.6 Conclusions

The use of ensemble data for process-based FFA ensures high physical reliability but incurs significant computational costs. Event-based simulation methods can mitigate these demands; however, careful consideration of precipitation variability is essential. This study assesses the performance of two such methods—AGE and precipitation stretching—both of which incorporate precipitation variability in different ways, using a 720-year ensemble dataset. Additionally, the study examines how different ensemble utilization strategies influence uncertainty propagation. Discharge quantiles for all river grids on Shikoku Island, estimated from 25,700 valid precipitation events, serve as reference values.

The results demonstrate that event-based methods can effectively capture precipitation spatiotemporal variability and accurately estimate flood quantiles across various basin locations, provided a multi-location, multi-scale event identification approach—such as the AGE method—is employed. Specifically, apart from a few river source grids, discharge quantiles estimated using AGE exhibit high accuracy across the basin, with BIAS values within ±10%. The method also maintains spatial consistency, with MAPE values of 6% for the entire basin and 2% at the basin outlet. While the precipitation stretching method considers multiple possible

precipitation distributions, its estimated quantiles show both overestimation and underestimation, with biases reaching ±40%. These errors are largely driven by event selection, leading to substantial uncertainty. The method performs better in downstream regions (RBA > 90%) than upstream, with MAPE values of 23% (PrecStre-S) and 16% (PrecStre-I) at the basin outlet.

Regarding ensemble utilization strategies, using all members or ensemble means does not significantly affect discharge quantile accuracy in downstream regions but has a notable impact on uncertainty propagation. When utilizing the full 720-year dataset, both the AGE method and PrecStre-I yield RCID values near zero across different RBA ranges. In contrast, using ensemble means (PrecStre-S) results in a median RCID of 0.25 to 0.50, indicating that the 95% confidence interval is inflated by 25% to 50% compared to reference results.

Thus, when computational resources allow, the AGE method is the optimal ensemble utilization approach. The precipitation stretching method remains viable for estimating downstream discharge quantiles. Due to its impact on uncertainty propagation, PrecStre-I is the preferred approach.

These findings offer valuable insights for disaster prevention applications of climate ensembles and regional climate change impact assessments.

5. Projecting future floods at multiscale rivers over Japan[1]

Abstract

This chapter addressed computational challenges in high-resolution, large-domain, process-based flood quantile estimation, focusing on Japan's future flood risks at a 150 m resolution. Using the Aggregating Grid Event (AGE) method, Rainfall-Runoff-Inundation (RRI) model, and Peaks-Over-Threshold (POT) approach, it incorporates 2,160-year precipitation from a 5-km dynamically downscaled ensemble (d4PDF DDSJP) across three climate stages (historical, +2˚C, +4˚C). The AGE method identified critical precipitation events for the flood quantile estimations and the POT method was employed to estimate 100-year discharge (Q100) for over 2.2 million river grid cells. Key findings include: (1) Nationwide, 100-year discharge (Q100) is projected to increase 1.16 times (+2˚C) and 1.37 times (+4˚C), with equivalent return periods reduced to 45 years (+2˚C) and 23 years (+4˚C). Northern regions (Hokkaido and Tohoku) are particularly climate-sensitive, exceeding national averages in Q100 increases. (2) Small river basins and transition zones from plains to mountains exhibit higher increase ratios, necessitating targeted flood prevention measures. (3) Flash flood risks are expected to rise, with most national A-class basins seeing flashiness increases of over 10% (+2˚C) and 20% (+4˚C). Southern Japan faces further flash flood intensification, while Northern Japan under +4˚C stage anticipates significant new challenges. The study underscores the urgency of adaptive flood management strategies to mitigate increasing risks, offering a foundation for informed policymaking and public-engaged mitigation. Simulation data opens pathways for further research on cascading disaster scenarios in +2˚C and +4˚C climates.

[1] This chapter is based on the publication:

Chen, J., Sayama, T., Yamada, M., Tanaka, T., Sugawara, Y. (2025) Projecting multiscale river flood changes across Japan at +2˚C and +4˚C climates. ***Earth's Future***, 13(5), e2024EF005884

5.1 Introduction

Global warming-induced changes in precipitation and floods are pressing concerns (Blöschl et al., 2019; Donat et al., 2016; Hirabayashi et al., 2013; Prein et al., 2017; Tellman et al., 2021; Winsemius et al., 2016). Human populations face heightened flood risks due to increased frequency of extreme precipitation events (Li et al., 2019; Qin et al., 2022). Decision makers, ranging from national governments to local residents, urgently require understanding of forthcoming flood characteristic changes, such as flood frequency, in their respective regions to formulate adaptation plans effectively (IPCC, 2022; Owen, 2020; Soergel et al., 2021).

Although the Clausius-Clapeyron equation suggests atmospheric water capacity increases about 6.5% per degree Celsius (Allen and Ingram, 2002), the actual increase in extreme precipitation may deviate from this value due to differences in storm dynamics and structure, as well as in larger scale weather patterns (Fowler et al., 2021; Moustakis et al., 2021; Wasko et al., 2021; Westra et al., 2014). Meanwhile, the nonlinear effects of basins further complicate the increase relation between extreme precipitation and floods (Quintero et al., 2022; Stephens et al., 2018; Vangelis et al., 2022). Currently, assessing the impact of future climate change on floods relies on the application of general circulation models (GCMs) and hydrological models.

To better represent the spatial structures of climatic variables, simulation results from GCMs require further dynamic downscaling through nested regional circulation models (RCMs) (Ishizaki, 2022; Sasaki et al., 2011; Sunyer et al., 2017). Studies indicate that kilometer-level grids can effectively capture mesoscale weather systems, closely linked to flash floods, while sub-daily extreme precipitation data improves flash flood simulations (Ficchì et al., 2016; Younis et al., 2008). Moreover, ensemble data adoption is critical to ensure robust conclusions, given the sensitivity of climate simulations to model structures and initial conditions (Ali et al., 2018; Cloke et al., 2013; Kim et al., 2020; Leduc et al., 2019; Michalek et al., 2023; Shiogama et al., 2021; Try et al., 2022).

A range of downscaled climate projection ensemble datasets have supported regional studies on climate change impacts (Ali et al., 2018; Gutowski Jr. et al., 2016; Jacob et al., 2020; Leduc et al., 2019; van der Linden and Mitchell, 2009). Most studies typically utilize emission scenario-based climate ensembles, whose future forcings such as greenhouse gases are designed according to representative concentration pathway

(RCP) and shared socioeconomic pathway (SSP) scenarios (James et al., 2017). Consequently, these ensembles offer transient insights into global warming, where warming levels vary over time. However, developing local adaptation strategies necessitates insights at specific target warming levels. To robustly project consequences of climate reaching specific stages, Mizuta et al. (2017) proposed a warming stage-based simulation scheme, culminating in the development of the database for Policy Decision making for Future climate change (d4PDF). This scheme extracts GCM outputs (from emission scenario-based simulations) when global-mean surface air temperature reach 2˚C or 4˚C warmer than preindustrial levels, serving as boundary conditions (Fujita et al., 2019). Over 5,000-year samples per warming stage were generated through extensive simulations. The ensemble dataset facilitates obtaining frequency of extreme events, including snow, precipitation, typhoons, and storm surges, while ensuring that the statistical characteristics of samples remain consistent over time (Hatsuzuka et al., 2020; Kawase et al., 2016; Mori et al., 2019; Tanaka et al., 2020, 2021; Zhao et al., 2023c). Recently, hourly d4PDF has undergone dynamic downscaling from 60 km to 20 km and further to 5 km resolutions (Ishii and Mori, 2020; Kawase et al., 2023).

With the goal of projecting future flood changes using climate ensembles, some focus on a global, continental scale, or major basins worldwide (i.e., macroscale), seeking to understand changing trends in flood occurrence across various regions to estimate associated risks and potential damages (Alfieri et al., 2015a, 2018; Arnell and Gosling, 2016; Chen et al., 2023; Hirabayashi et al., 2013; Lim et al., 2018; Try et al., 2022). Another subset of studies comprehensively investigates mechanisms and responses within a specific basin or sub-basin (i.e., microscale) using fine-scale models that consider complex processes (Shi and Shiraiwa, 2023; Silva and Portela, 2018; Tanaka et al., 2020; Yamamoto et al., 2021; Zhao et al., 2016). However, few studies recognize the importance of mesoscale analysis, which projects future floods using high-resolution, process-based hydrologic models on a national or regional scale. Mesoscale research serves to bridge the gap between macroscale and microscale studies, facilitating a comprehensive understanding of future flood changes. Moreover, mesoscale research addresses limitations of both macroscale and microscale approaches: macroscale research struggles to represent hydrological properties of all river channels including in small-to-medium rivers, while microscale research faces challenges in extracting general insights from a singular basin. Although mesoscale research offers various advantages as mentioned above, it has

not yet been widely conducted due to limitations in methodology, model efficiency, and computational resources.

To enhance understanding of future flood patterns across multi-scales in Japan, this study conducted high-resolution flood simulations (150 m spatial and 1-hour temporal resolution) from a mesoscale perspective, utilizing the d4PDF dataset, which encompasses 720-year data per climatic stage (historical, +2˚C, and +4˚C). This work has considered the data issue (i.e., resolution effects, representativeness of warming stages) and the scale issue (i.e., mesoscale flood simulations). To the best of our knowledge, this represents an unprecedented large-domain, high-resolution flood projection at specific warming levels. This study aims to investigate (1) the national patterns in extreme flood changes across warming stages; (2) the regional trends relate to basin attributes (basin size and elevation); (3) changes in flood processes. This study underscores the value of mesoscale studies for regional flood mitigation strategies, and providing future flood information with an easily perceptible resolution to enhance public understanding of climate change impacts. The simulated data is expected to support further studies on cascading impact assessment.

5.2 Study area and data description

5.2.1 Study area

Japan, situated in East Asia, comprises four major islands spanning approximately 378,000 km^2. About 75% of its terrain is hilly and mountainous, resulting in pronounced river gradients throughout the country (Yasuda et al., 2016). Meanwhile, due to the predominance of short river lengths, the flood types are dominated by flash floods, characterized by high destructiveness (Higashino and Stefan, 2019).

Lateral subsurface flow plays an important role in the runoff component because of the large area of mountains and forests, posing challenges for flood simulations. Extreme precipitation, primarily from typhoons and quasi-stationary frontal systems, notably impacts the southern (below about 36 ° N) and southwestern regions (Hirockawa et al., 2020; Kamahori and Arakawa, 2018; Kato, 2020). Historical events such as Typhoons Jebi and Hagibis have caused significant damage (Sayama et al., 2020; Takabatake et al., 2018; Tanaka et al., 2023). Typhoons originating from the Pacific Ocean typically move northward, primarily making landfall between Kyushu and Kanto. Frontal rainfall occurs in summer and autumn, initially affecting northern

Kyushu and gradually extending northward to Tohoku as autumn progresses. Typical weather system patterns can be referenced in Grossman et al. (2015), Osakada and Nakakita (2018) and Ohya and Yamada (2024). The population is densely concentrated in the coastal plains of the Kanto, Chubu, and Kinki regions, which are home to some of the world's most densely populated cities, including Tokyo, Nagoya, and Osaka. Japan faces a high flood risk due to the abovementioned factors of topography, climate, population distribution. To facilitate analysis, Japan is divided into 14 regions (Figure 5-1), primarily based on administrative divisions, with adjustments made to account for geographical characteristics and integrity of basins.

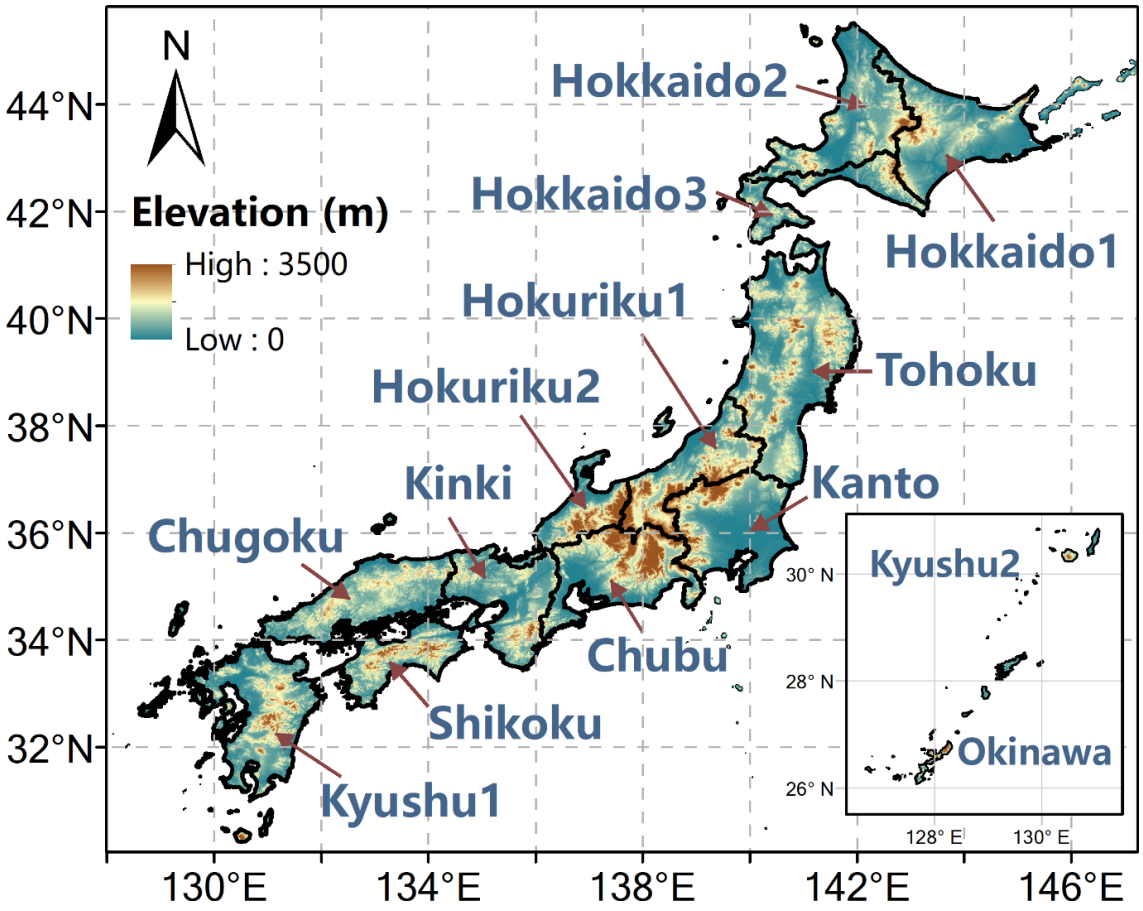


Figure 5-1 Topography of Japan and the locations of 14 regions, adjusted from official administrative divisions based on basin boundaries

5.2.2 Ensemble climate projection dataset

The hourly precipitation data used in this study sourced from the 5-km dynamically downscaled d4PDF (DDSJP), fully covering Japan and well reproduced the historical extreme precipitation (Kawase et al., 2023). The original d4PDF data was produced

through 60-km global experiments using the Meteorological Research Institute Atmospheric General Circulation Model 3.2 (MRI-AGCM3.2) (Mizuta et al., 2012, 2017). The 5-km version was further downscaled using the Non-Hydrostatic Regional Climate Model (NHRCM) (Sasaki et al., 2008). For details on the downscaling methodology, refer to Kawase et al. (2023). The DDSJP has 720-year sample for each warming stage (historical, +2˚C, and +4˚C). The +2˚C stage aligns with the goal of the Paris Agreement, while the +4˚C represents the status of far-future (circa 2100) under the RCP 8.5 scenario. The 720-year data of historical stage consists of 12 60-year members, each simulated with distinct initial perturbations spanning from 1951 to 2010. The data in future stages (720 years per stage) were generated through 60-year simulations based on 12 boundary conditions, comprising combinations of six sea surface temperatures (SSTs) from various GCMs and two perturbations (Mizuta et al., 2017). Notably, different from emission scenario-based simulation, d4PDF was designed for iteratively simulating at a specific warming stage, rendering the number of years in future stages as indicative of data size rather than a time concept. All meteorological events are considered from the same independent and identically distribution under the specified warming stage, thus the 720-year data was directly used for frequency analysis (Chen et al., 2024; Ishii and Mori, 2020; Kawase et al., 2023; Sasai et al., 2019; Zhao et al., 2023c). Compared with the 20-km version, the 5-km DDSJP was proved to have better reproducibility of typhoon-related, frontal, and localized extreme precipitation (Kawase et al., 2023).

5.3 Methodology

5.3.1 Event extraction method

Conducting 150-m resolution simulations nationwide with a large ensemble requires substantial computational resources, while sizable portion of 720-year hourly data does not significantly contribute to extreme floods. Regarding that precipitation is the dominant factor causing flooding, even in northern regions (Nguyen et al., 2020), thus, to enable feasible simulations, the aggregating grid event (AGE) method was employed to extract extreme precipitation events (Chen et al., 2025c). This method comprehensively identifies precipitation events that lead to basin and local floods through multi-scale grid-by-grid analysis. According to the average precipitation intensity during approximate river concentration time, the largest n events per precipitation grid were selected. As the final extracted events are used for flood

frequency analysis, *n* is set to 72, corresponding to a 10-year return period. Eventually, by aggregating the selected events from different grids and scales along the temporal axial, the start and end times of events for extraction were determined. The AGE method, rooted in hydrological concepts, comprehensively considers the impact of spatiotemporal precipitation variability, thereby aiding in the accurate estimation of discharge quantiles for every river grid, which had been proved in a previous study (Chen et al., 2025c).

5.3.2 Rainfall-Runoff-Inundation (RRI) model

The RRI model is a two dimensional (2D) distributed model, enabling simultaneously simulate river discharge and flood inundation (Sayama et al., 2012). It spatially classifies grids into river and land grids, employing one dimensional (1D) and 2D diffusion wave functions to describe water movement, respectively. The RRI model can well simulate lateral subsurface flow, vertical infiltration flow, and surface flow (Sayama and McDonnell, 2009). The numerical scheme, optimized using the fifth-order Runge-Kutta formula, ensures both accuracy and efficiency (Cash and Karp, 1990). Owing to the advantages of accuracy, efficiency, and extendibility, the RRI model has been widely applied in Southeast Asia and Japan (Bhagabati and Kawasaki, 2017; Rasmy et al., 2019; Sayama et al., 2017, 2020; Try et al., 2022; Yamamoto et al., 2021).

This study built a 150-m resolution RRI model covering Japan. This model operates with a unit timestep of smaller than 10 minutes in land grids and smaller than 1 minute in river grids, outputting hourly discharge and inundation processes. Hydraulic parameters (refer to the Table S5) were correlated with soil and land use type, enhancing the physical interpretability. The performance of validated RRI model can be obtained from the Figures S5 to S6. The 150-m RRI model integrated surveyed river cross-section data and 121 national dams, as indicated in the Figure S9 (Ly et al., 2021; Yamada et al., 2022). Simple operational ruler was used for simulating the effect of dams. Topography and flow direction data were sourced from 30-m Japan flow direction map (J-FlwDir) (Yamazaki et al., 2020), and upscaled using an algorithm developed by Masutani et al. (2006). River grids were identified when the number of upstream contributing grids exceeded 50, corresponding to an area larger than 1.125 km^2. This study encompassed over 2.2 million river grids in the RRI model.

5.3.3 Flood frequency analysis

The Peaks-Over-Threshold (POT) method is employed to estimate flood frequency curves by fitting the generalized Pareto distribution (GPD, Eq. 5-1) to extreme values exceeding a defined threshold (Chen et al., 2025c; Pan et al., 2022). A higher threshold effectively reduces data demand, while the POT method, due to its data-filtering approach, minimizes the risk of missing extreme values compared to the block maxima method (Chen et al., 2024; Cunnane, 1973; Madsen et al., 1997). The threshold of POT method can be an exact value or a specified probability. This study extracted the 72 largest discharge peaks for each river grid from extensive simulation results based on events identified using the AGE method. Given the utilization of 720-year data, the 72 largest values correspond to the 10-year return period threshold. The POT method was applied to all river grids to estimate the corresponding discharge at 100-year return period (Q100).

$$\boldsymbol{GPD}(\boldsymbol{x}) = \begin{cases} 1 - (1 + \xi\left(\frac{x-\mu}{\sigma}\right))^{-1/\xi} & for\ \xi \neq 0 \\ 1 - exp\left(-\frac{x-\mu}{\sigma}\right) & for\ \xi = 0 \end{cases} \quad (5\text{-}1)$$

where ξ, μ, and σ is the shape, location, scale parameter, respectively.

5.3.4 Evaluation method

The increase ratio (Eq. 5-2) was employed to describe the changes in flood peak at the same return period. This study focuses on quantiles corresponding to 100-year return period (i.e., Q100) as a common indicator for assessing the impact of climate change on floods. The historical stage was regarded as the baseline, and comparisons were made between the baseline and future stages (i.e., +2˚C or +4˚C). In Eq. 5-2, Q_b and Q_f represent the Q100 at historical and future stages, respectively.

Flashiness was used to assess the severity of flash floods (Li et al., 2023). As defined in Eq. 5-3, the flashiness (*F*) quantifies how quickly and how high discharge rises within a certain duration. Q_t represents discharge at timestep *t*; *d* is the duration, i.e., 6 hours in this study; CA denotes the upstream contribution area; and max() is a function that returns the maximum value. The unit of flashiness in this study is mm/h^2.

This study utilized a modified coefficient of variation (*M-CV*, Eq. 5-4) to assess the

variability of flood increase ratios within a region. Here, n is the total number of increase ratios, x_i is the i-th increase ratio, M is the median of the increase ratios. Compared with the conventional coefficient of variation, the *M-CV* replaces the mean with the median, resulting a more robust outcome.

$$Icrease\ Ratio = \frac{Q_f}{Q_b} \tag{5-2}$$

$$F = \frac{\max(Q_t - Q_{t-1}, Q_t - Q_{t-2}, \ldots, Q_t - Q_{t-d})}{CA \times d} \tag{5-3}$$

$$M\text{-}CV = \sqrt{\frac{1}{n-1}\sum(x_i - M)^2}\,/M \tag{5-4}$$

The Mann-Kendall (M-K) test is a non-parametric method for statistically assessing the presence of a monotonic trend in an ordered series, as outlined by Mann (1945) and Kendall (1975). The null hypothesis of the M–K test is that no monotonic trend exists. If the p-value of the M–K test is below 0.05, the null hypothesis can be rejected with 95% confidence. The test statistic, S is calculated by Eq. 5-5, where a positive (negative) value indicates an increasing (decreasing) trend.

$$S = \sum_{j-1}^{n-1}\sum_{i-j+1}^{n} sgn(m_i - m_j) \tag{5-5}$$

The M-K test is applied to detect trends in the median increase ratios across different basin sizes, with ratios grouped into 20 km² equally spaced basin area bins. Here, m_i is the increase ratio median for the i-th basin area (ordered from small to large); and $sgn()$ is an indicator function that returns 1, 0, or -1 based on the sign of $(m_i - m_j)$.

The Kolmogorov–Smirnov (KS) test is employed to evaluate whether two samples originate from the same distribution. The null hypothesis assumes that both samples come from the same distribution. In this study, the KS test evaluates the significance of flashiness changes across warming stages, with a 95% confidence level adopted to reject the null hypothesis.

5.4 Results

5.4.1 National trend

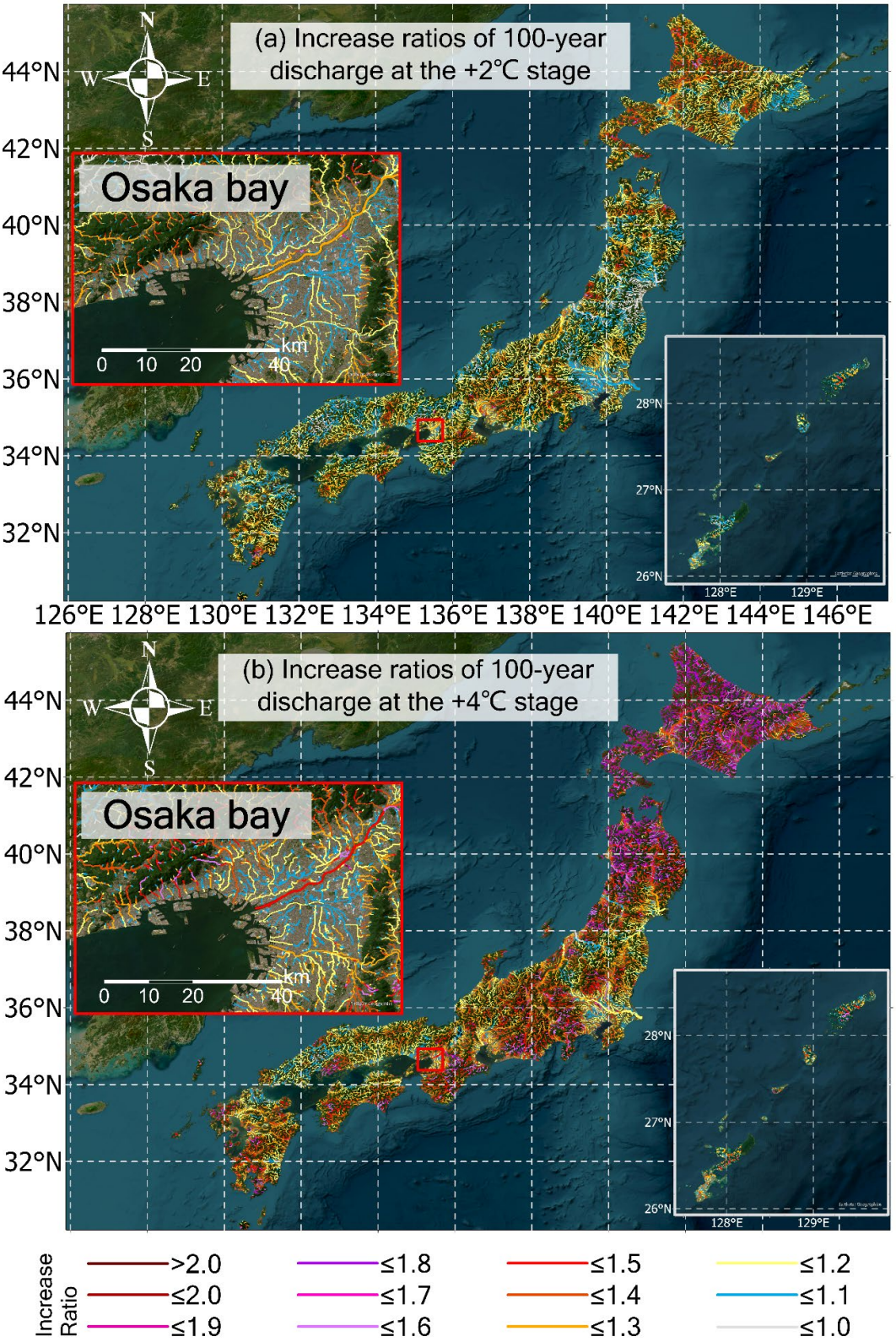


Figure 5-2 Spatial distribution of Q100 increase ratios at +2˚C (a) and +4˚C (b) stages. Osaka bay (red rectangle) is enlarged as an example to show tributary details in this study. Abbreviation: 100-year return period discharge (Q100)

The performance of discharge quantile reproducibility of the DDSJP can be found in the supplementary material Figure S10. In general, the DDSJP can well reproduce discharge quantiles on most regions. Figure 5-2 portrays the spatial distribution of the increase ratios in Q100 at the +2˚C and +4˚C stages. When the global climate is 2˚C warmer than the preindustrial era, predominantly the ratios range from 1.0 to 1.2. Higher increase ratios, between 1.2 and 1.4, are observed in the northern part (i.e., Hokkaido-1, -2, and -3 regions) and Chubu region. Although Q100s in Japan generally show an increasing trend at the +2˚C stage, a decreasing trend is observed in specific basins, such as those in the central Chugoku and southern Tohoku regions. These fine-grained patterns are revealed through high-resolution, dynamically downscaled ensembles, which effectively capture local extreme precipitation.

At the +4˚C stage, the spatial pattern of increase ratios shifts notably. Northern regions, including Tohoku and Hokkaido-1, -2, and -3, exhibit increase ratios between 1.5 and 2.0, followed by Chubu, southern coastal Kinki, Shikoku, and southwest Kyushu-1. Overall, the Q100 increase ratios at both stages follow a pattern of higher values in the north and relatively lower values in the south, with notable spatial variability within regions. The spatial distribution of increase ratios for the 50-year discharge (Q50) is shown in Figure S11. Overall, the national trend of Q50 increase ratios closely aligns with those of Q100, highlighting the representativeness of Q100.

Figure 5-3 shows the distributions of increase ratios and equivalent return period of historical Q100 on the national level and the 14 regions. The equivalent return period means estimating return period of +2˚C or +4˚C stage by the Q100 at historical stage. Because the threshold of the POT method is set to be 10-year return period, return periods shorter than 10 years cannot be estimated in this study and are marked as 0. Additionally, some river channels with decreased discharge result in return periods longer than 100 years (outliers). To highlight the main distribution, Figure 5-3 (b) presents results within the range of 0 to 100 years.

The results shown in Figure 5-3(a) indicate that Q100s increase by 1.16 and 1.37 times (medians of boxplots) for Japan at the +2˚C and +4˚C stages, respectively. The relatively wide “box” at the +4˚C stage indicates greater spatial variability in increase ratios. Regional distributions of increase ratios differ significantly, with medians in

Hokkaido-1, -2, -3, and Chubu regions surpassing the national median at +2˚C, and Tohoku joining these regions at +4˚C. Hokkaido-1, -2, -3, and Tohoku regions show wider discrepancy between +2˚C and +4˚C stages than other regions, suggesting heightened flood sensitivity to climate change in these areas. At the +4˚C stage, median increase ratios in Hokkaido-1, -2, and -3 exceed 1.65, well above the national median.

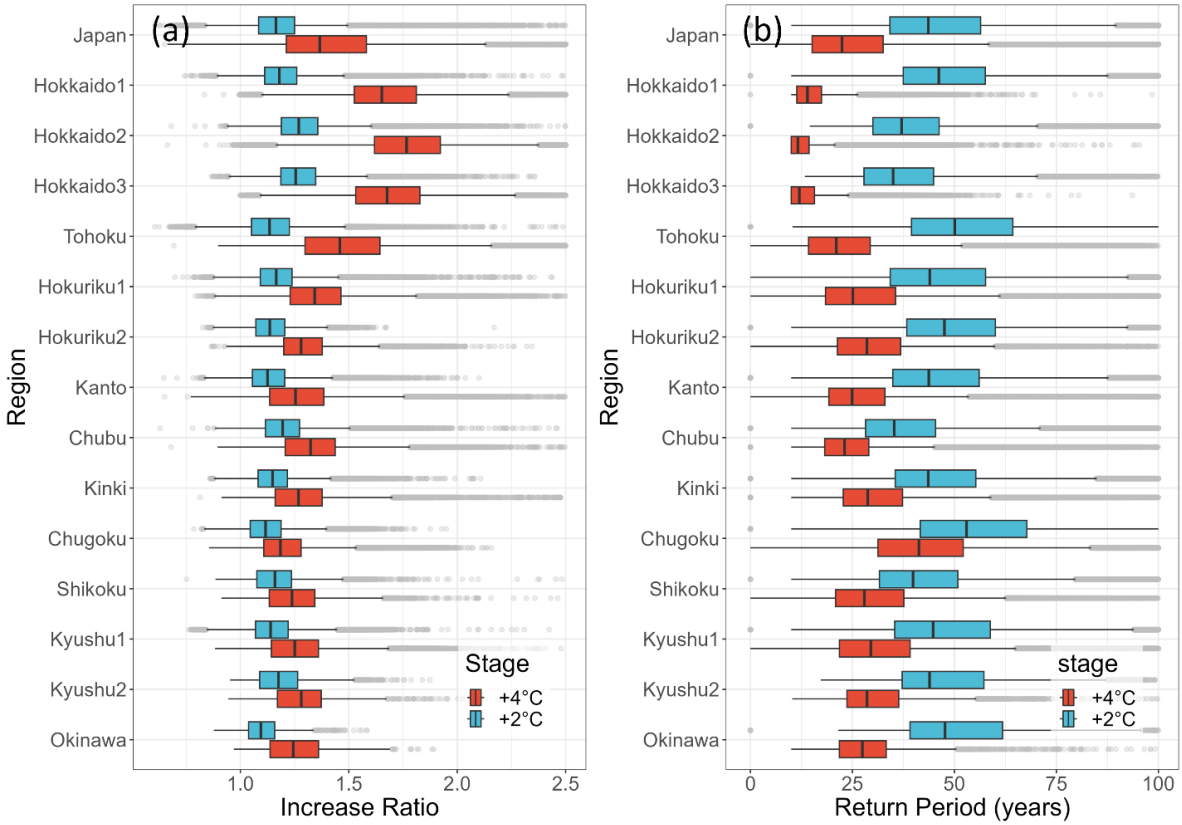


Figure 5-3 Distributions of increase ratios (a) and equivalent return period of historical Q100 (b) on the national level and 14 regions. Abbreviation: 100-year return period discharge (Q100)

Figure 5-3(b) illustrates that floods with a 100-year return period at the historical stage will occur more frequently, with most equivalent return periods shortening to less than 100 years. The medians of equivalent return periods at the national scale are 45 and 23 years at the +2˚C and +4˚C stages, respectively. Among regions, the medians fluctuated around the national medians, except in Hokkaido-2, -3, and Chubu regions (around 35 years) at the +2˚C stage and Hokkaido-1, -2, -3 regions (around 12 years) at the +4˚C stage.

In summary, (1) Q100s exhibit an overall increasing trend, by factors of 1.16 (+2˚C) and 1.37 (+4˚C) nationally; (2) equivalent return periods of Q100 shorten to 45 (+2˚C)

and 23 (+4˚C) years; (3) warmer climate conditions result in higher increase ratios with stronger spatial variability; (4) the northern regions (Hokkaido-1, -2, -3, and Tohoku) and Chubu have higher increase ratios, with the northern regions demonstrating greater climate sensitivity.

5.4.2 Regional trends

The flood patterns in upstream contribution areas (CAs) and the elevation are noteworthy, as they relate to future flood prevention and adaptation strategies. Typically, downstream regions of large river basins receive greater attention in flood prevention efforts, with more embankments and water gates due to higher population density and asset concentration. However, recent disasters reveal a situation that dikes in the upstream failed first and subsequently flooded the downstream areas (Nagumo et al., 2016; Yasuda et al., 2016), raising concerns about the climate change impact on floods in upstream areas.

Figures 5-4 and 5-5 display the Q100 increase ratio varying with CA at the +2˚C and +4˚C stages, respectively. Each sub-figure presents results within a region, featuring a logarithmic x-axis, a black line for medians, and a red dashed line for the M-CV. Point color indicates point density at each location. To robustly detect trends, grids with extremely small or large CA are excluded from the figures due to uncertainties and limited sample sizes; thus, the CA range in Figures 5-4 and 5-5 is restricted to 10 to 1,000. To highlight the increase ratio of most river grids, the y-axis is set between 0.3 and 2.5. Regions with few samples, such as Kyushu-2 and Okinawa, are excluded from the regional analysis. The M-CV, assessing data variability, shows a slight decrease as river basins become larger across regions and warming stages, with values centered around 0.1, indicating a reliable level for analysis. According to the M–K test, at the +2˚C stage, 4 regions exhibit a significant decreasing trend in medians, indicating higher increase ratios in small basins; 2 region shows the opposite pattern; 6 regions display no significant impact of basin sizes. Warmer conditions enhance these gradients and increase the number of the regions with significant decreasing trends. At the +4˚C stage, 6 regions show a decreasing trend in increase ratio medians, 2 increasing trends, and 4 no trend. Hokkaido-1, -3, and Hokuriku-1 retain the same trend at +4˚C, with Hokkaido-3 showing the most pronounced decrease from around 1.7 to 1.4. These findings indicate that small river basins may have comparable or even higher increase ratios than larger ones, underscoring the necessity of revisiting reginal flood prevention systems especially in small-to-medium sized rivers.

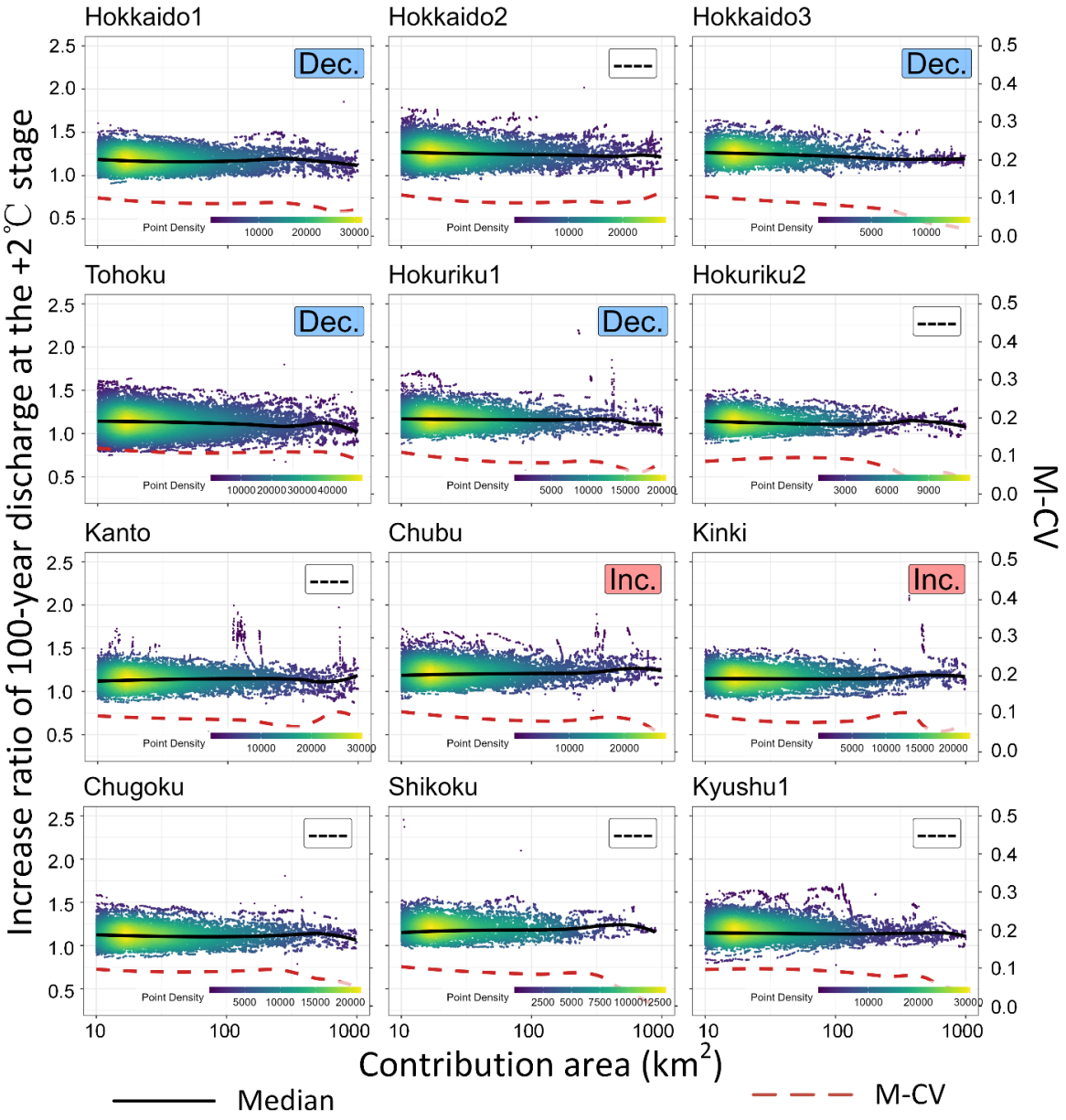


Figure 5-4 Q100 increase ratios of each region vary with contribution areas at the +2˚C stage.

"Dec." (blue background) and "Inc." (red background) represent monotonous decreasing and increasing trends, respectively, as identified by the M-K test at a 95% confidence level. "----" indicates no significant trend. Abbreviation: Mann-Kendall (M-K), modified coefficient of variation (*M-CV*)

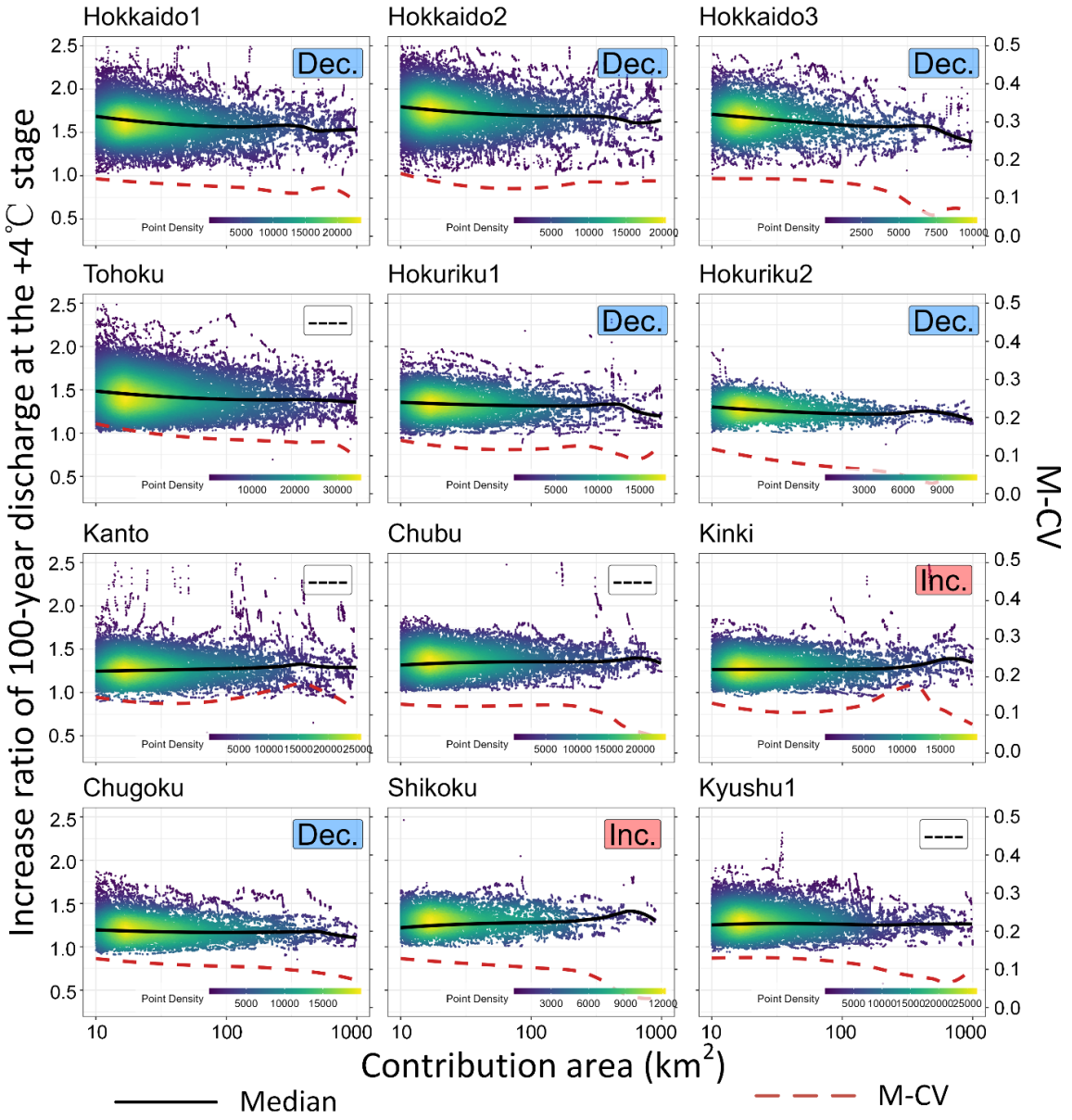


Figure 5-5 Q100 increase ratios of each region vary with contribution areas at the +4˚C stage.

"Dec." (blue background) and "Inc." (red background) represent monotonous decreasing and increasing trends, respectively, as identified by the M-K test at a 95% confidence level. "----" indicates no significant trend. Abbreviation: Mann-Kendall (M-K), modified coefficient of variation (*M-CV*)

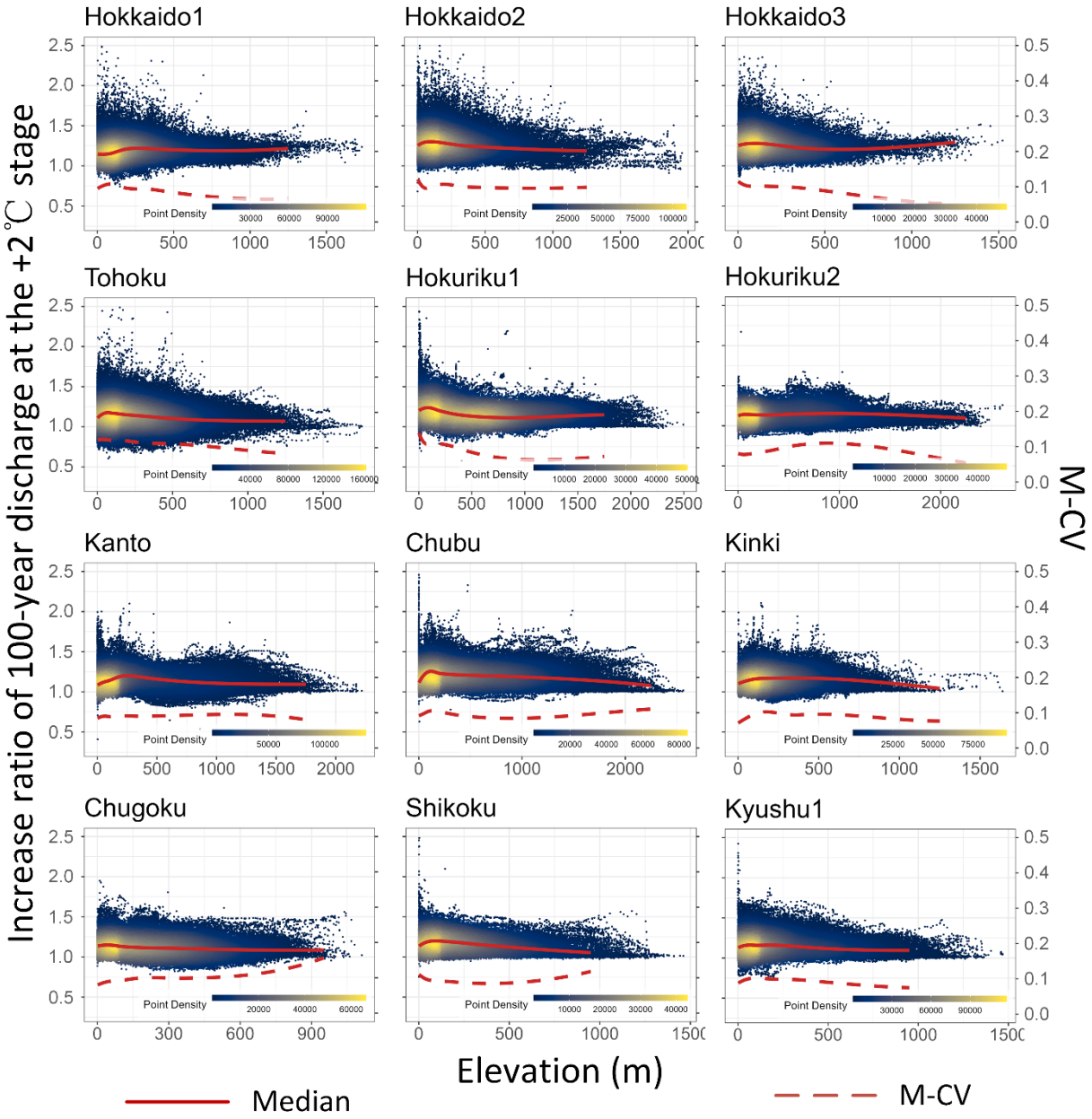


Figure 5-6 Q100 increase ratios of each region vary with elevation at the +2˚C stage. Abbreviation: modified coefficient of variation (*M-CV*)

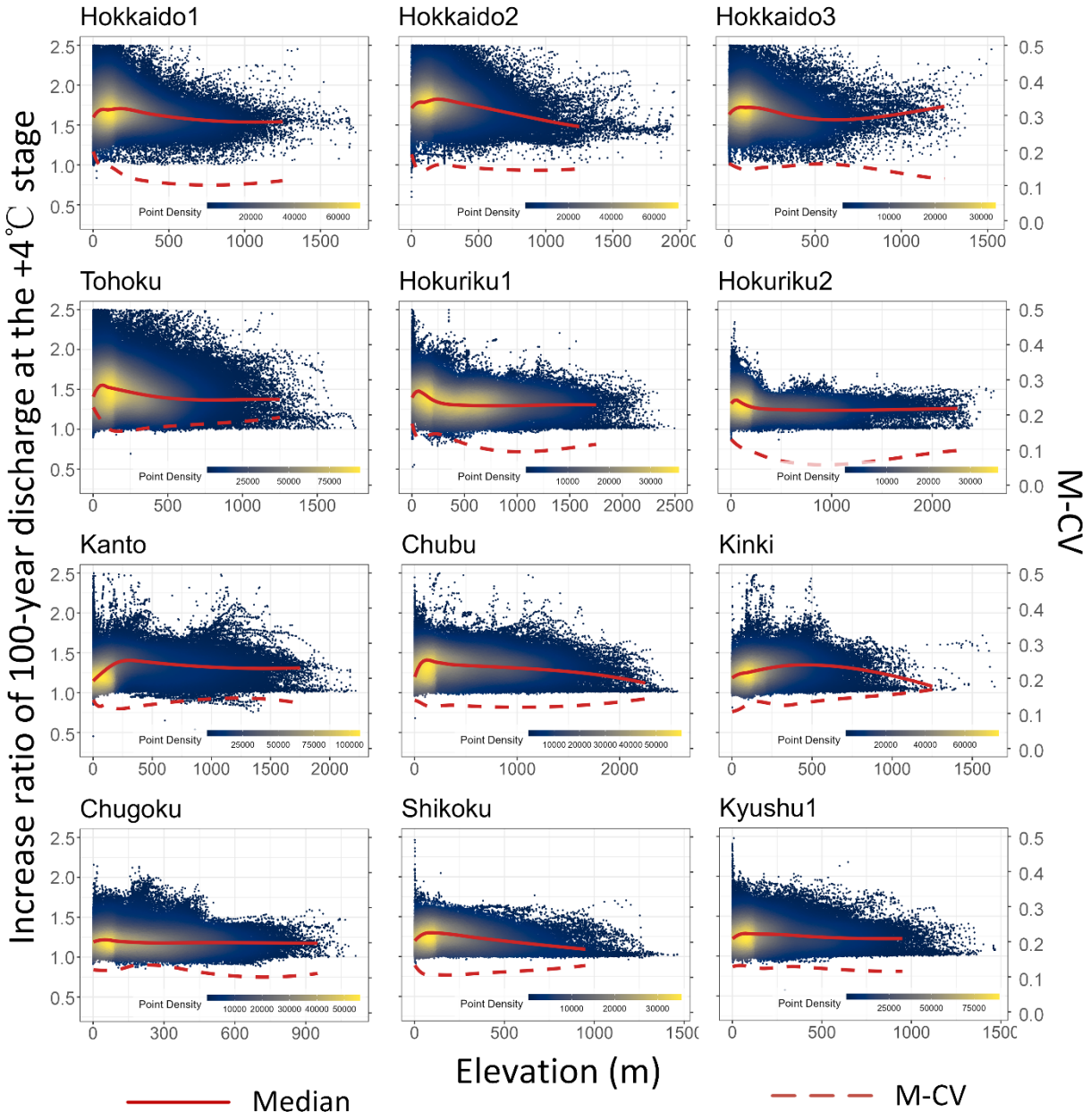


Figure 5-7 Q100 increase ratios of each region vary with elevation at the +4˚C stage. Abbreviation: modified coefficient of variation (*M-CV*)

Figures 5-6 and 5-7 show the Q100 increase ratios varying with elevation at the +2˚C and +4˚C stages. The M-CV values fluctuate around 0.1 at +2˚C and range between 0.1 to 0.2 at +4˚C. The median lines of increase ratios across regions reveal a similar trend that peaks appear at elevations between 30 m and 300 m, suggesting relatively higher flood risks in river sections at such elevations. Moreover, the impact of elevations becomes more significant at a warmer climate. Due to sample characteristics, grids with small CA, which are directly responsive to extreme precipitation, dominate each elevation range, indicating that the pattern mainly relates to precipitation. The

topography lifting effect on precipitation would be the main reason presenting such trend, where moist air masses, intensified by a warmer climate, contribute more to precipitation on hillsides. Figure S12, using the results at the +4˚C stage, displays the contours corresponding to median peaks for each region. These contours align with transition zones from mountains to plains, with elevation values varying by regional topography. Regions with gentler terrain exhibit higher elevation values. Overall, these regional patterns emphasize the need for proactive measures against future floods in transition zones, which are also critical areas for debris flows and landslides.

In summary, regional patterns linked to basin size and topography suggest that future flood risks in basins with small CAs and those located in transition zones are comparable to or exceed those in larger basins or other areas, highlighting the urgency of implementing countermeasures for these vulnerable regions.

5.4.3 Flood process changes

Beyond the flood peak changes, changes in flood process are also crucial as it relates to specific actions of flood management. Figure 5-8(a) presents the historical flashiness median of extreme events at 109 national river basin outlets. These basins, designated by the Japanese government, are recognized for their significance to the national economy. Generally, smaller basins exhibit higher flashiness, indicating more severe and rapid flood events. Southern regions, including Kyushu, Shikoku, and the coastal areas of Kinki and Kanto, which are typically impacted by typhoons, show elevated flashiness levels.

Figure 5-8(b) served as an example, showing the flashiness distributions for the Shinguu basin across the historical, +2˚C, and +4˚C stages, which clearly illustrates that the flashiness increased with the climate becomes warmer. The KS test identifies the significant difference in distribution across warming stages. The outline of basins in Figure 5-8 (c) and (d) will be plotted in black color if the distribution at the +2˚C and +4˚C stages have significant change compared with the one at the historical stage, respectively. In Figures 5-8(c) and (d), basin outlines are highlighted in black if the flashiness distribution at the +2˚C or +4˚C stage significantly deviates from the historical stage. Basin colors in these figures represent relative changes in flashiness medians, valid only if significant distribution changes are detected.

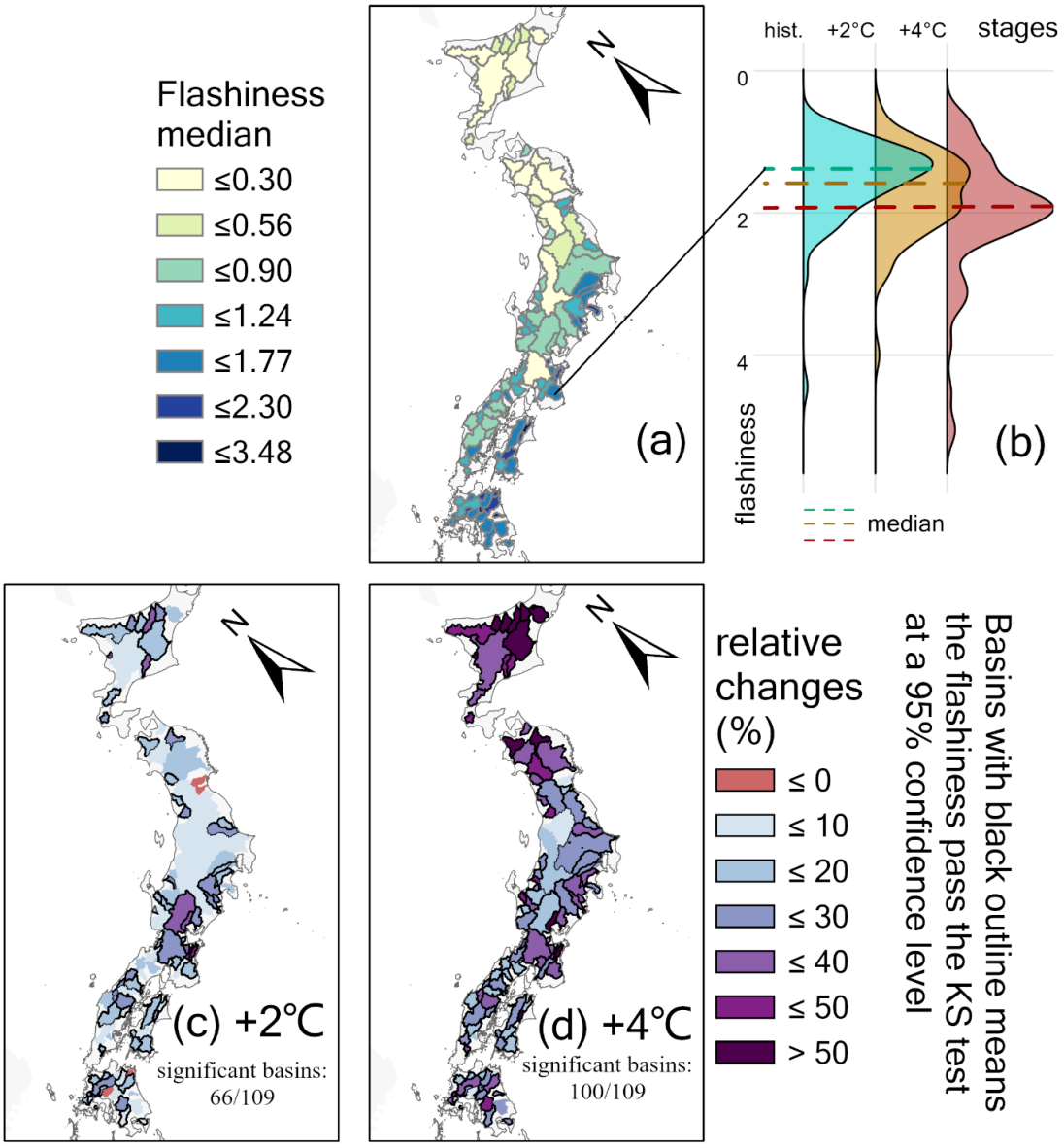


Figure 5-8 Spatial distribution of flashiness medians and their relative changes at the +2˚C and +4˚C stages.

(a) flashiness medians for 109 national basins at the historical stage; (b) flashiness distributions of Shinguu basin at the historical, +2˚C, and +4˚C stages; (c) relative changes in flashiness medians at the +2˚C stage; (d) relative changes in flashiness medians at the +4˚C stage.

At the +2˚C stage, 66 basins show significant distribution changes, with flashiness values rising by over 10%, predominantly in the south, where initial flashiness levels are already high. This intensifies challenges for local river management, as severe flash floods allow less time for preventive measures. Notably, northern basins also exhibit increased flashiness, suggesting a heightened susceptibility to flash floods in areas previously less prone to such events.

At the +4˚C stage, 100 basins exhibit significant changes in flashiness distribution, with over 20% relative increases in most cases, indicating an overall heightened flash flood risk. In particular, Hokkaido and northern Tohoku regions show relative changes exceeding 30%. Although absolute changes are smaller in these regions compared to those with initially high flashiness, the results still reveal an alarming change in flood types and subsequent flood-related preparation planning.

In summary, 66 and 100 of the 109 national basins show significant increases in flashiness by over 10% and 20% at the +2˚C and +4˚C stages, respectively. Southern Japan, already at high flash flood risk, faces further intensification, while northern Japan, especially at +4˚C, confronts new challenges with markedly increased flashiness, emphasizing the need for adaptive flood management strategies.

5.5 Discussion

This study projected floods under historical, +2˚C, and +4˚C climate stages for all river basins in Japan using a high-resolution (150 m) RRI model and a 5-km dynamically downscaled climate ensemble (d4PDF DDSJP). Simulation results were used to estimate peak discharge frequency curves via the POT method, and flashiness of extreme events was analyzed. National and regional trends in Q100 increase ratios, as well as changes in flood processes, were further investigated.

5.5.1 Increase ratio and flashiness at major basin outlets

This work provides perspectives of climate change impact on floods across multiple scales, from extremely small basins to the national level. In Figure 5-2, changes in the downstream regions of large river basins are challenging to visually distinguish due to the dense representation of small river channels. Figure 5-9 illustrates the increase ratio at the outlets of 109 national river basins. Generally, the increase ratios at most outlets align with those observed in most of the tributaries. However, there are exceptions, such as basins in Shikoku and Kanto regions (showing higher increase ratios than tributaries) and northern Tohoku and Hokkaido-1 regions (showing lower increase ratios than tributaries at the +2˚C stage). These inconsistencies may be attributed to geographical conditions and differences in dominant events.

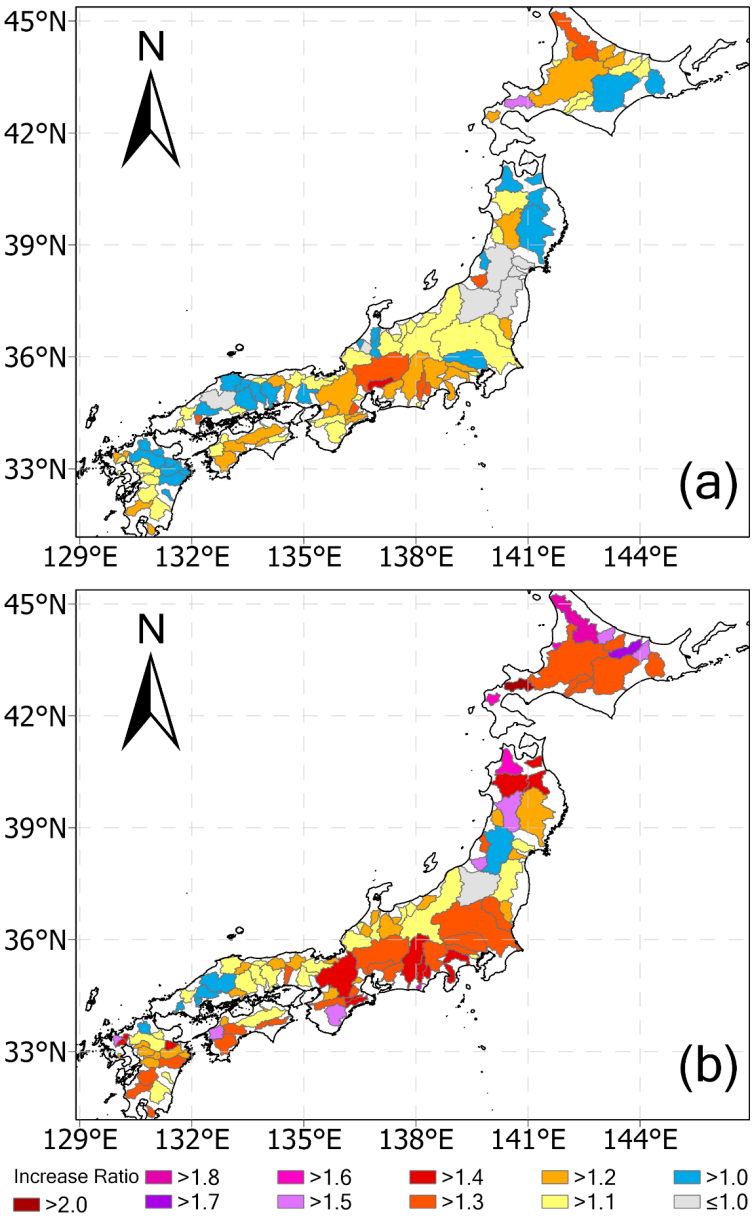


Figure 5-9 Spatial distribution of increase ratios for outlets of 109 national basins at the +2˚C (a) and +4˚C (b) stages.

A comparison between Figures 5-9 and 5-8 reveals a correlation between flashiness enhancement and discharge peak increase ratios; at the +4˚C stage, basins with higher increase ratios tend to show significant changes in flashiness. However, this correlation is not necessarily linear. For instance, at the +2˚C stage, a basin in Hokkaido-2 exhibits an increase ratio exceeding 1.2 without significant flashiness changes, whereas a basin in northern Tohoku shows an increase ratio above 1.0 with marked changes in flashiness. This indicates that flashiness changes are influenced not only by discharge volume but also by the spatiotemporal patterns of precipitation and other factors (Saharia et al., 2021).

5.5.2 Extreme precipitation pattern changes

Hokkaido-1, -2, -3, and Tohoku regions show higher increase ratios and greater sensitivity compared with other areas. Extreme precipitation in Japan is mainly driven by three weather systems: typhoons (Mei and Xie, 2016), the Baiu front (a stagnant front system) (Guo and Hibino, 2023), and senjo-kosuitai (a quasi-stationary band-shaped precipitation system) (Kato, 2020). The elevated increase ratios in these regions are likely related to the northward shift of the Baiu front and typhoon tracks. Projections from the d4PDF indicate a significant rise in the number of Baiu front-induced extreme precipitation events at the +4°C stage in northern regions that previously experienced few such events (Osakada and Nakakita, 2018). Additionally, typhoon tracks in the northwestern Pacific are projected to shift northwest (Kossin et al., 2016; Murakami et al., 2013; Nakamura et al., 2017; Studholme et al., 2022). Beyond climatic factors, local hydrological characteristics may also contribute to the higher increase ratios. Due to their high latitudes, these regions experience relatively lower baseline rainfall intensity and discharge, making them more sensitive to increases. Overall, the notable high increase ratios in these areas highlight the need further adaptations in previously inexperienced regions.

The similar increase ratio distribution pattern on elevation may be attributed to the topographic effect on precipitation. On the investigation of a severe flood event in Hokkaido-2, triggered by the remote effect of the tropical cyclone “Lionrock”, the topography was identified to be the primary forcing for reproducing the extreme precipitation (Nguyen-Le and Yamada, 2017). The 2021 Henan flood, caused by a record-breaking precipitation event with peak rainfall intensity of 201.9 mm/h, also highlights the important role of topography. The water vapor transported by two typhoons was blocked by the Taihang and Funiu Mountains in western Henan, leading to strong moisture convergence and high large-scale precipitation efficiency (Liang et al., 2022; Yin et al., 2023). Generally, the thermodynamic effects explain precipitation differences across various warming stages, while dynamic effects (i.e., topographic effect) account for spatial variations in precipitation. As reported, dynamical process exhausts vertically-integrated moisture more completely as climate warms, thus result in higher precipitation efficiency (Jun and Rind, 2024). The elevation-related flood increase patterns identified in this study further corroborate their findings, highlighting the consequent impacts on floods.

5.5.3 Comparison of flood projection studies

By correcting the bias of the 20-km d4PDF, Kobayashi et al. (2020) further projected floods at the +4˚C stage for the outlets of 109 national river basins in Japan. Their findings indicate that the increase ratios range from 1.0 to 1.2 in the Chugoku region, 1.2 to 1.5 in most other regions, and 1.5 to 2.0 in northern Hokkaido, aligning well with the results shown in Figure 5-9(b). Slight differences exist in certain basins, such as the Ishikari River Basin—the largest in Hokkaido-2. Nguyen et al. (2020), using 5-km dynamically downscaled d4PDF data specific to Hokkaido, projected an increase ratio of approximately 1.33 at the Ishikari River outlet and 1.4 to 1.6 in its tributaries, which closely matches the results shown in Figures 5-2 and 5-9. Overall, the increase ratios estimated in this study demonstrate strong agreement with previous d4PDF-based projections, while offering broader insights in terms of scale and coverage.

Some studies utilized scenario-based ensembles from the Coupled Model Intercomparison Project (CMIP), which are derived using experiment schemes distinct from the d4PDF. Nonetheless, comparing results from mid-century and far-future under the RCP8.5 scenario with those at +2˚C and +4˚C warming stages is still beneficial for contextualizing Japan's climate change impacts within a global framework. As reported, the relative changes of Q100s in Europe are at a range of ±30% (Di Sante et al., 2021) or ±40% (Alfieri et al., 2015b) by the far-future, showing a spatial pattern of positive changes in western and parts of eastern Europe, and negative changes in the northeast and southwest. The reduction in Q100 in northeastern Europe is linked to the reduction of snow accumulation, whereas extreme floods in northeastern Japan, primarily driven by intense precipitation events like typhoons (Heidarzadeh et al., 2021), are expected to be intensified. In the U.S., Yu et al. (2020) employed a process-based frequency analysis framework and convection-permitting RCM outputs to project floods at far-future for Turkey river under RCP8.5 scenario, revealing that smaller basins exhibited higher relative Q100 increases (over 30%) compared to larger basins (around 15%). Michalek et al. (2023) investigated future flood changes in Iowa, U.S. using high-resolution ensembles from CMIP6 HighResMIP tier, finding that 65% of communities are projected to experience a 20% increase in flood risk (though not statistically significant). Meanwhile, Budhathoki et al. (2022), using the 20-km d4PDF, projected a 1.3-time increase in Q100 for the Chao Phraya River Basin in Thailand at the +4˚C stage. Overall, future flood projections indicate that Japan is likely to experience comparable or even higher increase ratios

than other regions globally. Unlike areas where snowmelt reduction mitigates flood risks, Japan's high-latitude regions may see further flood intensification due to increased extreme precipitation. These findings underscore the urgency of implementing comprehensive, nation-wide measures to address escalating flood risks.

5.5.4 "by All" Policy

Comprehensive insights with 150-m resolution for everywhere in Japan are expected to serve for a national flood management policy. Limiting global warming to well below 2°C (i.e., the goal of the Paris Agreement) is more challenging than anticipated according to a recent study which successfully excluded the internal climate variability in the eastern tropical Pacific (Liang et al., 2024). To mitigate the warming trend and flood damage as much as possible, the flood risk management paradigms are shifting, calling for civilian participation (Nakamura and Oki, 2018). The Japanese government is promoting a policy called "River Basin Disaster Resilience and Sustainability by All" (Koike, 2021; MLIT, 2024a). This policy involves a series of measures with civilian participation to reduce exposure and vulnerability, including using paddy field dams to reduce flood peaks, providing flood risk information in real estate transactions, relocating important factories, and facilitating anti-inundation preparedness through financial tools (Suzuki et al., 2022; Yoshikawa et al., 2010). However, implementing this new policy faces resistance due to divergent stakeholder interests. For example, the inundation of rice plants during growth decreases yield, leading stakeholders to view the policy cautiously (Bark et al., 2021; Kotera et al., 2005). Increasing the awareness of climate change impacts and policies is essential to assist stakeholders making decisions that are in the long-term interest (Kawai et al., 2024). Thus, the perceptible high-resolution results of this study are expected to facilitate policy implementation and serve as a reference for other measures.

5.5.5 Limitations

Due to computational limitations, this study did not assess the agreement among ensemble members, leaving open the possibility that results may be more influenced by specific members. However, according to Hirabayashi et al. (2021), reported strong consensus on Q100 changes among Atmosphere–Ocean General Circulation Models (AOGCMs) for Japan. Additionally, extreme events identified in this study were not predominantly driven by any single ensemble member.

As stated in the introduction, this study focuses on mesoscale flood projections, primarily addressing fluvial floods. The simulations do not incorporate complex interactions such as storm surges, sea level changes, or urban drainage systems. This limitation prevents the direct application of our results to studies on compound or urban flooding. However, microscale research can still benefit from our simulations by using the outputs as boundary conditions for higher-resolution studies.

The aim of this work is not to quantitatively determine precise discharge quantiles for specific warming stages, given the inability to account for all potential future changes such as land use alterations, dam construction, or modifications in operational rules, alongside known systematic biases in the RRI model for certain regions. Instead, the study emphasizes the relative changes in flood peaks and processes, primarily linked to shifts in extreme precipitation patterns. Therefore, despite the aforementioned limitations, the insights and challenges highlighted remain robust and credible.

5.6 Conclusions

This work conducted a mesoscale analysis projecting future floods across Japan using the high-resolution (150 m) RRI model, delivering insights into national and regional flood risk trends and process changes at the +2˚C and +4˚C warming stages. Specifically, we utilized a 5-km dynamically downscaled climate ensemble (DDSJP) spanning 720 years for each stage, and employed the AGE method to identify critical extreme events. By analyzing hourly outputted discharges, including estimating Q100 for all river grids by the POT method and assessing flashiness for 109 national river basins, we identified critical regions for flood prevention from national and regional perspectives, and revealed an overall elevated flash flood risk across Japan. Specific findings are as follow:

(1) From the national perspective, overall, discharges of 100-year floods are expected to increase 1.16 (+2˚C) and 1.37 (+4˚C) times, with equivalent return period reduced to 45 (+2˚C) and 23 (+4˚C) years. Enhanced spatial variability in increase ratios with warming indicates that the northern regions (Hokkaido-1, -2, -3, and Tohoku), followed by Chubu, will experience relatively higher increases, with northern regions showing greater climate sensitivity.
(2) From the regional perspective, increase ratios in small river basins are comparable to or exceed those of large river basins, underscoring the need for

enhanced flood prevention in upstream areas. Additionally, rivers situated in transition zones between mountains and plains show higher increase ratios, necessitating further countermeasures for these vulnerable zones.

(3) Most of the national basins are projected to become more prone to flash floods with flashiness increase by over 10% at the +2°C stage and over 20% at the +4°C stage. Southern Japan, already at high risk of flash floods, is expected to experience further intensification. Northern Japan, particularly under +4°C warming, is poised to face new challenges with a pronounced increase in flashiness, highlighting the urgent need for adaptive flood management strategies.

Overall, this study provides comprehensive flood-related insights at multiple scales under future warming stages, contributing to informed decision-making and the implement of public-engaged flood mitigation policies.

6. Meteorological driver transitions of projected floods

Abstract

Climate change is expected to alter characteristics of weather systems such as Tropical Cyclones (TCs), while few studies have systematically examined their cascading impacts on projected regional floods. Based on the works in Chapter 5, this chapter utilizes a global TC track dataset to classify the projected floods into three categories: TC-induced, non-TC events in June–July (NT67, associated with Meiyu–Baiu fronts), and non-TC events in August–September (NT89, linked to autumnal fronts), revealing an increasingly complex and severe future flood regimes. These three categories collectively account for over 90% of historical floods in Japan, with TCs being the predominant driver (>50%). While the frequency of TC-driven floods is projected to decline—particularly in northern Japan—due to a reduction in TC number affecting Japan, shifts in TC tracks and intensification cause a ~20% increase in TC-driven flood events in the Chugoku region under +2 ˚C warming stage. Both TC and non-TC floods show increasing peak discharge and flashiness, with the contributions of NT67 and NT89 projected to rise by 20%–30%, exhibiting strong regional characteristics. The increasing complexity and intra-basin heterogeneity in flood causation challenge traditional flood management practices. A dominantly weakened scale effect of TC-induced floods suggest that flood potential in small basins has largely plateaued, and thus, mitigation efforts should prioritize peak discharge increases in large basins. In contrast, basins in northern Japan with intensified scale effects will see rising flood potential in both small and large basins, particularly necessitating focus on small-basin flood prevention. In frequently non-TC impacted regions, a consistent weakening of scale effects is observed under warmer climates, indicating that non-TC impacts will increasingly affect larger basins.

This chapter highlights the escalating challenges for flood risk management, emphasizing the importance of region- and design-specific assessments of changes in dominant weather systems and the urgent need to develop targeted flood management strategies for non-TC systems. This study provides critical data support and insights for future planning by regional flood control authorities.

6.1 Introduction

Extensive research has projected that climate change amplifies extreme precipitation, intensifying flood hazards and resulting in severe socio-economic impacts (Donat et al., 2016; Hirabayashi et al., 2021; Prein et al., 2017; Tellman et al., 2021; Winsemius et al., 2016, 2018). Mitigating these losses requires strategic planning, adaptive measures, and improved emergency responses—all of which depend on reliable future flood projections and a thorough understanding of their driving mechanisms (Blöschl, 2022; Owen, 2020; Soergel et al., 2021).

Extreme precipitation is associated with various weather systems, including tropical cyclones (TCs), frontal systems, and mesoscale convective systems (Kato, 2020; Sayama et al., 2020; Takemi, 2010). Among them, TCs are particularly destructive due to the compound effects of intense rainfall, strong winds, and storm surges. TCs pose significant threats to coastal areas and, in some cases, entire nations such as Japan. Historically, individual TCs have caused devastating impacts—e.g., Hurricane Katrina (2005) led to $125 billion in losses, while the Bhola cyclone (1970) claimed 300,000 lives (Peduzzi et al., 2012). Climate change is projected to double TC-related economic damages (Mendelsohn et al., 2012), prompting considerable interest in their future behavior under warming scenarios (Mei and Xie, 2016; Young and Hsiang, 2024; Zhu et al., 2022).

Recent studies reveal a poleward shift in TC tracks, particularly in the Northwest Pacific (Kossin et al., 2016; Nakamura et al., 2017; Studholme et al., 2022), along with earlier seasonal occurrence. Shan et al. (2023) found that the timing of lifetime peak intensity advanced by 3.7 and 3.2 days per decade in the Northern and Southern Hemispheres, respectively, between 1981 and 2017. Elevated sea surface temperatures enhance TC moisture and energy availability, increasing their destructive potential, although their duration may shorten (Knutson et al., 2010; Wang et al., 2020; Xu et al., 2020; Yamaguchi et al., 2020). Evidence suggests a consistent rise in TC destructiveness (Emanuel, 2005; Li et al., 2017; Tu et al., 2018). While the global annual frequency of TCs remains steady at ~80–90 (Patricola et al., 2022; Sobel et al., 2021), their future trends remain uncertain (Chand et al., 2022; Emanuel, 2021a, b). Nevertheless, intense TCs are projected to increase (Emanuel, 2021a; Kossin et al., 2020; Walsh et al., 2016; Yamada et al., 2017). Additionally, TC activity is found to be modulated by large-scale climate patterns such as the El Niño–Southern Oscillation (ENSO) and the Interdecadal Pacific Oscillation (IPO) (Patricola et al., 2018; Shan et al.,

2025).

While many studies have evaluated TC-induced flooding in coastal regions, historical records show that TCs can also trigger extreme floods inland (Yang et al., 2020). Some of the extreme floods are attributed to the remote effects of TCs (Deng et al., 2022; Liang et al., 2022; Qin et al., 2022), underscoring the far-reaching and complex influences of these systems. In some inland regions, TC-driven floods—though less frequent—can exceed the severity of coastal flooding during the same event, underscoring the need for comprehensive countermeasures (Chen et al., 2025a). Key mechanisms driving such floods include anomalous moisture transport, extratropical transition, and orographic enhancement (Liu et al., 2022b; Nayak and Takemi, 2020b). Pseudo Global Warming (PGW) experiments suggest that TCs with similar tracks will produce more rainfall and higher flood risks under future warming (Nayak and Takemi, 2019, 2020a; Takemi, 2019). Projected stronger winds and precipitation, and longer stalling durations, together with sea level rise are expected to further exacerbate TC-induced flood risks (Gori et al., 2020; Sarhadi et al., 2025; Zhu et al., 2021).

Despite these advances, most existing research relies on individual PGW-based TC case studies and lacks a systematic investigation linking macroscale TC changes with regional flood impacts under climate change. Outstanding questions remain, including: (1) Will the proportion of TC-induced floods decline in tandem with the projected decrease in TC frequency, or persist due to intensifying TC severity? (2) Do evolving precipitation patterns preferentially enhance flood potential in large basins or in small, more responsive catchments? (3) Are TC-induced floods intrinsically more hazardous or distinct from non-TC events in terms of hydrological characteristics? These questions cannot be resolved through analyses limited to TCs or individual flood events. A comprehensive understanding requires region-wide flood attribution to meteorological drivers, supported by high-resolution modeling that integrally captures the full spectrum of physical processes across broad spatial and temporal scales.

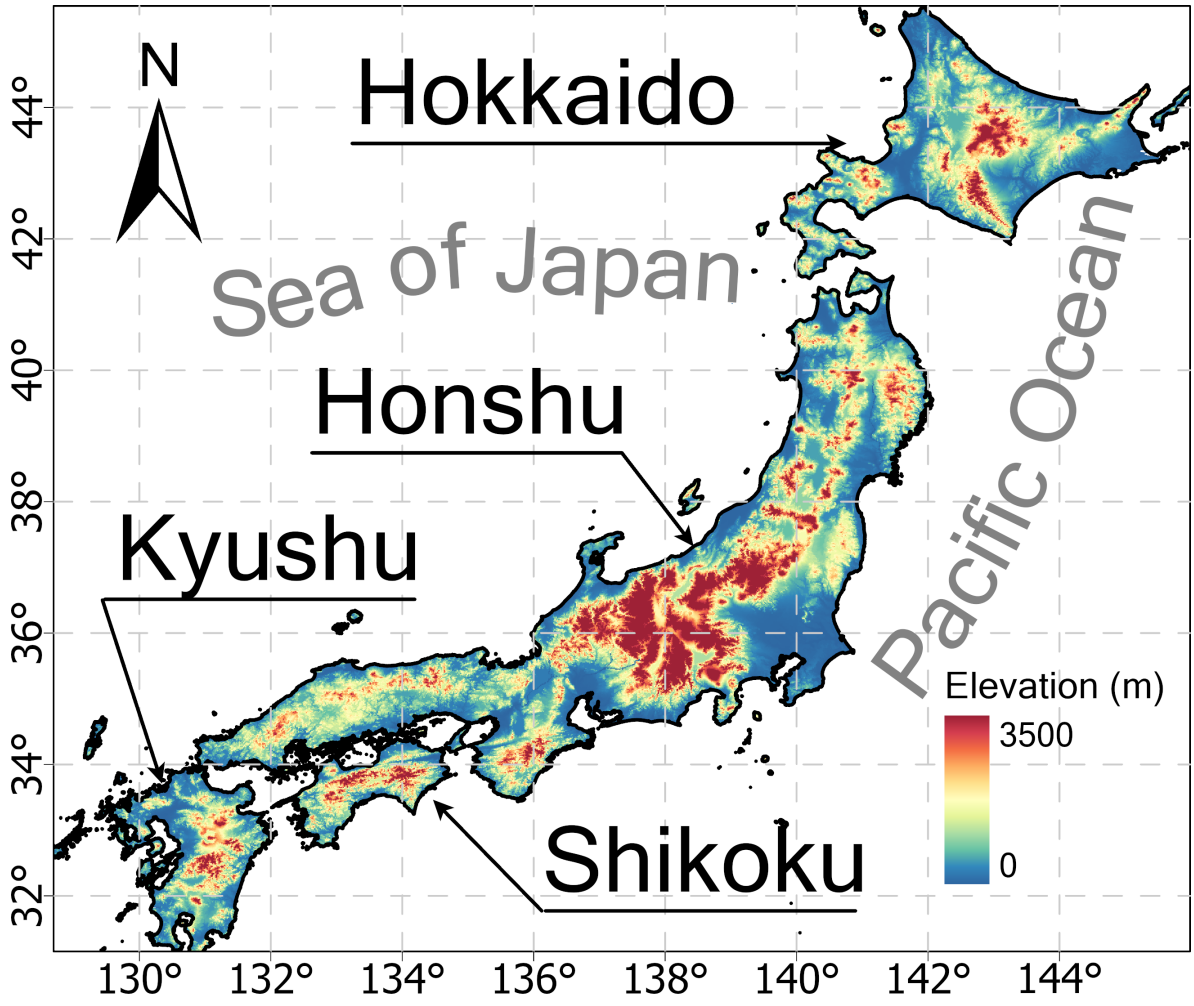


Figure 6-1 Overview of the four major islands in Japan

To address these challenges, this study utilizes a large dynamically downscaled climate projection ensemble, providing hourly precipitation at 5 km resolution, and simulates flooding across all Japanese rivers at 150 m resolution using a high-efficiency hydrologic model (Figure 1). For each region, around 3,000 to 6,000 extreme precipitation events were identified for simulation from the 720-year climate ensemble data of each climate stage. The top 72 events per river grid—ranked by peak discharge and corresponding to return periods $\geqslant 10$ years—were selected and attributed using a global TC track dataset. Floods are categorized into three groups: TC-induced, early-summer (June–July) non-TC (NT67), and late-summer/autumn (August–September) non-TC (NT89) events. This study quantifies the TC impact changes on regional floods relating to climate change by analyzing changes in their TC event proportion, basin scale effects, and flood responses, and compares these trends with those of non-TC. Results indicate a projected decline in TC-induced floods, particularly in northern Japan. However, despite their decreasing frequency, TC-

induced floods are expected to become more hazardous, with significantly higher peak discharges and increased flash flood risks nationwide. In some northern basins, TCs are projected to further elevate flood potential in small basins, while in most other regions, the increase is concentrated in large basins. Results indicate a projected decline in TC-induced floods, particularly in northern Japan. However, despite their decreasing frequency, TC-induced floods are expected to become more hazardous, with significantly higher peak discharges and increased flash flood risks nationwide. In some northern basins, TCs are projected to further elevate flood potential in small basins, while in most other regions, the increase is concentrated in large basins. In contrast, both NT67- and NT89-induced floods increase in number, discharge peak, flash flood risks. Meanwhile, non-TC, characterized by relatively spatiotemporally concentrated precipitation, is projected to impact larger basins. This work presents a research framework for investigating the impact of weather system changes on regional flood regimes under climate change, highlighting the distinct response patterns of different flood drivers and underscoring the need for weather-specific flood prevention, mitigation countermeasures.

6.2 Results

6.2.1 Changes in flood contributions

A total of 5,825 (past), 4,946 (+2 ˚C), and 3,757 (+4 ˚C) TC events traversing the seas surrounding Japan were extracted from 720 years (60 years × 12 ensemble members) of simulation data for each climate stage. The number of TCs exhibits a declining trend with rising global temperatures. By matching flood periods with the TC affecting periods, flood events were categorized. In Japan, non-typhoon events are primarily driven by Meiyu–Baiu frontal systems (Yin et al., 2024), autumnal frontal systems (Zhao et al., 2023a), and mesoscale convective systems (e.g., line-shaped rainband) (Kato, 2020; Ohya and Yamada, 2024), with NT67 and NT89 generally occupied by Meiyu–Baiu and autumnal fronts, respectively (Fumiaki and Jun, 2022; Iizuka and Nakamura, 2019).

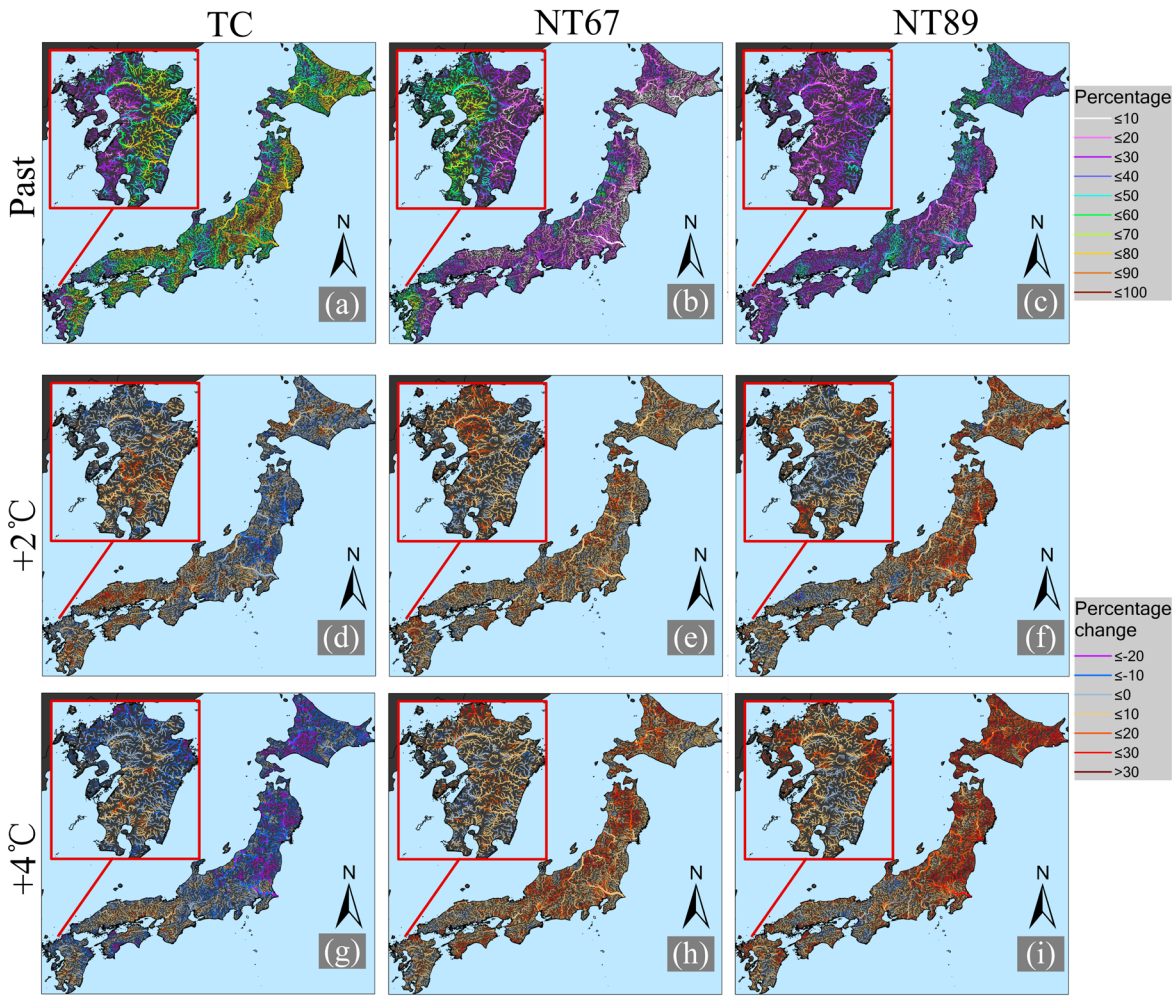


Figure 6-2 Proportion of TC-, NT67-, NT89-induced floods at the past climate stage and projected changes at the +2˚C and +4˚C stages.

Abbreviations: Tropical Cyclone, TC; Non-Tropical cyclone event between June and July, NT67; Non-Tropical cyclone event between August and September, NT89.

Figure 6-2 presents the spatial distribution of TC, NT67, and NT89 contributions to historical extreme floods, along with projected changes at the +2 ˚C and +4 ˚C warming stages. Historically, TCs accounted for over 50% of extreme floods across most of Japan, confirming their dominant role. In some inland areas, TC contributions exceeded 80%, reflecting their superior capacity to transport moisture and induce heavy rainfall in mountainous regions than other systems. NT67 contributed to 20–30% of extreme floods across much of Japan, with locally higher contributions (50–80%) in western Kyushu, parts of southwestern Honshu, and coastal northern Honshu along the Sea of Japan. This aligns with the historical prevalence of the Meiyu–Baiu front and mesoscale convective systems in these regions (Duan et al., 2014; Mukunoki et al., 2021). In contrast, NT67 accounted for less than 10% of floods on the Pacific

side of northern Honshu and eastern Hokkaido, which is also consistent with historical climatological patterns. NT89 similarly contributed to 20–30% of extreme floods across large areas, with stronger influence in higher latitudes, including western Hokkaido, northwestern Honshu, and parts of central Honshu—reflecting the southward shift of autumnal fronts from high latitudes following the retreat of the Pacific high. Collectively, TC, NT67, and NT89 were responsible for over 90% of past extreme floods nationwide.

At the +2 ˚C stage, TC contributions decline by 10–20% along the Pacific side of northern Honshu. Some areas where historical TC-induced flood shares exceeded 80% now reduced to 60–70%. In contrast, southwestern Honshu shows localized increases of 10–30%. At the +4 ˚C, TC-related flood contributions further decreased, especially in the north, where reductions exceed 20% in some river basins. Minor increases (<10%) are observed in certain southwestern rivers. Overall, declining TC frequency under warming reduces their share in extreme floods, though increased moisture and altered tracks contribute to localized increases at the +2 ˚C (Hu et al., 2018). By the +4 ˚C, the decline in TC frequency dominates over other factors, leading to a national decline trend. Nevertheless, TCs remain the primary driver of extreme floods in most regions, accounting for approximately 50% floods.

NT67 shows a consistent increase in flood contributions under warming. At the +2 ˚C, increases of 10–20% are observed in northern Kyushu and along the Sea of Japan coast in northern Honshu—regions already significantly influenced by NT67 historically. At the +4 ˚C, the regions with 10%-20% increase in northern Kyushu shrink northward, while those in northern Honshu and western Hokkaido expanded, aligning with the northward shift pattern of the Meiyu–Baiu front (Osakada and Nakakita, 2018). The spatial expansion of NT67-related floods highlights the need for preparedness in regions not previously regarded as critical factors.

NT89 also shows growing contribution under warming, particularly in northern Japan. At the +2 ˚C, the Pacific side of northern Honshu experiences 10–20% increases, which expand across northern Japan at the +4 ˚C, reaching 10–30% in many areas. Thus, both NT67 and NT89 are projected to play increasingly important roles in future extreme flooding, with distinct regional shifts: NT67 expanding northward along the Sea of Japan coast, and NT89 extending from the Pacific side to broader northern regions.

In summary, the TC-induced floods are projected to decline, but still account for over

50% floods in many regions. Floods triggered by NT67 and NT89 are expected to increase, emerging as significant contributors under warmer climate conditions. Regionally, northern Japan is projected to experience more pronounced changes, and TC-induced floods in southwestern Honshu significantly increasing at the +2°C stage, but showing no significant increase at the +4°C.

6.2.2 Basin scale effect changes

The maximum flood potential of a region and its variation with basin size—referred to as the scale effect—is primarily governed by intrinsic geographical and climatic characteristics and provides critical insights for flood management planning. The Regional Envelope Curve (REC) offers a simple yet effective means of quantifying these scale effects. Due to diminishing precipitation intensity with increasing basin area and the attenuation of flood waves during routing, smaller basins typically exhibit higher unit peak discharges (normalized by basin area) than larger ones. This relationship is mathematically expressed as a negative REC slope, with steeper negative slopes indicating stronger scale effects, i.e., greater disparities in flood potential between small and large basins. Points on the REC represent the upper bound of unit peak discharge for a given basin size.

Figure 6-3 illustrates REC slopes for 109 national basins at the past, +2°C, and +4°C climate stages, categorized by weather drivers: TC, NT67, and NT89. The Watari River Basin serves as an example, depicting RECs for TC-induced floods at each climate stage. High-resolution simulations enhance the accuracy of regional flood potential estimation, while basin-specific RECs reduce uncertainty associated with homogenous regional classifications. Results demonstrate spatial coherence and driver-specific patterns in REC slopes. At the past stage, TC-induced REC slopes generally range from –0.1 to –0.2, with some basins exhibiting steeper slopes (< –0.2). While NT67- and NT89-induced floods fall within a similar range, a greater number of basins exhibit steeper slopes than those driven by TCs, indicating stronger scale effects. This can be attributed to differences in precipitation patterns: non-TC events tend to produce more spatially and temporally concentrated rainfall, amplifying flood potential in small basins, whereas TCs distribute rainfall more broadly, reducing scale disparities.

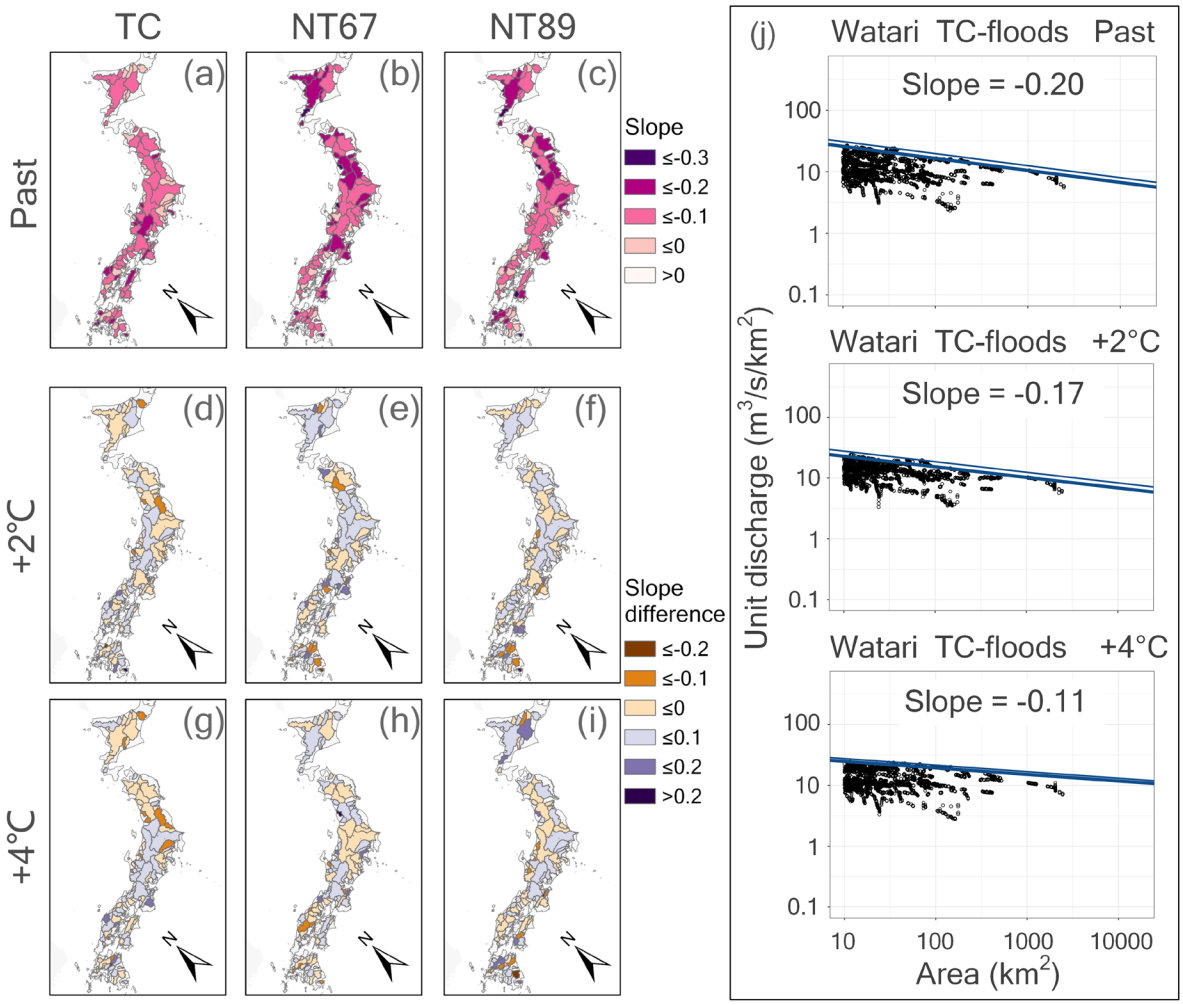


Figure 6-3 REC slope of TC-, NT67-, NT89-induced floods at the past climate stage, and their changes at the +2˚C, and +4˚C stages, with TC-induced floods in Watari River Basin as an example.

Abbreviations: Regional Envelope Curve, REC; Tropical Cyclone, TC; Non-Tropical cyclone event between June and July, NT67; Non-Tropical cyclone event between August and September, NT89.

Figures 6-3(d)–(i) show changes in REC slopes under warmer climates. Negative slope changes indicate intensifying scale effects, while positive changes suggest weakening. Regional significances of increase ratio trend along basin scales are presented in the supplemental material Figure S13-18. At +2˚C, TC-induced floods show intensified scale effects in northern Honshu and western Hokkaido, reflecting a shift toward more localized precipitation that disproportionately elevates flood potential in small basins—align with the current understandings and expectations (Haslinger et al., 2025; Yu et al., 2020; Zhao et al., 2023c; Zhou et al., 2021). However, weakened scale effects also exist and dominate overall. Figure 3(k) uses the Watari River Basin to illustrate this mechanism: despite the precipitation enhancement in a warmer climate, unit

peak discharge in small basins remains relatively unchanged, while large basins response by increasing flood potential, narrowing inter-basin differences. Differences in flood potential across basin scales result from a combination of factors, including changes in precipitation concentration, historical precipitation conditions, and geological characteristics, indicating the different flood protection priorities and strategies. The plateauing effect in small basins is likely attributable to either a substantial increase in rainfall amounts (compared with rainfall center) or pre-existing severe flood conditions in headwater areas, which limit the additional response capacity of these basins under further climate stress.

These findings imply that increased scale effects correspond to heightened risks in small basins, while decreased effects indicate an expansion of flood threats into medium and large basins. At the +4°C stage, TC-induced flood scale effects further weaken in most regions, with intensification largely confined to northern Japan. For NT67-induced floods, REC slope changes across +2°C and +4°C are inconsistent in some basins due to minimal fluctuations around zero. However, in regions with frequent NT67 events, a consistent weakening of scale effects is observed, indicating that flood impacts are expanding to larger basins. A similar trend is evident for NT89-induced floods, where weakened scale effects prevail in typically impacted regions. These patterns for both NT67 and NT89 can be attributed to their highly concentrated precipitation, which more easily reaches the flood potential plateau of small basins. Consequently, in a warmer climate, further increases in flood potential occur primarily in larger basins, leading to a weakened scale effect.

In summary, scale effects in flood potential exhibit both intensification and attenuation at warmer climates. For TC-induced floods, northern Japan is projected to experience stronger scale effects, underscoring the flood protection priority in small basins. In contrast, southern regions will require integrated strategies addressing both small and large basins due to a weakening scale effect. For non-TC-induced floods, a general weakening of scale effects suggests increasing flood risks in larger basins across typical impact zones.

6.2.4 Changes in flood responses

Beyond changes in frequency, variations in flood characteristics driven by different systems are also noteworthy. Figure 6-4 displays the median peak discharge—converted to equivalent precipitation intensity for basin-size comparability—for each

flood category at the outlets of 109 national basins, along with projected changes. Statistical significance of distributional changes is evaluated using the Kolmogorov–Smirnov (KS) test. Historically, regardless of the causative weather system, flood peaks generally exhibit a southwest-to-northeast decreasing gradient from the Pacific to the Sea of Japan side.

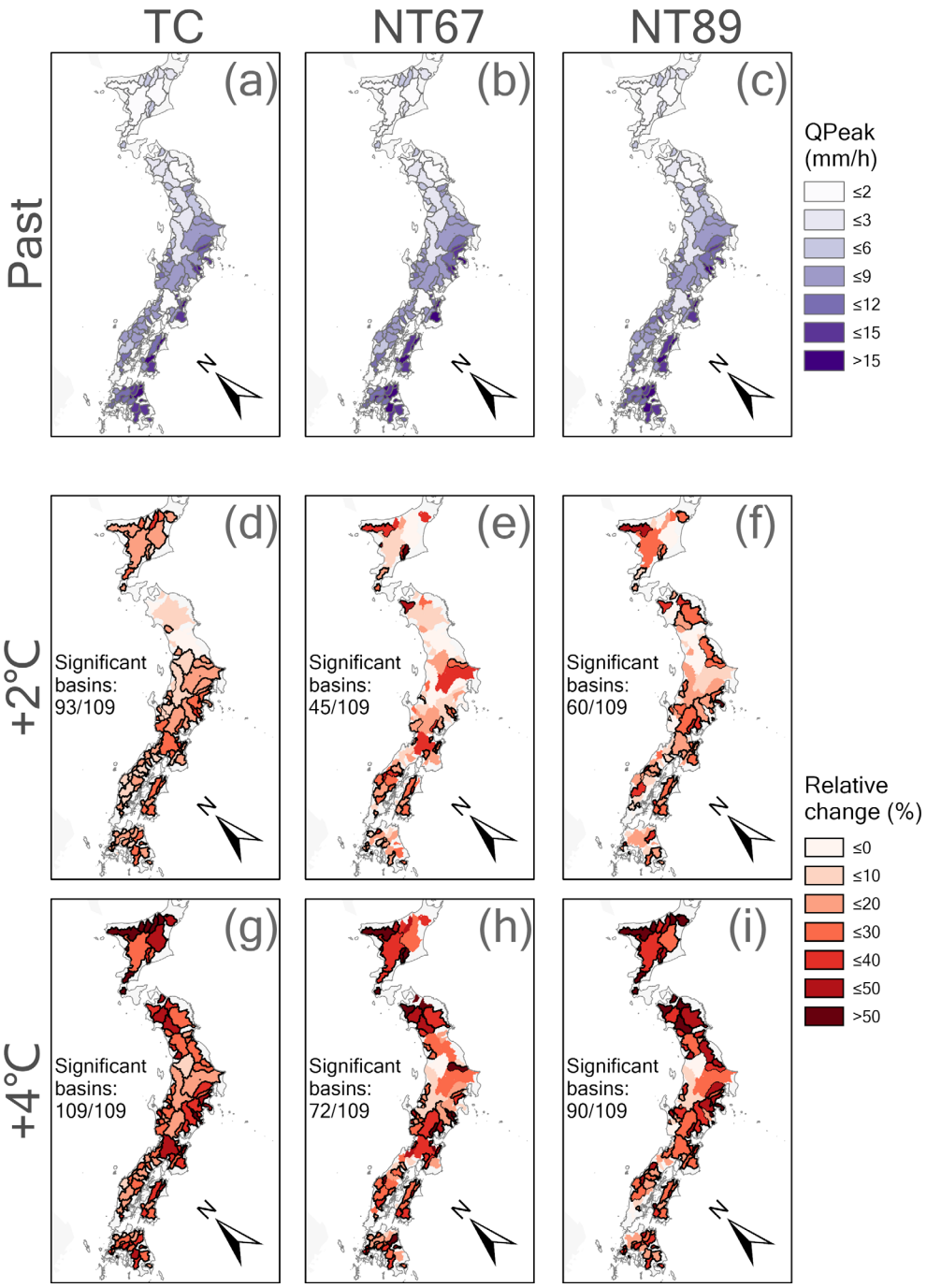


Figure 6-4 Discharge peak median of categorized floods at 109 national basin outlets under the past climate stage and the projected changes.

The black basin outlines indicate the statistically significant distribution changes at

a 95% confidence level according to the Kolmogorov–Smirnov test.

Within each warming stage, flood peak median changes are relatively consistent across categories, increasing by ~10–20% at +2°C and 20–50% at +4°C, reflecting the dominant influence of enhanced atmospheric water capacity (reflected by the Clausius–Clapeyron equation). The number of basins with significant increases follows the order: TC > NT89 > NT67. Both the magnitude of peak median increases and the number of significantly changed basins rise monotonically with warming. At the +4°C, TC-induced flood peaks increase significantly across all 109 basins, underscoring their broad-scale impact.

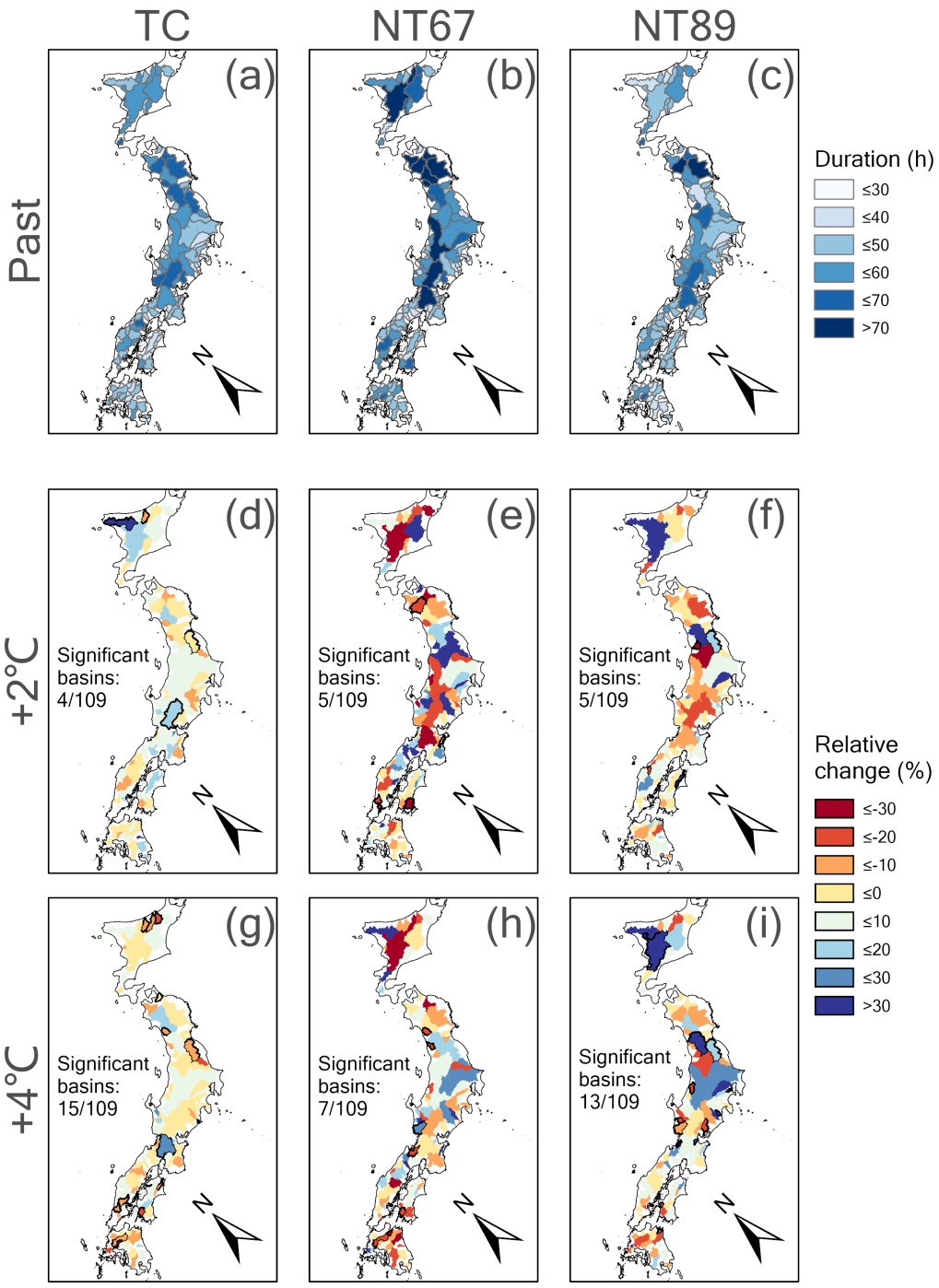


Figure 6-5 Effective duration median of categorized floods at 109 national basin outlets under the past climate stage and the projected changes.

The black basin outlines indicate the statistically significant distribution changes at a 95% confidence level according to the Kolmogorov–Smirnov test.

Figure 6-5 illustrates the median effective flood duration—defined as the period during which discharge exceeds 10% of the peak—for each flood category and its projected changes. Most basins exhibit duration medians of 30–70 hours, consistent with Japan's rapid-response hydrology. NT67- and NT89-induced floods tend to have

longer durations, with certain basins exceed 70 hours, reflecting the persistent rainfall associated with quasi-stationary systems like the Meiyu–Baiu front.

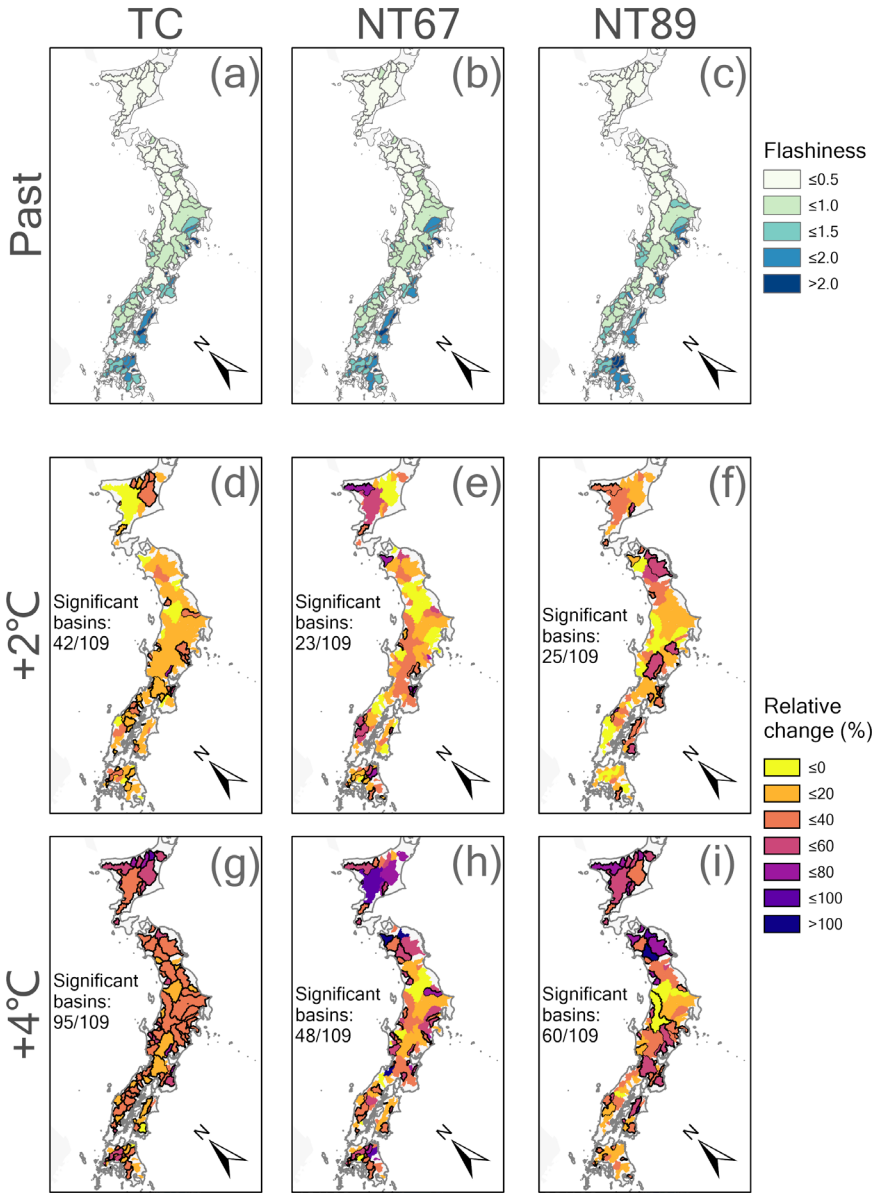


Figure 6-6 Flashiness of categorized floods at 109 national basin outlets under the past climate stage and the projected changes.

The black basin outlines indicate the statistically significant distribution changes at a 95% confidence level according to the Kolmogorov–Smirnov test.

TC-induced flood durations remain relatively stable under warming, with changes within ±10%. In contrast, NT67- and NT89-induced floods show more substantial variation with some basins exceed ±30%. However, few basins exhibit statistically significant changes. The large but insignificant change in non-TC flood durations is attributed to internal variability, as these categories encompass both short-duration

mesoscale convective events and long-duration rainfall from quasi-stationary systems, highlighting the heterogeneity of non-TC flood dynamics.

Figure 6-6 maps the spatial distribution of flashiness medians—an indicator of flash flood risk derived from hourly discharge data—and its future projections. Higher flashiness denotes faster, larger flood rises, implying greater flash flood risk. Historically, the flashiness median pattern closely aligns with the distribution of peak discharge median shown in Figure 6-4, with higher values along the southern Pacific coast.

At +2°C, significant flashiness increases occur mainly in smaller basins. At +4°C, TC-induced floods show significant increases in 95 of 109 basins with a relative change range of around 20–40%, reaffirming their widespread impact. NT67-induced floods exhibit flashiness increases primarily in small basins, while NT89-induced floods show notable increases even in some larger basins. Overall, non-TC-induced floods exhibit greater increases in flashiness than TC-induced floods, underscoring their critical role in amplifying future flash flood risks.

6.3 Discussion

The weather systems triggering floods in Japan are projected to undergo significant shifts due to climate change, typically reflected in changes in the flood compositional proportions. These shifts are likely to entail a range of social and environmental challenges. From a flood control perspective, TC tracks are relatively predictable, providing lead time for interventions such as reservoir drawdown (Trošelj and Lee, 2021). In contrast, non-typhoon-related extreme precipitation remains challenging to forecast (Sayama et al., 2020). Although the Meiyu–Baiu front (related to NT67) occurs during a predictable seasonal window, uncertainty in the location and intensity of associated front band limits the effectiveness of preparatory actions. Similarly, autumnal frontal systems (related to NT89) often trigger sudden, intense rainfall under unstable atmospheric conditions, leaving little warning time. The projected increases in NT67- and NT89-induced floods suggest these systems will become more prominent flood drivers in certain regions, presenting substantial challenges for future flood risk management.

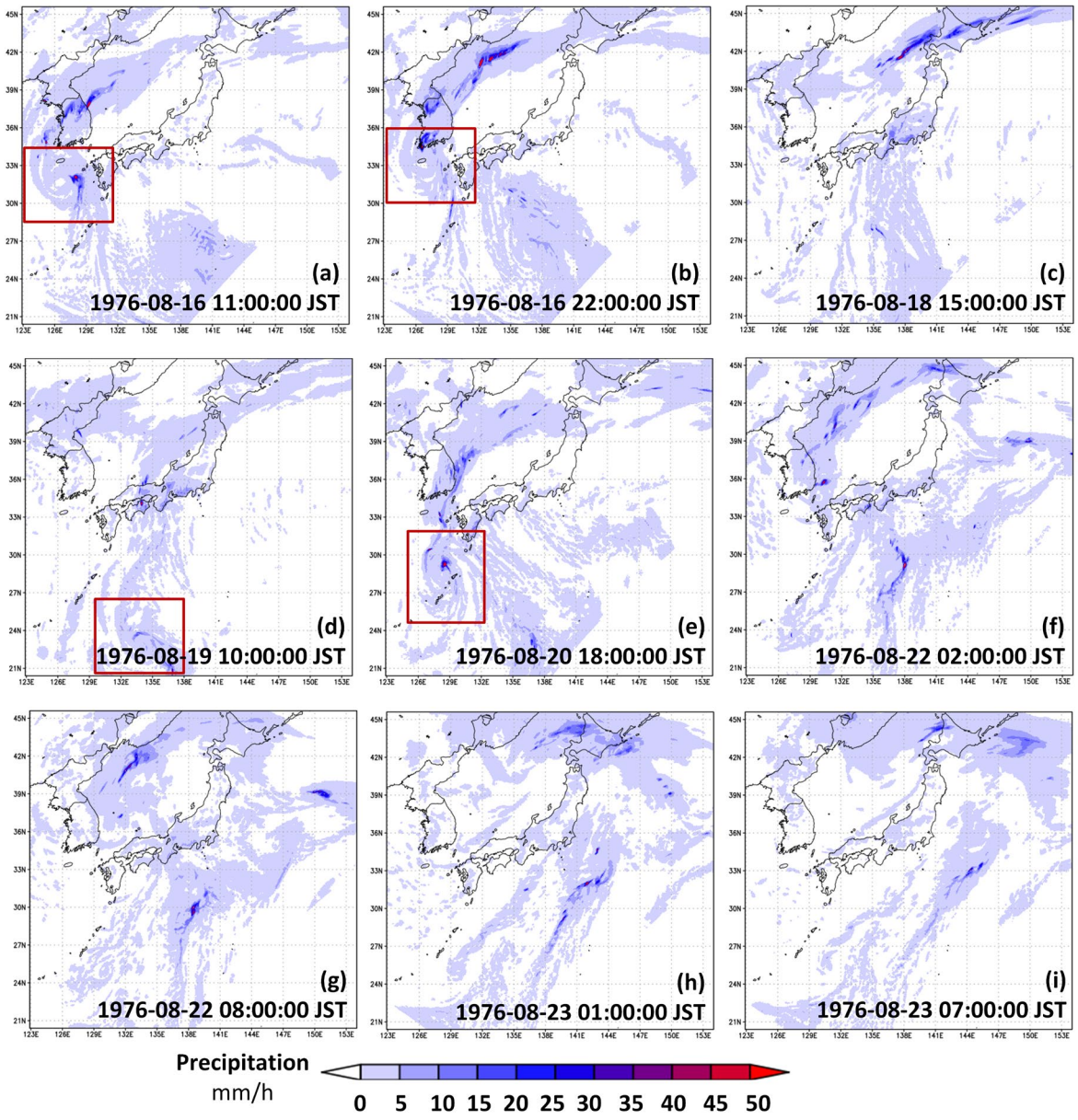


Figure 6-7 Representative precipitation processes of the largest flood event in Ishikari basin from the past climate ensemble.

Although direct TC landfalls in Hokkaido are rare, this study reveals that a considerable proportion of floods in the region are TC-induced. The precipitation process of a representative TC-induced flood event, shown in Figure 6-7, explains this phenomenon. This event resulted in the largest flood in the Ishikari basin, which is the largest basin in Hokkaido, from the climate ensemble data. Figures 6-7(a) and 6-7(b) show the TC center (red frame) positioned west of Kyushu. Despite the distance, substantial moisture was transported northeastward via the Sea of Japan, bypassing Honshu, and causing intense precipitation over Hokkaido (Figure 6-7c). Thus, even without direct landfall, TCs can remotely trigger flooding via atmospheric circulation.

The successful attribution of this event highlights the effectiveness of the matching approach employed in capturing such remote TC impacts. Notably, although the TC center was geographically closer to Kyushu, it did not produce severe rainfall there. This emphasizes the need for flood defense preparation that account for moisture transport pathways, not just TC tracks.

The extreme flooding in the Ishikari River basin was further exacerbated by the sequential influence of two TCs. As shown in Figures 6-7(d) and 6-7(e), before precipitation from the first TC subsided, a second TC developed at low latitudes over the Pacific, tracked toward western Kyushu, and followed a similar moisture pathway to high latitudes, initiating a second heavy rainfall in Hokkaido. Notably, this event, derived from one of the ensemble members, which used additional perturbation on historical boundaries, was not intended to replicate the exact historical timing or rainfall magnitude. Instead, it demonstrates the possibility of binary TC systems under similar climate boundaries and our simulations confirm their potential to produce floods with return periods exceeding 720 years.

Flood events driven by multiple TCs are increasingly reported (Kimura et al., 2018; Liang et al., 2022; Yu et al., 2015). For example, the devastating rainfall event in Henan, China in July 2021 has been linked to a binary TC system (Deng et al., 2022). The mechanisms underlying multiple TC interactions and their response to climate change require further investigation (Cha et al., 2021; Li et al., 2018; Yu et al., 2015). The simulated flood in the Ishikari basin caused by a binary TC system underscores that conventional flood design approaches—especially those used for long return periods (e.g., 200 years) or based on probable maximum precipitation—may underestimate flood magnitudes if they assume a fixed precipitation duration. This highlights the value of climate ensemble-based flood frequency analysis and demonstrates the advantages of the Aggregating Grid Event (AGE) method employed in this study, which identifies extreme events without relying on predefined time windows (Chen et al., 2025c).

The slowdown of TC translation speed is a widely discussed topic in climate science. Observations have shown a significant deceleration in TC movement over the Northwest Pacific (Kossin, 2018; Song et al., 2024; Yamaguchi et al., 2020), including during and after landfall (Wu et al., 2022). Studies have identified a positive correlation between slower TC movement and enhanced storm intensity (Mei et al., 2012; Walker et al., 2014; Zhao and Chan, 2017), resulting in higher regional rainfall

amount (Kossin, 2018; Lai et al., 2020). Climate change is expected to weaken large-scale atmospheric circulation, further contributing to this slowdown (Chu et al., 2012; Coumou et al., 2015; Kossin, 2018; Screen et al., 2018; Zhang et al., 2020). This trend implies elevated TC-related flood risks, as illustrated in Figure 6-4. However, studies explicitly examining the hydrological impacts of slower-moving TCs remain limited. According to Figure 6-5, despite the projected deceleration, this study found limited significant increases in effective flood duration for TC-induced floods, suggesting that the associated rainfall-runoff processes require further investigation.

At the historical stage, REC slopes predominantly range from –0.1 to –0.3, indicating weaker scale effects in Japan compared to Europe (Bertola et al., 2024). This phenomenon is primarily driven by two factors: (1) the classification of floods by weather drivers leads to similar rainfall patterns across basin sizes, inherently flattening the REC slopes; and (2) Japan's mountainous terrain provides higher gravitational potential energy for runoff and limits flood wave attenuation, with flash floods dominating—further reducing disparities in flood potential between small and large basins.

The changes in REC slopes must be interpreted within the broader context of regional hydrological characteristics and climate change impacts. In Japan, previous studies project increases in extreme precipitation, particularly for short-duration events (Zhao et al., 2023c), suggesting a likely rise in flood potential for small basins and, consequently, an intensification of the scale effect. When observed trends deviate from this expectation, they are attributed to the plateauing of flood potential in small basins. Given the already high unit peak discharges at the past stage, both trends signify rising flood risks, but underscore different priorities for mitigation: intensified attention on small basins when scale effects increase, and expanded risk management strategies for larger basins when scale effects weaken.

One limitation of this study is the exclusion of compound effects from sea-level rise and storm surge, which could lead to underestimation of flood peaks in coastal rivers. However, this limitation minimally affects the attribution analysis and primarily influences flood characteristics in coastal zones. The river outlets selected for flood characteristic assessment are key national flood control points, generally located upstream of coastal areas, where compound effects are attenuated. Therefore, the results remain robust.

Additionally, due to the complexity of identifying non-typhoon systems—particularly mesoscale convective systems such as line-shaped rainbands—automated detection methods within large ensemble datasets remain underdeveloped. Consequently, this study does not differentiate non-TC systems by their physical structures when analyzing individual impacts. This may obscure certain flood characteristics, such as effective duration. Nonetheless, for most metrics, the dominance of Meiyu–Baiu systems in June–July and autumnal fronts in August–September ensures that their impacts remain discernible.

6.4 Conclusions

This study integrates a large ensemble of climate projections with a high-resolution hydrologic model to assess changes in the proportion and characteristics of weather-specific floods in Japan at the past, +2 ˚C, and +4 ˚C climate stages. Historically, TC, NT67, and NT89 systems together account for over 90% of floods with return periods exceeding 10 years, with TCs alone contributing more than 50%, and NT67 and NT89 each contributing 20–30%.

Global warming is projected to reduce the frequency of TCs around Japan, leading to an overall decline in TC-induced flood occurrence. However, due to complex changes in TC tracks and intensities, some rivers in southwestern Japan are projected to experience increases of up to approximately 20% in the proportion of TC-induced floods at +2 ˚C, while northern Japan shows pronounced decreases exceeding 20%. Despite the decline in frequency, the impact of TC-induced floods—measured by peak discharge and flashiness—is projected to rise significantly across most basins, increasing by approximately 20–40% at +4 ˚C, indicating widespread national impacts. The weakening of scale effects under warmer climates suggests that flood potential in small basins has largely plateaued. Therefore, mitigation efforts should prioritize peak discharge increases in large basins. In contrast, basins in northern Japan with intensified scale effects will see rising flood potential in both small and large basins, necessitating greater focus on small-basin flood prevention.

Floods associated with NT67 and NT89 systems display strong regional variability, contributing 50–80% of floods in several regions. Both types are projected to increase their contributions in northern Japan, with non-TC systems becoming dominant drivers in some areas. NT67-induced floods are expected to rise along the Sea of Japan coast, while NT89-induced floods show more spatially uniform increases, typically

between 20–30%. Their peak discharges and flashiness are also projected to increase significantly, especially in small- to medium-sized basins. In frequently impacted regions, a consistent weakening of scale effects is projected under warmer climates, indicating that non-TC impacts will also increasingly affect larger basins.

This study reveals substantial shifts in the causation and characteristics of future floods in Japan, emphasizing the growing complexity of regional flood drivers and the distinct change patterns associated with TC-, NT67-, and NT89-induced events. The findings highlight escalating challenges for flood risk management and underscore the urgent need to develop targeted strategies, particularly for non-TC systems. The results offer critical data and insights to support future planning by regional flood control authorities.

6.5 Methods

6.5.1 Data sources

Hourly precipitation data for the past, +2 ˚C, and +4 ˚C warming stages were sourced from the 5-km dynamically downscaled d4PDF (Database for Policy Decision-making for Future climate change) project (Kawase et al., 2023). The original simulations were conducted using the Meteorological Research Institute Atmospheric General Circulation Model version 3.2 (MRI-AGCM3.2) at a horizontal resolution of 60 km (Mizuta et al., 2012, 2017). These outputs were subsequently downscaled over Japan to a 5-km resolution using the Non-Hydrostatic Regional Climate Model (NHRCM) (Sasaki et al., 2008), resulting in 720 years of simulations for each climate stage.

Historical simulations were forced by 1951–2010 boundary conditions with 12 ensemble members generated via perturbations. Future projections were driven by outputs from six Global Climate Models (GCMs), with 12 ensemble members generated by applying two perturbations to each GCM output. Further details on the experimental design are provided in (Mizuta et al., 2017) and (Kawase et al., 2023). The use of a pseudo global warming simulation scheme in the d4PDF project avoids non-stationarity issues, ensuring robustness in comparative analyses across climate stages.

To support flood attribution, a global tropical cyclone track dataset developed by (Webb et al., 2019) based on d4PDF outputs, was used. The TC track extraction methodology creating this dataset has been validated against the International Best

Track Archive for Climate Stewardship (IBTrACS), demonstrating high consistency, particularly in the Northern Hemisphere (Shimura et al., 2017; Webb et al., 2019).

Topographic data were obtained from the 30-m Japan Flow Direction map (J-FlwDir) developed by (Yamazaki et al., 2020), which integrates high-resolution digital elevation models and hydrological maps detailing streamlines and water surfaces. These data were upscaled to 150 m using the method proposed by (Masutani et al., 2006) for preserving the alignment of main stream locations.

6.5.2 Hydrodynamic model

Flood simulations were conducted using the Rainfall–Runoff–Inundation (RRI) model, which couples 1D diffusive wave equations for river flow with 2D diffusive wave equations for overland flow, enabling simultaneous simulation of runoff and inundation processes (Sayama et al., 2012, 2015). This internal coupling is essential for accurately modeling river–land water exchanges during flood events. The Green–Ampt infiltration model was applied for flat terrain (Green and Ampt, 1911), while a stage–discharge relationship was used to represent subsurface flow in mountainous regions (Sayama and McDonnell, 2009; Tachikawa et al., 2004). The model employs spatially distributed parameters, linking hydrological and hydraulic responses to underlying soil and land cover characteristics. Model calibration and validation details are provided in (Sayama et al., 2025). To account for reservoir operations, a simple dam module was implemented for 121 national dams (locations shown in Figure S9) (Ly et al., 2021). River grids were defined as cells with upstream contributing areas exceeding 1.1 km². The simulation was conducted at a spatial resolution of 150 m, with a time step of 1 min for rivers and 10 min for overland flow. The fifth-order Runge-Kutta method was used to solve ordinary differential equations and an adaptive time-step control scheme was used to improve numerical stability (Cash and Karp, 1990; Sayama et al., 2012). Hourly discharge outputs were generated for all simulations.

6.5.3 Extreme precipitation event extraction method

To reduce computational costs of hydrodynamic simulations over a large domain, this study employed the Aggregating Grid Event (AGE) method to identify critical flood-causative precipitation events from climate ensemble data (Chen et al., 2025c). The AGE method was developed based on hydrological concepts, enabling the extraction

of complete precipitation processes responsible for floods exceeding a target return period, accounting for heterogeneity in extreme event sets due to differences in basin sizes and locations within a region. This study targeted a 10-year return period, following regional definitions established in Chen et al. (2025b). Depending on the region's size and precipitation variability, approximately 3,000 to 6,000 events were extracted from the 5-km d4PDF dataset for each region at each climate stage.

6.5.4 Flood attribution method

For each river grid, the top 72 independent peak discharges were extracted. A TC was considered a potential influence Japan if its center passed through the region bounded by 123°E–150°E and 30°N–46°N. Flood events overlapping the temporal extent of any such TC were categorized as TC-induced floods. All remaining events were classified as non-TC floods and further grouped into NT67 (June–July) and NT89 (August–September), reflecting the typical occurrence periods of Meiyu–Baiu and autumnal fronts, respectively (Takaya et al., 2020; Zhao et al., 2023b).

6.5.5 Index and Statistical Testing

The Regional Envelope Curve (REC) was defined by Eqs. 1 and 2, and estimated with the largest discharge peak of all river grids. The slope b was estimated by quantile regression (Amponsah et al., 2020), choosing a 95% threshold, and the intercept a was further adjusted for covering all data, showing as two lines in Figure 3 (j).

$$\log(q_{max}) = a + b \times \log(CA) \tag{1}$$

$$q_{max} = \max\left(\frac{q_i}{CA}\right) \tag{2}$$

where, CA is the contributing area; q_i is the discharge peak of the i^{th} event; q_{max} is the maximum discharge peak among events; a and b are the intercept and slope of REC, respectively.

Flashiness (F), an indicator of flash flood risk (Li et al., 2022), was calculated based on the maximum increase in discharge over a fixed duration window (6 hours in this study). The discharge increase is normalized by the CA and duration, as shown in Eq. 6-2.

$$F = \frac{\max\left(Q_t - Q_{t-1}, Q_t - Q_{t-2}, \ldots, Q_t - Q_{t-d}\right)}{CA \times d} \tag{6-2}$$

where, Q_t denotes the discharge at time t, d is the duration.

To assess statistical significance in flood characteristic changes between historical and future climates, the Kolmogorov–Smirnov (KS) test was employed. This non-parametric test evaluates differences in cumulative distributions. A 95% confidence level was used to reject the null hypothesis of no significant difference.

7. Concluding remarks

To facilitate flood impact assessments under climate change at any location in Japan and support localized decision-making, this study develops a comprehensive methodology centered on the Aggregating Grid Event (AGE) method. Leveraging dynamically downscaled 5-km d4PDF climate ensemble data and a high-resolution (150 m, hourly) large-domain flood model—the Rainfall-Runoff-Inundation (RRI) model—floods exceeding the 10-year return period are projected for all river cross-sections in Japan. Preliminary analyses summarize changes in flood patterns and associated weather systems at the +2˚C and +4˚C warming stages.

Chapter 2 proposes an initial simulation framework—the regional approach—for extracting regional extreme event sets. This approach circumvents the infeasible computational cost of continuous simulations across the full climate ensemble by constructing extreme event sets based on regional annual maximum 48-hour precipitation. Given the ensemble includes 372 years per warming stage (31 years × 12 members), sufficient data are available for robust analysis. Over Shikoku Island, flood frequency analyses for eight major basins demonstrate that the regional method yields accurate discharge quantiles at basin outlets. The Peaks-Over-Threshold (POT) method outperforms the Block Maxima (BM) method by more effectively mitigating errors associated with high-frequency flood inconsistencies, which introduced by the regional approach. POT analyses using the top 10%–50% of flood peaks are recommended. However, fixed-duration event extraction fails to capture complete precipitation processes across all basins and overlooks variability in river concentration times, resulting in substantial bias in frequency estimates. Additionally, regional precipitation maxima may not represent floods driven by localized extremes in tributaries.

Chapter 3 addresses these limitations by introducing the AGE method, which extracts precipitation events causing floods above a specified return level at any river cross-section within a target region. The method identifies top-n precipitation events at each grid cell (including upscaled grids), and aggregates them into a regional extreme event set. The extracted events are selected by the contribution of rainfall within an approximate river concentration time of corresponding grid size. The value of n is determined by the ensemble size and return period (e.g., n = 72 for a 10-year flood in

a 720-year ensemble). From the 5-km d4PDF dataset over Shikoku Island, 25,700 valid events with at least one value exceeds 10 mm/h are extracted and used as the benchmark. In contrast, the AGE method extracts much less, with 2,966 events. Validation shows that AGE-based estimates of flood quantiles are highly accurate across all river grid cells, with relative bias for the 100-year flood generally within ±5%, slightly biased toward underestimation.

Chapter 4 compares the AGE method to the precipitation stretching method. Both of them can incorporate the spatiotemporal precipitation variability, but achieve in completely different ways. The AGE method relies on extracting events from climate ensemble, whereas the precipitation stretching method synthetizes events based on regional characteristics summarized from ensemble data. Results show the AGE method consistently achieves higher accuracy without introducing additional uncertainty. In contrast, the precipitation stretching method yields errors up to ±40% for 100-year discharge estimates over Shikoku, and the strategy that utilizing ensemble means increases uncertainty by 25%–50%. These findings underscore the robustness and accuracy of the AGE method for high-resolution, ensemble-based flood frequency estimation over a large domain.

Building on this, a complete methodological framework is established. The AGE method extracts regional extreme precipitation events from the 5-km d4PDF dataset, followed by RRI simulations to generate runoff for each river grid. The top 72 discharge peaks at each grid are analyzed using the POT method to derive frequency curves for floods exceeding a 10-year return period.

Chapter 5 applies this framework to all of Japan, dividing the country into 14 regions. Analysis of 100-year flood changes under warming shows nationwide discharge peak increases of 1.16× and 1.37× at +2˚C and +4˚C stages, respectively. Northern regions such as Tohoku and Hokkaido exhibit greater increases and higher climate sensitivity. Within regions, variability is substantial, with small basins and mountain–plain transition zones showing relatively higher increases. These newly identified high-risk zones warrant increased attention. Flood hydrographs are projected to become steeper, with 10%–20% faster rising limbs, indicating elevated flash flood risks. Statistically significant increases in flashiness across northern Japan suggest the need for incorporating emerging flash flood risks into future flood management strategies. This chapter also generates a large future flood database to support localized hazard and impact assessments.

Chapter 6 investigates meteorological drivers of future floods, focusing on the role of tropical cyclones (TCs). Unlike conventional studies that infer impacts from changes in weather patterns, this attribution is based directly on projected flood events, enabling more robust and clearer causal inferences. Using a d4PDF-based global TC track dataset, floods are categorized into TC-induced, non-TC events in June–July (NT67, linked to Meiyu–Baiu fronts), and non-TC events in August–September (NT89, linked to autumnal fronts). These three types account for over 90% of historical floods, with TCs being dominant (>50%). A general decline in the proportion of TC-driven floods is observed, particularly in northern Japan, due to fewer TCs in the western North Pacific. However, changes in TC tracks and intensification lead to a ~20% increase in TC-induced floods in the Chugoku region at +2°C. Despite reduced frequency, TC-driven flood peaks and flashiness intensify, with widespread national impacts. Contributions from NT67 and NT89 increase by 20%–30%, with pronounced regional variability. Their peak discharges and flashiness are also projected to rise. While TCs remain the primary driver nationally, flood causation becomes increasingly complex regionally, complicating flood management. Scale effects in flood potential exhibit both intensification and attenuation at warmer climates. For TC-induced floods, northern Japan is projected to experience stronger scale effects, underscoring the need for targeted flood peak management in small basins. In contrast, southern regions will require integrated strategies addressing both small and large basins due to a weakening scale effect. For non-TC-induced floods, a general weakening of scale effects suggests increasing flood risks in larger basins across typical impact zones.

In summary, this study presents a novel simulation framework enabling high-resolution, climate ensemble-based, nationwide flood projections. Through extensive simulations and analyses, it reveals evolving flood patterns and critical shifts in flood-generating mechanisms across Japan. The findings underscore the need to focus on newly identified high-risk areas and adapt to a more complex flood regime, urging further research to validate intensified flood risks in those regions and develop region-specific flood management strategies, thereby enhancing national resilience.

Supporting information

Supplemental figures

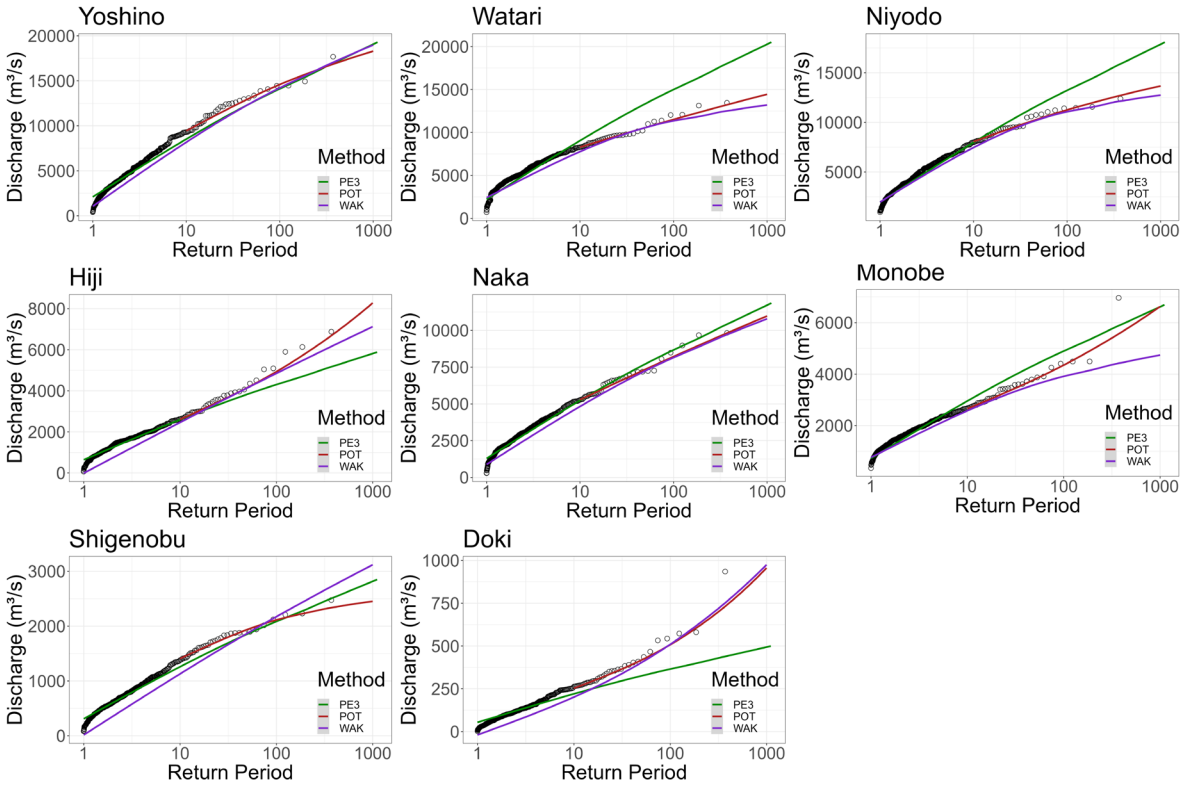


Figure S1 Comparison of fitting methods for basin annual maximum series.

The Wakeby (WAK) is a five-parameter distribution with advantage of assigning lower weight to lower values. POT method is able to screening out lower values. Both of them are the possible optimal method for obtaining reference results. Meanwhile, the reference results in this study are modeled based on the annual maximum discharge for each basin, making the goodness-of-fit Z equally applicable. Therefore, PE3 also appears to be a potential optimal distribution. Thus, we conducted a comparative analysis for the eight basins. The result shows in Figure S1. The five-parameter Wakeby distribution is more robust than the three-parameter PE3 and less prone to significant overestimation in long return periods. However, when focusing on return periods exceeding 10 years, the fitting performance is evidently inferior to the POT method with the top 10% peak discharges. Therefore, the POT with a threshold of top 10% peak discharges is selected to create reference frequency curves.

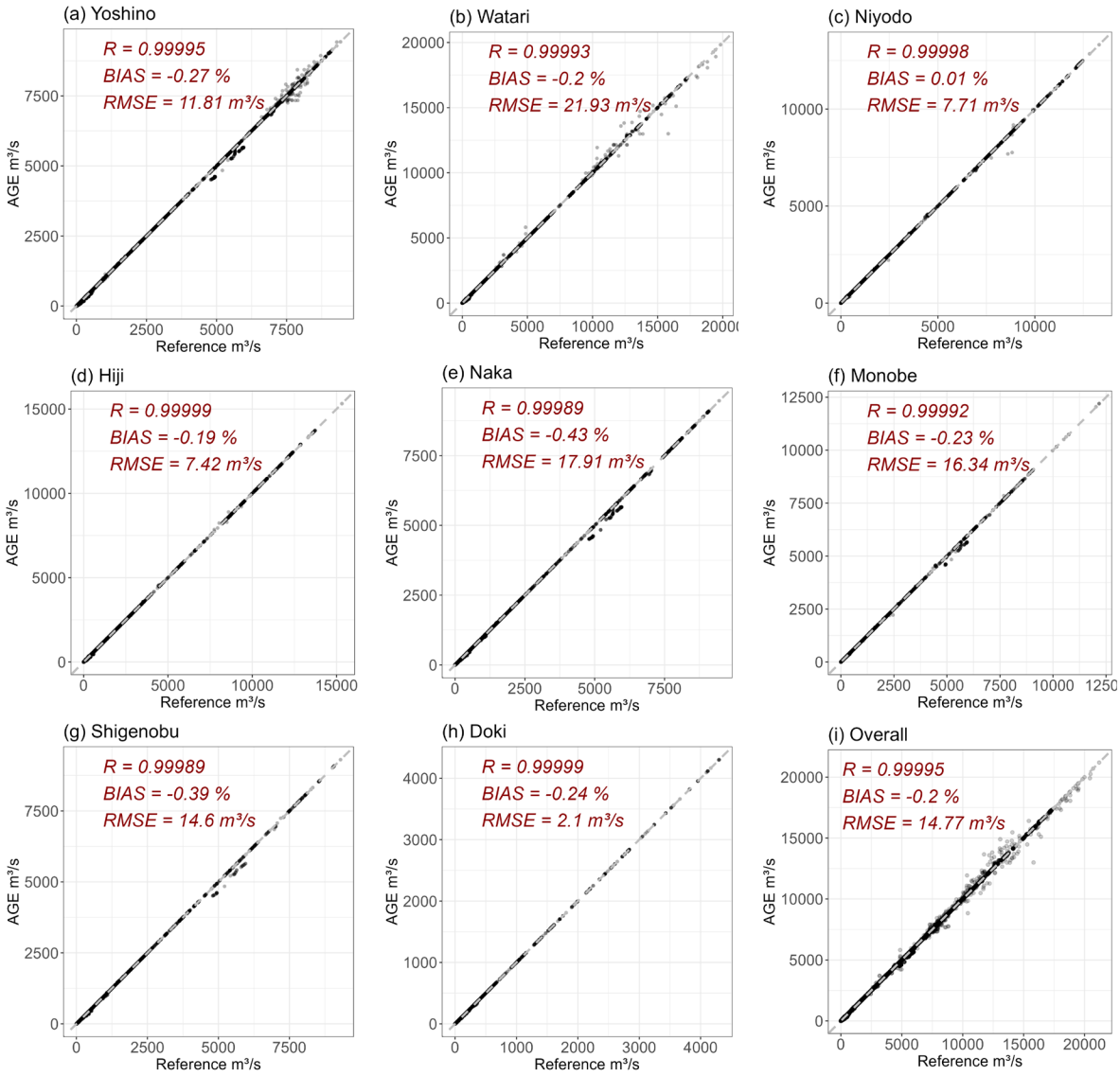


Figure S2 Evaluation of the peak discharges of all river grids, based on the events extracted by the aggregating grid event (AGE) method using the total rainfall (TR) indicator.

(a)~(h) portray the results for the eight major basins the Shikoku Island; (i) portrays the overall results for Shikoku Island. Abbreviations: correlation coefficient (R), relative bias (BIAS), root mean square error (RMSE).

In step 2 of the AGE method, selecting an appropriate ranking indicator is crucial to extract precipitation events most likely to result in discharges with an annual exceedance probability (AEP) $\leqslant$0.1. One potential option is utilizing the total rainfall (TR) of an event, stemming from the saturation excess theory.

As a preliminary experiment, we used 60-year data for examination. 122 events were

extracted by using TR as the ranking indicator. Subsequently, the highest six discharges for each river grid were selected after simulations. The evaluation results of these peak discharges are shown in Figure S2. (a)~(h) portray the results for the eight major basins the Shikoku Island; (i) portrays the overall results for Shikoku Island. The -0.2 % of BIAS and the 14.77 m3/s of RMSE for the overall Shikoku Island indicate that using TR as the ranking indicator can achieve highly accurate in peak discharge estimations. Therefore, TR emerges as a promising indicator for consideration in the AGE method.

Another potential option to rank events is using the rainfall during concentration time (RDCT). This indicator represents the highest rainfall intensity of an event, which is inspired by the infiltration excess theory. The approximate basin concentration time was used as the valid period for calculating the rainfall intensity, as we assume that the rainfall within this period will contribute to the same discharge peak.

We applied the RDCT to the AGE method and processed the same 60-year dataset. 161 events were extracted The RDCT theoretically enhances the identification of localized extreme precipitation events characterized by short durations and limited spatial extents, making them less prone to merging with other events during aggregation. Consequently, a larger number of precipitation events were extracted using RDCT compared with TR, with relatively shorter durations.

Similar to Figures 3-4 and 3-5, evaluation on RDCT-based peak discharges was conducted. Results show slightly higher accuracy compared to those based on TR, with a BIAS of 0.03% and an RMSE of -13.65 m3/s on Shikoku Island. This improved performance is likely attributed to the AGE method extracting more localized events based on RDCT, which is important for a small proportion of river grids. Overall, whether using TR or RDCT as the ranking indicator, there is not a significant impact on the accuracy of peak discharges in Shikoku Island.

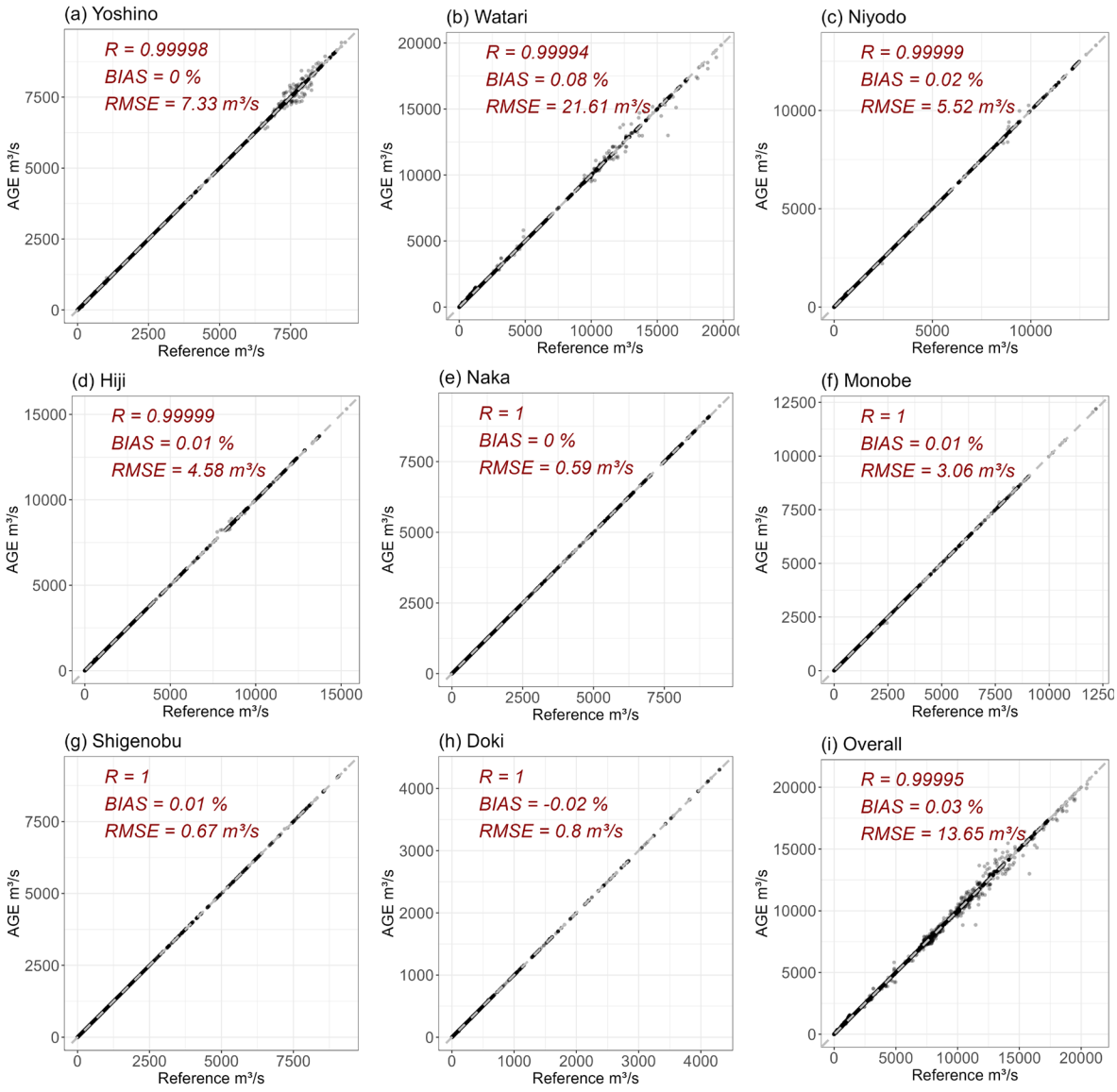


Figure S3 Evaluation of the peak discharges of all river grids, based on the events extracted by the aggregating grid event (AGE) method using the rainfall during concentration time (RDCT) indicator.

(a)~(h) portray the results for the eight major basins the Shikoku Island; (i) portrays the overall results for Shikoku Island. Abbreviations: correlation coefficient (R), relative bias (BIAS), root mean square error (RMSE).

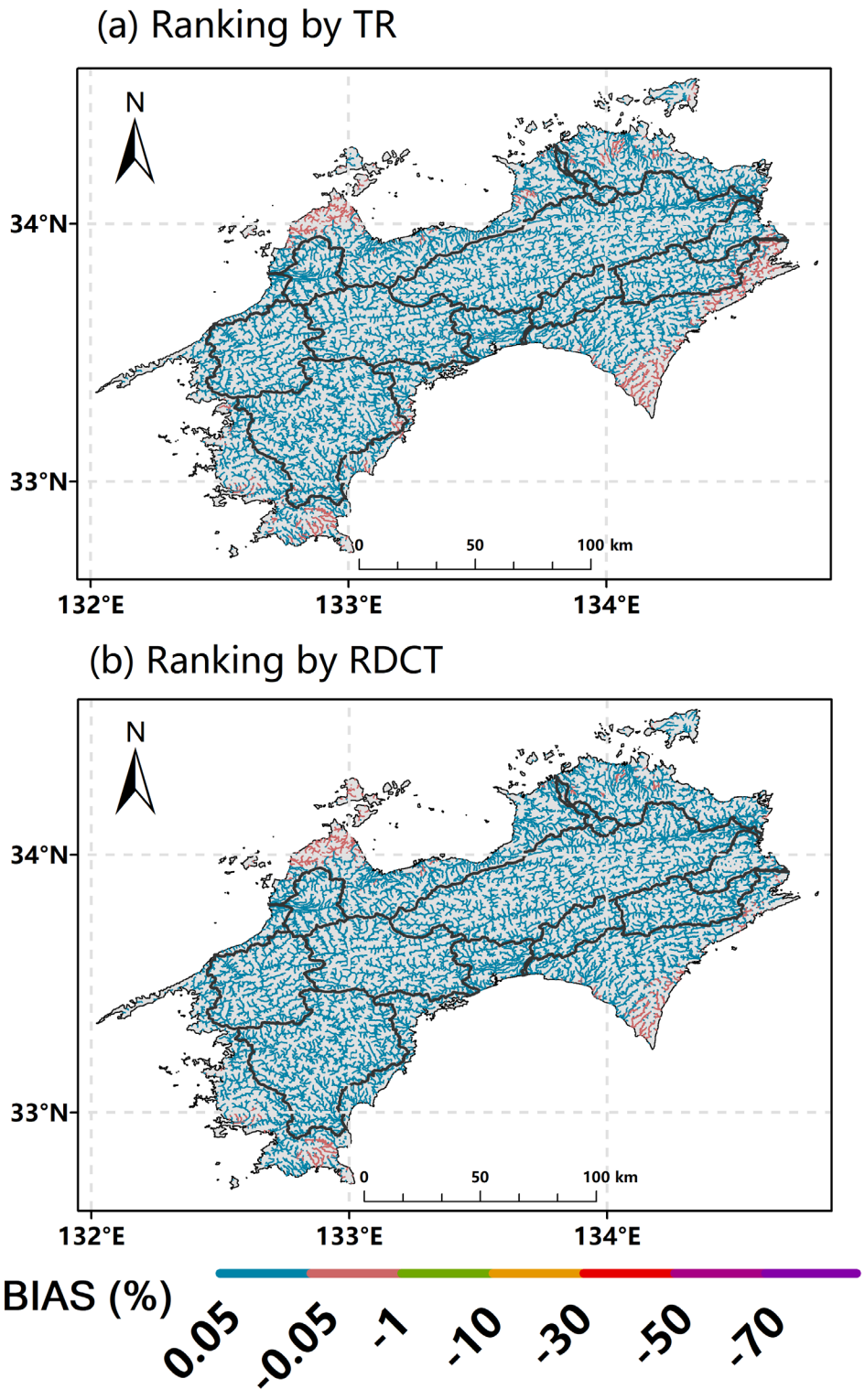


Figure S4 Spatial distribution of the relative bias (BIAS) values in the peak discharges, based on the aggregating grid event (AGE method) using the (a) total rainfall (TR) and (b) rainfall during concentration time (RDCT) indicators.

The spatial distribution of the BIAS was shown in Figure S4. Note that, a BIAS in this figure was calculated by the peak discharges of the corresponding river grid. Most

river grids exhibit a predominance of BIAS values falling between 0.05% and -0.05%. Notably, the spatial pattern of the BIAS does not demonstrate significant differences between utilizing the TR or RDCT indicator. Therefore, we ultimately opted to utilize RDCT as the ranking indicator for the AGE method in this study.

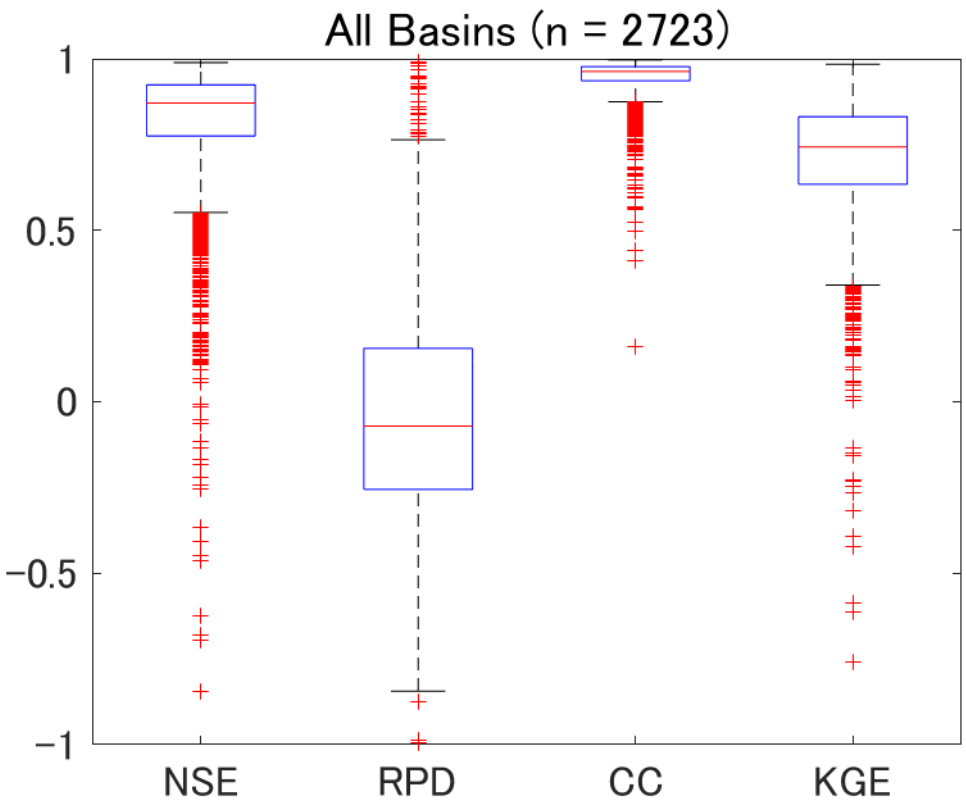


Figure S5 Box plots of the evaluation indices, including NSE, RPD, CC, and KGE at 711 national stations (2,723 events in total).

Abbreviations: Nash–Sutcliffe Efficiency (NSE), Relative Peak Difference (RPD), Correlation Coefficient (CC), Kling-Gupta Efficiency (KGE).

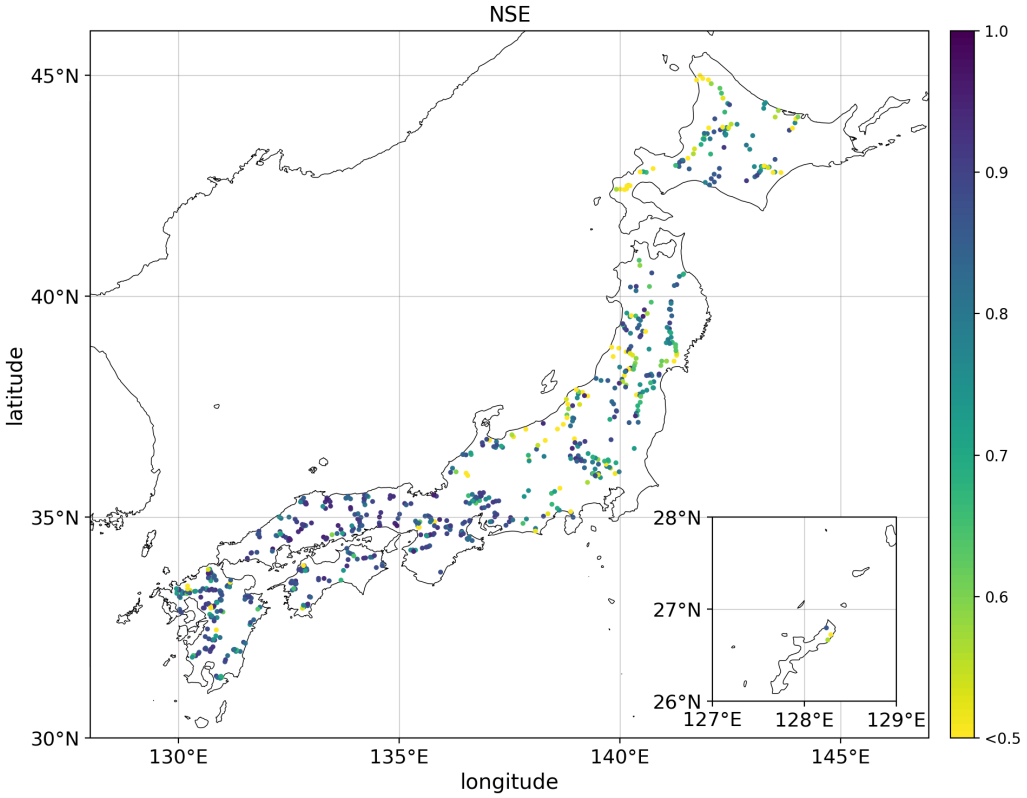


Figure S0-6 Spatial distribution of average NSE values at 711 national stations. Abbreviations: Nash–Sutcliffe Efficiency (NSE).

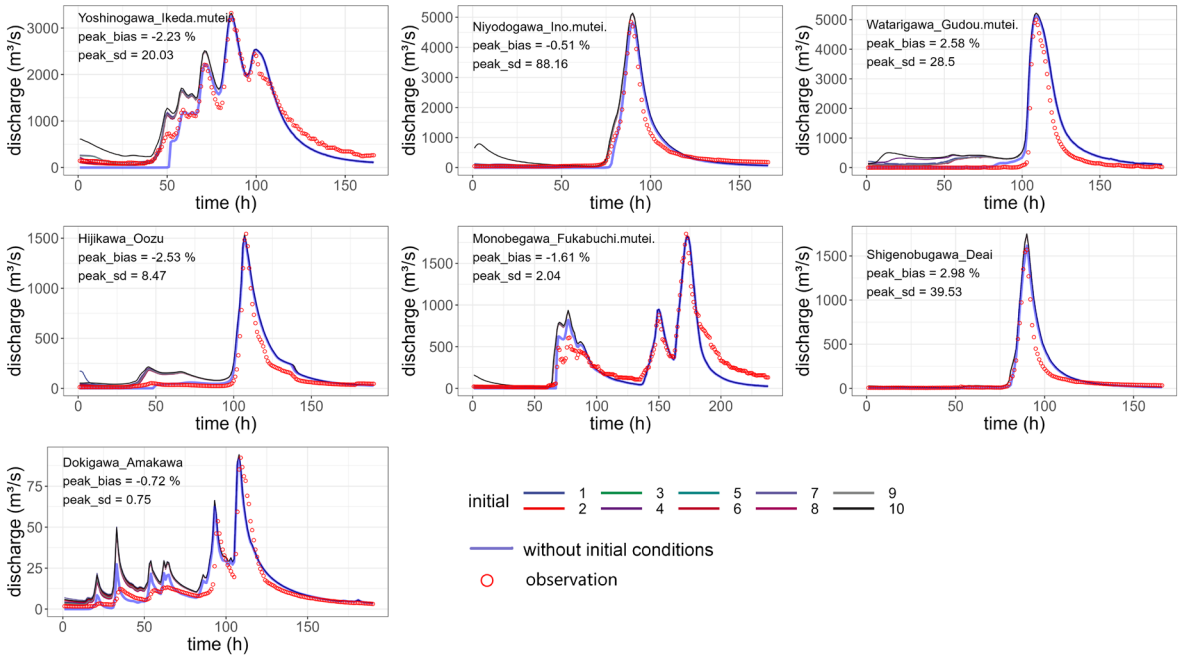


Figure S7 Comparisons of observed events against discharge simulated with and without initial conditions at the major basins of the study area.

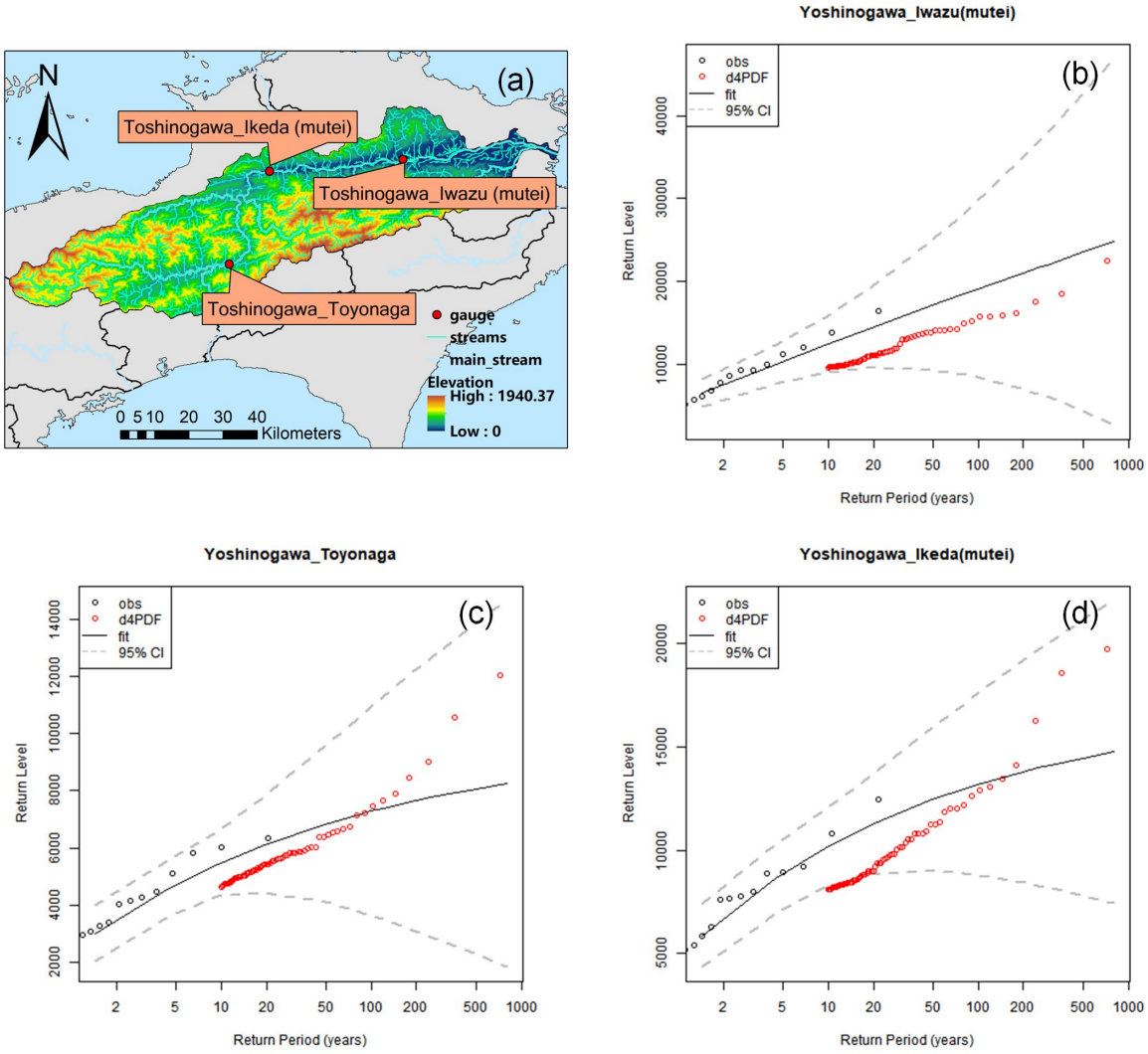


Figure S8 Locations of the discharge gauges (a) and comparisons between observation-based frequency curve and simulated extremes (b~d).

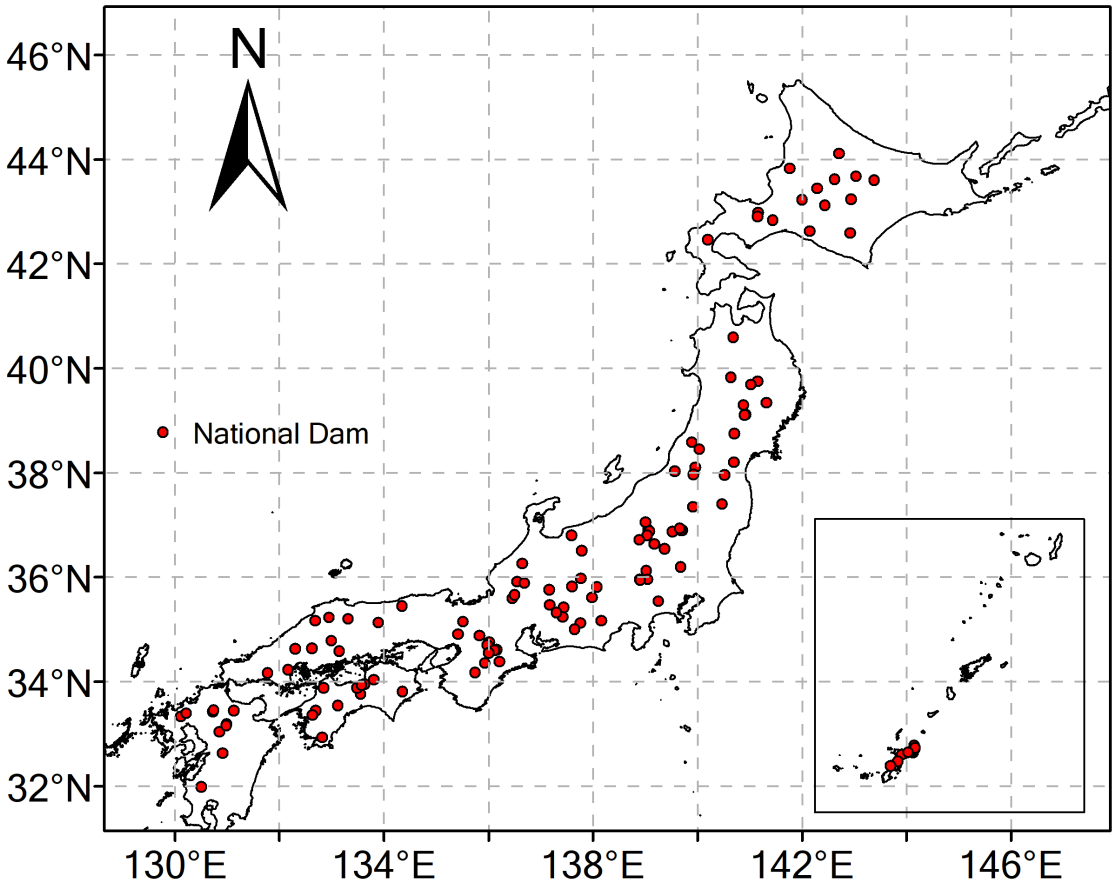


Figure S9 Spatial distribution of 121 national dams in the RRI model. Abbreviations: Rainfall-Runoff-Inundation (RRI)

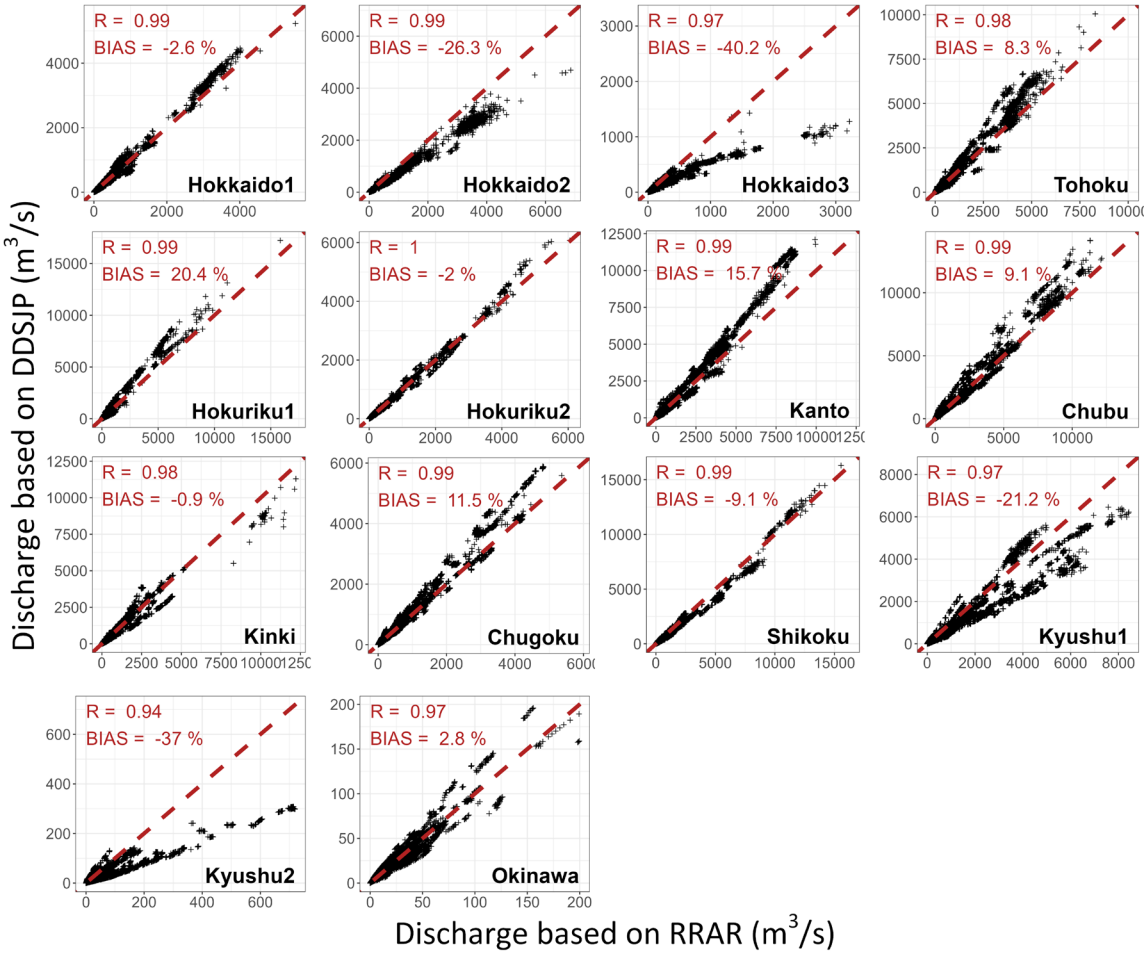


Figure S10 Comparison of 10-year discharge for each river grid across 14 regions of Japan.

Radar Rain gauge Analyzed Rainfall (RRAR) is a gridded precipitation dataset based on rain gauges and radar observations. In this study, precipitation from 1989 to 2010 were utilized as input for the RRI model to estimate 10-year discharge values across all river grids, serving as reference data.

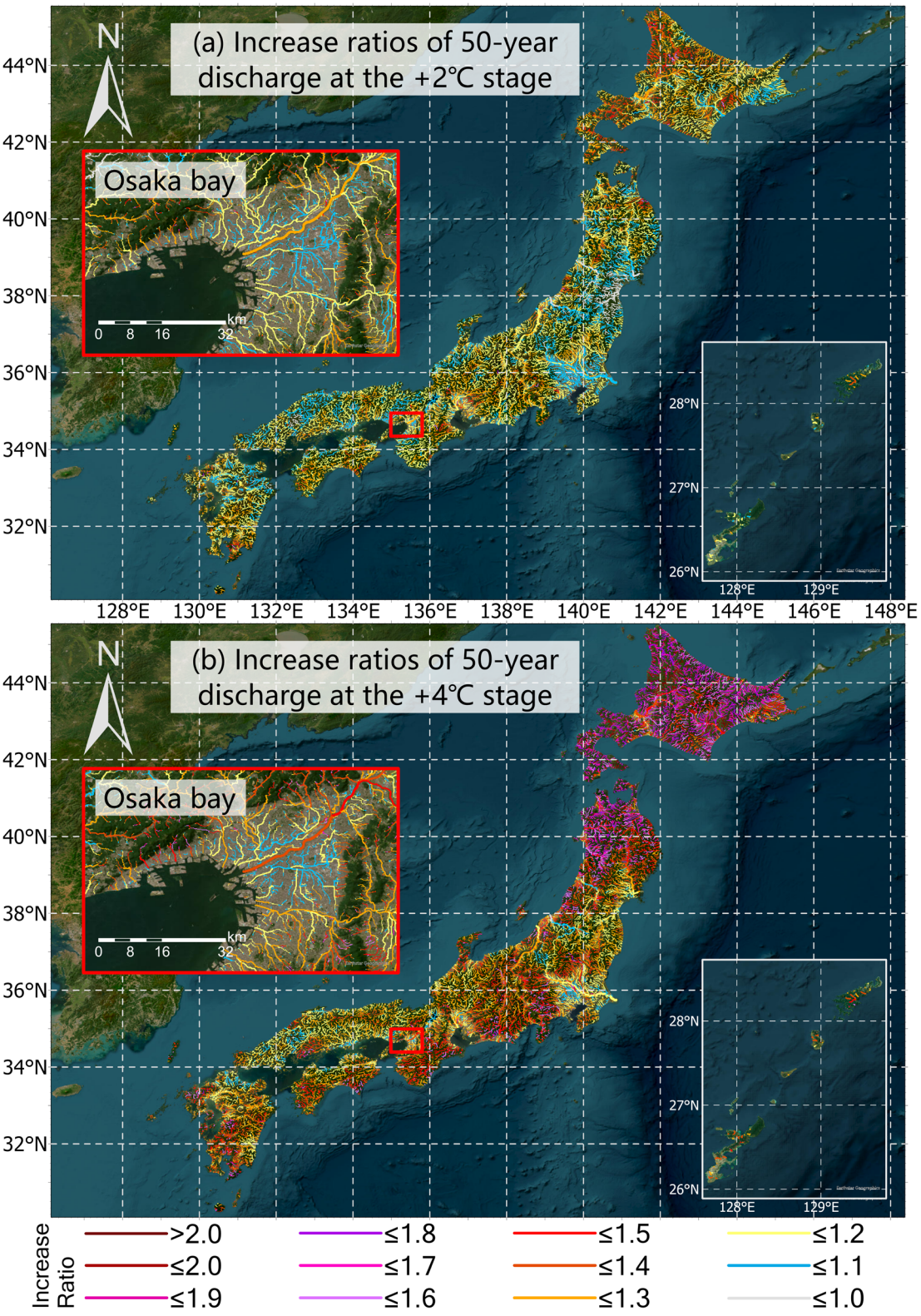


Figure S11 Spatial distribution of Q50 increase ratios at +2˚C (a) and +4˚C (b) stages. Osaka bay (red rectangle) is enlarged as an example to show tributary details in this study. Abbreviation: 50-year return period discharge (Q50).

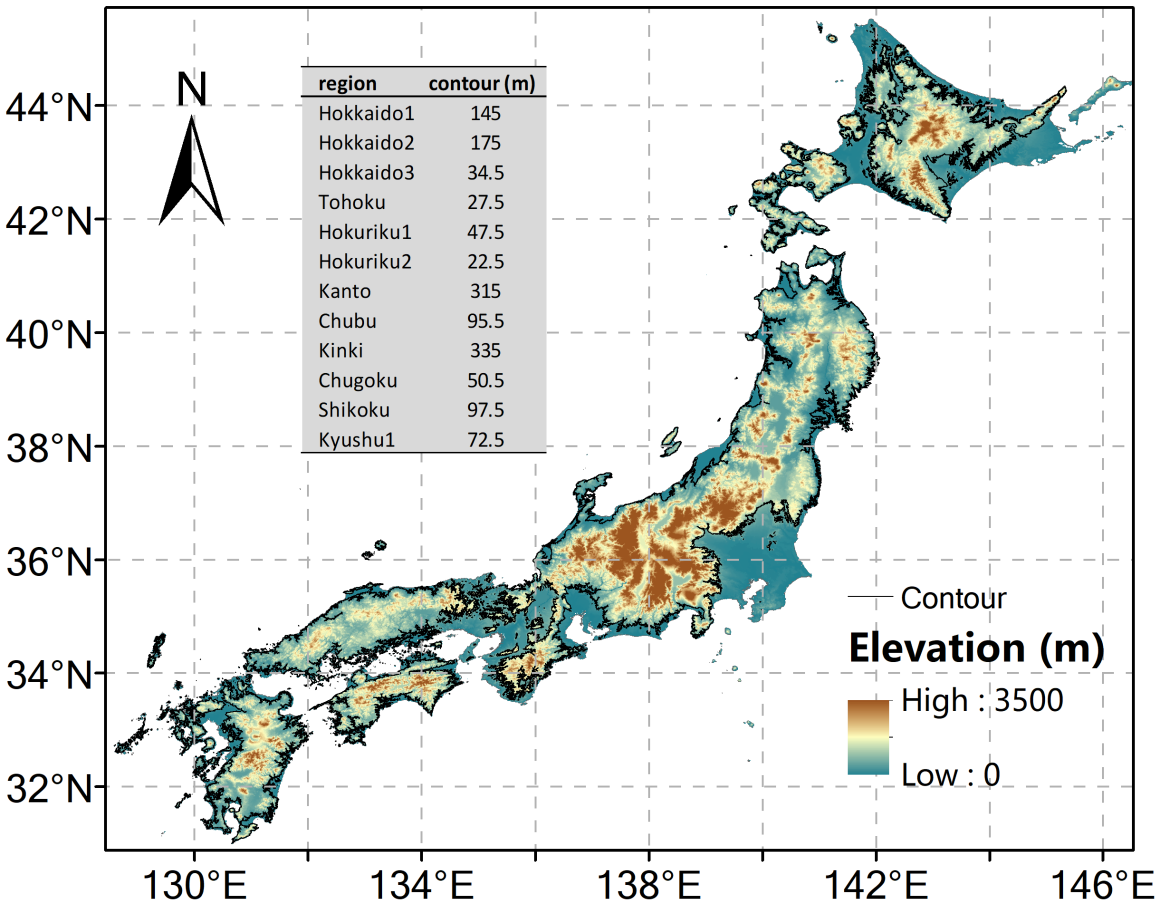


Figure S12 Spatial distribution of contours for increase ratio median peak in Figure 5-7. The attached table provides the contour values for the corresponding region.

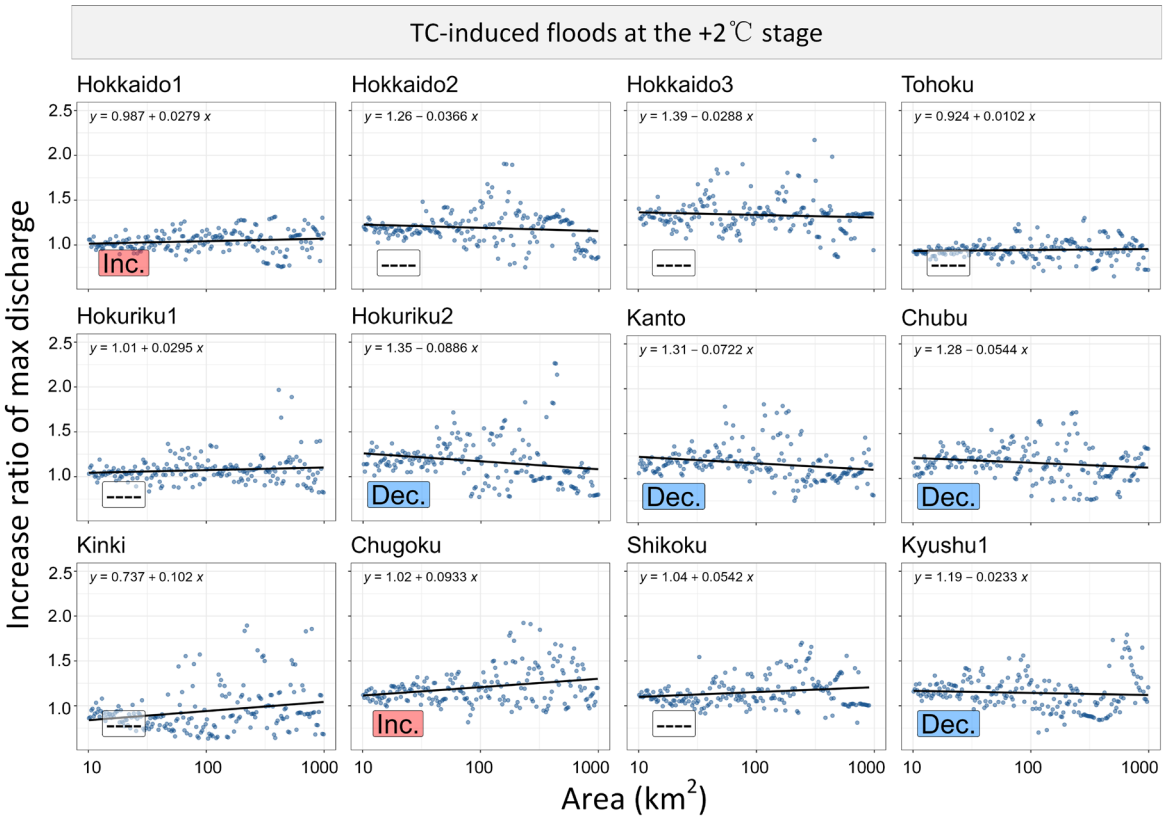


Figure S13 Increase ratio trend of TC-induced max discharge along basin area at the +2℃ stage.

"Dec." (blue background) and "Inc." (red background) represent monotonous decreasing and increasing trends, respectively, as identified by the M-K test at a 95% confidence level. "----" indicates no significant trend. Abbreviation: Mann-Kendall (M-K)

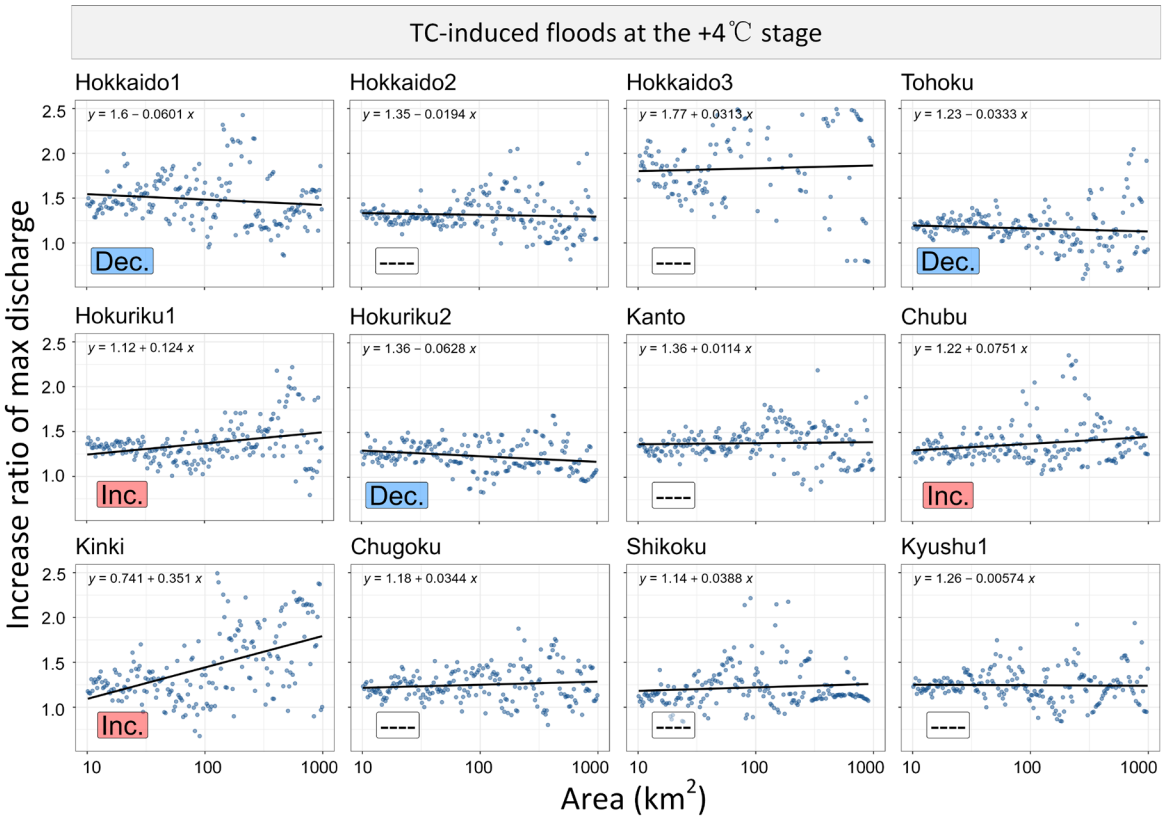


Figure S14 Increase ratio trend of TC-induced max discharge along basin area at the +4℃ stage.

"Dec." (blue background) and "Inc." (red background) represent monotonous decreasing and increasing trends, respectively, as identified by the M-K test at a 95% confidence level. "----" indicates no significant trend. Abbreviation: Mann-Kendall (M-K)

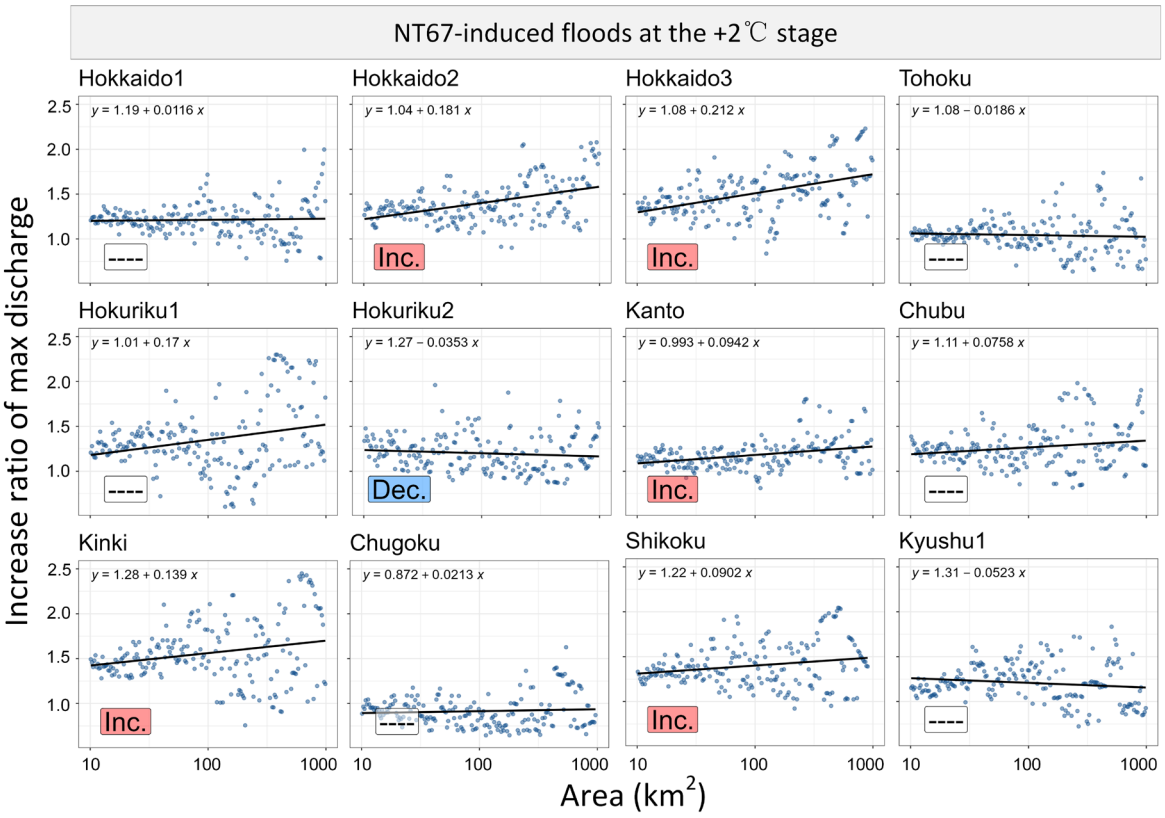


Figure S15 Increase ratio trend of NT67-induced max discharge along basin area at the +2℃ stage.

"Dec." (blue background) and "Inc." (red background) represent monotonous decreasing and increasing trends, respectively, as identified by the M-K test at a 95% confidence level. "----" indicates no significant trend. Abbreviation: Mann-Kendall (M-K)

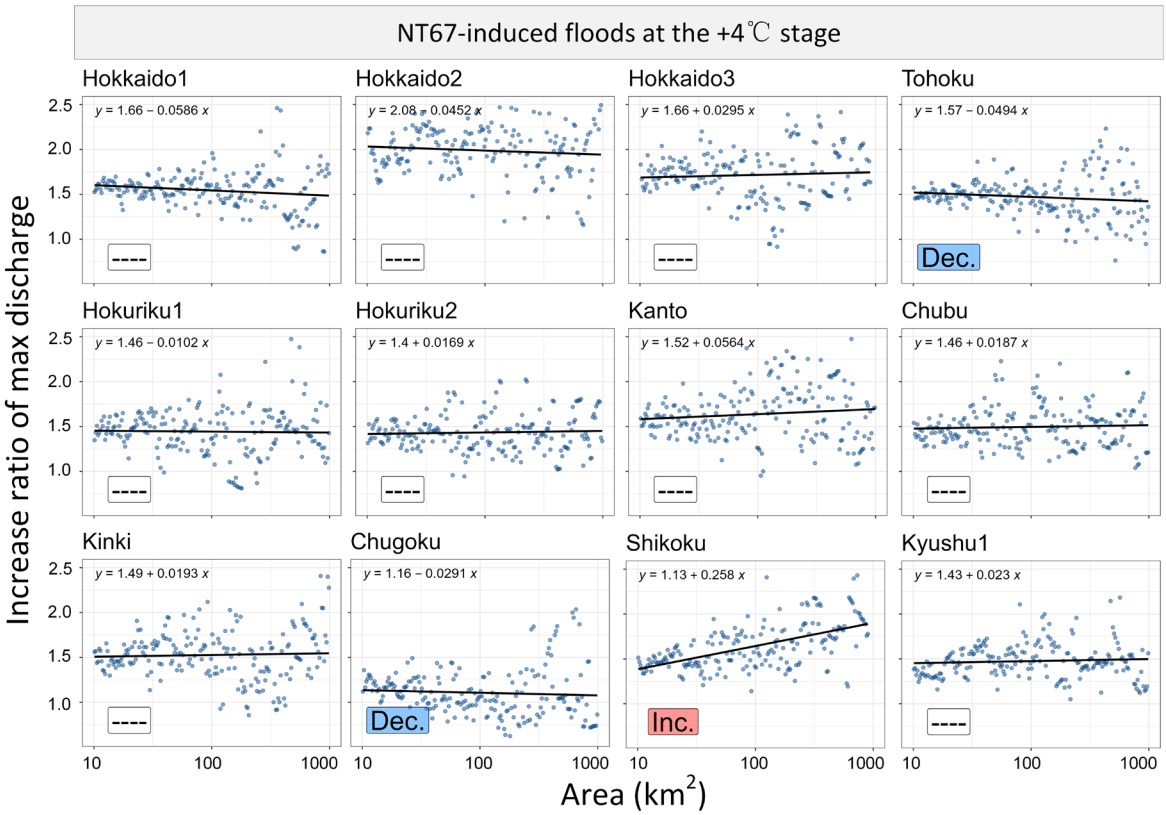


Figure S16 Increase ratio trend of NT67-induced max discharge along basin area at the +4℃ stage.

"Dec." (blue background) and "Inc." (red background) represent monotonous decreasing and increasing trends, respectively, as identified by the M-K test at a 95% confidence level. "----" indicates no significant trend. Abbreviation: Mann-Kendall (M-K)

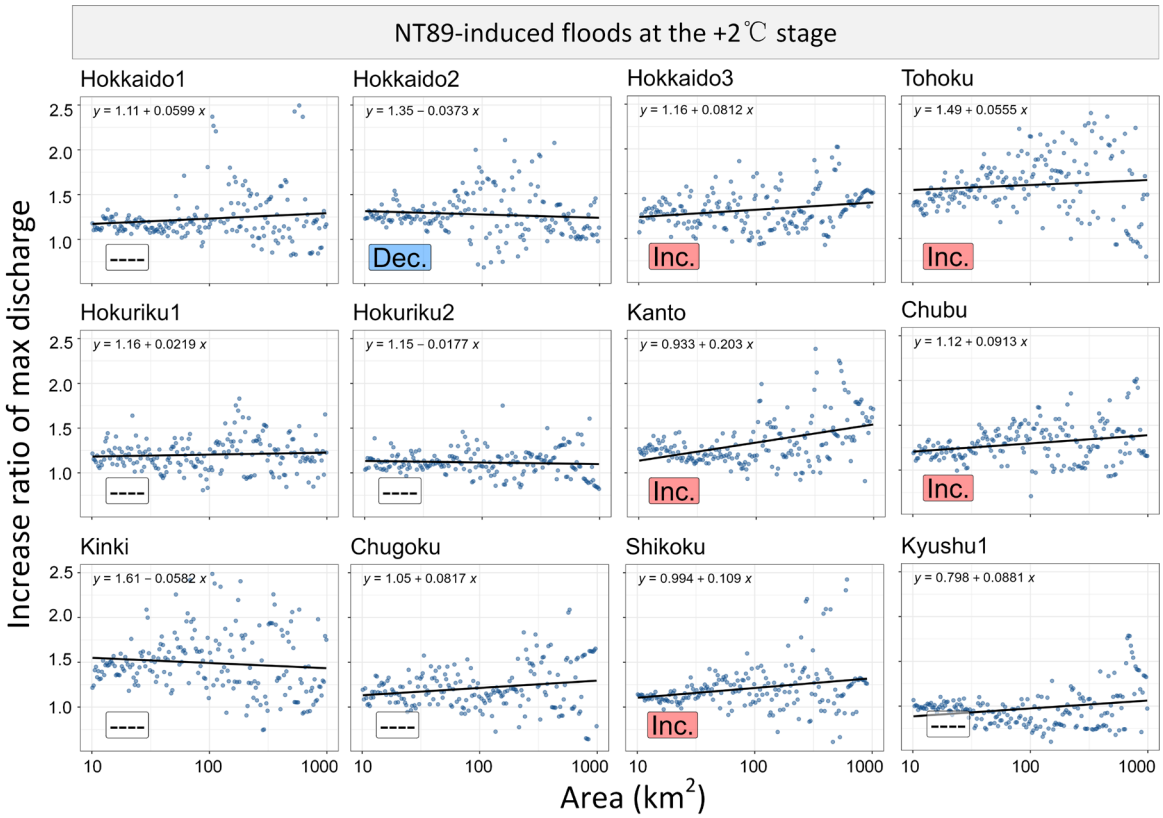


Figure S17 Increase ratio trend of NT89-induced max discharge along basin area at the +2℃ stage.

"Dec." (blue background) and "Inc." (red background) represent monotonous decreasing and increasing trends, respectively, as identified by the M-K test at a 95% confidence level. "----" indicates no significant trend. Abbreviation: Mann-Kendall (M-K)

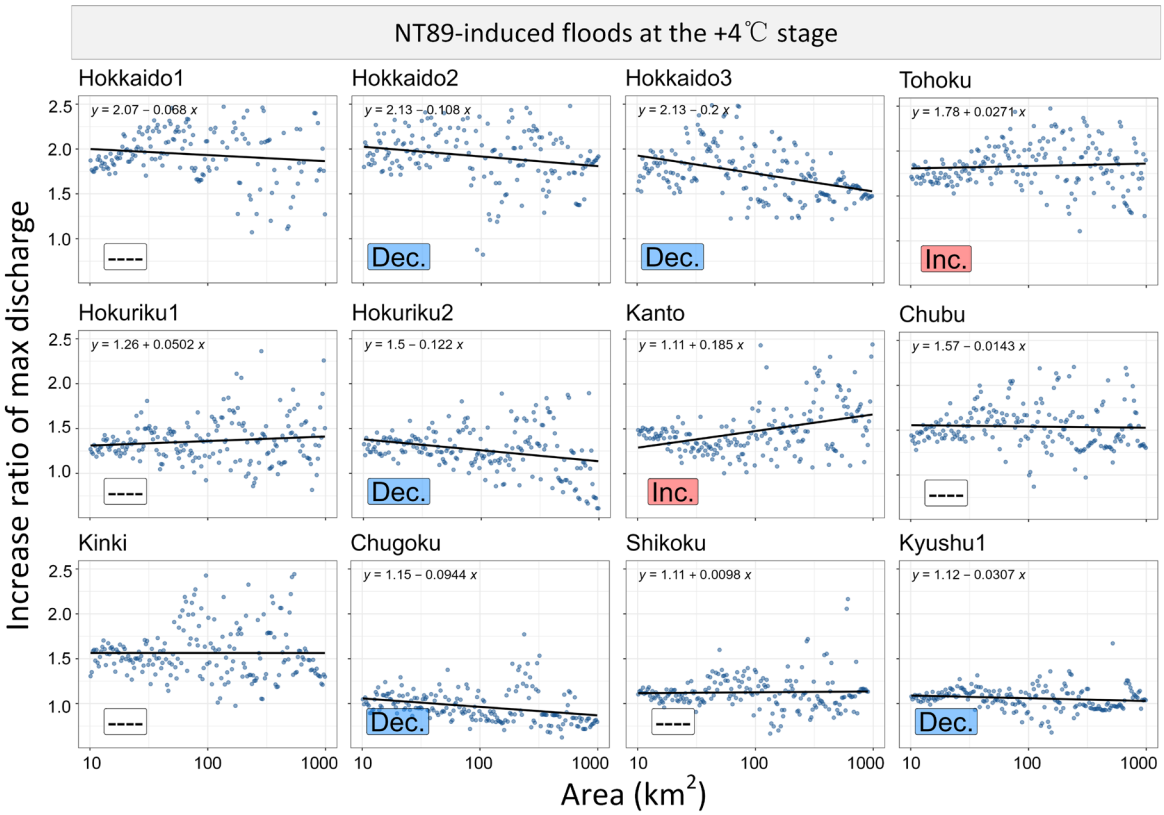


Figure S18 Increase ratio trend of NT89-induced max discharge along basin area at the +4℃ stage.

"Dec." (blue background) and "Inc." (red background) represent monotonous decreasing and increasing trends, respectively, as identified by the M-K test at a 95% confidence level. "----" indicates no significant trend. Abbreviation: Mann-Kendall (M-K)

Supplemental tables

The goodness-of-fit statistic Z (refer to Eq.S1) is utilized to assess the fitting performance of candidate distributions. When |Z| < 1.645, there is 95% confidence in selecting the corresponding distribution, with smaller |Z| values indicating better fit. In this study, the Generalized Logistic (GLO), Generalized Extreme Value (GEV), Generalized Normal (GNO), Generalized Pareto Distribution (GPD), and Pearson Type III (PE3) are employed as candidate distributions of the annual maximum sequences.

Tables S1 to S3 demonstrate that, in different scenarios, the eight major basins in the study area are more suitable for adopting PE3 as the optimal distribution for the block maximum method.

$$Z = \frac{\tau_4^C - \tau_4^S + \beta_4}{\sigma_4} \quad \text{Eq (S1)}$$

Where, τ_4^c is the L-kurtosis of the candidate distribution, τ_4^s is the L-kurtosis of samples, β_4 and σ_4 is the bias and standard deviation of sample L-kurtosis

Table S1 Goodness-of-fit Z of the eight basins under current scenario

Distribution	Yoshino	Watari	Niyodo	Hiji	Naka	Monobe	Shigenobu	Doki
GLO	3.278	3.398	3.447	3.589	3.428	3.396	3.346	3.426
GEV	1.922	1.971	2.013	2.093	1.988	1.988	1.959	2.001
GNO	1.185	1.194	1.234	1.280	1.205	1.222	1.204	1.226
PE3	-0.134	-0.195	-0.161	-0.175	-0.196	-0.149	-0.146	-0.161
GPD	-1.555	-1.691	-1.664	-1.742	-1.705	-1.625	-1.599	-1.654

Table S2 Goodness-of-fit Z of the eight basins under 2k scenario

Distribution	Yoshino	Watari	Niyodo	Hiji	Naka	Monobe	Shigenobu	Doki
GLO	3.107	3.234	3.305	3.311	3.205	3.268	3.229	3.318
GEV	1.558	1.625	1.637	1.640	1.605	1.616	1.603	1.650
GNO	0.948	0.993	0.981	0.983	0.976	0.966	0.964	0.995
PE3	-0.183	-0.182	-0.237	-0.237	-0.192	-0.241	-0.223	-0.223
GPD	-2.235	-2.312	-2.445	-2.450	-2.310	-2.428	-2.374	-2.431

Table S3 Goodness-of-fit Z of the eight basins under 4k scenario

Distribution	Yoshino	Watari	Niyodo	Hiji	Naka	Monobe	Shigenobu	Doki
GLO	3.396	3.324	3.314	3.376	3.415	3.392	3.446	3.450

GEV	2.090	2.035	2.050	2.058	2.090	2.094	2.131	2.100
GNO	1.275	1.229	1.261	1.234	1.262	1.283	1.310	1.257
PE3	-0.170	-0.197	-0.137	-0.224	-0.203	-0.153	-0.144	-0.235
GPD	-1.339	-1.351	-1.268	-1.404	-1.390	-1.315	-1.321	-1.444

Table S4 Relationship between pixel area and approximate basin concentration time.

Area (km²)	**Time (h)**
0~200	6
200~500	12
500~5000	24
≥5000	48

Table S4, showing the relation between basin area and approximate river concentration time, is summarized from the governmental flood control plans of major rivers in Japan. These plans, led by the Ministry of Land, Infrastructure, Transport and Tourism of Japan, take into account the geographic and hydrological characteristics of individual river and provide engineering guidelines based on extensive experiments. The planned precipitation durations in these plans are referred to the river concentration time, primarily influenced by the area of the basin. As the plans consider the rainfall recording frequency of local departments, they generally recommend a 24-hour for small basins, which differs from our original intention in using this indicator. So, for small basins, we mainly refer to the results of Kadoya formula, which is also commonly used for estimating river concentration time in Japan (Kadoya and Fukushima, 1976; Wakatsuki et al., 2022). It should be noted that precise river concentration time is influenced by hydroclimate conditions and basin geometrical characteristics. The approximate concentration time presented in Table S4 aims to provide a duration level, instead of an exact value, to ensure the independence of precipitation events.

Table S5 Parameter sets of the Rainfall-Runoff-Inundation model for each soil type.

Soil Name	n_{slope} $(m^{-1/3}/s)$	γ_a	γ_m	k_a (m/s)	β

Man-made soil	0.50	0.50	0.05	0.08	7
Organic soil	0.40	0.35	0.00	0.10	4
Podosols	0.40	0.35	0.00	0.10	4
Andosols	0.40	0.50	0.05	0.05	9
Dark red soils	0.50	0.50	0.10	0.05	5
Lowland soils	0.30	0.50	0.00	0.03	4
Red-yellow soils	0.50	0.50	0.05	0.08	7
Stagnant soils	0.50	0.50	0.10	0.05	5
Brown forest soils	0.50	0.50	0.05	0.08	7
Regosols	0.50	0.50	0.05	0.03	7
Bare rocks	0.30	0.40	0.05	0.20	6

where n_{slope} is the Manning's roughness on the slope, γ_a is the effective porosity, γ_m determines the threshold of happening unsaturated flow, k_a is the lateral saturated hydraulic conductivity β is a factor to compute the lateral hydraulic conductivity in unsaturated zone (k_m) from k_a ($k_m = k_a / \beta$)

Table S6 Estimated scaling ratios and corresponding upper and lower 95% limits for candidate events using in PrecStre-I.

Basins	Estimation	Lower limit	Upper limit
Yoshino	1.10	1.02	1.20
	1.07	0.99	1.16
	1.05	0.97	1.14
	1.05	0.96	1.13
	1.01	0.93	1.10
	1.00	0.92	1.08
Watari	1.12	1.05	1.20

	1.09	1.02	1.17
	1.04	0.97	1.11
	1.01	0.94	1.08
	1.00	0.93	1.07
	0.99	0.92	1.06
Niyodo	1.09	1.02	1.16
	1.08	1.01	1.15
	1.08	1.01	1.15
	1.07	1.01	1.14
	1.07	1.01	1.14
	1.05	0.98	1.11
Hiji	1.12	1.00	1.25
	1.11	0.99	1.25
	1.05	0.94	1.18
	1.05	0.94	1.18
	1.02	0.91	1.15
	0.99	0.88	1.11
Naka	1.07	1.01	1.15
	1.07	1.01	1.15
	1.07	1.01	1.15
	1.05	0.99	1.12
	1.01	0.95	1.08
	1.00	0.94	1.07
Monobe	1.08	1.01	1.15
	1.08	1.01	1.15
	1.06	0.99	1.14
	1.04	0.97	1.11
	1.04	0.97	1.11
	1.00	0.93	1.07
Shigenobu	1.12	1.00	1.27
	1.08	0.97	1.23
	1.08	0.97	1.23
	1.08	0.97	1.23
	1.06	0.95	1.21
	1.04	0.93	1.18
Doki	1.16	1.04	1.29
	1.16	1.03	1.29
	1.15	1.03	1.28
	1.15	1.03	1.28
	1.12	1.00	1.25
	1.10	0.98	1.22

Table S7 Estimated scaling ratios and corresponding upper and lower 95% limits for candidate events using in PrecStre-S.

Basins	Estimation	Lower limit	Upper limit
Yoshino	1.22	0.92	1.65

	1.29	0.97	1.74
	1.3	0.98	1.76
	1.31	0.98	1.76
	1.42	1.06	1.91
	1.46	1.1	1.97
Watari	0.96	0.75	1.24
	1.14	0.89	1.48
	1.26	0.99	1.64
	1.28	1	1.66
	1.3	1.02	1.68
	1.34	1.05	1.74
Niyodo	1.09	0.87	1.38
	1.13	0.9	1.43
	1.21	0.96	1.53
	1.23	0.98	1.56
	1.24	0.99	1.57
	1.37	1.09	1.73
Hiji	0.64	0.45	0.95
	1.41	0.99	2.09
	1.78	1.25	2.65
	1.8	1.26	2.68
	1.81	1.27	2.69
	1.86	1.31	2.78
Naka	1.11	0.88	1.43
	1.2	0.95	1.54
	1.25	0.99	1.6
	1.27	1.01	1.63
	1.33	1.05	1.71
	1.34	1.06	1.73
Monobe	1.15	0.91	1.48
	1.15	0.91	1.48
	1.23	0.97	1.58
	1.29	1.02	1.66
	1.29	1.02	1.66
	1.38	1.09	1.78
Shigenobu	1.23	0.85	1.83
	1.25	0.86	1.85
	1.3	0.9	1.93
	1.5	1.04	2.22
	1.52	1.05	2.26
	1.64	1.14	2.44
Doki	1.07	0.73	1.61
	1.36	0.93	2.06
	1.45	0.99	2.18
	1.46	1	2.2
	1.62	1.1	2.44
	1.68	1.15	2.53

References

Alfieri, L., Salamon, P., Bianchi, A., Neal, J., Bates, P., and Feyen, L.: Advances in pan-European flood hazard mapping, Hydrological Processes, 28, 4067–4077, https://doi.org/10.1002/hyp.9947, 2014.

Alfieri, L., Feyen, L., Dottori, F., and Bianchi, A.: Ensemble flood risk assessment in Europe under high end climate scenarios, Global Environmental Change, 35, 199–212, https://doi.org/10.1016/j.gloenvcha.2015.09.004, 2015a.

Alfieri, L., Burek, P., Feyen, L., and Forzieri, G.: Global warming increases the frequency of river floods in Europe, Hydrology and Earth System Sciences, 19, 2247–2260, https://doi.org/10.5194/hess-19-2247-2015, 2015b.

Alfieri, L., Dottori, F., Betts, R., Salamon, P., and Feyen, L.: Multi-Model Projections of River Flood Risk in Europe under Global Warming, Climate, 6, 6, https://doi.org/10.3390/cli6010006, 2018.

Ali, J., Syed, K. H., Gabriel, H. F., Saeed, F., Ahmad, B., and Bukhari, S. A. A.: Centennial Heat Wave Projections Over Pakistan Using Ensemble NEX GDDP Data Set, Earth Syst Environ, 2, 437–454, https://doi.org/10.1007/s41748-018-0064-8, 2018.

Allen, M. R. and Ingram, W. J.: Constraints on future changes in climate and the hydrologic cycle, Nature, 419, 224–232, https://doi.org/10.1038/nature01092, 2002.

Amponsah, W., Marra, F., Marchi, L., Roux, H., Braud, I., and Borga, M.: Objective Analysis of Envelope Curves for Peak Floods of European and Mediterranean Flash Floods, in: Climate Change, Hazards and Adaptation Options: Handling the Impacts of a Changing Climate, edited by: Leal Filho, W., Nagy, G. J., Borga, M., Chávez Muñoz, P. D., and Magnuszewski, A., Springer International Publishing, Cham, 267–276, https://doi.org/10.1007/978-3-030-37425-9_14, 2020.

Archer, L., Hatchard, S., Devitt, L., Neal, J. C., Coxon, G., Bates, P. D., Kendon, E. J., and Savage, J.: Future Change in Urban Flooding Using New Convection-Permitting Climate Projections, Water Resources Research, 60, e2023WR035533, https://doi.org/10.1029/2023WR035533, 2024.

Arnell, N. W. and Gosling, S. N.: The impacts of climate change on river flood risk at the global scale, Climatic Change, 134, 387–401, https://doi.org/10.1007/s10584-014-1084-5, 2016.

Babenko, A. and Lempitsky, V.: Aggregating Deep Convolutional Features for Image Retrieval, in: 2015 Ieee International Conference on Computer Vision (iccv), New York, 1269–1277, https://doi.org/10.1109/ICCV.2015.150, 2015.

Balbastre-Soldevila, R., García-Bartual, R., and Andrés-Doménech, I.: A Comparison of Design Storms for Urban Drainage System Applications, Water, 11, 757, https://doi.org/10.3390/w11040757, 2019.

Bao, Y. and Wen, X.: Projection of China's near- and long-term climate in a new high-resolution daily downscaled dataset NEX-GDDP, J Meteorol Res, 31, 236–249, https://doi.org/10.1007/s13351-017-6106-6, 2017.

Bark, R. H., Martin-Ortega, J., and Waylen, K. A.: Stakeholders' views on natural flood management: Implications for the nature-based solutions paradigm shift?, Environmental Science & Policy, 115, 91–98, https://doi.org/10.1016/j.envsci.2020.10.018, 2021.

Bates, P. D., Horritt, M. S., and Fewtrell, T. J.: A simple inertial formulation of the shallow water equations for efficient two-dimensional flood inundation modelling, Journal of Hydrology, 387, 33–45, https://doi.org/10.1016/j.jhydrol.2010.03.027, 2010.

Bates, P. D., Quinn, N., Sampson, C., Smith, A., Wing, O., Sosa, J., Savage, J., Olcese, G., Neal, J., Schumann, G., Giustarini, L., Coxon, G., Porter, J. R., Amodeo, M. F., Chu, Z., Lewis-Gruss, S., Freeman, N. B., Houser, T., Delgado, M., Hamidi, A., Bolliger, I., E. McCusker, K., Emanuel, K., Ferreira, C. M., Khalid, A., Haigh, I. D., Couasnon, A., E. Kopp, R., Hsiang, S., and Krajewski, W. F.: Combined Modeling of US Fluvial, Pluvial, and Coastal Flood Hazard Under Current and Future Climates, Water Resources Research, 57, e2020WR028673, https://doi.org/10.1029/2020WR028673, 2021.

Beguería, S.: Uncertainties in partial duration series modelling of extremes related to the choice of the threshold value, Journal of Hydrology, 303, 215–230, https://doi.org/10.1016/j.jhydrol.2004.07.015, 2005.

Benoit, L., Vrac, M., and Mariethoz, G.: Nonstationary stochastic rain type generation: accounting for climate drivers, Hydrology and Earth System Sciences, 24, 2841–2854, https://doi.org/10.5194/hess-24-2841-2020, 2020.

Bertola, M., Castellarin, A., Viglione, A., Valtancoli, E., and Blöschl, G.: Frequency and Spatial Variability of European Record Floods, Water Resources Research, 60, e2023WR036767, https://doi.org/10.1029/2023WR036767, 2024.

Bevacqua, E., Schleussner, C.-F., and Zscheischler, J.: A year above 1.5 °C signals that Earth is most probably within the 20-year period that will reach the Paris Agreement limit, Nat. Clim. Chang., 15, 262–265, https://doi.org/10.1038/s41558-025-02246-9, 2025.

Bezak, N., Brilly, M., and Šraj, M.: Comparison between the peaks-over-threshold method and the annual maximum method for flood frequency analysis, Hydrological Sciences Journal, 59, 959–977, https://doi.org/10.1080/02626667.2013.831174, 2014.

Bhagabati, S. S. and Kawasaki, A.: Consideration of the rainfall-runoff-inundation (RRI) model for flood mapping in a deltaic area of Myanmar, Hydrol. Res. Lett., 11, 155–160, https://doi.org/10.3178/hrl.11.155, 2017.

Blöschl, G.: Three hypotheses on changing river flood hazards, Hydrology and Earth System Sciences, 26, 5015–5033, https://doi.org/10.5194/hess-26-5015-2022, 2022.

Blöschl, G., Hall, J., Viglione, A., Perdigão, R. A. P., Parajka, J., Merz, B., Lun, D., Arheimer, B., Aronica, G. T., Bilibashi, A., Boháč, M., Bonacci, O., Borga, M., Čanjevac, I., Castellarin, A., Chirico, G. B., Claps, P., Frolova, N., Ganora, D., Gorbachova, L., Gül, A., Hannaford, J., Harrigan, S., Kireeva, M., Kiss, A., Kjeldsen, T. R., Kohnová, S., Koskela, J. J., Ledvinka, O., Macdonald, N., Mavrova-Guirguinova, M., Mediero, L., Merz, R., Molnar, P., Montanari, A., Murphy, C., Osuch, M., Ovcharuk, V., Radevski, I., Salinas, J. L., Sauquet, E., Šraj, M., Szolgay, J., Volpi, E., Wilson, D., Zaimi, K., and Živković, N.: Changing climate both increases and decreases European river floods, Nature, 573, 108–111, https://doi.org/10.1038/s41586-019-1495-6, 2019.

Boulange, J., Hanasaki, N., Yamazaki, D., and Pokhrel, Y.: Role of dams in reducing global flood exposure under climate change, Nat Commun, 12, 417, https://doi.org/10.1038/s41467-020-20704-0, 2021.

Breinl, K., Lun, D., Müller-Thomy, H., and Blöschl, G.: Understanding the relationship between rainfall and flood probabilities through combined intensity-duration-frequency analysis, Journal of Hydrology, 602, 126759, https://doi.org/10.1016/j.jhydrol.2021.126759, 2021.

Budhathoki, A., Tanaka, T., and Tachikawa, Y.: Correcting streamflow bias considering its spatial structure for impact assessment of climate change on floods using d4PDF in the Chao Phraya River Basin, Thailand, Journal of Hydrology: Regional Studies, 42, 101150, https://doi.org/10.1016/j.ejrh.2022.101150, 2022.

Cabinet Office: On disaster damage by the Heavy Rainfall in July 2018 (in Japanese), Government of Japan, 2019.

Cabinet Office: On disaster damage by the Typhoon No. 19 (Hagibis) in 2019 (in Japanese), Government of Japan, 2020.

Cabinet Office: On disaster damage by the heavy rainfall since 2024.09.20 (in Japanese), Government of Japan, 2024.

Caseri, A., Javelle, P., Ramos, M. h., and Leblois, E.: Generating precipitation ensembles for flood alert and risk management, Journal of Flood Risk Management, 9, 402–415, https://doi.org/10.1111/jfr3.12203, 2016.

Cash, J. and Karp, A.: A Variable Order Runge-Kutta Method for Initial-Value Problems with Rapidly Varying Right-Hand Sides, ACM Trans. Math. Softw., 16, 201–222, https://doi.org/10.1145/79505.79507, 1990.

Cea, L. and Fraga, I.: Incorporating Antecedent Moisture Conditions and Intraevent Variability of Rainfall on Flood Frequency Analysis in Poorly Gauged Basins, Water Resources Research, 54, 8774–8791, https://doi.org/10.1029/2018WR023194, 2018.

Ceola, S., Laio, F., and Montanari, A.: Satellite nighttime lights reveal increasing human exposure to floods worldwide, Geophysical Research Letters, 41, 7184–7190, https://doi.org/10.1002/2014GL061859, 2014.

Cha, E.-J., Yun, S., Moon, I.-J., and Kim, D.-H.: Binary interaction of typhoons Soulik and Cimaron in 2018 – Part I: Observational characteristics and forecast error, Tropical Cyclone Research and Review, 10, 32–42, https://doi.org/10.1016/j.tcrr.2021.03.001, 2021.

Chand, S. S., Walsh, K. J. E., Camargo, S. J., Kossin, J. P., Tory, K. J., Wehner, M. F., Chan, J. C. L., Klotzbach, P. J., Dowdy, A. J., Bell, S. S., Ramsay, H. A., and Murakami, H.: Declining tropical cyclone frequency under global warming, Nat. Clim. Chang., 12, 655–661, https://doi.org/10.1038/s41558-022-01388-4, 2022.

Chen, H., Han, L., Tang, Y., Chen, J., Lei, C., and Li, X.: Impacts of tropical cyclones on extreme precipitation and flooding in a humid subtropical inland basin of China, Journal of Hydrology: Regional Studies, 57, 102096, https://doi.org/10.1016/j.ejrh.2024.102096, 2025a.

Chen, J., Shi, X., Gu, L., Wu, G., Su, T., Wang, H.-M., Kim, J.-S., Zhang, L., and Xiong, L.: Impacts of climate warming on global floods and their implication to current flood defense standards, Journal of Hydrology, 618, 129236, https://doi.org/10.1016/j.jhydrol.2023.129236, 2023.

Chen, J., Sayama, T., Yamada, M., and Sugawara, Y.: Regional event-based flood quantile estimation method for large climate projection ensembles, Progress in Earth and Planetary Science, 11, 16, https://doi.org/10.1186/s40645-024-00618-x, 2024.

Chen, J., Sayama, T., Yamada, M., Tanaka, T., and Sugawara, Y.: Projecting Multiscale River Flood Changes Across Japan at +2°C and +4°C Climates, Earth's Future, 13, e2024EF005884, https://doi.org/10.1029/2024EF005884, 2025b.

Chen, J., Sayama, T., Yamada, M., and Sugawara, Y.: Reducing the computational cost of process-based

flood frequency estimation by extracting precipitation events from a large-ensemble climate dataset, Journal of Hydrology, 655, 132946, https://doi.org/10.1016/j.jhydrol.2025.132946, 2025c.

Chen, Y., Paschalis, A., Kendon, E., Kim, D., and Onof, C.: Changing Spatial Structure of Summer Heavy Rainfall, Using Convection-Permitting Ensemble, Geophysical Research Letters, 48, e2020GL090903, https://doi.org/10.1029/2020GL090903, 2021a.

Chen, Y., Paschalis, A., Kendon, E., Kim, D., and Onof, C.: Changing Spatial Structure of Summer Heavy Rainfall, Using Convection-Permitting Ensemble, Geophysical Research Letters, 48, e2020GL090903, https://doi.org/10.1029/2020GL090903, 2021b.

Cheng, D., Shimizu, K., and Yamada, T. J.: Hydrological frequency analysis of large-ensemble climate simulation data using control density as a statistical control, Hydrological Research Letters, 15, 84–91, https://doi.org/10.3178/hrl.15.84, 2021.

Chu, P.-S., Kim, J.-H., and Ruan Chen, Y.: Have steering flows in the western North Pacific and the South China Sea changed over the last 50 years?, Geophysical Research Letters, 39, https://doi.org/10.1029/2012GL051709, 2012.

Ciervo, F., Papa, M. n., Medina, V., and Bateman, A.: Simulation of flash floods in ungauged basins using post-event surveys and numerical modelling, Journal of Flood Risk Management, 8, 343–355, https://doi.org/10.1111/jfr3.12103, 2015.

Clark, M. P., Wilby, R. L., Gutmann, E. D., Vano, J. A., Gangopadhyay, S., Wood, A. W., Fowler, H. J., Prudhomme, C., Arnold, J. R., and Brekke, L. D.: Characterizing Uncertainty of the Hydrologic Impacts of Climate Change, Curr Clim Change Rep, 2, 55–64, https://doi.org/10.1007/s40641-016-0034-x, 2016.

Cloke, H. L., Wetterhall, F., He, Y., Freer, J. E., and Pappenberger, F.: Modelling climate impact on floods with ensemble climate projections, Quarterly Journal of the Royal Meteorological Society, 139, 282–297, https://doi.org/10.1002/qj.1998, 2013.

Collier, C. G.: Flash flood forecasting: What are the limits of predictability?, Quarterly Journal of the Royal Meteorological Society, 133, 3–23, https://doi.org/10.1002/qj.29, 2007.

Coumou, D., Lehmann, J., and Beckmann, J.: The weakening summer circulation in the Northern Hemisphere mid-latitudes, Science, 348, 324–327, https://doi.org/10.1126/science.1261768, 2015.

Cunnane, C.: A particular comparison of annual maxima and partial duration series methods of flood frequency prediction, Journal of Hydrology, 18, 257–271, https://doi.org/10.1016/0022-1694(73)90051-6, 1973.

Deng, L., Feng, J., Zhao, Y., Bao, X., Huang, W., Hu, H., and Duan, Y.: The Remote Effect of Binary Typhoon Infa and Cempaka on the “21.7” Heavy Rainfall in Henan Province, China, Journal of Geophysical Research: Atmospheres, 127, e2021JD036260, https://doi.org/10.1029/2021JD036260, 2022.

Deser, C., Phillips, A., Bourdette, V., and Teng, H.: Uncertainty in climate change projections: the role of internal variability, Clim Dyn, 38, 527–546, https://doi.org/10.1007/s00382-010-0977-x, 2012.

Deser, C., Phillips, A. S., Alexander, M. A., and Smoliak, B. V.: Projecting North American Climate over the Next 50 Years: Uncertainty due to Internal Variability, Journal of Climate, 27, 2271–2296, https://doi.org/10.1175/JCLI-D-13-00451.1, 2014.

Deushi, M. and Shibata, K.: Development of a Meteorological Research Institute Chemistry-Climate Model version 2 for the Study of Tropospheric and Stratospheric Chemistry, Papers in Meteorology and Geophysics, 62, 1–46, https://doi.org/10.2467/mripapers.62.1, 2011.

Di Sante, F., Coppola, E., and Giorgi, F.: Projections of river floods in Europe using EURO-CORDEX, CMIP5 and CMIP6 simulations, Intl Journal of Climatology, 41, 3203–3221, https://doi.org/10.1002/joc.7014, 2021.

Donat, M. G., Lowry, A. L., Alexander, L. V., O'Gorman, P. A., and Maher, N.: More extreme precipitation in the world's dry and wet regions, Nature Clim Change, 6, 508–513, https://doi.org/10.1038/nclimate2941, 2016.

Dong, G., Jiang, Z., Tian, Z., Buonomo, E., Sun, L., and Fan, D.: Projecting Changes in Mean and Extreme Precipitation Over Eastern China During 2041–2060, Earth and Space Science, 7, e2019EA001024, https://doi.org/10.1029/2019EA001024, 2020.

Dottori, F., Salamon, P., Bianchi, A., Alfieri, L., Hirpa, F. A., and Feyen, L.: Development and evaluation of a framework for global flood hazard mapping, Advances in Water Resources, 94, 87–102, https://doi.org/10.1016/j.advwatres.2016.05.002, 2016.

Duan, W., He, B., Takara, K., Luo, P., Nover, D., Yamashiki, Y., and Huang, W.: Anomalous atmospheric events leading to Kyushu's flash floods, July 11–14, 2012, Nat Hazards, 73, 1255–1267, https://doi.org/10.1007/s11069-014-1134-3, 2014.

Emanuel, K.: Increasing destructiveness of tropical cyclones over the past 30 years, Nature, 436, 686–688, https://doi.org/10.1038/nature03906, 2005.

Emanuel, K.: Atlantic tropical cyclones downscaled from climate reanalyses show increasing activity over past 150 years, Nat Commun, 12, 7027, https://doi.org/10.1038/s41467-021-27364-8, 2021a.

Emanuel, K.: Response of Global Tropical Cyclone Activity to Increasing CO2: Results from Downscaling CMIP6 Models, Journal of Climate, 34, 57–70, https://doi.org/10.1175/JCLI-D-20-0367.1, 2021b.

Eyring, V., Bony, S., Meehl, G. A., Senior, C. A., Stevens, B., Stouffer, R. J., and Taylor, K. E.: Overview of the Coupled Model Intercomparison Project Phase 6 (CMIP6) experimental design and organization, Geoscientific Model Development, 9, 1937–1958, https://doi.org/10.5194/gmd-9-1937-2016, 2016.

Ferreira, A. and de Haan, L.: On the block maxima method in extreme value theory: PWM estimators, Ann. Statist., 43, https://doi.org/10.1214/14-AOS1280, 2015.

Ficchì, A., Perrin, C., and Andréassian, V.: Impact of temporal resolution of inputs on hydrological model performance: An analysis based on 2400 flood events, Journal of Hydrology, 538, 454–470, https://doi.org/10.1016/j.jhydrol.2016.04.016, 2016.

Fowler, H. J., Lenderink, G., Prein, A. F., Westra, S., Allan, R. P., Ban, N., Barbero, R., Berg, P., Blenkinsop, S., Do, H. X., Guerreiro, S., Haerter, J. O., Kendon, E. J., Lewis, E., Schaer, C., Sharma, A., Villarini, G., Wasko, C., and Zhang, X.: Anthropogenic intensification of short-duration rainfall extremes, Nat Rev Earth Environ, 2, 107–122, https://doi.org/10.1038/s43017-020-00128-6, 2021.

Fujita, M., Mizuta, R., Ishii, M., Endo, H., Sato, T., Okada, Y., Kawazoe, S., Sugimoto, S., Ishihara, K., and Watanabe, S.: Precipitation Changes in a Climate With 2-K Surface Warming From Large Ensemble Simulations Using 60-km Global and 20-km Regional Atmospheric Models, Geophysical Research Letters, 46, 435–442, https://doi.org/10.1029/2018GL079885, 2019.

Fumiaki, F. and Jun, M.: Regional Features Related to Timing of Maximum and Minimum Precipitation during the Warm Season in Japan, Geographical review of Japan series B, 95, 55–68, https://doi.org/10.4157/geogrevjapanb.95.55, 2022.

Gellens, D.: Combining regional approach and data extension procedure for assessing GEV distribution

of extreme precipitation in Belgium, Journal of Hydrology, 268, 113–126, https://doi.org/10.1016/S0022-1694(02)00160-9, 2002.

Georgakakos, K. P.: On the Design of National, Real-Time Warning Systems with Capability for Site-Specific, Flash-Flood Forecasts, 1986.

Gori, A., Lin, N., and Smith, J.: Assessing Compound Flooding From Landfalling Tropical Cyclones on the North Carolina Coast, Water Resources Research, 56, e2019WR026788, https://doi.org/10.1029/2019WR026788, 2020.

Green, W. H. and Ampt, G. A.: Studies on Soil Phyics., The Journal of Agricultural Science, 4, 1–24, https://doi.org/10.1017/S0021859600001441, 1911.

Grimaldi, S., Petroselli, A., and Serinaldi, F.: Design hydrograph estimation in small and ungauged watersheds: continuous simulation method versus event-based approach, Hydrological Processes, 26, 3124–3134, https://doi.org/10.1002/hyp.8384, 2012.

Grossman, M. J., Zaiki, M., and Nagata, R.: Interannual and interdecadal variations in typhoon tracks around Japan, International Journal of Climatology, 35, 2514–2527, https://doi.org/10.1002/joc.4156, 2015.

Guo, Q. and Hibino, K.: Physical responses of Baiu extreme precipitation to future warming: Examples of the 2018 and 2020 western Japan events, Weather and Climate Extremes, 39, 100547, https://doi.org/10.1016/j.wace.2022.100547, 2023.

Gutowski Jr., W. J., Giorgi, F., Timbal, B., Frigon, A., Jacob, D., Kang, H.-S., Raghavan, K., Lee, B., Lennard, C., Nikulin, G., O'Rourke, E., Rixen, M., Solman, S., Stephenson, T., and Tangang, F.: WCRP COordinated Regional Downscaling EXperiment (CORDEX): a diagnostic MIP for CMIP6, Geoscientific Model Development, 9, 4087–4095, https://doi.org/10.5194/gmd-9-4087-2016, 2016.

Habata, S., Yokokawa, M., and Kitawaki, S.: The earth simulator system, NEC Res. Dev., 44, 21–26, 2003.

Habata, S., Umezawa, K., Yokokawa, M., and Kitawaki, S.: Hardware system of the Earth Simulator, Parallel Comput., 30, 1287–1313, https://doi.org/10.1016/j.parco.2004.09.004, 2004.

Hanazaki, R., Yamazaki, D., and Yoshimura, K.: Development of a Reservoir Flood Control Scheme for Global Flood Models, Journal of Advances in Modeling Earth Systems, 14, e2021MS002944, https://doi.org/10.1029/2021MS002944, 2022.

Haslinger, K., Breinl, K., Pavlin, L., Pistotnik, G., Bertola, M., Olefs, M., Greilinger, M., Schöner, W., and Blöschl, G.: Increasing hourly heavy rainfall in Austria reflected in flood changes, Nature, 639, 667–672, https://doi.org/10.1038/s41586-025-08647-2, 2025.

Hatsuzuka, D., Sato, T., Yoshida, K., Ishii, M., and Mizuta, R.: Regional Projection of Tropical-Cyclone-Induced Extreme Precipitation around Japan Based on Large Ensemble Simulations, Sola, 16, 23–29, https://doi.org/10.2151/sola.2020-005, 2020.

Heidarzadeh, M., Iwamoto, T., Takagawa, T., and Takagi, H.: Field surveys and numerical modeling of the August 2016 Typhoon Lionrock along the northeastern coast of Japan: the first typhoon making landfall in Tohoku region, Nat Hazards, 105, 1–19, https://doi.org/10.1007/s11069-020-04112-7, 2021.

Hernes, R. R., Gragne, A. S., Abdalla, E. M. H., Braskerud, B. C., Alfredsen, K., and Muthanna, T. M.: Assessing the effects of four SUDS scenarios on combined sewer overflows in Oslo, Norway: evaluating the low-impact development module of the Mike Urban model, Hydrology Research, 51, 1437–1454, https://doi.org/10.2166/nh.2020.070, 2020.

Higashino, M. and Stefan, H. G.: Variability and change of precipitation and flood discharge in a Japanese river basin, Journal of Hydrology: Regional Studies, 21, 68–79, https://doi.org/10.1016/j.ejrh.2018.12.003, 2019.

Hirabayashi, Y., Mahendran, R., Koirala, S., Konoshima, L., Yamazaki, D., Watanabe, S., Kim, H., and Kanae, S.: Global flood risk under climate change, Nature Clim Change, 3, 816–821, https://doi.org/10.1038/nclimate1911, 2013.

Hirabayashi, Y., Tanoue, M., Sasaki, O., Zhou, X., and Yamazaki, D.: Global exposure to flooding from the new CMIP6 climate model projections, Sci Rep, 11, 3740, https://doi.org/10.1038/s41598-021-83279-w, 2021.

Hirockawa, Y., Kato, T., Tsuguti, H., and Seino, N.: Identification and Classification of Heavy Rainfall Areas and their Characteristic Features in Japan, Journal of the Meteorological Society of Japan, 98, 835–857, https://doi.org/10.2151/jmsj.2020-043, 2020.

Hoch, J. M. and Trigg, M. A.: Advancing global flood hazard simulations by improving comparability, benchmarking, and integration of global flood models, Environ. Res. Lett., 14, 034001, https://doi.org/10.1088/1748-9326/aaf3d3, 2019.

Hoegh-Guldberg, O., Jacob, D., Taylor, M., Guillén Bolaños, T., Bindi, M., Brown, S., Camilloni, I. A., Diedhiou, A., Djalante, R., Ebi, K., Engelbrecht, F., Guiot, J., Hijioka, Y., Mehrotra, S., Hope, C. W., Payne, A. J., Pörtner, H.-O., Seneviratne, S. I., Thomas, A., Warren, R., and Zhou, G.: The human imperative of stabilizing global climate change at 1.5°C, Science, 365, eaaw6974, https://doi.org/10.1126/science.aaw6974, 2019.

Hosking, J. R. M. and Wallis, J. R.: Some statistics useful in regional frequency analysis, Water Resour. Res., 29, 271–281, https://doi.org/10.1029/92WR01980, 1993.

Hu, F., Li, T., Liu, J., Bi, M., and Peng, M.: Decrease of tropical cyclone genesis frequency in the western North Pacific since 1960s, Dynamics of Atmospheres and Oceans, 81, 42–50, https://doi.org/10.1016/j.dynatmoce.2017.11.003, 2018.

Huang, C.-W., Yang, F.-P.-Y., Huang, L.-H., Chou, J.-F., Lien, H.-C., and Chang, C.-W.: Optimal design of interception for flood control: An integrated simulation approach, Journal of Hydro-environment Research, 19, 103–116, https://doi.org/10.1016/j.jher.2018.02.001, 2018.

Huang, S., Krysanova, V., and Hattermann, F.: Projections of climate change impacts on floods and droughts in Germany using an ensemble of climate change scenarios, Reg Environ Change, 15, 461–473, https://doi.org/10.1007/s10113-014-0606-z, 2015.

Huang, W., Zhang, Y. J., Liu, Z., Yu, H., Liu, Y., Lamont, S., Zhang, Y., Hirpa, F., Li, T., Bakker, B., Zhan, W., Patel, S., and Mori, N.: Simulation of compound flooding in Japan using a nationwide model, Natural Hazards, 117, 2693–2713, https://doi.org/10.1007/s11069-023-05962-7, 2023.

Iizuka, S. and Nakamura, H.: Sensitivity of Midlatitude Heavy Precipitation to SST: A Case Study in the Sea of Japan Area on 9 August 2013, Journal of Geophysical Research: Atmospheres, 124, 4365–4381, https://doi.org/10.1029/2018JD029503, 2019.

Ikeda, N., Narama, C., and Gyalson, S.: Knowledge Sharing for Disaster Risk Reduction: Insights from a Glacier Lake Workshop in the Ladakh Region, Indian Himalayas, mred, 36, 31–40, https://doi.org/10.1659/MRD-JOURNAL-D-15-00035.1, 2016.

Institute of Hydrology: Flood Estimation Handbook, Wallingford: Institute of Hydrology, 1999.

IPCC: Climate Change 2021: The Physical Science Basis. Contribution of Working Group I to the Sixth

Assessment Report of the Intergovernmental Panel on Climate Change, Cambridge University Press, Cambridge, United Kingdom and New York, NY, USA, 2391 pp., 2021.

IPCC: Climate Change 2022: Impacts, Adaptation and Vulnerability. Contribution of Working Group II to the Sixth Assessment Report of the Intergovernmental Panel on Climate Change, Cambridge University Press, Cambridge, UK and New York, USA, 3056 pp., 2022.

Ishii, M. and Mori, N.: d4PDF: large-ensemble and high-resolution climate simulations for global warming risk assessment, Progress in Earth and Planetary Science, 7, 58, https://doi.org/10.1186/s40645-020-00367-7, 2020.

Ishizaki, N.: Bias corrected climate scenarios over Japan based on NHRCM02 using monthly CDFDM (Ver.1), https://doi.org/10.17595/20220415.001, 2022.

Ivers, L. C. and Ryan, E. T.: Infectious diseases of severe weather-related and flood-related natural disasters, Current Opinion in Infectious Diseases, 19, 408, https://doi.org/10.1097/01.qco.0000244044.85393.9e, 2006.

Jacob, D., Teichmann, C., Sobolowski, S., Katragkou, E., Anders, I., Belda, M., Benestad, R., Boberg, F., Buonomo, E., Cardoso, R. M., Casanueva, A., Christensen, O. B., Christensen, J. H., Coppola, E., De Cruz, L., Davin, E. L., Dobler, A., Domínguez, M., Fealy, R., Fernandez, J., Gaertner, M. A., García-Díez, M., Giorgi, F., Gobiet, A., Goergen, K., Gómez-Navarro, J. J., Alemán, J. J. G., Gutiérrez, C., Gutiérrez, J. M., Güttler, I., Haensler, A., Halenka, T., Jerez, S., Jiménez-Guerrero, P., Jones, R. G., Keuler, K., Kjellström, E., Knist, S., Kotlarski, S., Maraun, D., van Meijgaard, E., Mercogliano, P., Montávez, J. P., Navarra, A., Nikulin, G., de Noblet-Ducoudré, N., Panitz, H.-J., Pfeifer, S., Piazza, M., Pichelli, E., Pietikäinen, J.-P., Prein, A. F., Preuschmann, S., Rechid, D., Rockel, B., Romera, R., Sánchez, E., Sieck, K., Soares, P. M. M., Somot, S., Srnec, L., Sørland, S. L., Termonia, P., Truhetz, H., Vautard, R., Warrach-Sagi, K., and Wulfmeyer, V.: Regional climate downscaling over Europe: perspectives from the EURO-CORDEX community, Reg Environ Change, 20, 51, https://doi.org/10.1007/s10113-020-01606-9, 2020.

James, R., Washington, R., Schleussner, C.-F., Rogelj, J., and Conway, D.: Characterizing half-a-degree difference: a review of methods for identifying regional climate responses to global warming targets, WIREs Climate Change, 8, e457, https://doi.org/10.1002/wcc.457, 2017.

Ji, H. K., Mirzaei, M., Lai, S. H., Dehghani, A., and Dehghani, A.: Implementing generative adversarial network (GAN) as a data-driven multi-site stochastic weather generator for flood frequency estimation, Environmental Modelling & Software, 172, 105896, https://doi.org/10.1016/j.envsoft.2023.105896, 2024.

Jun, T. and Rind, D.: Increasing contribution of the atmospheric vertical motion to precipitation in a warming climate, Commun Earth Environ, 5, 1–13, https://doi.org/10.1038/s43247-024-01676-1, 2024.

Kadoya, M. and Fukushima, A.: Concentration time of flood in small or medium river basins, Annuals of the Disaster Prevention Research Institute, Kyoto University, B-2, 19, 143–152, 1976.

Kamahori, H. and Arakawa, O.: Tropical Cyclone Induced Precipitation over Japan Using Observational Data, SOLA, 14, 165–169, https://doi.org/10.2151/sola.2018-029, 2018.

Kato, T.: Quasi-stationary Band-Shaped Precipitation Systems, Named “Senjo-Kousuitai”, Causing Localized Heavy Rainfall in Japan, Journal of the Meteorological Society of Japan. Ser. II, 98, 485–509, https://doi.org/10.2151/jmsj.2020-029, 2020.

Kawai, H., Toyoda, R., Tebekari, T., Yoshida, K., and Noda, K.: The gap between farmers and beneficiaries in terms of awareness and expectations regarding the paddy field dam project, Paddy Water

Environ, https://doi.org/10.1007/s10333-024-00978-6, 2024.

Kawase, H., Murata, A., Mizuta, R., Sasaki, H., Nosaka, M., Ishii, M., and Takayabu, I.: Enhancement of heavy daily snowfall in central Japan due to global warming as projected by large ensemble of regional climate simulations, Climatic Change, 139, 265–278, https://doi.org/10.1007/s10584-016-1781-3, 2016.

Kawase, H., Imada, Y., Tsuguti, H., Nakaegawa, T., Seino, N., Murata, A., and Takayabu, I.: The Heavy Rain Event of July 2018 in Japan Enhanced by Historical Warming, Bulletin of the American Meteorological Society, 101, S109–S114, https://doi.org/10.1175/BAMS-D-19-0173.1, 2020.

Kawase, H., Nosaka, M., Watanabe, S. I., Yamamoto, K., Shimura, T., Naka, Y., Wu, Y.-H., Okachi, H., Hoshino, T., Ito, R., Sugimoto, S., Suzuki, C., Fukui, S., Takemi, T., Ishikawa, Y., Mori, N., Nakakita, E., Yamada, T. J., Murata, A., Nakaegawa, T., and Takayabu, I.: Identifying Robust Changes of Extreme Precipitation in Japan From Large Ensemble 5-km-Grid Regional Experiments for 4K Warming Scenario, Journal of Geophysical Research: Atmospheres, 128, e2023JD038513, https://doi.org/10.1029/2023JD038513, 2023.

Kendall, M., George,: Rank Correlation Methods, 4th Edition., Griffin, London, 1975.

Kim, J., Johnson, L., Cifelli, R., Thorstensen, A., and Chandrasekar, V.: Assessment of antecedent moisture condition on flood frequency: An experimental study in Napa River Basin, CA, Journal of Hydrology: Regional Studies, 26, 100629, https://doi.org/10.1016/j.ejrh.2019.100629, 2019.

Kim, Y.-H., Min, S.-K., Zhang, X., Sillmann, J., and Sandstad, M.: Evaluation of the CMIP6 multi-model ensemble for climate extreme indices, Weather Clim. Extremes, 29, 100269, https://doi.org/10.1016/j.wace.2020.100269, 2020.

Kimura, N., Kiri, H., and Kitagawa, I.: The Impact of Multiple Typhoons on Severe Floods in the Mid-Latitude Region (Hokkaido), Water, 10, 843, https://doi.org/10.3390/w10070843, 2018.

Kita, Y. and Yamazaki, D.: Uncertainty of internal climate variability in probabilistic flood simulations using d4PDF, Hydrological Research Letters, 17, 15–20, https://doi.org/10.3178/hrl.17.15, 2023.

Kitoh, A., Ose, T., and Takayabu, I.: Dynamical Downscaling for Climate Projection with High-Resolution MRI AGCM-RCM, Journal of the Meteorological Society of Japan. Ser. II, 94A, 1–16, https://doi.org/10.2151/jmsj.2015-022, 2016a.

Kitoh, A., Ose, T., and Takayabu, I.: Dynamical Downscaling for Climate Projection with High-Resolution MRI AGCM-RCM, Journal of the Meteorological Society of Japan, 94A, 1–16, https://doi.org/10.2151/jmsj.2015-022, 2016b.

Knutson, T. R., McBride, J. L., Chan, J., Emanuel, K., Holland, G., Landsea, C., Held, I., Kossin, J. P., Srivastava, A. K., and Sugi, M.: Tropical cyclones and climate change, Nature Geosci, 3, 157–163, https://doi.org/10.1038/ngeo779, 2010.

Kobayashi, K., Tanaka, T., Shinohara, M., and Tachikawa, Y.: Analyzing future changes of extreme river discharge in Japan using d4PDF, Journal of Japan Society of Civil Engineers, Ser. B1 (Hydraulic Engineering), 76, 140–152, https://doi.org/10.2208/jscejhe.76.1_140, 2020.

Koike, T.: Evolution of Japan's flood control planning and policy in response to climate change risks and social changes, Water Policy, 23, 77–84, https://doi.org/10.2166/wp.2021.287, 2021.

Koks, E. E., Rozenberg, J., Zorn, C., Tariverdi, M., Vousdoukas, M., Fraser, S. A., Hall, J. W., and Hallegatte, S.: A global multi-hazard risk analysis of road and railway infrastructure assets, Nat Commun, 10, 2677, https://doi.org/10.1038/s41467-019-10442-3, 2019.

Köplin, N., Schädler, B., Viviroli, D., and Weingartner, R.: Seasonality and magnitude of floods in Switzerland under future climate change, Hydrological Processes, 28, 2567–2578, https://doi.org/10.1002/hyp.9757, 2014.

Kossin, J. P.: A global slowdown of tropical-cyclone translation speed, Nature, 558, 104–107, https://doi.org/10.1038/s41586-018-0158-3, 2018.

Kossin, J. P., Emanuel, K. A., and Camargo, S. J.: Past and Projected Changes in Western North Pacific Tropical Cyclone Exposure, Journal of Climate, 29, 5725–5739, https://doi.org/10.1175/JCLI-D-16-0076.1, 2016.

Kossin, J. P., Knapp, K. R., Olander, T. L., and Velden, C. S.: Global increase in major tropical cyclone exceedance probability over the past four decades, Proceedings of the National Academy of Sciences, 117, 11975–11980, https://doi.org/10.1073/pnas.1920849117, 2020.

Kotera, A., Nawata, E., Thao, L. V., Vuong, N. V., and Sakuratani, T.: Effect of Submergence on Rice Yield in the Red River Delta, Vietnam, Japanese Journal of Tropical Agriculture, 49, 197–206, https://doi.org/10.11248/jsta1957.49.197, 2005.

Kusunoki, S. and Mizuta, R.: Changes in precipitation intensity over East Asia during the 20th and 21st centuries simulated by a global atmospheric model with a 60 km grid size, Journal of Geophysical Research: Atmospheres, 118, 11,007-11,016, https://doi.org/10.1002/jgrd.50877, 2013.

Lai, Y., Li, J., Gu, X., Chen, Y. D., Kong, D., Gan, T. Y., Liu, M., Li, Q., and Wu, G.: Greater flood risks in response to slowdown of tropical cyclones over the coast of China, Proceedings of the National Academy of Sciences, 117, 14751–14755, https://doi.org/10.1073/pnas.1918987117, 2020.

Lang, M., Ouarda, T., and Bobee, B.: Towards operational guidelines for over-threshold modeling, J. Hydrol., 225, 103–117, https://doi.org/10.1016/S0022-1694(99)00167-5, 1999.

Langousis, A., Mamalakis, A., Puliga, M., and Deidda, R.: Threshold detection for the generalized Pareto distribution: Review of representative methods and application to the NOAA NCDC daily rainfall database, Water Resour. Res., 52, 2659–2681, https://doi.org/10.1002/2015WR018502, 2016.

Leduc, M., Mailhot, A., Frigon, A., Martel, J.-L., Ludwig, R., Brietzke, G. B., Giguère, M., Brissette, F., Turcotte, R., Braun, M., and Scinocca, J.: The ClimEx Project: A 50-Member Ensemble of Climate Change Projections at 12-km Resolution over Europe and Northeastern North America with the Canadian Regional Climate Model (CRCM5), Journal of Applied Meteorology and Climatology, 58, 663–693, https://doi.org/10.1175/JAMC-D-18-0021.1, 2019.

Li, C., Zwiers, F., Zhang, X., Chen, G., Lu, J., Li, G., Norris, J., Tan, Y., Sun, Y., and Liu, M.: Larger Increases in More Extreme Local Precipitation Events as Climate Warms, Geophys. Res. Lett., 46, 6885–6891, https://doi.org/10.1029/2019GL082908, 2019.

Li, J., Thyer, M., Lambert, M., Kuczera, G., and Metcalfe, A.: An efficient causative event-based approach for deriving the annual flood frequency distribution, Journal of Hydrology, 510, 412–423, https://doi.org/10.1016/j.jhydrol.2013.12.035, 2014.

Li, Q.-H., Lu, H.-C., Zhong, W., Wang, W.-C., Guo, X.-L., and Yuan, M.: Meso-scale transport characteristics and budget diagnoses of water vapor in binary typhoons, Acta Phys. Sin., 67, 039201, https://doi.org/10.7498/aps.67.20170455, 2018.

Li, R. C. Y., Zhou, W., Shun, C. M., and Lee, T. C.: Change in Destructiveness of Landfalling Tropical Cyclones over China in Recent Decades, Journal of Climate, 30, 3367–3379, https://doi.org/10.1175/JCLI-D-16-0258.1, 2017.

Li, Z., Gao, S., Chen, M., Gourley, J. J., Liu, C., Prein, A. F., and Hong, Y.: The conterminous United States are projected to become more prone to flash floods in a high-end emissions scenario, Commun Earth Environ, 3, 1–9, https://doi.org/10.1038/s43247-022-00409-6, 2022.

Li, Z., Gao, S., Chen, M., Zhang, J., Gourley, J. J., Wen, Y., Yang, T., and Hong, Y.: Introducing Flashiness-Intensity-Duration-Frequency (F-IDF): A New Metric to Quantify Flash Flood Intensity, Geophysical Research Letters, 50, e2023GL104992, https://doi.org/10.1029/2023GL104992, 2023.

Liang, X., Xia, R., Bao, X., Zhang, X., Wang, X., Su, A., Fu, J., Li, H., Wu, C., Yu, M., Hu, H., Yang, J., Liu, L., Xu, H., Zhu, C., Liu, B., Hu, N., Wang, X., Chen, G., and Chen, L.: Preliminary investigation on the extreme rainfall event during July 2021 in Henan Province and its multi-scale processes, CSB, 67, 997–1011, https://doi.org/10.1360/TB-2021-0827, 2022.

Liang, Y., Gillett, N. P., and Monahan, A. H.: Accounting for Pacific climate variability increases projected global warming, Nat. Clim. Chang., 14, 608–614, https://doi.org/10.1038/s41558-024-02017-y, 2024.

Lim, W. H., Yamazaki, D., Koirala, S., Hirabayashi, Y., Kanae, S., Dadson, S. J., Hall, J. W., and Sun, F.: Long-Term Changes in Global Socioeconomic Benefits of Flood Defenses and Residual Risk Based on CMIP5 Climate Models, Earth's Future, 6, 938–954, https://doi.org/10.1002/2017EF000671, 2018.

van der Linden, P. and Mitchell, J., editors: ENSEMBLES: Climate Change and its Impacts: Summary of research and results from the ENSEMBLES project, Met Office Hadley Centre, FitzRoy Road, Exeter EX1 3PB, UK, 160, 2009.

Liu, J., Feng, S., Gu, X., Zhang, Y., Beck, H. E., Zhang, J., and Yan, S.: Global changes in floods and their drivers, Journal of Hydrology, 614, 128553, https://doi.org/10.1016/j.jhydrol.2022.128553, 2022a.

Liu, M., Smith, J. A., Yang, L., and Vecchi, G. A.: Tropical Cyclone Flooding in the Carolinas, Journal of Hydrometeorology, 23, 53–70, https://doi.org/10.1175/JHM-D-21-0113.1, 2022b.

Liu, Q., Zhang, N., Wang, L., Yu, K., Wu, J., Wang, J., and Ma, M.: Flash flood simulation based on distributed hydrological model in future scenarios, Front. Earth Sci., 12, https://doi.org/10.3389/feart.2024.1537486, 2025.

Liu, Y., Liu, Y., Hao, Y., Wang, T., Yeh, T.-C. J., Fan, Y., and Zhang, Q.: Probabilistic Analysis of Extreme Discharges and Precipitations with a Nonparametric Copula Model, Water, 10, 823, https://doi.org/10.3390/w10070823, 2018.

Liu, Z., Ding, G., Zhang, Y., Lao, J., Liu, Y., Zhang, J., Lu, L., Liu, Q., and Jiang, B.: Identifying different types of flood–sensitive diarrheal diseases from 2006 to 2010 in Guangxi, China, Environmental Research, 170, 359–365, https://doi.org/10.1016/j.envres.2018.12.067, 2019.

Lorenz, E. N.: Deterministic Nonperiodic Flow, 1963.

Ly, S., Try, S., and Sayama, T.: Hydrological Changes in the Mekong River Basin Under Future Hydropower Development and Reservoir Operations, Journal of Japan Society of Civil Engineers, Ser. B1 (Hydraulic Engineering), 77, I_259-I_264, https://doi.org/10.2208/jscejhe.77.2_I_259, 2021.

Madsen, H., Rasmussen, P. F., and Rosbjerg, D.: Comparison of annual maximum series and partial duration series methods for modeling extreme hydrologic events: 1. At-site modeling, Water Resources Research, 33, 747–757, https://doi.org/10.1029/96WR03848, 1997.

Mahbod, M. and Rafiee, M. R.: Trend analysis of extreme precipitation events across Iran using percentile indices, International Journal of Climatology, 41, 952–969, https://doi.org/10.1002/joc.6708, 2021.

Mann, H. B.: Nonparametric Tests Against Trend, Econometrica, 13, 245–259, https://doi.org/10.2307/1907187, 1945.

Marchi, L., Borga, M., Preciso, E., and Gaume, E.: Characterisation of selected extreme flash floods in Europe and implications for flood risk management, Journal of Hydrology, 394, 118–133, https://doi.org/10.1016/j.jhydrol.2010.07.017, 2010.

Martínez, C., Sanchez, A., Toloh, B., and Vojinovic, Z.: Multi-objective Evaluation of Urban Drainage Networks Using a 1D/2D Flood Inundation Model, Water Resour Manage, 32, 4329–4343, https://doi.org/10.1007/s11269-018-2054-x, 2018.

Mascaro, G., Deidda, R., and Hellies, M.: On the nature of rainfall intermittency as revealed by different metrics and sampling approaches, Hydrology and Earth System Sciences, 17, 355–369, https://doi.org/10.5194/hess-17-355-2013, 2013.

Masutani, K., Akai, K., and Magome, J.: A New Scaling Algorithm of Gridded River Networks, JOURNAL OF JAPAN SOCIETY OF HYDROLOGY & WATER RESOURCES, 19, 139–150, https://doi.org/10.3178/jjshwr.19.139, 2006.

Maymandi, N., Hummel, M. A., and Zhang, Y.: Compound Coastal, Fluvial, and Pluvial Flooding During Historical Hurricane Events in the Sabine–Neches Estuary, Texas, Water Resources Research, 58, e2022WR033144, https://doi.org/10.1029/2022WR033144, 2022.

Meade, R. H., Rayol, J. M., Da Conceicão, S. C., and Natividade, J. R. G.: Backwater effects in the Amazon River basin of Brazil, Environ. Geol. Water Sci, 18, 105–114, https://doi.org/10.1007/BF01704664, 1991.

Mei, C., Liu, J., Wang, H., Li, Z., Yang, Z., Shao, W., Ding, X., Weng, B., Yu, Y., and Yan, D.: Urban flood inundation and damage assessment based on numerical simulations of design rainstorms with different characteristics, Sci. China Technol. Sci., 63, 2292–2304, https://doi.org/10.1007/s11431-019-1523-2, 2020.

Mei, W. and Xie, S.-P.: Intensification of landfalling typhoons over the northwest Pacific since the late 1970s, Nature Geosci, 9, 753–757, https://doi.org/10.1038/ngeo2792, 2016.

Mei, W., Pasquero, C., and Primeau, F.: The effect of translation speed upon the intensity of tropical cyclones over the tropical ocean, Geophysical Research Letters, 39, https://doi.org/10.1029/2011GL050765, 2012.

Mendelsohn, R., Emanuel, K., Chonabayashi, S., and Bakkensen, L.: The impact of climate change on global tropical cyclone damage, Nature Clim Change, 2, 205–209, https://doi.org/10.1038/nclimate1357, 2012.

Michalek, A. T., Villarini, G., Kim, T., Quintero, F., Krajewski, W. F., and Scoccimarro, E.: Evaluation of CMIP6 HighResMIP for Hydrologic Modeling of Annual Maximum Discharge in Iowa, Water Resources Research, 59, e2022WR034166, https://doi.org/10.1029/2022WR034166, 2023.

Miller, J. D., Kim, H., Kjeldsen, T. R., Packman, J., Grebby, S., and Dearden, R.: Assessing the impact of urbanization on storm runoff in a peri-urban catchment using historical change in impervious cover, Journal of Hydrology, 515, 59–70, https://doi.org/10.1016/j.jhydrol.2014.04.011, 2014.

Milly, P. C. D., Betancourt, J., Falkenmark, M., Hirsch, R. M., Kundzewicz, Z. W., Lettenmaier, D. P., and Stouffer, R. J.: Stationarity Is Dead: Whither Water Management?, Science, 319, 573–574, https://doi.org/10.1126/science.1151915, 2008.

Mirhosseini, G., Srivastava, P., and Stefanova, L.: The impact of climate change on rainfall Intensity-

Duration-Frequency (IDF) curves in Alabama, Reg. Envir. Chang., 13, S25–S33, https://doi.org/10.1007/s10113-012-0375-5, 2013.

Mitková, V. B., Pekárová, P., Miklánek, P., and Pekár, J.: Hydrological simulation of flood transformations in the upper Danube River: Case study of large flood events, Journal of Hydrology and Hydromechanics, 64, 337–348, https://doi.org/10.1515/johh-2016-0050, 2016.

Mitu, M. F., Sofia, G., Shen, X., and Anagnostou, E. N.: Assessing the compound flood risk in coastal areas: Framework formulation and demonstration, Journal of Hydrology, 626, 130278, https://doi.org/10.1016/j.jhydrol.2023.130278, 2023.

Miyasaka, T., Kawase, H., Nakaegawa, T., Imada, Y., and Takayabu, I.: Future Projections of Heavy Precipitation in Kanto and Associated Weather Patterns Using Large Ensemble High-Resolution Simulations, Sola, 16, 125–131, https://doi.org/10.2151/sola.2020-022, 2020.

Mizuta, R., Yoshimura, H., Murakami, H., Matsueda, M., Endo, H., Ose, T., Kamiguchi, K., Hosaka, M., Sugi, M., Yukimoto, S., Kusunoki, S., and Kitoh, A.: Climate Simulations Using MRI-AGCM3.2 with 20-km Grid, Journal of the Meteorological Society of Japan. Ser. II, 90A, 233–258, https://doi.org/10.2151/jmsj.2012-A12, 2012.

Mizuta, R., Murata, A., Ishii, M., Shiogama, H., Hibino, K., Mori, N., Arakawa, O., Imada, Y., Yoshida, K., Aoyagi, T., Kawase, H., Mori, M., Okada, Y., Shimura, T., Nagatomo, T., Ikeda, M., Endo, H., Nosaka, M., Arai, M., Takahashi, C., Tanaka, K., Takemi, T., Tachikawa, Y., Temur, K., Kamae, Y., Watanabe, M., Sasaki, H., Kitoh, A., Takayabu, I., Nakakita, E., and Kimoto, M.: Over 5,000 Years of Ensemble Future Climate Simulations by 60-km Global and 20-km Regional Atmospheric Models, Bulletin of the American Meteorological Society, 98, 1383–1398, https://doi.org/10.1175/BAMS-D-16-0099.1, 2017.

MLIT: On disaster damage by the Heavy Rainfall in 2018 (in Japanese), (Ministry of Land Infrastructure, Transport and Tourism), 2019.

MLIT: On disaster damage by the Typhoon No. 19 (Hagibis) in 2019 (in Japanese), (Ministry of Land Infrastructure, Transport and Tourism), 2020.

MLIT: River Basin Disaster Resilience and Sustainability by All, 2024a.

MLIT: Technical Criteria for River Works: Practical Guide for Planning, (Japanese Ministry of Land, Infrastructure, Transport and Tourism), 2024b.

Mori, N., Shimura, T., Yoshida, K., Mizuta, R., Okada, Y., Fujita, M., Khujanazarov, T., and Nakakita, E.: Future changes in extreme storm surges based on mega-ensemble projection using 60-km resolution atmospheric global circulation model, Coastal Engineering Journal, 61, 295–307, https://doi.org/10.1080/21664250.2019.1586290, 2019.

Mori, S. and Ono, K.: Landslide disasters in Ehime Prefecture resulting from the July 2018 heavy rain event in Japan, Soils and Foundations, 59, 2396–2409, https://doi.org/10.1016/j.sandf.2019.11.009, 2019.

Mostofi Zadeh, S., Durocher, M., Burn, D. H., and Ashkar, F.: Pooled flood frequency analysis: a comparison based on peaks-over-threshold and annual maximum series, Hydrological Sciences Journal, 64, 121–136, https://doi.org/10.1080/02626667.2019.1577556, 2019.

Moustakis, Y., Papalexiou, S. M., Onof, C. J., and Paschalis, A.: Seasonality, Intensity, and Duration of Rainfall Extremes Change in a Warmer Climate, Earth's Future, 9, e2020EF001824, https://doi.org/10.1029/2020EF001824, 2021.

Mukunoki, T., Suetsugu, D., Sako, K., Murakami, S., Fukubayashi, Y., Ishikura, R., Hino, T., Sugimoto, S., Wakinaka, K., Ito, S., and Koyama, A.: Reconnaissance report on geotechnical damage caused by a localized torrential downpour with emergency warning level in Kyushu, Japan, Soils and Foundations, 61, 600–620, https://doi.org/10.1016/j.sandf.2021.01.008, 2021.

Murakami, H., Wang, B., Li, T., and Kitoh, A.: Projected increase in tropical cyclones near Hawaii, Nature Clim Change, 3, 749–754, https://doi.org/10.1038/nclimate1890, 2013.

Nagumo, N., Ohara, M., Kuribayashi, D., and Sawano, H.: The 2015 Flood Impact due to the Overflow and Dike Breach of Kinu River in Joso City, Japan, Journal of Disaster Research, 11, 1112–1127, https://doi.org/10.20965/jdr.2016.p1112, 2016.

Najibi, N. and Devineni, N.: Scaling of Floods With Geomorphologic Characteristics and Precipitation Variability Across the Conterminous United States, Water Resources Research, 59, e2022WR032815, https://doi.org/10.1029/2022WR032815, 2023.

Nakamura, J., Camargo, S. J., Sobel, A. H., Henderson, N., Emanuel, K. A., Kumar, A., LaRow, T. E., Murakami, H., Roberts, M. J., Scoccimarro, E., Vidale, P. L., Wang, H., Wehner, M. F., and Zhao, M.: Western North Pacific Tropical Cyclone Model Tracks in Present and Future Climates, Journal of Geophysical Research: Atmospheres, 122, 9721–9744, https://doi.org/10.1002/2017JD027007, 2017.

Nakamura, S. and Oki, T.: Paradigm Shifts on Flood Risk Management in Japan: Detecting Triggers of Design Flood Revisions in the Modern Era, Water Resources Research, 54, 5504–5515, https://doi.org/10.1029/2017WR022509, 2018.

Nayak, S. and Takemi, T.: Quantitative estimations of hazards resulting from Typhoon Chanthu (2016) for assessing the impact in current and future climate, Hydrological Research Letters, 13, 20–27, https://doi.org/10.3178/hrl.13.20, 2019.

Nayak, S. and Takemi, T.: Robust responses of typhoon hazards in northern Japan to global warming climate: cases of landfalling typhoons in 2016, Meteorological Applications, 27, e1954, https://doi.org/10.1002/met.1954, 2020a.

Nayak, S. and Takemi, T.: Typhoon-induced precipitation characterization over northern Japan: a case study for typhoons in 2016, Progress in Earth and Planetary Science, 7, 39, https://doi.org/10.1186/s40645-020-00347-x, 2020b.

Nguyen, T. T., Nakatsugawa, M., Yamada, T. J., and Hoshino, T.: Assessing climate change impacts on extreme rainfall and severe flooding during the summer monsoon season in the Ishikari River basin, Japan, Hydrological Research Letters, 14, 155–161, https://doi.org/10.3178/hrl.14.155, 2020.

Nguyen-Le, D. and Yamada, T. J.: SIMULATION OF TROPICAL CYCLONE 201610 (LIONROCK) AND ITS REMOTE EFFECT ON HEAVY RAINFALL IN HOKKAIDO, J. JSCE, Ser. B1, 73, I_199-I_204, https://doi.org/10.2208/jscejhe.73.I_199, 2017.

Ohba, M. and Sugimoto, S.: Differences in climate change impacts between weather patterns: possible effects on spatial heterogeneous changes in future extreme rainfall, Clim Dyn, 52, 4177–4191, https://doi.org/10.1007/s00382-018-4374-1, 2019.

Ohba, M., Arai, R., Toyoda, Y., and Sato, T.: Impact of weather regime on projected future changes in streamflow in a heavy snowfall area of Japan, Clim Dyn, 59, 939–950, https://doi.org/10.1007/s00382-022-06163-x, 2022.

Ohya, Y. and Yamada, T. J.: Meteorological characteristics of line-shaped rainbands in northern Japan and its surrounding seas under climate change, Journal of Hydroinformatics, 26, 397–407, https://doi.org/10.2166/hydro.2024.121, 2024.

Osakada, Y. and Nakakita, E.: Future Change of Occurrence Frequency of Baiu Heavy Rainfall and Its Linked Atmospheric Patterns by Multiscale Analysis, Sola, 14, 79–85, https://doi.org/10.2151/sola.2018-014, 2018.

Otaki, T., Fudeyasu, H., Kohno, N., Takemi, T., Mori, N., and Iida, K.: Investigation of Characteristics of Maximum Storm Surges in Japanese Coastal Regions Caused by Typhoon Jebi (2018) Based on Typhoon Track Ensemble Simulations, J. Meteorol. Soc. Jpn., 100, 661–676, https://doi.org/10.2151/jmsj.2022-034661, 2022.

Owen, G.: What makes climate change adaptation effective? A systematic review of the literature, Global Environmental Change, 62, 102071, https://doi.org/10.1016/j.gloenvcha.2020.102071, 2020.

Packman, J. C. and Kidd, C. H. R.: A logical approach to the design storm concept, Water Resources Research, 16, 994–1000, https://doi.org/10.1029/WR016i006p00994, 1980.

Palmer, T. N.: A Nonlinear Dynamical Perspective on Climate Prediction, 1999.

Pan, X., Rahman, A., Haddad, K., and Ouarda, T. B. M. J.: Peaks-over-threshold model in flood frequency analysis: a scoping review, Stoch Environ Res Risk Assess, 36, 2419–2435, https://doi.org/10.1007/s00477-022-02174-6, 2022.

Pappenberger, F., Dutra, E., Wetterhall, F., and Cloke, H. L.: Deriving global flood hazard maps of fluvial floods through a physical model cascade, Hydrology and Earth System Sciences, 16, 4143–4156, https://doi.org/10.5194/hess-16-4143-2012, 2012.

Patricola, C. M., Camargo, S. J., Klotzbach, P. J., Saravanan, R., and Chang, P.: The Influence of ENSO Flavors on Western North Pacific Tropical Cyclone Activity, Journal of Climate, 31, 5395–5416, https://doi.org/10.1175/JCLI-D-17-0678.1, 2018.

Patricola, C. M., Cassidy, D. J., and Klotzbach, P. J.: Tropical Oceanic Influences on Observed Global Tropical Cyclone Frequency, Geophysical Research Letters, 49, e2022GL099354, https://doi.org/10.1029/2022GL099354, 2022.

Peduzzi, P., Chatenoux, B., Dao, H., De Bono, A., Herold, C., Kossin, J., Mouton, F., and Nordbeck, O.: Global trends in tropical cyclone risk, Nature Clim Change, 2, 289–294, https://doi.org/10.1038/nclimate1410, 2012.

Peleg, N. and Morin, E.: Stochastic convective rain-field simulation using a high-resolution synoptically conditioned weather generator (HiReS-WG), Water Resources Research, 50, 2124–2139, https://doi.org/10.1002/2013WR014836, 2014.

Peleg, N., Fatichi, S., Paschalis, A., Molnar, P., and Burlando, P.: An advanced stochastic weather generator for simulating 2-D high-resolution climate variables, Journal of Advances in Modeling Earth Systems, 9, 1595–1627, https://doi.org/10.1002/2016MS000854, 2017.

Pendergrass, A. G.: Changing Degree of Convective Organization as a Mechanism for Dynamic Changes in Extreme Precipitation, Curr Clim Change Rep, 6, 47–54, https://doi.org/10.1007/s40641-020-00157-9, 2020.

Pontoppidan, M., Reuder, J., Mayer, S., and Kolstad, E. W.: Downscaling an intense precipitation event in complex terrain: the importance of high grid resolution, Tellus A: Dynamic Meteorology and Oceanography, 69, 2017.

Prein, A. F., Langhans, W., Fosser, G., Ferrone, A., Ban, N., Goergen, K., Keller, M., Tölle, M., Gutjahr, O., Feser, F., Brisson, E., Kollet, S., Schmidli, J., van Lipzig, N. P. M., and Leung, R.: A review on regional convection-permitting climate modeling: Demonstrations, prospects, and challenges, Reviews

of Geophysics, 53, 323–361, https://doi.org/10.1002/2014RG000475, 2015.

Prein, A. F., Rasmussen, R. M., Ikeda, K., Liu, C., Clark, M. P., and Holland, G. J.: The future intensification of hourly precipitation extremes, Nature Clim Change, 7, 48–52, https://doi.org/10.1038/nclimate3168, 2017.

Qin, H., Yuan, W., Wang, J., Chen, Y., Dai, P., Sobel, A. H., Meng, Z., and Nie, J.: Climate change attribution of the 2021 Henan extreme precipitation: Impacts of convective organization, Sci. China Earth Sci., 65, 1837–1846, https://doi.org/10.1007/s11430-022-9953-0, 2022.

Quintero, F., Villarini, G., Prein, A. F., Zhang, W., and Krajewski, W. F.: Discharge and floods projected to increase more than precipitation extremes, Hydrol. Process., 36, e14738, https://doi.org/10.1002/hyp.14738, 2022.

Rasmussen, R., Ikeda, K., Liu, C., Gochis, D., Clark, M., Dai, A., Gutmann, E., Dudhia, J., Chen, F., Barlage, M., Yates, D., and Zhang, G.: Climate Change Impacts on the Water Balance of the Colorado Headwaters: High-Resolution Regional Climate Model Simulations, https://doi.org/10.1175/JHM-D-13-0118.1, 2014.

Rasmy, M., Sayama, T., and Koike, T.: Development of water and energy Budget-based Rainfall-Runoff-Inundation model (WEB-RRI) and its verification in the Kalu and Mundeni River Basins, Sri Lanka, Journal of Hydrology, 579, 124163, https://doi.org/10.1016/j.jhydrol.2019.124163, 2019.

Raynaud, D., Thielen, J., Salamon, P., Burek, P., Anquetin, S., and Alfieri, L.: A dynamic runoff co-efficient to improve flash flood early warning in Europe: evaluation on the 2013 central European floods in Germany, Meteorological Applications, 22, 410–418, https://doi.org/10.1002/met.1469, 2015.

Riahi, K., van Vuuren, D. P., Kriegler, E., Edmonds, J., O'Neill, B. C., Fujimori, S., Bauer, N., Calvin, K., Dellink, R., Fricko, O., Lutz, W., Popp, A., Cuaresma, J. C., Kc, S., Leimbach, M., Jiang, L., Kram, T., Rao, S., Emmerling, J., Ebi, K., Hasegawa, T., Havlik, P., Humpenöder, F., Da Silva, L. A., Smith, S., Stehfest, E., Bosetti, V., Eom, J., Gernaat, D., Masui, T., Rogelj, J., Strefler, J., Drouet, L., Krey, V., Luderer, G., Harmsen, M., Takahashi, K., Baumstark, L., Doelman, J. C., Kainuma, M., Klimont, Z., Marangoni, G., Lotze-Campen, H., Obersteiner, M., Tabeau, A., and Tavoni, M.: The Shared Socioeconomic Pathways and their energy, land use, and greenhouse gas emissions implications: An overview, Global Environmental Change, 42, 153–168, https://doi.org/10.1016/j.gloenvcha.2016.05.009, 2017.

Rosenfeld, D., Andreae, M. O., Asmi, A., Chin, M., de Leeuw, G., Donovan, D. P., Kahn, R., Kinne, S., Kivekäs, N., Kulmala, M., Lau, W., Schmidt, K. S., Suni, T., Wagner, T., Wild, M., and Quaas, J.: Global observations of aerosol-cloud-precipitation-climate interactions, Reviews of Geophysics, 52, 750–808, https://doi.org/10.1002/2013RG000441, 2014.

Saharia, M., Kirstetter, P.-E., Vergara, H., Gourley, J. J., Emmanuel, I., and Andrieu, H.: On the Impact of Rainfall Spatial Variability, Geomorphology, and Climatology on Flash Floods, Water Resour. Res., 57, e2020WR029124, https://doi.org/10.1029/2020WR029124, 2021.

Saito, M., Ishida, T., Kojima, J., Maeda, Y., and Okabe, M.: Study on design flood setting method considering the increase in rainfall due to climate change, Advances in river engineering, 28, 433-438 (in Japanese), https://doi-org.kyoto-u.idm.oclc.org/10.11532/river.28.0_433, 2022.

Salgado-Cassiani, J. J., Coronado-Hernández, O. E., Gatica, G., Linfati, R., and Coronado-Hernández, J. R.: Probabilistic Approach to Determine the Spatial Distribution of the Antecedent Moisture Conditions for Different Return Periods in the Atlántico Region, Colombia, Water, 14, 1217, https://doi.org/10.3390/w14081217, 2022.

Sampson, C. C., Smith, A. M., Bates, P. D., Neal, J. C., Alfieri, L., and Freer, J. E.: A high-resolution global flood hazard model, Water Resources Research, 51, 7358–7381, https://doi.org/10.1002/2015WR016954, 2015.

dos Santos, C. M., Escobedo, J. F., Teramoto, É. T., and da Silva, S. H. M. G.: Assessment of ANN and SVM models for estimating normal direct irradiation (Hb), Energy Conversion and Management, 126, 826–836, https://doi.org/10.1016/j.enconman.2016.08.020, 2016.

Sarhadi, A., Rousseau-Rizzi, R., and Emanuel, K.: Physics-Based Hazard Assessment of Compound Flooding From Tropical and Extratropical Cyclones in a Warming Climate, Earth's Future, 13, e2024EF005078, https://doi.org/10.1029/2024EF005078, 2025.

Sasai, T., Kawase, H., Kanno, Y., Yamaguchi, J., Sugimoto, S., Yamazaki, T., Sasaki, H., Fujita, M., and Iwasaki, T.: Future Projection of Extreme Heavy Snowfall Events With a 5-km Large Ensemble Regional Climate Simulation, Journal of Geophysical Research: Atmospheres, 124, 13975–13990, https://doi.org/10.1029/2019JD030781, 2019.

Sasaki, H., Kurihara, K., Takayabu, I., and Uchiyama, T.: Preliminary Experiments of Reproducing the Present Climate Using the Non-hydrostatic Regional Climate Model, Sola, 4, 25–28, https://doi.org/10.2151/sola.2008-007, 2008.

Sasaki, H., Murata, A., Hanafusa, M., Oh'izumi, M., and Kurihara, K.: Reproducibility of Present Climate in a Non-Hydrostatic Regional Climate Model Nested within an Atmosphere General Circulation Model, Sola, 7, 173–176, https://doi.org/10.2151/sola.2011-044, 2011.

Satoh, M., Noda, A. T., Seiki, T., Chen, Y.-W., Kodama, C., Yamada, Y., Kuba, N., and Sato, Y.: Toward reduction of the uncertainties in climate sensitivity due to cloud processes using a global non-hydrostatic atmospheric model, Progress in Earth and Planetary Science, 5, 67, https://doi.org/10.1186/s40645-018-0226-1, 2018.

Sayama, T. and McDonnell, J. J.: A new time-space accounting scheme to predict stream water residence time and hydrograph source components at the watershed scale, Water Resour. Res., 45, W07401, https://doi.org/10.1029/2008WR007549, 2009.

Sayama, T., Ozawa, G., Kawakami, T., Nabesaka, S., and Fukami, K.: Rainfall-runoff-inundation analysis of the 2010 Pakistan flood in the Kabul River basin, Hydrol. Sci. J., 57, 298–312, https://doi.org/10.1080/02626667.2011.644245, 2012.

Sayama, T., Tatebe, Y., Iwami, Y., and Tanaka, S.: Hydrologic sensitivity of flood runoff and inundation: 2011 Thailand floods in the Chao Phraya River basin, Nat. Hazards Earth Syst. Sci., 15, 1617–1630, https://doi.org/10.5194/nhess-15-1617-2015, 2015.

Sayama, T., Tatebe, Y., and Tanaka, S.: An emergency response-type rainfall-runoff-inundation simulation for 2011 Thailand floods, J. Flood Risk Manag., 10, 65–78, https://doi.org/10.1111/jfr3.12147, 2017.

Sayama, T., Yamada, M., Sugawara, Y., and Yamazaki, D.: Ensemble flash flood predictions using a high-resolution nationwide distributed rainfall-runoff model: case study of the heavy rain event of July 2018 and Typhoon Hagibis in 2019, Progress in Earth and Planetary Science, 7, 75, https://doi.org/10.1186/s40645-020-00391-7, 2020.

Sayama, T., Yamada, M., Yamakita, A., and Sugawara, Y.: Parameter regionalization of large-scale distributed rainfall–runoff models using a conditional probability method, Progress in Earth and Planetary Science, 12, 17, https://doi.org/10.1186/s40645-025-00691-w, 2025.

Schumann, G. J.-P., Stampoulis, D., Smith, A. M., Sampson, C. C., Andreadis, K. M., Neal, J. C., and

Bates, P. D.: Rethinking flood hazard at the global scale, Geophysical Research Letters, 43, 10,249-10,256, https://doi.org/10.1002/2016GL070260, 2016.

Screen, J. A., Deser, C., Smith, D. M., Zhang, X., Blackport, R., Kushner, P. J., Oudar, T., McCusker, K. E., and Sun, L.: Consistency and discrepancy in the atmospheric response to Arctic sea-ice loss across climate models, Nature Geosci, 11, 155–163, https://doi.org/10.1038/s41561-018-0059-y, 2018.

Shan, K., Lin, Y., Chu, P.-S., Yu, X., and Song, F.: Seasonal advance of intense tropical cyclones in a warming climate, Nature, 623, 83–89, https://doi.org/10.1038/s41586-023-06544-0, 2023.

Shan, K., Song, F., Lin, Y., Chu, W., He, C., Chu, P.-S., Wu, L., and Yu, X.: How does globally accumulated tropical cyclone energy vary in response to a changing climate?, Science Bulletin, 70, 943–950, https://doi.org/10.1016/j.scib.2024.12.036, 2025.

Shehata, M. and Mizunaga, H.: Flash Flood Risk Assessment for Kyushu Island, Japan, Environ Earth Sci, 77, 76, https://doi.org/10.1007/s12665-018-7250-8, 2018.

Shepherd, T. G.: Atmospheric circulation as a source of uncertainty in climate change projections, Nature Geosci, 7, 703–708, https://doi.org/10.1038/ngeo2253, 2014.

Shepherd, T. G., Boyd, E., Calel, R. A., Chapman, S. C., Dessai, S., Dima-West, I. M., Fowler, H. J., James, R., Maraun, D., Martius, O., Senior, C. A., Sobel, A. H., Stainforth, D. A., Tett, S. F. B., Trenberth, K. E., van den Hurk, B. J. J. M., Watkins, N. W., Wilby, R. L., and Zenghelis, D. A.: Storylines: an alternative approach to representing uncertainty in physical aspects of climate change, Clim. Change, 151, 555–571, https://doi.org/10.1007/s10584-018-2317-9, 2018.

Shi, M. and Shiraiwa, T.: Estimating future streamflow under climate and land use change conditions in northeastern Hokkaido, Japan, Journal of Hydrology: Regional Studies, 50, 101555, https://doi.org/10.1016/j.ejrh.2023.101555, 2023.

Shimura, T., Mori, N., and Hemer, M. A.: Projection of tropical cyclone-generated extreme wave climate based on CMIP5 multi-model ensemble in the Western North Pacific, Clim Dyn, 49, 1449–1462, https://doi.org/10.1007/s00382-016-3390-2, 2017.

Shiogama, H., Ishizaki, N. N., Hanasaki, N., Takahashi, K., Emori, S., Ito, R., Nakaegawa, T., Takayabu, I., Hijioka, Y., Takayabu, Y. N., and Shibuya, R.: Selecting CMIP6-Based Future Climate Scenarios for Impact and Adaptation Studies, Sola, 17, 57–62, https://doi.org/10.2151/sola.2021-009, 2021.

Shokri, A., Shokri, A., and Koupai, J. A.: Pre-event base flow as a useful indicator for flood forecasting, Advances in Water Resources, 180, 104539, https://doi.org/10.1016/j.advwatres.2023.104539, 2023.

Shugar, D. H., Burr, A., Haritashya, U. K., Kargel, J. S., Watson, C. S., Kennedy, M. C., Bevington, A. R., Betts, R. A., Harrison, S., and Strattman, K.: Rapid worldwide growth of glacial lakes since 1990, Nat. Clim. Chang., 10, 939–945, https://doi.org/10.1038/s41558-020-0855-4, 2020.

Silva, A. T. and Portela, M. M.: Using Climate-Flood Links and CMIP5 Projections to Assess Flood Design Levels Under Climate Change Scenarios: A Case Study in Southern Brazil, Water Resour Manage, 32, 4879–4893, https://doi.org/10.1007/s11269-018-2058-6, 2018.

Singh, V., Lohani, A. K., and Jain, S. K.: Reconstruction of extreme flood events by performing integrated real-time and probabilistic flood modeling in the Periyar river basin, Southern India, Nat Hazards, 112, 2433–2463, https://doi.org/10.1007/s11069-022-05272-4, 2022.

Smith, A., Freer, J., Bates, P., and Sampson, C.: Comparing ensemble projections of flooding against flood estimation by continuous simulation, Journal of Hydrology, 511, 205–219, https://doi.org/10.1016/j.jhydrol.2014.01.045, 2014.

Smith, A., Sampson, C., and Bates, P.: Regional flood frequency analysis at the global scale, Water Resources Research, 51, 539–553, https://doi.org/10.1002/2014WR015814, 2015.

Sobel, A. H., Wing, A. A., Camargo, S. J., Patricola, C. M., Vecchi, G. A., Lee, C.-Y., and Tippett, M. K.: Tropical Cyclone Frequency, Earth's Future, 9, e2021EF002275, https://doi.org/10.1029/2021EF002275, 2021.

Soergel, B., Kriegler, E., Weindl, I., Rauner, S., Dirnaichner, A., Ruhe, C., Hofmann, M., Bauer, N., Bertram, C., Bodirsky, B. L., Leimbach, M., Leininger, J., Levesque, A., Luderer, G., Pehl, M., Wingens, C., Baumstark, L., Beier, F., Dietrich, J. P., Humpenöder, F., von Jeetze, P., Klein, D., Koch, J., Pietzcker, R., Strefler, J., Lotze-Campen, H., and Popp, A.: A sustainable development pathway for climate action within the UN 2030 Agenda, Nat. Clim. Chang., 11, 656–664, https://doi.org/10.1038/s41558-021-01098-3, 2021.

Song, J., Klotzbach, P. J., Dai, Y., and Duan, Y.: A Slowdown in Translation Speed of Western North Pacific Tropical Cyclones Undergoing Rapid Intensification, Geophysical Research Letters, 51, e2024GL110220, https://doi.org/10.1029/2024GL110220, 2024.

Soriano, E., Mediero, L., and Garijo, C.: Quantification of Expected Changes in Peak Flow Quantiles in Climate Change by Combining Continuous Hydrological Modelling with the Modified Curve Number Method, Water Resour Manage, 34, 4381–4397, https://doi.org/10.1007/s11269-020-02670-w, 2020.

Stephens, C. M., Johnson, F. M., and Marshall, L. A.: Implications of future climate change for event-based hydrologic models, Advances in Water Resources, 119, 95–110, https://doi.org/10.1016/j.advwatres.2018.07.004, 2018.

Studholme, J., Fedorov, A. V., Gulev, S. K., Emanuel, K., and Hodges, K.: Poleward expansion of tropical cyclone latitudes in warming climates, Nat. Geosci., 15, 14–28, https://doi.org/10.1038/s41561-021-00859-1, 2022.

Sun, Q., Zhang, X., Zwiers, F., Westra, S., and Alexander, L. V.: A Global, Continental, and Regional Analysis of Changes in Extreme Precipitation, Journal of Climate, 34, 243–258, https://doi.org/10.1175/JCLI-D-19-0892.1, 2021.

Sun, Y., Dong, S., Hu, T., Zhang, X., and Stott, P.: Anthropogenic Influence on the Heaviest June Precipitation in Southeastern China since 1961, https://doi.org/10.1175/BAMS-D-18-0114.1, 2019a.

Sun, Y., Wendi, D., Kim, D. E., and Liong, S.-Y.: Deriving intensity–duration–frequency (IDF) curves using downscaled in situ rainfall assimilated with remote sensing data, Geoscience Letters, 6, 17, https://doi.org/10.1186/s40562-019-0147-x, 2019b.

Sunyer, M. A., Luchner, J., Onof, C., Madsen, H., and Arnbjerg-Nielsen, K.: Assessing the importance of spatio-temporal RCM resolution when estimating sub-daily extreme precipitation under current and future climate conditions, International Journal of Climatology, 37, 688–705, https://doi.org/10.1002/joc.4733, 2017.

Suzuki, Y., Nakamura, K., and Hama, T.: Peak discharge mitigation effects in different rainfall patterns at a paddy plot with a runoff control plate, Journal of Hydrology: Regional Studies, 42, 101165, https://doi.org/10.1016/j.ejrh.2022.101165, 2022.

Swetapadma, S. and Ojha, C. S. P.: Technical Note: Flood frequency study using partial duration series coupled with entropy principle, Hydrology and Earth System Sciences Discussions, 1–23, https://doi.org/10.5194/hess-2021-570, 2021.

Tachikawa, Y., Nagatani, G., and Takara, K.: Development of Stage-Discharge Relationship Equation Incorporationg Saturated-Unsaturated Flow Mechanism, Proceedings of Hydraulic Engineering, 48, 7–

12, https://doi.org/10.2208/prohe.48.7, 2004.

Tada, H., Uchiyama, Y., and Masunaga, E.: Impacts of two super typhoons on the Kuroshio and marginal seas on the Pacific coast of Japan, Deep-Sea Res. Part I-Oceanogr. Res. Pap., 132, 80–93, https://doi.org/10.1016/j.dsr.2017.12.007, 2018.

Takabatake, T., Mäll, M., Esteban, M., Nakamura, R., Kyaw, T. O., Ishii, H., Valdez, J. J., Nishida, Y., Noya, F., and Shibayama, T.: Field Survey of 2018 Typhoon Jebi in Japan: Lessons for Disaster Risk Management, Geosciences, 8, 412, https://doi.org/10.3390/geosciences8110412, 2018.

Takaya, Y., Ishikawa, I., Kobayashi, C., Endo, H., and Ose, T.: Enhanced Meiyu-Baiu Rainfall in Early Summer 2020: Aftermath of the 2019 Super IOD Event, Geophysical Research Letters, 47, e2020GL090671, https://doi.org/10.1029/2020GL090671, 2020.

Takemi, T.: Dependence of the precipitation intensity in mesoscale convective systems to temperature lapse rate, Atmospheric Research, 96, 273–285, https://doi.org/10.1016/j.atmosres.2009.09.002, 2010.

Takemi, T.: Impacts of Global Warming on Extreme Rainfall of a Slow-Moving Typhoon: A Case Study for Typhoon Talas (2011), Sola, 15, 125–131, https://doi.org/10.2151/sola.2019-023, 2019.

Tamm, O., Kokkonen, T., Warsta, L., Dubovik, M., and Koivusalo, H.: Modelling urban stormwater management changes using SWMM and convection-permitting climate simulations in cold areas, Journal of Hydrology, 622, 129656, https://doi.org/10.1016/j.jhydrol.2023.129656, 2023.

Tan, X., Wu, X., and Liu, B.: Global changes in the spatial extents of precipitation extremes, Environ. Res. Lett., 16, 054017, https://doi.org/10.1088/1748-9326/abf462, 2021.

Tanaka, T., Tachikawa, Y., Ichikawa, Y., and Yorozu, K.: Flood risk curve development with probabilistic rainfall modelling and large ensemble climate simulation data: a case study for the Yodo River basin, Hydrological Research Letters, 12, 28–33, https://doi.org/10.3178/hrl.12.28, 2018.

Tanaka, T., Kiyohara, K., and Tachikawa, Y.: Comparison of fluvial and pluvial flood risk curves in urban cities derived from a large ensemble climate simulation dataset: A case study in Nagoya, Japan, Journal of Hydrology, 584, 124706, https://doi.org/10.1016/j.jhydrol.2020.124706, 2020.

Tanaka, T., Kobayashi, K., and Tachikawa, Y.: Simultaneous flood risk analysis and its future change among all the 109 class-A river basins in Japan using a large ensemble climate simulation database d4PDF, Environ. Res. Lett., 16, 074059, https://doi.org/10.1088/1748-9326/abfb2b, 2021.

Tanaka, T., Kawase, H., Imada, Y., Kawai, Y., and Watanabe, S.: Risk-based versus storyline approaches for global warming impact assessment on basin-averaged extreme rainfall: a case study for Typhoon Hagibis in eastern Japan, Environ. Res. Lett., 18, 054010, https://doi.org/10.1088/1748-9326/accc24, 2023.

Tang, Z., Wang, P., Li, Y., Sheng, Y., Wang, B., Popovych, N., and Hu, T.: Contributions of climate change and urbanization to urban flood hazard changes in China's 293 major cities since 1980, Journal of Environmental Management, 353, 120113, https://doi.org/10.1016/j.jenvman.2024.120113, 2024.

Taniguchi, K., Kotone, K., and Shibuo, Y.: Simulation-based assessment of inundation risk potential considering the nonstationarity of extreme flood events under climate change, Journal of Hydrology, 613, 128434, https://doi.org/10.1016/j.jhydrol.2022.128434, 2022.

Tellman, B., Sullivan, J. A., Kuhn, C., Kettner, A. J., Doyle, C. S., Brakenridge, G. R., Erickson, T. A., and Slayback, D. A.: Satellite imaging reveals increased proportion of population exposed to floods, Nature, 596, 80–86, https://doi.org/10.1038/s41586-021-03695-w, 2021.

Tezuka, S., Takiguchi, H., Kazama, S., Sato, A., Kawagoe, S., and Sarukkalige, R.: Estimation of the effects of climate change on flood-triggered economic losses in Japan, International Journal of Disaster Risk Reduction, 9, 58–67, https://doi.org/10.1016/j.ijdrr.2014.03.004, 2014.

Thomassen, E. D., Kendon, E. J., Sørup, H. J. D., Chan, S. C., Langen, P. L., Christensen, O. B., and Arnbjerg-Nielsen, K.: Differences in representation of extreme precipitation events in two high resolution models, Clim Dyn, 57, 3029–3043, https://doi.org/10.1007/s00382-021-05854-1, 2021.

Trošelj, J. and Lee, H. S.: Modelling typhoon-induced extreme river discharges: A case study of Typhoon Hagibis in Japan, Journal of Hydrology: Regional Studies, 34, 100776, https://doi.org/10.1016/j.ejrh.2021.100776, 2021.

Try, S., Tanaka, S., Tanaka, K., Sayama, T., Hu, M., Sok, T., and Oeurng, C.: Projection of extreme flood inundation in the Mekong River basin under 4K increasing scenario using large ensemble climate data, Hydrological Processes, 34, 4350–4364, https://doi.org/10.1002/hyp.13859, 2020.

Try, S., Tanaka, S., Tanaka, K., Sayama, T., Khujanazarov, T., and Oeurng, C.: Comparison of CMIP5 and CMIP6 GCM performance for flood projections in the Mekong River Basin, Journal of Hydrology: Regional Studies, 40, 101035, https://doi.org/10.1016/j.ejrh.2022.101035, 2022.

Tu, S., Xu, F., and Xu, J.: Regime shift in the destructiveness of tropical cyclones over the western North Pacific, Environ. Res. Lett., 13, 094021, https://doi.org/10.1088/1748-9326/aade3a, 2018.

Vacondio, R., Dal Palù, A., and Mignosa, P.: GPU-enhanced Finite Volume Shallow Water solver for fast flood simulations, Environmental Modelling & Software, 57, 60–75, https://doi.org/10.1016/j.envsoft.2014.02.003, 2014.

Vangelis, H., Zotou, I., Kourtis, I. M., Bellos, V., and Tsihrintzis, V. A.: Relationship of Rainfall and Flood Return Periods through Hydrologic and Hydraulic Modeling, Water, 14, 3618, https://doi.org/10.3390/w14223618, 2022.

Verdin, A., Rajagopalan, B., Kleiber, W., Podestá, G., and Bert, F.: A conditional stochastic weather generator for seasonal to multi-decadal simulations, Journal of Hydrology, 556, 835–846, https://doi.org/10.1016/j.jhydrol.2015.12.036, 2018.

Verschuur, J., Fernández-Pérez, A., Mühlhofer, E., Nirandjan, S., Borgomeo, E., Becher, O., Voskaki, A., Oughton, E. J., Stankovski, A., Greco, S. F., Koks, E. E., Pant, R., and Hall, J. W.: Quantifying climate risks to infrastructure systems: A comparative review of developments across infrastructure sectors, PLOS Climate, 3, e0000331, https://doi.org/10.1371/journal.pclm.0000331, 2024.

Vestby, J., Schutte, S., Tollefsen, A. F., and Buhaug, H.: Societal determinants of flood-induced displacement, Proceedings of the National Academy of Sciences, 121, e2206188120, https://doi.org/10.1073/pnas.2206188120, 2024.

Vetter, T., Reinhardt, J., Flörke, M., van Griensven, A., Hattermann, F., Huang, S., Koch, H., Pechlivanidis, I. G., Plötner, S., Seidou, O., Su, B., Vervoort, R. W., and Krysanova, V.: Evaluation of sources of uncertainty in projected hydrological changes under climate change in 12 large-scale river basins, Climatic Change, 141, 419–433, https://doi.org/10.1007/s10584-016-1794-y, 2017.

van Vuuren, D. P., Edmonds, J., Kainuma, M., Riahi, K., Thomson, A., Hibbard, K., Hurtt, G. C., Kram, T., Krey, V., Lamarque, J.-F., Masui, T., Meinshausen, M., Nakicenovic, N., Smith, S. J., and Rose, S. K.: The representative concentration pathways: an overview, Climatic Change, 109, 5, https://doi.org/10.1007/s10584-011-0148-z, 2011.

Wakatsuki, Y., Nakane, H., and Hashino, T.: River Stage Modeling with a Deep Neural Network Using Long-Term Rainfall Time Series as Input Data: Application to the Shimanto-River Watershed, Water,

14, 452, https://doi.org/10.3390/w14030452, 2022.

Walker, N. D., Leben, R. R., Pilley, C. T., Shannon, M., Herndon, D. C., Pun, I.-F., Lin, I.-I., and Gentemann, C. L.: Slow translation speed causes rapid collapse of northeast Pacific Hurricane Kenneth over cold core eddy, Geophysical Research Letters, 41, 7595–7601, https://doi.org/10.1002/2014GL061584, 2014.

Wallemacq, P., UNISDR, and CRED: Economic Losses, Poverty and Disasters 1998-2017, https://doi.org/10.13140/RG.2.2.35610.08643, 2018.

Walsh, K. J. E., McBride, J. L., Klotzbach, P. J., Balachandran, S., Camargo, S. J., Holland, G., Knutson, T. R., Kossin, J. P., Lee, T., Sobel, A., and Sugi, M.: Tropical cyclones and climate change, WIREs Climate Change, 7, 65–89, https://doi.org/10.1002/wcc.371, 2016.

Wang, S., Rashid, T., Throp, H., and Toumi, R.: A Shortening of the Life Cycle of Major Tropical Cyclones, Geophysical Research Letters, 47, e2020GL088589, https://doi.org/10.1029/2020GL088589, 2020.

Wang, X., Zhai, X., Zhang, Y., and Guo, L.: Evaluating flash flood simulation capability with respect to rainfall temporal variability in a small mountainous catchment, Journal of Geographical Science, 33, 2530–2548, https://doi.org/10.1007/s11442-023-2188-5, 2023.

Wang, Z., Chen, Y., Zeng, Z., Li, R., Li, Z., Li, X., and Lai, C.: Compound effects in complex estuary-ocean interaction region under various combination patterns of storm surge and fluvial floods, Urban Climate, 58, 102186, https://doi.org/10.1016/j.uclim.2024.102186, 2024.

Ward, P. J., Couasnon, A., Eilander, D., Haigh, I. D., Hendry, A., Muis, S., Veldkamp, T. I. E., Winsemius, H. C., and Wahl, T.: Dependence between high sea-level and high river discharge increases flood hazard in global deltas and estuaries, Environ. Res. Lett., 13, 084012, https://doi.org/10.1088/1748-9326/aad400, 2018.

Wasko, C., Nathan, R., Stein, L., and O'Shea, D.: Evidence of shorter more extreme rainfalls and increased flood variability under climate change, Journal of Hydrology, 603, 126994, https://doi.org/10.1016/j.jhydrol.2021.126994, 2021.

Watt, E. and Marsalek, J.: Critical review of the evolution of the design storm event concept, Can. J. Civ. Eng., 40, 105–113, https://doi.org/10.1139/cjce-2011-0594, 2013.

Webb, A., Shimura, T., and Mori, N.: Global Tropical Cyclone Track Detection and Analysis of the d4PDF Mega-ensemble Projection, Journal of Japan Society of Civil Engineers, Ser. B2 (Coastal Engineering), 75, I_1207-I_1212, https://doi.org/10.2208/kaigan.75.I_1207, 2019.

Westra, S., Fowler, H. J., Evans, J. P., Alexander, L. V., Berg, P., Johnson, F., Kendon, E. J., Lenderink, G., and Roberts, N. M.: Future changes to the intensity and frequency of short-duration extreme rainfall, Reviews of Geophysics, 52, 522–555, https://doi.org/10.1002/2014RG000464, 2014.

Wing, O. E. J., Bates, P. D., Sampson, C. C., Smith, A. M., Johnson, K. A., and Erickson, T. A.: Validation of a 30 m resolution flood hazard model of the conterminous United States, Water Resour. Res., 53, 7968–7986, https://doi.org/10.1002/2017WR020917, 2017.

Wing, O. E. J., Smith, A. M., Marston, M. L., Porter, J. R., Amodeo, M. F., Sampson, C. C., and Bates, P. D.: Simulating historical flood events at the continental scale: observational validation of a large-scale hydrodynamic model, Natural Hazards and Earth System Sciences, https://doi.org/10.5194/nhess-2020-344, 2020.

Winsemius, H. C., Van Beek, L. P. H., Jongman, B., Ward, P. J., and Bouwman, A.: A framework for

global river flood risk assessments, Hydrology and Earth System Sciences, 17, 1871–1892, https://doi.org/10.5194/hess-17-1871-2013, 2013.

Winsemius, H. C., Aerts, J. C. J. H., van Beek, L. P. H., Bierkens, M. F. P., Bouwman, A., Jongman, B., Kwadijk, J. C. J., Ligtvoet, W., Lucas, P. L., van Vuuren, D. P., and Ward, P. J.: Global drivers of future river flood risk, Nature Clim Change, 6, 381–385, https://doi.org/10.1038/nclimate2893, 2016.

Winsemius, H. C., Jongman, B., Veldkamp, T. I. E., Hallegatte, S., Bangalore, M., and Ward, P. J.: Disaster risk, climate change, and poverty: assessing the global exposure of poor people to floods and droughts, Environment and Development Economics, 23, 328–348, https://doi.org/10.1017/S1355770X17000444, 2018.

Wright, D. B., Smith, J. A., and Baeck, M. L.: Flood frequency analysis using radar rainfall fields and stochastic storm transposition, Water Resources Research, 50, 1592–1615, https://doi.org/10.1002/2013WR014224, 2014.

Wright, D. B., Mantilla, R., and Peters-Lidard, C. D.: A remote sensing-based tool for assessing rainfall-driven hazards, Environmental Modelling & Software, 90, 34–54, https://doi.org/10.1016/j.envsoft.2016.12.006, 2017.

Wright, D. B., Yu, G., and England, J. F.: Six decades of rainfall and flood frequency analysis using stochastic storm transposition: Review, progress, and prospects, Journal of Hydrology, 585, 124816, https://doi.org/10.1016/j.jhydrol.2020.124816, 2020.

Wu, K., Wang, C., Wu, L., Zhao, H., and Cao, J.: Slowdown in Landfalling Tropical Cyclone Motion in South China, Geophysical Research Letters, 49, e2022GL100428, https://doi.org/10.1029/2022GL100428, 2022.

Xu, L., Wang, A., Yu, W., and Yang, S.: Hot spots of extreme precipitation change under 1.5 and 2 °C global warming scenarios, Weather and Climate Extremes, 33, 100357, https://doi.org/10.1016/j.wace.2021.100357, 2021.

Xu, Z., Sun, Y., Li, T., Zhong, Z., Liu, J., and Ma, C.: Tropical Cyclone Size Change under Ocean Warming and Associated Responses of Tropical Cyclone Destructiveness: Idealized Experiments, J Meteorol Res, 34, 163–175, https://doi.org/10.1007/s13351-020-8164-4, 2020.

Yamada, M., Sayama, T., Yamazaki, D., and Watanabe, M.: Development of Methodology for Introducing Surveyed River Cross-Sections into Nationwide Distributed Hydrological Model Throughout Japan, and Its Effect on Water Level Prediction Accuracy, Journal of Japan Society of Civil Engineers, Ser. B1 (Hydraulic Engineering), 78, 7–22, https://doi.org/10.2208/jscejhe.78.1_7, 2022.

Yamada, Y., Satoh, M., Sugi, M., Kodama, C., Noda, A. T., Nakano, M., and Nasuno, T.: Response of Tropical Cyclone Activity and Structure to Global Warming in a High-Resolution Global Nonhydrostatic Model, Journal of Climate, 30, 9703–9724, https://doi.org/10.1175/JCLI-D-17-0068.1, 2017.

Yamaguchi, M., Chan, J. C. L., Moon, I.-J., Yoshida, K., and Mizuta, R.: Global warming changes tropical cyclone translation speed, Nat Commun, 11, 47, https://doi.org/10.1038/s41467-019-13902-y, 2020.

Yamakita, A.: Parameter regionalization of a nationwide hydrologic model and its validation at multiple locations, Master's Thesis, Kyoto University, Graduate School of Engineering, 91 pp., 2023.

Yamamoto, K., Sayama, T., and Apip: Impact of climate change on flood inundation in a tropical river basin in Indonesia, Progress in Earth and Planetary Science, 8, 5, https://doi.org/10.1186/s40645-020-00386-4, 2021.

Yamazaki, D., de Almeida, G. A. M., and Bates, P. D.: Improving computational efficiency in global river models by implementing the local inertial flow equation and a vector-based river network map, Water Resources Research, 49, 7221–7235, https://doi.org/10.1002/wrcr.20552, 2013.

Yamazaki, D., Togashi, S., Takeshima, A., and Sayama, T.: High-Resolution Flow Direction Map of Japan, Journal of JSCE, 8, 234–240, https://doi.org/10.2208/journalofjsce.8.1_234, 2020.

Yan, C., Zhao, G., Yue, T., Chen, C., Liu, J., Li, H., and Su, N.: Speeding up the high-accuracy surface modelling method with GPU, Environ. Earth Sci., 74, 6511–6523, https://doi.org/10.1007/s12665-015-4138-8, 2015.

Yan, Z., Xia, J., Song, J., Zhao, L., and Pang, G.: Research progress on design hyetographs in small and medium-scale basins, Progress in Geography, 39, 1224–1235, https://doi.org/10.18306/dlkxjz.2020.07.014, 2020.

Yang, L., Villarini, G., Zeng, Z., Smith, J., Liu, M., Li, X., Wang, L., and Hou, A.: Riverine Flooding and Landfalling Tropical Cyclones Over China, Earth's Future, 8, e2019EF001451, https://doi.org/10.1029/2019EF001451, 2020.

Yao, H. X. and Creed, I. F.: Determining spatially-distributed annual water balances for ungauged locations on Shikoku Island, Japan: a comparison of two interpolators, Hydrol. Sci. J.-J. Sci. Hydrol., 50, 245–263, https://doi.org/10.1623/hysj.50.2.245.60647, 2005.

Yasuda, S., Shimizu, Y., and Deguchi, K.: Investigation of the mechanism of the 2015 failure of a dike on Kinu River, Soils and Foundations, 56, 581–592, https://doi.org/10.1016/j.sandf.2016.07.001, 2016.

Ye, M., Ward, P. J., Bloemendaal, N., Nirandjan, S., and Koks, E. E.: Risk of Tropical Cyclones and Floods to Power Grids in Southeast and East Asia, Int J Disaster Risk Sci, 15, 494–507, https://doi.org/10.1007/s13753-024-00573-7, 2024.

Yin, L., Ping, F., Mao, J., and Jin, S.: Analysis on Precipitation Efficiency of the "21.7" Henan Extremely Heavy Rainfall Event, Adv. Atmos. Sci., 40, 374–392, https://doi.org/10.1007/s00376-022-2054-x, 2023.

Yin, Z., Song, X., Zhou, B., Jiang, W., Chen, H., and Wang, H.: Traditional Meiyu–Baiu has been suspended by global warming, National Science Review, 11, nwae166, https://doi.org/10.1093/nsr/nwae166, 2024.

Yokoya, N., Yamanoi, K., He, W., Baier, G., Adriano, B., Miura, H., and Oishi, S.: Breaking Limits of Remote Sensing by Deep Learning From Simulated Data for Flood and Debris-Flow Mapping, IEEE Transactions on Geoscience and Remote Sensing, 60, 1–15, https://doi.org/10.1109/TGRS.2020.3035469, 2022.

Yoshida, R., Iizumi, T., Nishimori, M., and Yokozawa, M.: Impacts of land-use changes on surface warming rates and rice yield in Shikoku, western Japan, Geophysical Research Letters, 39, https://doi.org/10.1029/2012GL053711, 2012.

Yoshikawa, N., Nagao, N., and Misawa, S.: Evaluation of the flood mitigation effect of a Paddy Field Dam project, Agricultural Water Management, 97, 259–270, https://doi.org/10.1016/j.agwat.2009.09.017, 2010.

Young, R. and Hsiang, S.: Mortality caused by tropical cyclones in the United States, Nature, 635, 121–128, https://doi.org/10.1038/s41586-024-07945-5, 2024.

Younis, J., Anquetin, S., and Thielen, J.: The benefit of high-resolution operational weather forecasts for flash flood warning, Hydrology and Earth System Sciences, 12, 1039–1051, https://doi.org/10.5194/hess-12-1039-2008, 2008.

Yu, G., Wright, D. B., Zhu, Z., Smith, C., and Holman, K. D.: Process-based flood frequency analysis in an agricultural watershed exhibiting nonstationary flood seasonality, Hydrology and Earth System Sciences, 23, 2225–2243, https://doi.org/10.5194/hess-23-2225-2019, 2019.

Yu, G., Wright, D. B., and Li, Z.: The Upper Tail of Precipitation in Convection-Permitting Regional Climate Models and Their Utility in Nonstationary Rainfall and Flood Frequency Analysis, Earth's Future, 8, e2020EF001613, https://doi.org/10.1029/2020EF001613, 2020.

Yu, Z., Ji, C., Xu, J., Bao, S., and Qiu, J.: Numerical simulation and analysis of the Yangtze River Delta Rainstorm on 8 October 2013 caused by binary typhoons, Atmospheric Research, 166, 33–48, https://doi.org/10.1016/j.atmosres.2015.06.014, 2015.

Yukimoto, S., Adachi, Y., Hosaka, M., Sakami, T., Yoshimura, H., Hirabara, M., Tanaka, T. Y., Shindo, E., Tsujino, H., Deushi, M., Mizuta, R., Yabu, S., Obata, A., Nakano, H., Koshiro, T., Ose, T., and Kitoh, A.: A New Global Climate Model of the Meteorological Research Institute: MRI-CGCM3 —Model Description and Basic Performance, Journal of the Meteorological Society of Japan. Ser. II, 90A, 23–64, https://doi.org/10.2151/jmsj.2012-A02, 2012.

Zelinka, M. D., Randall, D. A., Webb, M. J., and Klein, S. A.: Clearing clouds of uncertainty, Nature Clim Change, 7, 674–678, https://doi.org/10.1038/nclimate3402, 2017.

Zeng, Z., Wang, Z., and Lai, C.: Simulation Performance Evaluation and Uncertainty Analysis on a Coupled Inundation Model Combining SWMM and WCA2D, Int. J. Disaster Risk Sci., 13, 448–464, https://doi.org/10.1007/s13753-022-00416-3, 2022.

Zhai, X., Guo, L., Liu, R., Zhang, Y., and Zhang, Y.: Comparing Three Hydrological Models for Flash Flood Simulations in 13 Humid and Semi-humid Mountainous Catchments, Water Resources Management, 35, 1547–1571, https://doi.org/10.1007/s11269-021-02801-x, 2021.

Zhang, G., Murakami, H., Knutson, T. R., Mizuta, R., and Yoshida, K.: Tropical cyclone motion in a changing climate, Science Advances, 6, eaaz7610, https://doi.org/10.1126/sciadv.aaz7610, 2020.

Zhang, W., Villarini, G., Vecchi, G. A., and Smith, J. A.: Urbanization exacerbated the rainfall and flooding caused by hurricane Harvey in Houston, Nature, 563, 384–388, https://doi.org/10.1038/s41586-018-0676-z, 2018.

Zhao, C., Sun, Y., Yang, J., Li, J., Zhou, Y., Yang, Y., Fan, H., and Zhao, X.: Observational evidence and mechanisms of aerosol effects on precipitation, Science Bulletin, 69, 1569–1580, https://doi.org/10.1016/j.scib.2024.03.014, 2024.

Zhao, F., Veldkamp, T. I. E., Frieler, K., Schewe, J., Ostberg, S., Willner, S., Schauberger, B., Gosling, S. N., Schmied, H. M., Portmann, F. T., Leng, G., Huang, M., Liu, X., Tang, Q., Hanasaki, N., Biemans, H., Gerten, D., Satoh, Y., Pokhrel, Y., Stacke, T., Ciais, P., Chang, J., Ducharne, A., Guimberteau, M., Wada, Y., Kim, H., and Yamazaki, D.: The critical role of the routing scheme in simulating peak river discharge in global hydrological models, Environ. Res. Lett., 12, 075003, https://doi.org/10.1088/1748-9326/aa7250, 2017.

Zhao, G., Gao, H., and Cuo, L.: Effects of Urbanization and Climate Change on Peak Flows over the San Antonio River Basin, Texas, Journal of Hydrometeorology, 17, 2371–2389, https://doi.org/10.1175/JHM-D-15-0216.1, 2016.

Zhao, N., Wu, P., Manda, A., Guo, X., and Wang, B.: Moisture Sources of the Tohoku Heavy Rainfalls in August 2022 and the Influences of Tropical Storms, Geophysical Research Letters, 50, e2023GL104166, https://doi.org/10.1029/2023GL104166, 2023a.

Zhao, N., Wu, P., Manda, A., Guo, X., and Wang, B.: Moisture Sources of the Tohoku Heavy Rainfalls

in August 2022 and the Influences of Tropical Storms, Geophysical Research Letters, 50, e2023GL104166, https://doi.org/10.1029/2023GL104166, 2023b.

Zhao, W., Abhishek, Takhellambam, B. S., Zhang, J., Zhao, Y., and Kinouchi, T.: Spatiotemporal Variability of Current and Future Sub-Daily Rainfall in Japan Using State-Of-The-Art High-Quality Data Sets, Water Resources Research, 59, e2022WR034305, https://doi.org/10.1029/2022WR034305, 2023c.

Zhao, X. and Chan, J. C. L.: Changes in tropical cyclone intensity with translation speed and mixed-layer depth: idealized WRF-ROMS coupled model simulations, Quarterly Journal of the Royal Meteorological Society, 143, 152–163, https://doi.org/10.1002/qj.2905, 2017.

Zhou, Y.: Exploring multidecadal changes in climate and reservoir storage for assessing nonstationarity in flood peaks and risks worldwide by an integrated frequency analysis approach, Water Research, 185, 116265, https://doi.org/10.1016/j.watres.2020.116265, 2020.

Zhou, Z., Smith, J. A., Baeck, M. L., Wright, D. B., Smith, B. K., and Liu, S.: The impact of the spatiotemporal structure of rainfall on flood frequency over a small urban watershed: an approach coupling stochastic storm transposition and hydrologic modeling, Hydrology and Earth System Sciences, 25, 4701–4717, https://doi.org/10.5194/hess-25-4701-2021, 2021.

Zhu, L., Emanuel, K., and Quiring, S. M.: Elevated risk of tropical cyclone precipitation and pluvial flood in Houston under global warming, Environ. Res. Lett., 16, 094030, https://doi.org/10.1088/1748-9326/ac1e3d, 2021.

Zhu, Y.-J., Collins, J. M., Klotzbach, P. J., and Schreck, C. J.: Hurricane Ida (2021): Rapid Intensification Followed by Slow Inland Decay, Bulletin of the American Meteorological Society, 103, E2354–E2369, https://doi.org/10.1175/BAMS-D-21-0240.1, 2022.

Zou, N., Volgushev, S., and Buecher, A.: Multiple Block Sizes and Overlapping Blocks for Multivariate Time Series Extremes, Ann. Stat., 49, 295–320, https://doi.org/10.1214/20-AOS1957, 2021.

Zsoter, E., Prudhomme, C., Stephens, E., Pappenberger, F., and Cloke, H.: Using ensemble reforecasts to generate flood thresholds for improved global flood forecasting, Journal of Flood Risk Management, 13, e12658, https://doi.org/10.1111/jfr3.12658, 2020.